DEPARTMENT OF CHEMISTRY, UNIVERSITY OF JYVÄSKYLÄ
RESEARCH REPORT No. 207

THEORETICAL AND COMPUTATIONAL STUDIES OF MAGNETIC ANISOTROPY AND EXCHANGE COUPLING IN MOLECULAR SYSTEMS

BY

AKSELI MANSIKKAMÄKI

Academic Dissertation for the Degree of
Doctor of Philosophy

To be presented,
by permission of the Faculty of Mathematics and Science of the University of Jyväskylä
for public examination in Auditorium KEM4, on April 20th, 2018 at 12 noon.

UNIVERSITY OF JYVÄSKYLÄ

Jyväskylä, Finland
ISBN 978-951-39-7386-5 (print)
ISBN 978-951-39-7387-2 (electronic)
ISSN 0357-346X

ABSTRACT

Mansikkamäki, Akseli
Theoretical and Computational Studies of Magnetic Anisotropy and Exchange Coupling in Molecular Systems
Jyväskylä: University of Jyväskylä, 2018, 190 p. (+included articles)
(Department of Chemistry, University of Jyväskylä Research Report Series
ISSN 0357-346X)
ISBN 978-951-39-7386-5 (print)
ISBN 978-951-39-7387-2 (electronic)

The field of molecular magnetism studies the magnetic properties of molecular systems as opposed to conventional metal-based magnets. The high chemical modifiability of the constituting molecules makes such materials highly versatile, and the small size of the building blocks leads to the rise of various quantum mechanical phenomena, such as tunneling and entanglement. These phenomena can then be further utilized in the construction of nanoscale quantum devices.

This dissertation describes computational and theoretical studies in the field of molecular magnetism using state-of-the-art quantum chemical methods based on *ab initio* multireference approaches and broken symmetry density functional theory. Of the eight papers included in this work, the first three describe the experimental and computational characterization of magnetic interactions between organic radicals, transition metal ions, and lanthanide ions. The next paper introduces an approach to design ferromagnetically coupled organic radical dimers, which can be used in the construction of magnets consisting of purely organic molecules. This theory can also be extended to the design of organo-main-group radical systems and ferromagnetically coupled metal–radical complexes. The following three papers focus on the study of magnetic anisotropy in mono- and polymetallic Dy(III) coordination complexes. The last paper develops a theoretical model for the description of anisotropic spin-dependent delocalization and applies this model to study the magnetic interactions in excited states of bilanthanide endohedral metallo-fullerenes. In all cases where computational tools are applied to experimentally characterized systems, the computations offer more insight into the electronic structure and chemical properties of the systems, giving rise to the various macroscopically observed magnetic phenomena than what could be obtained by experimental tools only. The results contribute to our understanding of magnetically interesting molecular systems and suggest new research directions in the field.

Keywords: molecular magnetism, single-molecule magnets, organic magnets, endohedral metallo-fullerenes, lanthanides, magnetic anisotropy, exchange interaction, spin-orbit coupling, quantum chemistry, broken symmetry DFT, DFT, CASSCF, CASPT2, NEVPT2

Author's address

Akseli Mansikkamäki
Department of Chemistry
P. O. Box 35
40014 University of Jyväskylä
Jyväskylä, Finland
akseli.mansikkamaki@jyu.fi

Supervisor

Professor Heikki M. Tuononen
Department of Chemistry
University of Jyväskylä
Jyväskylä, Finland

Reviewers

Professor Emeritus Pekka Pyykkö
Department of Chemistry
University of Helsinki
Helsinki, Finland

Doctor Stephen M. Winter
Institute for Theoretical Physics
Goethe University Frankfurt
Frankfurt am Main, Germany

Opponent

Professor Juha Vaara
NMR Research Unit
University of Oulu
Oulu, Finland

PREFACE

The research presented in this dissertation has been carried out at the University of Jyväskylä during the period from January 2014 to February 2018, and at KU Leuven from January to July 2016. Quite a few people have made an impact to this work—either small or large. The list of people is far too vast and this preface far too short to list everyone and their contribution in detail. I will nonetheless make an effort to list some of them.

First and foremost I would like to thank my supervisor Prof. Heikki M. Tuononen for making this Ph. D. dissertation possible in the first place and for entrusting me with considerable freedom to pursue research I found worthwhile and interesting. Secondly, I would like to thank Prof. Liviu F. Chibotaru for allowing me to work in his group and for supporting me during my visit at KU Leuven and ever since. Much of the work in this dissertation is based on experimental work conducted by collaborators, and I gratefully acknowledge the work of Dr. Rodolphe Clérac, Prof. Philip P. Power, Prof. Ming-Liang Tong, and Prof. Richard A. Layfield, as well as the members of their research groups. I have had many helpful, productive, and inspiring discussions with various co-workers, including Dr. Jani O. Moilanen, Dr. Mikko M. Hänninen, Dr. Aaron Mailman, and Dr. Ian S. Morgan at the University of Jyväskylä, and Dr. Naoya Iwahara, Dr. Liviu Ungur, and Dr. Veacheslav Vieru at KU Leuven. I would also like to thank the reviewers Prof. Pekka Pyykkö and Dr. Stephen M. Winter for their insightful comments on the manuscript of this thesis.

This work could not have been possible without the financial support provided by the Foundation for Research of Natural Resources in Finland and the Academy of Finland. Additional funding, which has enabled me to participate in conferences across the globe, has been provided by the Magnus Ehrnrooth Foundation, the Alfred Kordelin Foundation (Gustaf Komppa fund), and the University of Jyväskylä. Computational resources have been provided by the University of Jyväskylä, by CSC – IT Center for Science, Finland, by the Finnish Grid and Cloud Infrastructure, and by KU Leuven. The contributions of all these organizations are gratefully acknowledged.

In many ways I feel that this dissertation is not just the culmination of the four years I have spent doing the research, but rather of the eight and half years I have spent at University of Jyväskylä, first as an undergraduate student and later as a Ph. D candidate. During this time, which accounts for more than a quarter of my life, I have come to know quite a few people; some I have studied with, some I have worked with, some I have shared office space with, some I have had lunch with, and some I have consumed excessive amounts of alcohol with. The group of people I call friends now spreads over several continents, and I am lucky to say that during my time in Jyväskylä the words ‘co-worker’ and ‘friend’ have become largely synonymous. All of these people have—directly or indirectly—contributed to this thesis. It is mostly due to these people that the past eight and a half years have been some of the best in my life, and that during

this time not once have I felt regret that I made the choice to study in Jyväskylä or that I chose to pursue my Ph. D. here. During these eight and a half years I have met some of the greatest friends I have ever had, and during these eight and a half years I met and married my wife Susanna.

Jyväskylä, February 2018
Akseli Mansikkamäki

LIST OF ABBREVIATIONS

ωB97X	2008 range-separated hybrid exchange-correlation functional by Chai and Head-Gordon
ωPBE	2003 range-separated GGA exchange-correlation functional by Heyd, Scuseria, and Ernzerhof using the PBE GGA functional
ac	alternating current
ADF	Amsterdam Density Functional
AFM	anti-ferromagnetic
AILFT	*ab initio* ligand-field theory
ANO-RCC	relativistically contracted atomic natural orbital
AO	atomic orbital
B1B95	1995 hybrid exchange-correlation functional by Becke using one-parameter Fock exchange mixing, B88 GGA exchange, and B95 GGA correlation
B3LYP	1994 hybrid exchange-correlation functional by Stephens and co-workers using the B3PW91 parameterization, B88 GGA exchange, and LYP GGA correlation
B3PW91	1993 hybrid exchange-correlation functional by Becke using the B88 GGA exchange and PW91 GGA correlation
B88	1988 GGA exchange functional by Becke
B95	1995 GGA correlation functional by Becke
B97	1997 GGA and hybrid exchange-correlation functional by Becke
B97-1	1998 modification to B97 by Handy and co-workers
B97-2	2001 modification to B97 by Tozer and co-workers
B98	1998 modification to B97 by Becke
BHHLYP	A hybrid functional based on the 1993 half-and-half functional of Becke using B88 GGA exchange, LYP GGA correlation, and 50% of Fock exchange
BJ	Becke–Johnson
BMK	2004 meta-GGA and hybrid exchange-correlation functional by Bose and Martin
BQ	2,5-bisoxide-1,4-benzoquinone
BS	broken symmetry
BSSE	basis set superposition error

CAM	Coulomb-attenuating method
CAM-B3LYP	2004 range-separated parameterization of the B3LYP functional by Yanai and co-workers
CAS	complete active space
CASCI	complete active space configuration interaction
CASPT2	complete active space perturbation theory at second order
CASSCF	complete active space self-consistent field
CCI	complete configuration interaction
CCSD(T)	coupled cluster theory with single, double, and perturbative triple excitations
CD	Cholesky decomposition
CF	crystal-field
CG	Clebsch–Gordan
CI	configuration interaction
CIS	configuration interaction singles and doubles
COSX	chain of spheres exchange
CPD	Chang–Pelissier–Durand
CSF	configuration state function
dc	direct current
DDCI	difference-dedicated configuration interaction
DFT	density functional theory
DKH	Douglas–Kroll–Heß
DKH2	Douglas–Kroll-Heß transformation up to second order
DLPNO	domain-based local pair-natural orbital
DLPNO-CCSD(T)	domain-based local pair-natural orbital coupled cluster theory with single, double, and perturbative triple excitations
DLPNO-NEVPT2	domain-based local pair-natural orbital N-electron valence state perturbation theory at second order
DM	Dzyaloshinsky–Moriya
DMRG	density matrix renormalization group
ECP	Effective core potential
EMF	endohedral metallo-fullerene
EPR	electron paramagnetic resonance
ESR	electron spin resonance
FC	field-cooled

FCI	full configuration interaction
FM	ferromagnetic
FOIS	first-order interacting space
GASSCF	generalized active space self-consistent field
GGA	generalized gradient approximation
GM	Girerd–Münck
GTO	Gaussian-type orbital
HCTH	A family of GGA and hybrid exchange-correlation functionals by Handy and co-workers
HEG	Homogeneous electron gas
hfac	hexafluoroacetylacetonate
HF	Hartree–Fock
HK	Hohenberg–Kohn
HOMO	highest occupied molecular orbital
HS	high-spin
HSE	2003 range-separated hybrid exchange-correlation functional by Heyd, Scuseria, and Ernzerhof using the ωPBE range-separated GGA functional
HSE03	2003 modification of the HSE functional by Heyd and Scuseria
HSE06	2006 or 2009 modification of the HSE functional Scuseria, Henderson, and co-workers
ICE-CI	iterative configuration expansion configuration interaction
IORA	infinite-order regular approximation
IPEA	ionization potential electron affinity
ITO	irreducible tensor operator
KS	Kohn–Sham
LC-ωHPBE	2009 modification of the LC-ωPBE functional by Henderson and co-workers
LC-ωPBE	2006 range-separated hybrid exchange-correlation functional by Vydrov and Scuseria using the ωPBE range-separated GGA functional
LL	Levy–Lieb
LS	low-spin
LSDA	local spin density approximation
LUMO	lowest unoccupied molecular orbital
LYP	1988 GGA correlation functional by Lee, Yang, and Parr

M05	2005 hybrid exchange-correlation functional by Truhlar and co-workers
M05-2X	2005 hybrid exchange-correlation functional by Truhlar and co-workers with double Fock exchange
M06	2006 hybrid exchange-correlation functional by Truhlar and co-workers
M06-2X	2006 hybrid exchange-correlation functional by Truhlar and co-workers with double Fock exchange
M06-HF	2006 hybrid exchange-correlation functional by Truhlar and co-workers with 100% of Fock exchange
M06-L	2006 meta-GGA exchange-correlation functional by Truhlar and co-workers
M08-HX	2008 hybrid exchange-correlation functional by Truhlar and co-workers
M08-SO	2008 hybrid exchange-correlation functional by Truhlar and co-workers
M11	2011 range-separated hybrid exchange-correlation functional by Truhlar and co-workers using the range-separated M11-L meta-GGA functional
M11-L	2011 range-separated meta-GGA exchange-correlation functional by Truhlar and co-workers
MCSCF	multiconfigurational self-consistent field
MN12-L	2012 range-separated meta-GGA exchange-correlation functional by Truhlar and co-workers
MN12-SX	2012 range-separated hybrid exchange-correlation functional by Truhlar and co-workers using the range-separated MN12-L meta-GGA functional
MN15	2015 hybrid exchange-correlation functional by Truhlar and co-workers using the range-separated MN15-L meta-GGA functional
MN15-L	2015 range-separated meta-GGA exchange-correlation functional by Truhlar and co-workers
MO	molecular orbital
MP2	Møller–Plesset perturbation theory at second order
MRCI	multireference configuration interaction
MRCISD	multireference configuration interaction with single and double excitations
MS-CASPT2	multistate complete active space perturbation theory at second order

N12	2012 range-separated meta-GGA exchange-correlation functional by Truhlar and co-workers
N12-SX	2012 range-separated hybrid exchange-correlation functional by Truhlar and co-workers using the range-separated N12 meta-GGA functional
NEVPT2	*N*-electron valence state perturbation theory at second order
NMR	nuclear magnetic resonance
NO	natural orbital
NOON	natural orbital occupation number
OEP	optimized effective potential
ON	occupation number
P86	1986 GGA exchange functional by Perdew
PBE	1996 GGA exchange-correlation functional by Perdew, Burke, and Ernzerhof
PBE0	1999 hybrid exchange-correlation functional by Ernzerhof and Scuseria, and by Adamo and Barone using the PBE GGA
PBE1PBE	An alternative name to PBE0
Ph	phenyl
PW86	1986 GGA correlation functional by Perdew and Wang
PW91	1991 GGA exchange-correlation functional by Perdew and Wang
QD-NEVPT2	quasi-degenerate *N*-electron valence state perturbation theory at second order
QDPT	quasi-degenerate perturbation theory
QTM	quantum tunneling of magnetization
RASSCF	restricted active space self-consistent field
RASSI	restricted active space state-interaction
REKS	restricted ensemble-referenced Kohn–Sham
RHF	restricted Hartree–Fock
RI	resolution of identity
ROCIS	restricted open-shell configuration interaction singles
RPA	random phase approximation
SA-CASSCF	state-averaged complete active space self-consistent field
SARC	segmented all-electron relativistically contracted
SCF	self-consistent field
SIM	single-ion magnet

SMM	single-molecule magnet
SOC	spin-orbit coupling
SOGGA11	2011 GGA exchange-correlation functional by Truhlar and co-workers
SOGGA11X	2011 hybrid exchange-correlation functional by Truhlar and co-workers based on the SOGGA11 GGA
SOMO	singly occupied molecular orbital
SO-RASSI	spin-orbit restricted active space state-interaction
SQUID	superconducting quantum interference device
STO	Slater-type orbital
tbacac	2,2,6,6-tetramethyl-3,5-heptane-dionato
*t*Bu	*tert*-butyl
THF	tetrahydrofuran
TPSS	2003 meta-GGA exchange-correlation functional by Tao, Perdew, Staroverov, and Scuseria
TPSSh	A hybrid version of TPSS by Tao, Perdew, Staroverov, and Scuseria
UHF	unrestricted Hartree–Fock
VWN	A parameterization of the LSDA correlation by Vosko, Wilk, and Nusair
VWN5	A parameterization of the LSDA correlation by Vosko, Wilk, and Nusair
X2C	exact decoupling into two components
XC	exchange-correlation
XMS-CASPT2	extended multistate complete active space perturbation theory at second order
ZFC	zero-field-cooled
ZFS	zero-field splitting
ZORA	zeroth-order regular approximation

LIST OF INCLUDED ARTICLES

I I. S. Morgan, A. Mansikkamäki, P. A. Koutentis, G. A. Zissimou, M. Rouzières, R. Clérac, and H. M. Tuononen. **Coordination Complexes of a Neutral Benzo-1,2,4-Triazinyl Radical Ligand: Synthesis, Molecular and Electronic Structures, and Magnetic Properties.** *Chem. Eur. J.*, **2015**, *21*, 15843–15853.

II I. S. Morgan, A. Mansikkamäki, M. Rouzières, R. Clérac, and H. M. Tuononen. **Coexistence of long-range antiferromagnetic order and slow relaxation of the magnetization in the first lanthanide complex of a 1,2,4-benzotriazinyl radical.** *Dalton Trans.*, **2017**, *46*, 12790–12793.

III M. Faust, A. M. Bryan, A. Mansikkamäki, P. Vasko, M. M. Olmstead, H. M. Tuononen, F. Grandjean, G. J. Long, and P. P. Power. **The Instability of $Ni\{N(SiMe_3)_2\}_2$: A Fifty Year Old Transition Metal Silyamide Mystery.** *Angew. Chem. Int. Ed.*, **2015**, *54*, 12914–12917.

IV A. Mansikkamäki and H. M. Tuononen. **The role of orbital symmetries in enforcing ferromagnetic ground state in mixed radical dimers. 2018**, *manuscript in preparation*.

V Y.-C. Chen, J.-L. Liu, Y. Lan, Z.-Q. Zhong, A. Mansikkamäki, L. Ungur, Q.-W. Li, J.-H. Jia, L. F. Chibotaru, J. Han, W. Wernsdorfer, X.-M. Chen, and M. Tong. **Dynamic Magnetism and Optical Insight into a Pentagonal Bipyramidal Dy(III) Single-Ion Magnet.** *Chem. Eur. J.*, **2017**, *23*, 5708–5715.

VI F.-S. Guo, B. M. Day, Y.-C. Cheng, M.-L. Tong, A. Mansikkamäki, and R. A. Layfield. **A Dysprosium Metallocene Single-Molecule Magnet Functioning at the Axial Limit.** *Angew. Chem. Int. Ed.*, **2017**, *56*, 11445–11449.

VII J. O. Moilanen, A. Mansikkamäki, M. Lahtinen, F.-S. Guo, E. Kalenius, R. A. Layfield, and L. F. Chibotaru. **Thermal expansion and magnetic properties of benzoquinone-bridged dinuclear rare-earth complexes.** *Dalton Trans.*, **2017**, *46*, 13582–13589.

VIII A. Mansikkamäki, A. A. Popov, Q. Deng, N. Iwahara, and L. F. Chibotaru. **Interplay of spin-dependent delocalization and magnetic anisotropy in the ground and excited states of $[Gd_2@C_{78}]^-$ and $[Gd_2@C_{80}]^-$.** *J. Chem. Phys.*, **2017**, *147*, 124305.

Author's contribution

The author of the present dissertation has carried out all computational work in papers **I–VIII** except the geometry optimizations in Paper **VIII**. The author is the principal investigator and writer of papers **IV** and **VIII**, and has written the first drafts of sections relevant to his work in the other manuscripts. The author has carried out all theoretical derivations in Paper **VIII**.

CONTENTS

ABSTRACT
PREFACE
LIST OF ABBREVIATIONS
LIST OF INCLUDED ARTICLES
CONTENTS

1 INTRODUCTION 19
1.1 Historical outline and current state of the field 20
1.2 Aim of this study 24
1.3 Notation and conventions 25

I Theory **27**

2 QUANTUM MECHANICAL DESCRIPTION OF MANY-PARTICLE SYSTEMS 29
2.1 Molecular orbital description of non-interacting many-particle states 29
2.2 Fock-space description of many-particle states and second quantization 30
2.2.1 States and operators in the Fock space 30
2.2.2 Expectation values and reduced density matrices 33
2.2.3 Spin properties of states in the Fock space 34
2.3 The electron density 35

3 QUANTUM THEORY OF MOLECULAR MAGNETISM 37
3.1 Macroscopic magnetic properties 38
3.2 Microscopic theory of angular momentum 39
3.2.1 Angular momentum and rotations 39
3.2.2 Coupling of angular momenta 41
3.2.3 Irreducible tensor operators 41
3.2.4 Time-reversal symmetry and Kramers' theorem 43
3.2.5 The microscopic magnetization 44
3.3 Model Hamiltonians 44
3.3.1 Spin and pseudospin Hamiltonians 44
3.3.2 Effective Hamiltonian theory 47
3.4 Electronic structure of metal ions in molecular complexes 48
3.4.1 Classification of metal ions 48
3.4.2 The microscopic Hamiltonian 50
3.4.3 Spin and pseudospin Hamiltonians for monometallic complexes 52
3.5 Exchange interaction 55
3.5.1 Direct exchange mechanism 55

3.5.2 Superexchange mechanism 57
3.5.3 Double-exchange mechanism 58
3.5.4 Spin Hamiltonians for isotropic exchange 61
3.5.5 Spin Hamiltonians for weak anisotropic exchange 63
3.5.6 Pseudospin Hamiltonians for strongly anisotropic exchange 63
3.6 Dynamic magnetic properties 64
3.7 On experimental techniques 68

4 WAVE-FUNCTION-BASED QUANTUM CHEMISTRY OF STRONGLY CORRELATED SYSTEMS 71
4.1 Basics of electronic structure calculations 72
4.1.1 Variation of energy 72
4.1.2 The Hartree–Fock method 75
4.1.3 Electron correlation 77
4.2 The complete active space self-consistent field method 79
4.3 Multireference perturbation methods 83
4.3.1 General remarks 83
4.3.2 The CASPT2 method 84
4.3.3 The NEVPT2 method 87
4.3.4 Beyond perturbation theory 89
4.4 Relativistic corrections and properties 90
4.4.1 Four- two- and one-component theories 90
4.4.2 Zeroth-order regular approximation 92
4.4.3 Douglas–Kroll–Heß transformation 93
4.4.4 Exact decoupling methods 94
4.4.5 Spin-orbit coupling 95
4.4.6 Zeeman interaction 98
4.5 Extraction of spin Hamiltonian parameters from *ab initio* calculations 98
4.5.1 **g**-, $\tilde{\mathbf{g}}$-, and **D**-tensors 98
4.5.2 Isotropic exchange coupling constants 99
4.5.3 Parameters for anisotropic exchange 100
4.5.4 *Ab initio* crystal-field for lanthanides 101
4.5.5 Qualitative relaxation barrier 101

5 DENSITY FUNCTIONAL THEORY OF STRONGLY CORRELATED SYSTEMS 103
5.1 Density functional theory 104
5.1.1 Fundamental proofs 104
5.1.2 The Kohn–Sham theory 105
5.1.3 The exchange-correlation functional 107
5.2 The broken symmetry method for strongly correlated systems 112
5.2.1 Energy difference between spin states in the context of DFT 112
5.2.2 Broken symmetry method in the context of Hartree–Fock theory 114

5.2.3 Broken symmetry method in the context of DFT 116
5.2.4 On the choice of exchange-correlation functional 118
5.3 Calculation of **g**- and **D**-tensors using DFT 119

II Results **121**

6 COMPUTATIONAL MODELING OF ISOTROPIC EXCHANGE INTERACTIONS AND WEAK ANISOTROPY 123
6.1 Computational details 124
6.2 Computational analysis of exchange interactions in transition-metal, lanthanide, and radical systems 126
6.2.1 3d metal complexes of a 1,2,4-benzotriazinyl radical 126
6.2.2 Dy(III) complexes of a 1,2,4-benzotriazinyl radical 129
6.2.3 $[Ni\{N(SiMe_3)_2\}]_4$ tetramer 131
6.3 Design of organic radical systems with ferromagnetic interaction. 134
6.3.1 Theoretical framework 134
6.3.2 Model systems for a proof-of-concept study 136
6.3.3 Validation studies 137
6.3.4 Results 140

7 COMPUTATIONAL MODELING OF STRONGLY ANISOTROPIC MAGNETIC PROPERTIES 142
7.1 Computational details 142
7.2 Monometallic Dy(III) complexes 144
7.2.1 $Dy[(CyPh_2PO)_2(H_2O)_5]Br_3$ complex 144
7.2.2 Dysprocenium complexes 147
7.3 Bimetallic $[BQ\{DyCl_2(THF)_3\}_2]$ complex 150

8 THEORETICAL DESCRIPTION OF ANISOTROPIC SPIN-DEPENDENT DELOCALIZATION 153
8.1 Computational details 154
8.2 Electronic structures of $[Gd_2@C_{78}]^-$ and $[Gd_2@C_{80}]^-$ 155
8.3 Spin Hamiltonian description 157
8.3.1 Exchange interaction in Σ states 157
8.3.2 Exchange interaction in Π and Δ states 159
8.4 Numerical results 160

9 CONCLUSIONS 165
9.1 Outlook 166

REFERENCES 168

INCLUDED ARTICLES

1 INTRODUCTION

In 1927, Walter Heitler and Fritz London published a paper titled "Wechselwirkung neutraler Atome und homöopolare Bindung nach der Quantenmechanik" in Zeitschrift für Physik.[1] The title can be freely translated to English as "Interaction of Neutral Atoms and Homopolar Binding in Terms of Quantum Mechanics", and the paper constitutes the first application of modern quantum theory to a chemical problem. It is arguably one of the most important, if not *the* most important, contribution to our understanding of the concept of the chemical bond. In their work, Heitler and London explain the interaction of two hydrogen atoms and the formation of a chemical bond using the wave mechanics formulation of quantum theory published by Schrödinger the previous year.[2–6] An important aspect of the work of Heitler and London, and a key to its ultimate success, was the correct enforcement of anti-symmetry relative to particle exchange on their trial wave function. This leads to correct realization of the Pauli principle and is the origin of a phenomenon that came to be known as exchange interaction.[7–14] The following year Heisenberg published his nominal paper "Zur Theorie des Ferromagnetismus" ("On the Theory of Ferromagnetism"), in which he took the concept of exchange interaction further and used it to explain the spin-ordering of electrons in ferromagnetic (FM) metals.[15] Heisenberg's theory forms the basis of our understanding of the quantum mechanical effects, which lead to the formation of permanent magnets.

Thus, the genesis of the fundamental quantum theories of both chemistry and magnetism lies in the concept of exchange interaction; and it is reasonable to state that magnetism and the electronic structure of molecules are closely related on a microscopic level. For the better part of the 20th century, however, these two fields of study remained rather segregated. The magnetic properties of molecular systems certainly were widely studied as analytical tools in the context of nuclear magnetic resonance (NMR) spectroscopy,[16–18] electron paramagnetic resonance (EPR) spectroscopy,[19–21] and in the field of mangnetochemistry,[22,23] which studied paramagnetic properties of molecules as a tool for structural determination. It was not until the early 1980s when advances in the understanding of the magnetic properties of molecules and in experimental techniques initiated a paradigm shift

in the field of magnetochemistry, which moved the field from the analysis of structures on the basis of their paramagnetism towards designing structures with specific and novel magnetic properties.[24–26] This newborn research field became known as molecular magnetism and is the topic of this dissertation.

1.1 Historical outline and current state of the field

Early work in the field of molecular magnetism focused on controlling the magnetic properties of molecules through their chemical structure.[26,27] A true hallmark in this regard was achieved in 1982 when Kahn and co-workers induced FM interaction between transition-metal ions by exploiting orbital symmetries of different ions introduced into the same ligand framework (Figure 1a).[28] The focus then moved towards designing systems with three-dimensional long-range magnetic order using the so-called bottom-up approach where one begins with tailoring the interaction between neighboring molecules and then moves towards longer and longer ranges of interactions.[29] In 1987 long-range order was achieved in an organometallic decamethylferrocene–tetracyanoethylene salt (Figure 1d)[30] and in 1991 in the β-phase of purely organic *para*-nitrophenyl nitronyl nitroxide radical (Figure 1b).[31] The design of organometallic, purely organic, and organo-main-group magnets remains an active research field.[32–35] One of the main goals is the design of systems with higher ordering temperatures. The current record is 36 K observed in a material consisting of a dithiadiazolyl radical (Figure 1c).[36] Some recent advances have also been achieved by introducing heavier main-group atoms into the radical frameworks to induce spin-orbit coupling (SOC)[37,38] and by introducing spin-canting.[39]

A true renaissance of molecular magnetism started in 1993 when Sessoli *et al*. discovered slow relaxation of magnetization in $[Mn_{12}O_{12}(PhCOO)_{16}(H_2O)_4]$ or, as it is commonly known as, Mn_{12} (Figure 2a).[40,41] The anisotropy is a consequence of the interplay of SOC at the Mn ions and the crystal-field (CF) potential of the ligands. What is truly remarkable about the observation is that the slow relaxation is not a property of the bulk material but emerges at the single-molecule level. In other words, if a single Mn_{12} complex was doped into a diamagnetic crystal lattice, the slow magnetic relaxation would still be observed. What this means is that if the magnetic moment of a given Mn_{12} complex is oriented in a specific direction by an external magnetic field and the field is then switched off, the molecule will *remember* this direction over some finite time. Considering the extremely small size of the system (~ 1 nm), this "magnetic memory" is coupled with quantum phenomena, such as quantum entanglement, tunneling, and decoherence. This has immediate implications to potential technological applications in molecular-size quantum technologies, such as microscopic digital memory,[42,43] spintronics,[44–46] and quantum computing.[46,47] Systems demonstrating slow relaxation of magnetization emerging at the molecular level can be considered as zero-dimensional magnets and are commonly known as single-molecule magnets

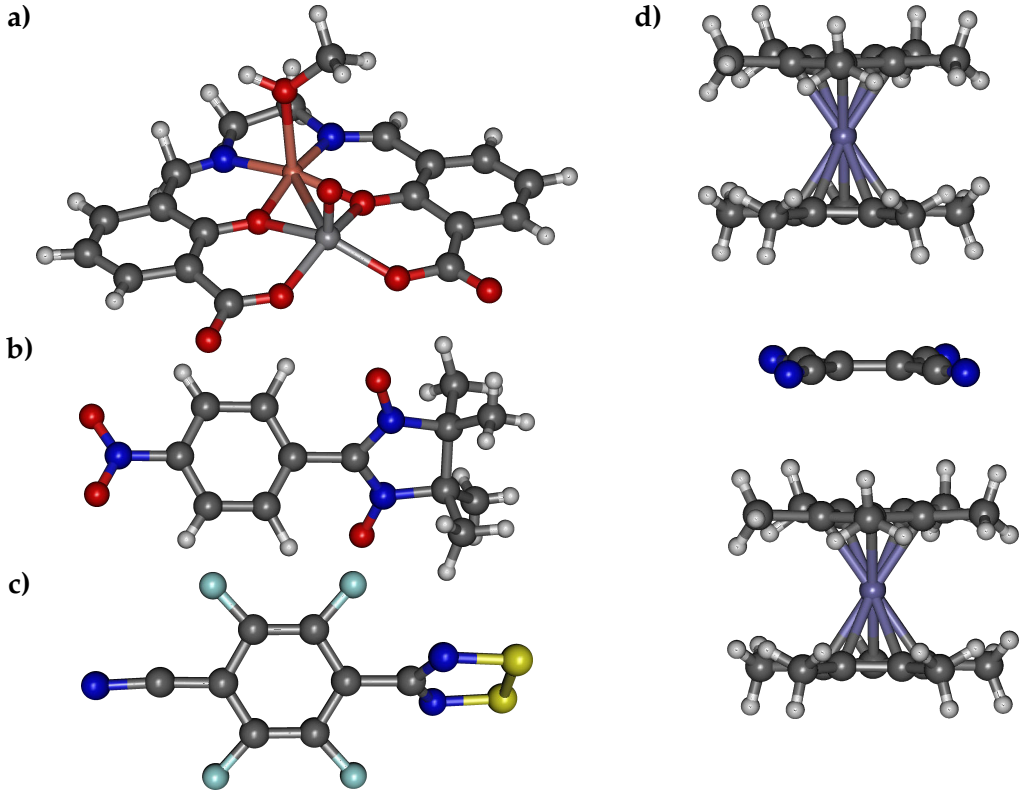

FIGURE 1 **a)** Ferromagnetically coupled complex of Kahn and co-workers, **b)** *para*-nitrophenyl nitronyl nitroxide radical, which orders ferromagnetically, **c)** a dithiadiazolyl radical of Rawson and co-workers, which orders ferromagnetically below 36 K, and **d)** decamethylferrocene–tetracyanoethylene salt, which orders ferrimagnetically.

(SMMs). The discovery of Mn_{12} led to a shift of focus from three-dimensional magnetic systems to zero-dimensional systems constructed using polymetallic high-spin complexes. The main aim was, and still is, to design systems with higher blocking temperatures. The blocking temperature has several definitions but can be considered as the highest temperature where the slow relaxation of magnetization can be observed at a "mechanical timescale" sometimes standardized as 100 s.[25] In most SMMs, the blocking temperature is in the range of a few kelvins above absolute zero.

An important aspect in the development of new systems has been the use of theoretical models and computational tools, which have afforded insight into the features of the chemical structure leading to the desired magnetic functionality. Theoretical calculations have been carried out on magnetic systems for several decades, and calculations on the magnetic properties of atoms using self-consistent field methods were well-established already in the 1930s.[48] However, application to larger molecular systems was severely limited by the available computational hardware until the 1990s. EPR parameters of small systems were calculated by semi-empirical methods with rather stringent approximations starting from the 1970s.[21,49] More accurate calculations for systems where SOC could be treated using low-order perturbation theory started to appear in the

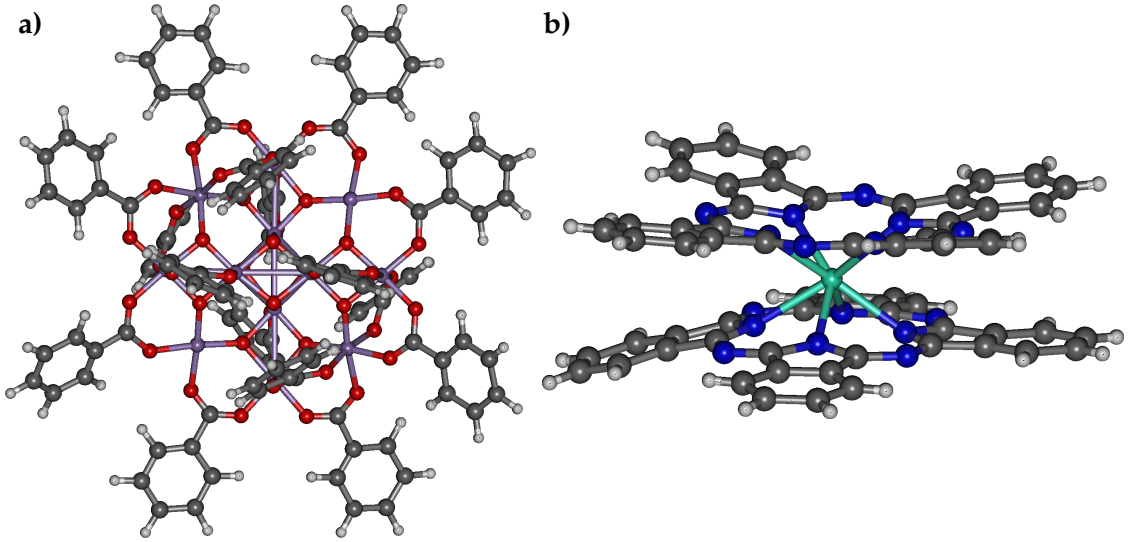

FIGURE 2 **a)** Structure of $[Mn_{12}O_{12}(CH_3COO)_{16}(H_2O)_4]$ and **b)** structure of a phthalocyanine–lanthanide(III) double-decker complex.

late 1990s in the context of density functional theory (DFT) methods[50–65] and wave-function-based *ab initio* methods.[66–69] Isotropic exchange coupling constants were calculated starting from the early 1980s,[70–75] and by the early 2000s, calculation on small to moderate size third-row transition-metal complexes using multireference *ab initio* methods were well established.[76,77] Accurate estimates of exchange coupling constants can also be made using DFT in the so-called broken symmetry formalism, which was developed in the 1980s.[70–73] The method is widely used (for examples see reviews 61, 78, 79, and the references therein), but its formal interpretation in the context of DFT remains somewhat controversial.[80–86] Starting from the turn of the millenia, anisotropic magnetic properties could be described by using multireference *ab initio* methods, where SOC was introduced in a non-perturbative manner.[87–89]

The need for high-level theoretical calculations of highly anisotropic magnetic properties became more apparent when in 2003 Ishikawa and co-workers demonstrated that phthalocyanine–lanthanide complexes with just one metal ion (Figure 2b) can show very pronounced SMM behavior.[90,91] This led to a huge surge in the research on lanthanide-based SMMs.[92,93] By that time, computational methods for the multireference treatment of systems with strong SOC were available,[94] and the physics of the magnetic properties of lanthanide ions were already well-established in the book of Abragam and Bleaney published in 1970.[20] The tools to put the calculated results in correspondence with various empirical quantities used to characterize these systems, however, were still missing for the most part. These were developed during the 2000s by Ungur, Chibotaru, and co-workers[95–101] with contributions by Atanasov, Neese, and co-workers.[102,103]

The theoretical results showed that more pronounced SMM behavior could be achieved by using simpler complexes with just one metal ion as opposed to complicated polymetallic systems.[104] Such systems are sometimes referred to as single-ion magnets (SIMs). It was further shown by Ungur and Chibotaru that the

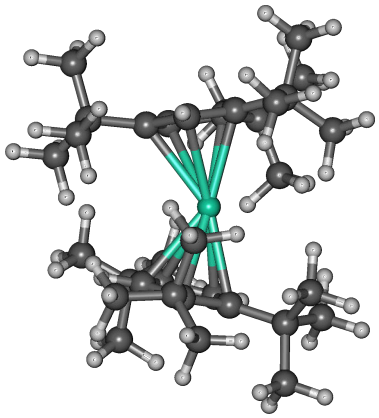

FIGURE 3 Structure of a dysprocenium SMM.

optimal system should have a highly axial CF with strong anionic ligands in axial positions of the coordination sphere and weak neutral or, better yet, no ligands at all in the equatorial positions.[105] A similar conclusion can also be drawn from the simple and highly successful electrostatic model introduced by Rineheart and Long[106] (based on earlier work by Sievers[107]), and from later theoretical works by various authors.[108–110] Most of the recent hallmarks in the field of SMMs have been achieved using this strategy.[VI,111–114] The SMM that currently has the highest blocking temperature up to 60 K is a dysprocenium cation with no equatorial ligands (Figure 3).[VI,114] The operational temperature of this SMM is approaching the temperature of liquid nitrogen (77 K), which can be considered as a lower temperature limit for actual industrial applications.

Another important trend in the design of SMMs is the construction of systems with a few, strongly exchange-coupled lanthanide ions. This design strategy started with the observation of a blocking temperature of 14 K in a N_2^{3-} radical-bridged Tb complex $\{[(Me_3Si)_2N]_2(THF)Tb\}_2(\mu\text{-}\eta^2\text{:}\eta^2\text{-}N_2)$ (Figure 4a).[115] The Gd–N_2^{3-} exchange coupling in the Gd analogue was the strongest observed in any lanthanide system[116] and the remains the highest observed in any coordination complex. The $\{[(Me_3Si)_2N]_2(THF)Tb\}_2(\mu\text{-}\eta^2\text{:}\eta^2\text{-}N_2)$ complex was very recently further improved by replacing the $(Me_3Si)_2N$ and THF auxiliary ligands with cyclopentadienyls raising the blocking temperature to 20 K. Stronger exchange coupling has since been achieved in an endohedral metallofullerene $Dy_2@C_{80}(CH_2Ph)$ (Figure 4b) with a blocking temperature of 18 K.[117] The theoretical description of the anisotropic interaction between strongly spin-orbit-coupled ions is extremely complicated. Usually in lanthanide systems, the exchange interactions are weak and are described within the framework of the Lines model[118] by introducing one empirical parameter, which is fitted to experimental data.[96,98,99] The exact expression for the interaction has been derived but has seen very limited use so far due to its complicated form.[119–121] This complexity greatly hinders the development of new polymetallic SMMs in a rational way. In the case of SIMs, theoretical calculations can be used to predict anisotropic magnetic properties of the systems,[108,109] but in the case of polymetallic systems, one is still largely confined to explaining the properties observed experimentally.

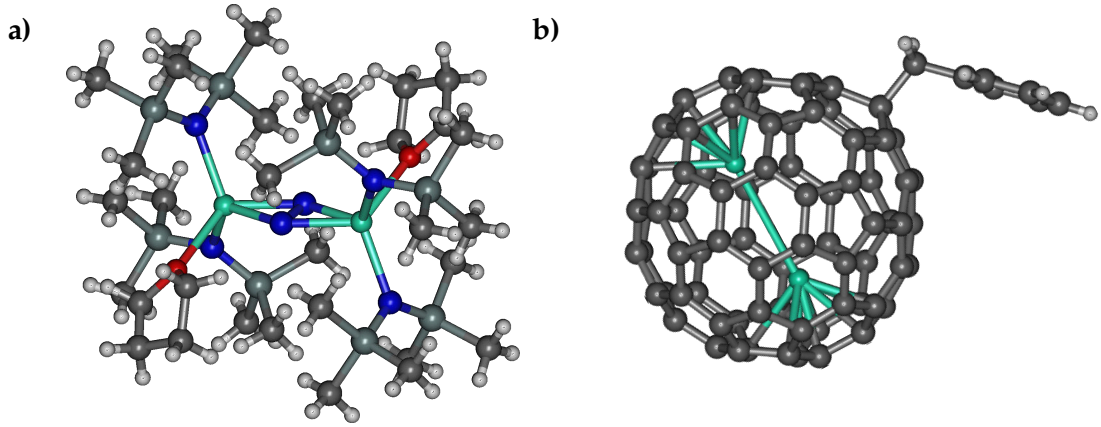

FIGURE 4 **a)** Structure of $\{[(Me_3Si)_2N]_2(THF)Tb\}_2(\mu\text{-}\eta^2\text{:}\eta^2\text{-}N_2)$ and **b)** structure of $Dy_2@C_{80}(CH_2Ph)$.

Theoretical models and calculations on the interaction between SMMs and the surrounding lattice, which results in magnetic relaxation, have also started to emerge very recently.[122,123] The theoretical developments in this regard are still in many ways in their infancy, but understanding the structural effects on the coupling between the phonons of the bulk lattice and the magnetic state of the SMM will most likely provide some new design criteria for high-temperature SMMs in the future.

A key problem in all of molecular magnetism is the need to achieve higher operational temperatures. In the case of SMMs, this means higher blocking temperatures, and in the case of organic magnets, higher ordering temperatures. This all comes down to design of chemical structures, which give rise to the desired properties in a controlled manner. The research effort is approached on three fronts: firstly, there is the synthetic effort of chemists to produce structures suggested by theory; secondly, there is the analytical effort both by chemists and by experimental physicists to observe the magnetic properties in the first place and to get more insight into the electronic structure and magnetic properties of the molecular magnets so that they can be compared with predictions made by theory; and thirdly, there is the theoretical and computational effort of theoreticians in understanding the relationship between the chemical structure and the magnetic properties on a microscopic level and in predicting new structures. The present work contributes to the latter.

1.2 Aim of this study

This dissertation focuses on the theoretical and computational study of molecular magnetic systems. The aim of the present work is threefold:

i) to analyze isotropic exchange interactions in molecular metal–radical and radical–radical systems using state-of-the art computational tools, and to use these results in the design of new organic ferromagnets;

ii) to analyze anisotropic magnetic properties of mono- and polymetallic transition-metal and lanthanide systems using state-of-the-art computational tools to better understand the relationship between the chemical structure of the complexes and their magnetic properties; and

iii) to develop theoretical models for the understanding of novel exchange interaction mechanism encountered in the field of molecular magnetism, which cannot be properly described by any pre-existing model.

This dissertation has been divided into eight chapters. Following this introduction, the next four chapters provide some background on the theoretical and computational tools used in this work. The next three chapters discuss the results of the three main topics of this work: the computational analysis of isotropic exchange interactions and the use of these results to design new molecular systems, the computational analysis of anisotropic magnetic properties, and the theoretical derivation of a new model of spin-dependent delocalization. The last chapter provides conclusions and discusses the outlook of the results.

1.3 Notation and conventions

In addition to the SI units, two systems of units will be used in this work with some notable exceptions. In discussion of quantum chemistry and density functional theory, the Hartree atomic units[124] will be used throughout. In this system of units, the electron mass (m_e), the reduced Planck constant ($\hbar = h/2\pi$), the magnitude of the elementary charge $|e|$, and the Coulomb constant $1/4\pi\epsilon_0$ are all set to unity by definition, and all other units follow from these. Most notably, the speed of light is $c \approx 137$. In relativistic equations, the electron mass may be explicitly written following the convention in the field. When discussing general theory of angular momentum, the convention $\hbar = 1$ will also be applied.

The field of molecular magnetism has (in our opinion rather unfortunately) inherited the use of the cgsemu system of units from the field of magnetochemistry. Since this is the system of units used in practically all literature in the field, we will stick with this choice. The easiest way to understand the cgsemu system is to consider that molar magnetization has the same dimension as the product of Avogadro's constant (N_A) and the Bohr magneton (μ_B): $N_A\mu_B = 5585\,\mathrm{cm^3\,G\,mol^{-1}}$, and to derive other units from this result. In the literature, it is (again unfortunately) rather common that oersted, which is the unit of magnetic field strength, and gauss, which is the unit of magnetic induction, are used interchangeably. Sometimes even tesla, which is the SI unit for magnetic induction, is used with oersteds in the same work. In cgsemu, the value of the permeability of vacuum is $\mu_0 = 1$, which is important to note when converting expressions from cgsemu to other systems of units. When reporting energies, again following convention, we use the wave number $\mathrm{cm^{-1}}$, which is neither part of the Hartree atomic units nor the cgsemu system (nor the SI system, for that

matter). With this choice of units the conversion factor

$$\frac{N_A {\mu_B}^2}{3k_B} = 0.125048612\,\mathrm{cm}^3\,\mathrm{mol}^{-1}, \tag{1}$$

where k_B is the Boltzmann constant, is very useful and can be used to relate energies and other quantities with the SI system. Other common convention in the field is to express energies in kelvin. Both kelvin and cm^{-1} are of the same order of magnitude and are related by the Boltzmann constant: $k_B = 0.69503877\,\mathrm{cm}^{-1}\,\mathrm{K}^{-1}$. In the context of thermochemistry, the SI unit $\mathrm{kJ\,mol}^{-1}$ will be used. More detailed discussion on the cgsemu system in the context of magnetochemistry and molecular magnetism is available, for example, in the books of Mabbs and Machin[23] and of Kahn.[24]

The relevant energy scale in molecular magnetism is set by the thermal energy from liquid helium temperature to ambient conditions, which is roughly $1.4\,\mathrm{cm}^{-1}$ to $210\,\mathrm{cm}^{-1}$. Thus, when referring to interaction as "weak", we are referring to interaction energies of the order $10^{-1}\,\mathrm{cm}^{-1}$ or less. Likewise, when stating that something is "energetically well separated", we are implying that the energy difference is considerably larger than the available thermal energy and thus of the order $10^3\,\mathrm{cm}^{-1}$ or greater.

Following the convention set by Russell *et al*. for quantum numbers, we will use lowercase symbols for quantum numbers of individual particles or quasi-particles and uppercase symbols for quantum numbers associated with some ensemble of particles.[125] In the mathematical notation, we will use regular italic symbols for scalars, bold symbols for vectors, matrices, and tensors, and calligraphic symbols for more general entities, such as vector spaces or operators on vector spaces. The hat symbol will be used for operators acting within vector spaces and the superscript asterisk and the dagger for complex conjugates and Hermitian conjugates, respectively. The tilde symbol will be used for pseudospin, and in the case of pseudospin operators we will not use the hat symbol. In CASSCF and related theories (Chapter 4), specific indices will run over specific one-particle states, but these will be indicated when relevant. In other parts of the text specific symbols used for indices do not carry any special implications.

We will be using notation from several different fields of physics, which unavoidably leads to the use of the same symbol for different quantities. Avoiding this would result in very unconventional notation, and we see overlapping symbols as a smaller problem than deviating from common conventions. The same symbols will, however, be used in very different contexts, making confusion unlikely. In cases where confusion is possible, an explanation will be explicitly stated.

Part I

Theory

2 QUANTUM MECHANICAL DESCRIPTION OF MANY-PARTICLE SYSTEMS

Any analysis of the magnetic properties of molecular systems requires understanding of the electronic structure of the molecules. The computational methods to obtain these properties will be discussed in Chapter 4, but first one must establish how the many-particle states arising from the electronic structure can be represented. In the present work, we will describe non-interacting many-particle states using the common molecular orbital approach, whereas interacting many-particle states will be described using the abstract concept of occupation number vectors and the formalism of second quantization.

2.1 Molecular orbital description of non-interacting many-particle states

Let us consider N electrons, which do not interact with each other but do interact with an external electric potential $V_{\text{ext}}(\mathbf{r})$, which can be, for example, the Coulombic potential of atomic nuclei. Each one-particle state is described by a one-particle function $\varphi_i(\mathbf{r}, m_s)$ known as a spinorbital, where $\mathbf{r}$ is the spatial coordinate and m_s is the projection of the particle spin. The one-particle states exist in an infinite-dimensional one-particle Hilbert space $\mathcal{H}$, and the N-particle system can then be described by a state in an N-particle Hilbert space

$$\mathcal{H}^{\otimes N} = \underbrace{\mathcal{H} \otimes \mathcal{H} \otimes \cdots \otimes \mathcal{H}}_{N}. \tag{2}$$

The simplest N-particle wave function in $\mathcal{H}^{\otimes N}$ would be a simple product $\varphi_1(\mathbf{r}_1 m_{s1})\varphi_2(\mathbf{r}_2 m_{s2}) \cdots \varphi_N(\mathbf{r}_N m_{sN})$ of the one-particle states of the N electrons known as a Hartree product.[124,126,127] The particles in such a state would neither be indistinguishable nor would they have the correct symmetry under permutation of particle indices.[7,10–13] To correctly enforce these properties, one needs to take a linear combination of all the possible permutations of the particle

indices in the Hartree product with the signs of each term determined by the number of particles permuted in each term. Such a structure is known as a Slater determinant:[127–129]

$$\Phi(\{\mathbf{r}_i, m_{si}\}) = \frac{1}{\sqrt{N!}} \begin{vmatrix} \varphi_1(\mathbf{r}_1, m_{s1}) & \varphi_2(\mathbf{r}_1, m_{s1}) & \cdots & \varphi_N(\mathbf{r}_1, m_{s1}) \\ \varphi_1(\mathbf{r}_2, m_{s2}) & \varphi_2(\mathbf{r}_2, m_{s2}) & \cdots & \varphi_N(\mathbf{r}_2, m_{s2}) \\ \vdots & \vdots & \ddots & \vdots \\ \varphi_1(\mathbf{r}_N, m_{sN}) & \varphi_2(\mathbf{r}_N, m_{sN}) & \cdots & \varphi_N(\mathbf{r}_N, m_{sN}) \end{vmatrix}, \quad (3)$$

where $\{\mathbf{r}_i, m_{si}\}$ is the set of spatial and spin coordinates of all electrons and $1/\sqrt{N!}$ is a normalization factor.

$\Phi(\{\mathbf{r}_i, m_{si}\})$ is an exact solution to the Schrödinger equation for a system of non-interacting fermions in some external electric potential $V_{\text{ext}}(\mathbf{r})$. A Slater determinant describes a single electronic configuration where each spinorbital in the determinant is occupied by exactly one electron. The spinorbitals can be separated into a spatial orbital (or simply a molecular orbital, MO) $\phi_i(\mathbf{r})$ and a spin function $\sigma(m_s)$:

$$\varphi_i(\mathbf{r}, m_s) = \phi_{i\sigma}(\mathbf{r})\sigma(m_s). \quad (4)$$

There exist two orthonormal spin functions $\sigma(m_s) \in \alpha(m_s), \beta(m_s)$, and they have the following properties:

$$\alpha(-1/2) = 0, \quad \alpha(1/2) = 1, \quad \beta(-1/2) = 1, \quad \text{and} \quad \beta(1/2) = 0. \quad (5)$$

The spin index σ in $\phi_{i\sigma}(\mathbf{r})$ can be replaced by adding a bar over the orbital symbol for β orbitals: $\phi_{i\alpha}(\mathbf{r}) \equiv \phi_i(\mathbf{r})$ and $\phi_{i\beta}(\mathbf{r}) \equiv \bar{\phi}_i(\mathbf{r})$. A rather common situation in electronic structure theory is the so-called restricted case where an α and a β electron share the same spatial function: $\phi_i(\mathbf{r}) = \bar{\phi}_i(\mathbf{r})$ and the spin index or bar notation can be dropped altogether. In this case, i indexes unique spatial orbitals and not individual particles. The opposite (more general) case when $\phi_i(\mathbf{r}) \neq \bar{\phi}_i(\mathbf{r})$ is called the unrestricted case. A rarer situation is the so-called restricted open-shell case where some orbitals are doubly occupied and share the same spatial orbital and a few valence orbitals are singly occupied and differ in the spatial part.

2.2 Fock-space description of many-particle states and second quantization

2.2.1 States and operators in the Fock space

The molecular orbital description of many-particle states introduced in section 2.1 is very useful for the description of non-interacting many-particle systems, and it can be extended to interacting systems as well. The interacting situation, however, is perhaps easiest to treat using the formalism of second quantization[130–135] where the many particle system is represented by a superposition of occupation

number (ON) vectors. The ON vectors used in second quantization are in many ways similar to the Slater determinants used in wave function approaches. It is therefore very common in the literature to use the terms ON vector and Slater determinant interchangeably; we will, however, always speak of ON vectors in the context of second quantization. The state vectors describing the system are entities in the Fock space $\mathcal{F}$.[131] The Fock space is a direct sum over all antisymmetrized M-particle Hilbert spaces $\mathcal{H}^{\otimes M}$ where M ranges from zero to infinity. Such a construct can be formally expressed as

$$\mathcal{F} = \bigoplus_{M=0}^{\infty} \mathcal{S}_- \mathcal{H}^{\otimes M} = \mathbb{C} \oplus \mathcal{H} \oplus \mathcal{S}_-(\mathcal{H} \otimes \mathcal{H}) \oplus \mathcal{S}_-(\mathcal{H} \otimes \mathcal{H} \otimes \mathcal{H}) \oplus \cdots, \quad (6)$$

where $\mathbb{C}$ is the set of complex numbers and $\mathcal{S}_-$ is an antisymmetrizising operator. A state vector in an antisymmetrized M-particle Hilbert space is given as $|n_1, n_2, \cdots\rangle$ where n_1 is the number of particles occupying one-particle state 1, n_2 is the number of particles occupying the one-particle state 2, *etc.*, and $\sum n_i = M$. The allowed ONs are 0 or 1 since two or more fermions may not occupy the same state due to the Pauli principle.[136,137] Like in section 2.1, the one-particle states are represented in the Cartesian space by a spinorbital $\varphi_i(\mathbf{r}, m_s)$. The antisymmetrizing operator $\mathcal{S}_-$ ensures the correct permutation symmetry of the electrons:

$$|\cdots n_i \cdots n_j \cdots\rangle = -|\cdots n_j \cdots n_j \cdots\rangle. \quad (7)$$

The Fock space can also be constructed for an ensemble of bosons in which case a symmetrizing operator is used instead. Such a system is, however, of no interest to us here.

A general state in the Fock space is given by a linear combination of ON vectors:

$$|\psi\rangle = \sum_{\mathbf{k}} C_{\mathbf{k}} |n_1^{\mathbf{k}}, n_2^{\mathbf{k}}, \cdots\rangle \equiv \sum_{\mathbf{k}} C_{\mathbf{k}} |\mathbf{k}\rangle, \quad (8)$$

where the expansion coefficients $C_{\mathbf{k}}$ are called configuration interaction (CI) coefficients and where we have simplified the notation so that the vector $\mathbf{k}$ corresponds to a specific set of the ONs: $\mathbf{k} = \{n_1^{\mathbf{k}}, n_2^{\mathbf{k}}, \cdots\}$. Different $|\mathbf{k}\rangle$ in the same expansion may have different numbers of particles but in chemistry we are only interested in operators which conserve the particle number.

The states in the Fock space are operated by creations and annihilation operators $\hat{a}_P^\dagger$ and $\hat{a}_P$, respectively. Like their name suggests, the operators add or remove particles from the states and therefore couple subspaces of the Fock space with different total particle numbers. As is evident from the notation they are Hermitian conjugates of each other. The effect of the operators on state vectors is defined as

$$\hat{a}_P^\dagger |\cdots, n_P, \cdots\rangle = \delta_{n_P,1} (-1)^{\sum_{Q<P} n_Q} |\cdots, n_P + 1, \cdots\rangle \quad (9)$$

$$\hat{a}_P |\cdots, n_P, \cdots\rangle = \delta_{n_P,0} (-1)^{\sum_{Q<P} n_Q} |\cdots, n_P - 1, \cdots\rangle, \quad (10)$$

where the phase factor $(-1)^{\sum_{Q<P} n_Q}$ ensures that the correct permutational symmetry is conserved. The phase factor can be read as even if the number of

occupied particle states "left" to the state being operated on is even and odd in the opposite case. Any ON vector in the Fock space can be constructed by sequential application of creation operators to the vacuum state $|\text{vac}\rangle = |0, 0, \cdots, 0\rangle$. The vacuum state should not be confused with a zero vector. The fermionic creation and annihilation operators have the following anticommutation relations

$$[\hat{a}_P, \hat{a}_Q]_+ = 0, \quad [\hat{a}_P^\dagger, \hat{a}_Q^\dagger]_+ = 0, \quad \text{and} \quad [\hat{a}_P, \hat{a}_Q^\dagger]_+ = \delta_{PQ} \tag{11}$$

and all other properties follow from them.[133,134] The consecutive operation on the same one-particle state by an annihilation and a creation operator returns the occupation number of that state. This operator $\hat{n}_p = \hat{a}_p^\dagger a_p$ is called the occupation number operator and the action on an ON vector is

$$\hat{n}_p |\cdots, n_p, \cdots\rangle = n_p |\cdots, n_p, \cdots\rangle. \tag{12}$$

The total particle number operator $\hat{N}$ is defined as the sum of occupation number operators: $\hat{N} = \sum_p \hat{n}_p$.

The upper case indices P and Q labeling the one-particle states contain all information on the spatial and spin properties of the one-particle state. It is often more practical to consider a less general coordinate by setting $P \to p, \sigma$, where p is the spatial index of the one-particle state and $\sigma \in \alpha, \beta$ is a spin index. This is very much analogous to the concept of spinorbital and spatial orbital introduced in section 2.1. Thus, for each one-particle state p there exists an α state and a β state. The creation and annihilation operators act on both the spin and spatial parts of the one-particle states and therefore the substitution $P \to p, \sigma$ leads to two indices on the creation and annihilation operators $\hat{a}_P \to \hat{a}_{p\sigma}$.

If the one-particle states are represented by restricted orbitals, lot of the following notation will be simplified by introducing the spin-free one- and two-particle excitation (or replacement) operators

$$\begin{aligned} \hat{E}_{pq} &= \hat{E}_{pq}^\alpha + \hat{E}_{pq}^\beta = \hat{a}_{p\alpha}^\dagger \hat{a}_{q\alpha} + \hat{a}_{p\beta}^\dagger \hat{a}_{q\beta} = \sum_\sigma \hat{a}_{p\sigma}^\dagger \hat{a}_{q\sigma} \\ \hat{E}_{pq,rs} &= \hat{E}_{pq}\hat{E}_{rs} - \delta_{qr}\hat{E}_{ps} = \sum_{\sigma,\tau} \hat{a}_{p\sigma}^\dagger \hat{a}_{r\tau}^\dagger \hat{a}_{s\tau} \hat{a}_{q\sigma} \end{aligned} \tag{13}$$

Both $\hat{E}_{pq}$ and $\hat{E}_{pq,rs}$ create and annihilate the same amount of α and β electrons and therefore they do not alter the total particle number or the total spin projection M_S of the system. The spin-free one-particle excitation operator $\hat{E}_{pq}$ can be considered as a singlet excitation operator (up to a scaling factor of $\sqrt{2}$) which are irreducible tensor operators of rank zero.[133,138] Therefore, $\hat{E}_{pq}$ does not add or remove any spin or orbital angular momentum from the state it operates on. Since the two-particle spin-free excitation operator $\hat{E}_{pq,rs}$ is constructed from the one-particle operators, it also conserves the angular momenta of the state it operates on. Irreducible tensor operators will be discussed in more detail in section 3.2.3.

2.2.2 Expectation values and reduced density matrices

Spin-free one- and two-particle operators, $\hat{h}$ and $\hat{g}$, can be constructed from the spin-free excitation operators as

$$\hat{h} = \sum_{p,q} h_{pq} \hat{E}_{pq} \quad \text{and} \quad \hat{g} = \frac{1}{2} \sum_{p,q,r,s} g_{pqrs} \hat{E}_{pq,rs}, \tag{14}$$

where h_{pq} and g_{pqrs} are the so-called one- and two-electron integrals over the spatial representation of the one-particle states $\phi_p(\mathbf{r})$:

$$h_{pq} = \int \phi_p^*(\mathbf{r}) \hat{h}_C(\mathbf{r}) \phi_q^*(\mathbf{r}) \mathrm{d}\mathbf{r} \tag{15}$$

$$g_{pqrs} = \iint \phi_p^*(\mathbf{r}_1) \phi_r^*(\mathbf{r}_2) \hat{g}_C(\mathbf{r}_1, \mathbf{r}_2) \phi_q(\mathbf{r}_1) \phi_s(\mathbf{r}_2) \mathrm{d}\mathbf{r}_1 \mathrm{d}\mathbf{r}_2 \tag{16}$$

$\hat{h}_C(\mathbf{r})$ and $\hat{g}_C(\mathbf{r}_1, \mathbf{r}_2)$ are spatial representations of the operators (i. e. operators in the wave function representation). The two-particle operator we are mostly interested in is the Coulomb operator. Its integrals are usually referred to simply as two-electron integrals and have special notation:

$$\iint \phi_p^*(\mathbf{r}_1) \phi_r^*(\mathbf{r}_2) \frac{1}{|\mathbf{r}_1 - \mathbf{r}_2|} \phi_q(\mathbf{r}_1) \phi_s(\mathbf{r}_2) \mathrm{d}\mathbf{r}_1 \mathrm{d}\mathbf{r}_2 \equiv (pq|rs). \tag{17}$$

It is important to take note of the order of the indices. The respective matrix elements over states of the type (8) are given as

$$\langle \psi | \hat{h} | \psi' \rangle = \sum_{p,q} h_{pq} \langle \psi | \hat{E}_{pq} | \psi' \rangle = \sum_{p,q} h_{pq} \gamma_{pq} \tag{18}$$

$$\langle \psi | \hat{g} | \psi' \rangle = \sum_{p,q,r,s} g_{pqrs} \langle \psi | \hat{E}_{pq,rs} | \psi' \rangle = \sum_{p,q,r,s} g_{pqrs} \Gamma_{pqrs}, \tag{19}$$

where $\gamma_{pq} = \langle \psi | \hat{E}_{pq} | \psi' \rangle$ and $\Gamma_{pqrs} = \langle \psi | \hat{E}_{pq,rs} | \psi' \rangle$ are the one- and two-particle reduced density matrices, respectively.[133,134] Reduced density matrices play a key role in quantum chemistry and all relevant physics can be formulated through them.[139–143] The reduced density matrices will be discussed in the context of the electron density in the Cartesian space in section 2.3. In the literature on quantum chemistry, the one-particle reduced density matrix is often referred to simply as the density matrix. It is also common to drop the term 'reduced' and simply speak of one- and two-particle density matrices or even just one- and two-matrices. We will follow this convention in the present work. It should be noted that all dependence on the spatial aspects in the expectation values (18) and (19) is confined to the integrals h_{pq} and g_{pqrs} and all dependence on the CI coefficients is contained in the density matrices.

The one- and two-particle density matrices are the matrix representations of the one- and two-particle density operators $\hat{\gamma} = \sum_{p,q} E_{pq}$ and $\hat{\Gamma} = \sum_{p,q,r,s} E_{pq,rs}$. The one-particle density operator can be split into one-particle spin density operators

$$\hat{\gamma} = \hat{\gamma}^\alpha + \hat{\gamma}^\beta = \sum_{p,q} \left(\hat{E}_{pq}^\alpha + \hat{E}_{pq}^\beta \right). \tag{20}$$

2.2.3 Spin properties of states in the Fock space

It is well-known that the non-relativistic Hamiltonian in the absence of external magnetic fields commutes with the total spin operator $\hat{S}^2$ and the spin-projection operator $\hat{S}_z$.[144,145] This results from the fact that the Hamiltonian is an irreducible tensor operator of rank zero (i. e. a singlet operator, see section 3.2.3).[133] Therefore it is always possible to choose the eigenstates of the Hamiltonian in such a way that they are also eigenstates of $\hat{S}^2$ and $\hat{S}_z$. It should be noted that this is strictly the case only for *exact* eigenstates of the Hamiltonian and not necessarily for approximate eigenstates we encounter in practical calculations. It is nonetheless useful in most cases to enforce the correct spin symmetry on the optimized state. One main advantage of this is that the size of the variational space can be reduced significantly. A rather notable exception to this is the broken symmetry Hartree–Fock and DFT methods discussed in chapter 5 where the spin symmetry is deliberately broken to offer *more* variational flexibility.

A given ON vector $|\mathbf{k}\rangle$ has a well-defined number of α and β electrons and is therefore an eigenstate of the particle number operator $\hat{N}_\sigma$ which returns the number of particles of given spin when operating on $|\mathbf{k}\rangle$:

$$\hat{N}_\sigma|\mathbf{k}\rangle = \sum_p \hat{a}^\dagger_{p\sigma}\hat{a}_{p\sigma}|\mathbf{k}\rangle = \sum_p n_{p\sigma}|\mathbf{k}\rangle = N_\sigma|\mathbf{k}\rangle, \tag{21}$$

where N_σ is the number of electrons with spin σ. The $\hat{S}_z$ commutes with $\hat{N}_\sigma$[133] and since there are no degeneracies in the eigenvalue of $\hat{N}_\sigma$, $|\mathbf{k}\rangle$ is an eigenstate of $\hat{S}_z$. However, $\hat{S}^2$ does not commute with $\hat{N}_\sigma$ and therefore $|\mathbf{k}\rangle$ is in general not an eigenstate of $\hat{S}^2$. A very common exception to this is the case when $|\mathbf{k}\rangle$ contains only closed shell orbitals.[133] However, it turns out that in the case of restricted orbitals it is always possible to construct some spin-adapted basis where all states are eigenstates of $\hat{S}^2$ by taking finite linear combinations in $\{|\mathbf{k}\rangle\}$. These eigenstates are called configuration state functions (CSFs). Each ON vector in a CSF has the same spatial occupations and only differs in the spin indices. All of the ON vectors in this set, $\{|\mathbf{m}\rangle\}$, have the same total spin projection M_S. The CSF $|\Phi_{S,M_S}\rangle$ with spin S and projection M_S can then be expanded as

$$|\Phi_{S,M_S}\rangle = \sum_{\mathbf{m}} B_{\mathbf{m}}|\mathbf{m}\rangle. \tag{22}$$

There are multiple ways of constructing CSFs from a restricted ON vector basis. The most popular methods today are based on the graphical unitary group approach (GUGA) initially formulated by Paldus[146] and Shavitt.[147,148] The details of this procedure are deeply rooted in group and graph theories and will not be discussed here. An excellent and highly detailed description of the construction of CSFs is given in the book of Pauncz.[149]

When considering practical aspects, the use of CSFs usually leads to shorter CI expansions but the use of ON vectors leads to simpler expressions for expectation values and therefore either choice as a basis requires some compromise. For a long time, the CSF basis was preferred over the ON vector basis but more

recent work using modern computers is starting to question this choice.[150] Most of the theory presented in this work is general enough that it can be applied both to ON vector and to CSF bases. When CSFs are required in a given expression, this is indicated by explicitly labeling the states with the spin quantum numbers.

2.3 The electron density

The electron density $\rho(\mathbf{r})$ gives the probability of finding an electron at $\mathbf{r}$ when the position of all other electron is arbitrary.[151] Likewise, the spin densities $\rho^\alpha(\mathbf{r})$ and $\rho^\beta(\mathbf{r})$ give the probabilities of finding an electron with an α or a β spin at $\mathbf{r}$. All three densities are functions in the Cartesian space and can, in principle, be determined experimentally. They therefore contribute a very important link between the electronic structure theory and experimental reality. They also form the basis for density functional methods discussed in chapter 5. The electron density is related to the wave function by

$$\rho(\mathbf{r}) = \int \psi^*(\mathbf{r}_1, m_{s1}, \mathbf{r}_2, m_{s2}, \cdots)\psi(\mathbf{r}_1, m_{s1}, \mathbf{r}_2, m_{s2}, \cdots)\mathrm{d}m_{s1}\mathrm{d}\mathbf{r}_2\mathrm{d}m_{s2}\cdots, \qquad (23)$$

where the integration over the values of m_s in practice means summation as m_s can only have two values. The integrand in (23) is the conditional probability density of the N-particle system which gives the probability of finding an electron with spin m_{s1} infitesimally close to $\mathbf{r}_1$, electron with spin m_{s2} infitesimally close to $\mathbf{r}_2$, etc. The electron density is then obtained from this distribution by integrating out all the degrees of freedom associated with all particles except one. The spin-densities are obtained by integrating out the degrees of freedom associated with the opposite spin as well. It should be noted that the electron density integrates to the number of particles, not to unity.

The relationship with the density in the formulation so far has been made through the abstract representation of the density operators in the Fock space. In second quantization the connection with the electron density in the Cartesian space can be made through the so-called electron field operators:[130,132,135]

$$\hat{\psi}_\sigma(\mathbf{r}) = \sum_p \phi_{p\sigma}(\mathbf{r})\hat{a}_{p\sigma} \quad \text{and} \quad \hat{\psi}^\dagger_\sigma(\mathbf{r}) = \sum_p \phi^*_{p\sigma}(\mathbf{r})\hat{a}^\dagger_{p\sigma}. \qquad (24)$$

The action of the field operators on the Cartesian space can be considered as creating or annihilating an electron with spin σ at $\mathbf{r}$. The spatial representation of $\hat{\gamma}^\alpha$ and $\hat{\gamma}^\beta$ is obtained by the substitution $\hat{a}_{p\sigma} \to \hat{\psi}_{p\sigma}(\mathbf{r})$:

$$\hat{\gamma}^\sigma \to \hat{\gamma}^\sigma(\mathbf{r};\mathbf{r}') = \sum_{p,q} \phi^*_{p\sigma}(\mathbf{r}')\phi_{q\sigma}(\mathbf{r})\hat{E}^\sigma_{pq} \qquad (25)$$

The respective matrix elements are the one-particle spin density matrices in the spatial representation:

$$\gamma^\sigma(\mathbf{r};\mathbf{r}') = \sum_{p,q} \phi^*_{p\sigma}(\mathbf{r}')\phi_{q\sigma}(\mathbf{r})\gamma^\sigma_{pq}, \qquad (26)$$

where $\gamma^{\sigma}_{pq} = \langle\psi|\hat{E}^{\sigma}_{pq}|\psi'\rangle$. The one-particle density matrix is simply the sum of the spin density matrices

$$\gamma(\mathbf{r};\mathbf{r}') = \gamma^{\alpha}(\mathbf{r};\mathbf{r}') + \gamma^{\beta}(\mathbf{r};\mathbf{r}'). \tag{27}$$

The density matrix is the kernel of the density operator in the wave function representation.[143,151] The name 'density matrix' is somewhat misleading here as $\gamma(\mathbf{r};\mathbf{r}')$ is clearly a function. McWeeney has noted that the term "density kernel" would be a better choice.[143] The electron density and spin densities are given by the "diagonal" values of the density matrices:

$$\rho(\mathbf{r}) = \gamma(\mathbf{r};\mathbf{r}), \quad \rho^{\alpha}(\mathbf{r}) = \gamma^{\alpha}(\mathbf{r};\mathbf{r}), \quad \text{and} \quad \rho^{\beta}(\mathbf{r}) = \gamma^{\beta}(\mathbf{r};\mathbf{r}). \tag{28}$$

The one-particle density matrix can be brought to a diagonal form by a proper unitary rotation of the MOs, giving

$$\gamma(\mathbf{r};\mathbf{r}') = \sum_{p} \omega_p \eta_p^*(\mathbf{r}')\eta_p(\mathbf{r}), \tag{29}$$

where the eigenfunctions $\eta_p(\mathbf{r})$ are called the natural orbitals (NOs) and the eigenvalues ω_p are known as the natural orbital occupation numbers (NOONs).[139,140] NOONs have a very important physical interpretation as they give the probability amplitudes for finding a particle in the respective one-particle state in the N-particle ensemble. The two-particle density matrix can also be diagonalized to yield functions known as the natural geminals. The corresponding eigenvalues give the probability amplitudes for finding two particles in a specific two-particle state.

3 QUANTUM THEORY OF MOLECULAR MAGNETISM

The main overall goal in the field of molecular magnetism is to tailor the macroscopic magnetic properties of a molecular material by chemical design and modification of the constituent molecules. It is, therefore, of critical importance to understand the relationship between the electronic structure of the molecules and the microscopic magnetic properties, and how these give rise to various macroscopic phenomena. The magnetic properties are most often discussed in terms of spin or pseudospin Hamiltonians, which act in reduced Hilbert spaces and reproduce the lowest-lying energy levels of the system.[20,97] In the (pseudo)spin description, the complicated electronic structure is compressed into a small set of scalar, vector, and tensor parameters, which have some physical interpretation. The Hamiltonian parameters can be calculated from first principles and, to an extent, extracted from experiment. In the words of Griffith, (pseudo)spin Hamiltonians provide "a convenient resting place during the long trek from fundamental theory to [the results of experiments]."[152]

Thus, the quantum theory of molecular magnetism consists of three layers: the macroscopic magnetic properties observed experimentally, the microscopic magnetic properties arising from the quantum realm of the electronic structure, and the (pseudo)spin description of the electronic structure used to reduce the complexity of the problem and to provide a "language" to discuss the properties therein. The connection between the macroscopic and microscopic properties is achieved through statistical mechanics, whereas the formal connection between the microscopic magnetic properties and (pseudo)spin Hamiltonians is achieved through the theory of effective Hamiltonians.[97,153–155] In the present chapter, we will introduce the relevant theoretical foundations of these three layers and briefly discuss dynamics of the magnetic properties and the experimental methods used to determine them.

3.1 Macroscopic magnetic properties

Two main properties of bulk materials that are used to probe their magnetic properties are magnetization (**M**) and the magnetic susceptibility (χ).[24–26,156] Magnetization is a vector, and the magnetic susceptibility is a second rank tensor. In practical experiments on powdered samples, however, only the isotropic spherical averages will be observed, which are noted by the scalars M and χ. We will focus here on molar magnetization and molar magnetic susceptibility, which give the quantities in terms of one mole of material. We will drop the term 'molar' in further discussion but will bear in mind that we are always discussing molar quantities unless stated otherwise.

Both **M** and χ describe the materials response to some external homogeneous magnetic field **B**. The term "magnetic field" is used rather ubiquitously in the field of molecular magnetism to describe both magnetic field strength (**H**) and magnetic induction (**B**). This stems from the fact that in vacuum, the two are related by $\mathbf{B} = \mu_0\mathbf{H}$ and in the cgsemu system $\mu_0 = 1$. Therefore, for all practical intents and purposes, **B** and **H** are often considered equivalent and are sometimes used interchangeably in the literature. This is no longer the case in the SI system nor is this the case inside materials where the material itself produces a demagnetizing field as a response to the external field. We will ignore this complication and simply bear in mind that this needs to be accounted for when considering experimentally measured values. A more detailed account of these considerations is given, for example, in the book of Gatteschi *et al*.[25]

Each energy eigenstate of a quantum mechanical system with energies $E_1, E_2, \cdots$, has a microscopic magnetization

$$\boldsymbol{\mu}_i = -\frac{\partial E_i(\mathbf{B})}{\partial \mathbf{B}}, \tag{30}$$

which describes the response of the state to the magnetic field. The magnetization **M** can then be obtained by summing the Boltzmann-weighted microscopic magnetization of each state in the ensemble as

$$\mathbf{M} = N_A \frac{\sum_i \boldsymbol{\mu}_i \exp\left(-\frac{E_i(\mathbf{B})}{k_B T}\right)}{\sum_i \exp\left(-\frac{E_i(\mathbf{B})}{k_B T}\right)}, \tag{31}$$

which can be written in a more compact form as

$$\mathbf{M} = N_A k_B T \frac{\partial \log Z(T, \mathbf{B})}{\partial \mathbf{B}}, \tag{32}$$

where log is the natural logarithm and

$$Z(T, \mathbf{B}) = \sum_i \exp\left(-\frac{E_i(\mathbf{B})}{k_B T}\right) \tag{33}$$

is the partition function. Magnetization is a vector quantity describing "how magnetic a material is" and its given in units equivalent to Bohr magneton per unit mole. The scalar magnetization is given by averaging **M** over all rotational angles.

Components of the magnetic susceptibility tensor are given as

$$\chi_{\alpha\beta} = N_A k_B T \frac{\partial^2 \log Z(T, \mathbf{H})}{\partial B_\alpha \partial B_\beta}, \tag{34}$$

where $\alpha, \beta \in x, y, z$ and the spherically averaged scalar susceptibility is then obtained from the trace as:

$$\chi = \frac{\chi_{xx} + \chi_{yy} + \chi_{zz}}{3}. \tag{35}$$

It is common to assume that the magnetic field is weak so that $M = \chi B$, where B is the field strength.

3.2 Microscopic theory of angular momentum

3.2.1 Angular momentum and rotations

The total angular momentum **J** of a many-particle system is described by the total angular momentum quantum number J and the angular momentum projection quantum number M_J, which describes the projection of **J** on the quantization axis. Common convention is that the quantization axis is chosen as the z axis of the coordinate system. M_J can have $2J + 1$ values $-J, -J + 1, \cdots, J$ and is the eigenvalue of the operator $\hat{J}_z$, which describes the z component of the angular momentum. The other two Cartesian components can be defined in terms of the so-called lowering and raising operators $\hat{J}_+$ and $\hat{J}_-$ as

$$\hat{J}_x = \frac{1}{2}\left(\hat{J}_+ + \hat{J}_-\right) \quad \text{and} \quad \hat{J}_y = -\frac{i}{2}\left(\hat{J}_+ - \hat{J}_-\right). \tag{36}$$

The operators for the Cartesian components of the total angular momentum of a many-particle system can be expressed as sums of the one-particle operators $\hat{j}_\alpha$ ($\alpha \in x, y, z$) acting on individual particles: $\hat{J}_\alpha = \sum_i \hat{j}_{i\alpha}$. The action of $\hat{J}_z$, $\hat{J}_\pm$, and the squared total angular momentum operator $\hat{\mathbf{J}}^2$ on a general angular momentum state $|JM_J\rangle$ is given as

$$\hat{J}_z|JM_J\rangle = M_J|JM_J\rangle, \tag{37}$$

$$\hat{J}_\pm|JM_J\rangle = \sqrt{J(J+1) - M_J(M_J \pm 1)}|JM_J \pm 1\rangle, \text{ and} \tag{38}$$

$$\hat{\mathbf{J}}^2|JM_J\rangle = J(J+1)|JM_J\rangle. \tag{39}$$

Thus, $|JM_J\rangle$ is an eigenstate of $\hat{\mathbf{J}}^2$ and $\hat{J}_z$ but not of $\hat{J}_\pm$. In general, all the operators for the Cartesian components commute with $\hat{\mathbf{J}}^2$, but not with each other. The

commutators of the Cartesian operators are

$$[\hat{J}_x, \hat{J}_y] = i\hat{J}_z, \quad [\hat{J}_y, \hat{J}_z] = i\hat{J}_x, \quad \text{and} \quad [\hat{J}_z, \hat{J}_x] = i\hat{J}_y, \tag{40}$$

and the lowering and raising operators follow

$$[\hat{\mathbf{J}}^2, \hat{J}_\pm] = 0, \quad [\hat{J}_z, \hat{J}_\pm] = \pm\hat{J}_\pm, \quad \text{and} \quad [\hat{J}_+, \hat{J}_-] = 2\hat{J}_z. \tag{41}$$

The Cartesian operators $\hat{J}_x$, $\hat{J}_y$, and $\hat{J}_z$ can be interpreted as the generators of finite rotations of the system.[157] A rotation $\hat{R}(\alpha, \beta, \gamma)$ over the Euler angles α, β, and γ is given as

$$\hat{R}(\alpha, \beta, \gamma) = \exp\left(i\gamma\hat{J}_z\right) \exp\left(i\beta\hat{J}_y\right) \exp\left(i\alpha\hat{J}_z\right). \tag{42}$$

Matrix elements of $\hat{R}(\alpha, \beta, \gamma)$ are given by the Wigner matrices[157,158]

$$\mathcal{D}^{(J)}_{M_J, M'_J}(\alpha, \beta, \gamma) = \langle JM_J|\hat{R}(\alpha, \beta, \gamma)|JM'_J\rangle, \tag{43}$$

which have tabulated values.[159] The set of states $\{|JM_J\rangle\}$ defined by one value of J and all allowed values of M_J forms an irreducible representation of the rotation group.[157,158] Therefore, no rotation can take a state $|JM_J\rangle$ to state $|J'M'_J\rangle$, where $J \neq J'$. Interpretation of the angular momentum operators as generators of rotations also explains why the Cartesian operators do not commute; for example, a rotation around x axis means that rotation around y axis is no longer the same rotation if the rotation around x axis was not carried out.

The equations given so far are perfectly general to any type angular momentum. In molecular magnetism, one encounters three types of angular momenta, the spin $\mathbf{S}$ described by the quantum numbers S and M_S, the orbital angular momentum $\mathbf{L}$ described by L and M_L, and the total angular momentum $\mathbf{J} = \mathbf{L} + \mathbf{S}$ described by the quantum numbers J and M_J. The operators and commutation relations associated with these angular momenta can be obtained by simply replacing J and M_J with the respective quantum numbers. In spherically symmetric systems (such as an atom or an ion), all six are good quantum numbers if SOC is neglected. Under SOC, the spin and orbital angular momentum eigenstates become mixed and only J and M_J remain good quantum numbers. When the symmetry is lowered from spherical to the finite point groups of molecular systems, none of the above remain good quantum numbers. An exception to this is linear molecules, which conserve the angular momentum projection and where the M_L, M_S (in the absence of SOC), and M_J remain good quantum numbers. If SOC is neglected and no external magnetic field is present, then S and M_S are good quantum numbers also in molecular systems as the spin is not coupled to the external potential in any way, and the correct rotational symmetry of the spin is conserved. This is approximately the case for light elements in low symmetries.

The angular momentum is not strictly conserved in practically any of the systems of interest to us in molecular magnetism. The quantum numbers are, however, still a useful starting point when characterizing distinct manifolds of states and form the foundation for the construction of spin and pseudospin Hamiltonians as explained in section 3.3.

3.2.2 Coupling of angular momenta

The addition of different angular momenta arises in several contexts in molecular magnetism: in the coupling of one-particle angular momenta to yield the many-particle momentum, in SOC, and in the coupling of different magnetic sites in a polymetallic system. Let us consider two sets of angular momentum states $\{|j_1 m_{j1}\rangle\}$ and $\{|j_2 m_{j2}\rangle\}$ for some fixed values of j_1 and j_2. The two sets span Hilbert spaces $\mathcal{H}_1$ and $\mathcal{H}_2$ with dimensions $2j_1+1$ and $2j_2+1$, respectively. A coupled state $|JM_J\rangle$ in a $(2j_1+1)(2j_2+1)$-dimensional direct product space $\mathcal{H}_1 \otimes \mathcal{H}_2$ can then be formed so that $\mathbf{J} = \mathbf{j}_1 + \mathbf{j}_2$. The state $|JM_J\rangle$ can be expanded as

$$|JM_J\rangle = \sum_{m_{j1}, m_{j2}} C^{JM_J}_{j_1 m_{j1}, j_2 m_{j2}} |j_1 m_{j1}\rangle \otimes |j_2 m_{j2}\rangle, \tag{44}$$

where

$$C^{JM_J}_{j_1 m_{j1}, j_2 m_{j_2}} = \left(\langle j_1 m_{j1}| \otimes \langle j_2 m_{j2}|\right) |JM_J\rangle \tag{45}$$

is a Clebsch–Gordan (CG) coefficient.[144,157,159,160] A general expression for the coefficients is available but it is so complicated that usually pre-tabulated or computer-generated values are used.[159] The CG coefficients are real, but one should play close attention to the phase convention used in a specific table of values as this can vary. Further angular momentum can be coupled to $|JM_J\rangle$ in a similar manner. It should be noted that in expansion (44) quantum numbers J, M_J, j_1 and j_2 are conserved; therefore, the coupled state $|JM_J\rangle$ should be more generally labeled as $|j_1 j_2 JM_J\rangle$. The basis set $\{|j_1 m_{j1}\rangle \otimes |j_2 m_{j2}\rangle\}$ is called the uncoupled basis, and the expansion (44) constitutes a transformation between the coupled and uncoupled bases.

Probably the most concrete example of angular momentum coupling in molecular magnetism is represented by SOC. In this case, the coupled basis is given by the total angular momentum states $\{|JM_J\rangle\}$ and the uncoupled basis by the direct product of orbital angular momentum and spin states $\{|LM_L\rangle \otimes |SM_S\rangle\}$. In the case of weak or vanishing SOC, the uncoupled basis forms a better representation of the electronic states, whereas at the limit of strong SOC, the coupled basis is the more natural representation. A special case of the coupled basis is the so-called Russell–Saunders or LS coupling scheme, where the $|JM_J\rangle$ state is formed from a set of uncoupled states with one specific value of L and one specific value of S.[48,161] These states are called multiplets and are labeled as $|LSJM_J\rangle$ or, following the standard spectroscopic notation,[48] as ${}^{2S+1}L_J$. In the same notation, the uncoupled states are called terms and are labeled as ${}^{2S+1}L$. Due to historical reasons, the orbital angular momentum L is labeled using a letter $S, P, D, F, G, H, I, K, L, \cdots$ standing for $0, 1, 2, 3, 4, 5, 6, 7, 8, \cdots$.

3.2.3 Irreducible tensor operators

Irreducible tensor operators (ITOs) are entities very closely related to angular momentum. A general ITO $\hat{\mathbf{T}}_k$ of rank k is a collection of $2k+1$ operators $\hat{T}_{kq}$, where

$q = -k, -k+1, \cdots, k$ labels the components of the operator.[144,157,159,162,163] The set of operators $\{\hat{T}_{kq}\}$ for a fixed value of the rank k (i. e., the operators in the set defined by $\hat{\mathbf{T}}_k$) form a basis for an irreducible representation of the rotation group and transform under rotations as

$$\hat{R}^{\dagger}(\alpha,\beta,\gamma)\hat{T}_{kq}\hat{R}(\alpha,\beta,\gamma) = \sum_{q'=-k}^{k} \hat{T}_{kq}\mathcal{D}^{(k)}_{q',q}(\alpha,\beta,\gamma). \tag{46}$$

ITOs have the following commutation relations with the primitive angular momentum operators $\hat{J}_z$ and $\hat{J}_{\pm}$:[162]

$$[\hat{J}_z, \hat{T}_{kq}] = q\hat{T}_{kq} \quad \text{and} \quad [\hat{J}_{\pm}, \hat{T}_{kq}] = \sqrt{(k \mp q)(k \pm q + 1)}\hat{T}_{kq\pm 1}. \tag{47}$$

Since the Cartesian components of a vector transform into each other under rotation and form a complete set, or in other words, they form a basis for an irreducible representation of the rotation group, any Cartesian vector operator can be represented as an ITO of rank 1. More specifically, a vector operator $\hat{\mathbf{v}}$ can be written in terms of spherical components $\hat{v}_{-1}$, $\hat{v}_0$, and $\hat{v}_{+1}$, which can be related to the Cartesian components as

$$\hat{v}_0 = \hat{v}_z \quad \text{and} \quad \hat{v}_{\pm 1} = \mp\frac{\hat{v}_x \pm i\hat{v}_y}{\sqrt{2}}. \tag{48}$$

The action of an ITO component $\hat{T}_{kq}$ on an angular momentum state can be considered as adding angular momentum k with projection q to the angular momentum state. Therefore, an ITO with rank zero conserves the angular momentum of the state and does not couple states with different angular momenta. Rank one ITOs couple states that differ by one quanta of angular momentum and so on.

The main advantage of using ITOs comes from the Wigner–Eckart theorem[158,164] which states that the matrix elements of ITO components $\hat{T}_{kq}$ in a basis of angular momentum eigenstates $\{|JM_J\rangle, |J'M'_J\rangle\}$ can be expressed as a product of a CG coefficient and a reduced matrix element that is independent of the values of M_J, M'_J, and q:

$$\langle JM_J|\hat{T}_{kq}|J'M'_J\rangle = C^{JM_J}_{J'M'_J,kq}\langle J||\hat{\mathbf{T}}||J'\rangle. \tag{49}$$

Thus, for each value of J, J', and k, one only needs to evaluate one matrix element to obtain a value of the reduced matrix element $\langle J||\hat{\mathbf{T}}||J'\rangle$ and all other matrix elements can be generated from this by simple multiplications with CG coefficients.

One very efficient use of ITOs is the decomposition of multiples or powers of angular momentum operators. A special case of the ITOs are the spherical tensor operators $Y_{kq}(\hat{\mathbf{J}})$, which are obtained from the Cartesian spherical harmonics $Y_{kq}(\mathbf{r}/r)$[157] by the replacement $\mathbf{r}/r \to \hat{\mathbf{J}}$ or in a similar manner in the case of

operators $\hat{\mathbf{S}}$ and $\hat{\mathbf{L}}$. Each multiple of angular momentum operators in the replacement needs to be an averaged sum of all possible permutations of the respective operators due to the noncommutativity of the quantum mechanical operators. The Wigner–Eckart theorem can be applied to the angular momentum operators expressed in terms of $Y_{kq}(\hat{\mathbf{J}})$ to greatly simplify the resulting expressions. A further useful property of the spherical tensor operators is that the resulting non-zero matrix elements in angular momentum state basis are proportional to a CG coefficient $C^{JM_J}_{kq,JM_J}$. From the properties of the CG coefficients, it is possible to show that coefficient is zero unless $k \leq 2J$.[159] This sets a limit for the highest rank of operators entering the expressions. The equivalence between the sets of operators $\{Y_{kq}(\hat{\mathbf{J}})\}$ and $\{Y_{kq}(\mathbf{r}/r)\}$ also means that is is possible to expand local multiplicative electrostatic potential operators of the form $\hat{V}(\mathbf{r})$ in terms of the spherical tensor operators. This is called the method of equivalent operators and is widely used in the theory of crystal-fields.[20,165] The matrix elements of the equivalent operators can be easily calculated in the basis of the angular momentum states $\{|JM_J\rangle\}$.

3.2.4 Time-reversal symmetry and Kramers' theorem

Symmetry under reversal of time is one of the fundamental symmetries of nature resulting from the fact that the laws of physics are invariant under the replacement $t \to -t$. We are mostly interested in the time-reversal of the angular momentum states $|JM_J\rangle$. If we consider a state $|\psi\rangle = \sum_{J,M_J} C_{JM_J}|JM_J\rangle$ expanded in angular momentum states, the effect of the time-reversal operator $\hat{\theta}$ is

$$|\tilde{\psi}\rangle = \hat{\theta}|\psi\rangle = \sum_{J,M_J} C^*_{JM_J}(-1)^{J-M_J}|J - M_J\rangle, \tag{50}$$

where $|\tilde{\psi}\rangle$ denotes the time-reversal conjugate of $|\psi\rangle$.[20] The time-reversal operator is anti-unitary and anti-linear. The latter means that, in general, $\hat{\theta}$ does not commute with complex numbers. In the absence of external magnetic fields, the Hamiltonian is invariant under time reversal, and thus, the energy of the system must be conserved under the operation of time-reversal. This is true if $|\psi\rangle$ and $|\tilde{\psi}\rangle$ are degenerate or if $|\psi\rangle = |\tilde{\psi}\rangle$. It turns out that if the system has a non-integer total angular momentum (i. e., odd number of electrons) $|\psi\rangle \neq |\tilde{\psi}\rangle$ always holds, and the system must be at least doubly degenerate. This is proved in Kramers' theorem[166] and the resulting degeneracy is called Kramers degeneracy. If the symmetry of the system is less than cubic under the action of the CF, the states of the system will be split into doublets known as Kramers doublets.[167] This conservation of degeneracy has rather important consequences,[20] and systems with odd number of electrons are called Kramers systems, whereas systems with an even number of electrons are known as non-Kramers systems. It should be noted that when the point-group symmetry of the system has doubly degenerate representations (trigonal symmetry or higher), Kramers degeneracy does not necessarily introduce any new degeneracies but can coincide with the spatial degeneracies.

If an external magnetic field is present, the time-reversal invariance is broken, and the Kramers' theorem no longer holds. This means that Kramers doublets can split and mix under the Zeeman interaction. This breaking of time-reversal symmetry does not imply that electrodynamics are not invariant under time-reversal; this is a consequence of the fact that we have not included the current producing the magnetic field into the system. If the full system was considered, the time-reversal operation would reverse the direction of the current producing the magnetic field, and the system would remain invariant.[145]

3.2.5 The microscopic magnetization

The microscopic magnetization $\boldsymbol{\mu}_i$ in equation (30) can be expressed as

$$\boldsymbol{\mu}_i = \frac{\partial E_i}{\partial \mathbf{B}} = \left\langle \psi_i \left| \frac{\partial \hat{H}}{\partial \mathbf{B}} \right| \psi_i \right\rangle , \tag{51}$$

where we have used the Hellmann–Feynman theorem[168,169] and $|\psi_i\rangle$ is the electronic state. The only part of the Hamiltonian, which depends on the magnetic field (assuming that the field is relatively weak compared to the Coulomb interaction), is the Zeeman term

$$\hat{H}_{\mathrm{Zee}} = -\mu_B \mathbf{B} \cdot \left(\hat{\mathbf{L}} + g_e \hat{\mathbf{S}} \right) , \tag{52}$$

where g_e is the free electron g value. Thus, the microscopic magnetization can be given as

$$\boldsymbol{\mu}_i = -\mu_B \left(\langle \hat{\mathbf{L}} \rangle_i + g_e \langle \hat{\mathbf{S}} \rangle_i \right) \tag{53}$$

where $\langle \hat{\mathbf{L}} \rangle_i$ and $\langle \hat{\mathbf{S}} \rangle_i$ are the expectation values of the orbital and spin angular momenta of state i. It is easy to see from (53) and (31) that all magnetic properties of a molecular material arise from the angular momenta of the many-particle system.

3.3 Model Hamiltonians

3.3.1 Spin and pseudospin Hamiltonians

The concept of spin and pseudospin Hamiltonians was introduced in the 1950s by Pryce and Abragam,[170,171] Bleaney and Stevens,[19,172] and Koster and Statz.[173,174] The initial work introduced them as model Hamiltonians determined on phenomenological grounds to explain experimental observations related to the low-energy spectrum of magnetic insulators. The theory related to the concept is rather well formulated in the book of Abragam and Bleaney.[20] The idea behind (pseudo)spin Hamiltonians is to reduce the massive number of degrees of freedom in a many-particle system to only a few, in many cases just one, spin degree of freedom. An effective Hamiltonian can then be constructed purely in terms

of angular momentum operators, which greatly reduces the dimension of the Hilbert space one needs to work with. The other physical properties not related to spin are absorbed into effective parameters expressed as scalars, vectors, or tensors. If the dimension of the space spanned by the (pseudo)spin states is chosen in a reasonable way, the effective parameters have clear physical interpretation. The two concepts introduced here, spin and pseudospin Hamiltonians, are closely related but distinct concepts, and only the latter can be used in the most general case to build a connection between experimental observations and the full microscopic Hamiltonian of the system under study.

Spin Hamiltonians are operators written in terms of spin operators: $\hat{H}_{\text{spin}} = \hat{H}_{\text{spin}}(\hat{\mathbf{S}}_1, \hat{\mathbf{S}}_2, \cdots)$ and operate in a Hilbert space known as the model space $\mathcal{P}_0$ spanned by the states $\{|S_1 M_{S1}\rangle \otimes |S_2 M_{S2}\rangle \otimes \cdots\}$.[155,175] The dimension of $\mathcal{P}_0$ is $\dim(\mathcal{P}_0) = (2S_1 + 1)(2S_2 + 1) \cdots$. Let us then consider a magnetic molecular system with several spin sites with spins $\mathbf{S}_1, \mathbf{S}_2, \cdots$. The spins are coupled in some way in the ground state to yield a ground spin-state with total spin $\mathbf{S}$, and if we neglect all SOC, the $2S + 1$ states of the ground manifold are degenerate. The full Hamiltonian of the system $\hat{H}$ commutes with $\hat{\mathbf{S}}^2$ and $\hat{S}_z$; therefore, the states in the $(2S + 1)$-fold degenerate manifold can be represented by the set $\{|SM_S\rangle\}$. The space spanned by these states is called the target space $\mathcal{P}'$, and it constitutes a subspace of the full space $\mathcal{P}$ spanned by all eigenstates of the full Hamiltonian of the system. The basis set $\{|S_1 M_{S1}\rangle \otimes |S_2 M_{S2}\rangle \otimes \cdots\}$ spanning $\mathcal{P}_0$ is isodimensional to the basis $\{|SM_S\rangle\}$ spanning $\mathcal{P}'$. The two are related by a unitary transformation. Thus, it is very easy to see that in this case the spectrum of the spin Hamiltonian $\hat{H}_{\text{spin}}$ acting in the model space $\mathcal{P}_0$ and of the full Hamiltonian $\hat{H}$ acting in the target space $\mathcal{P}'$ can be made fully equivalent.

The situation becomes more complicated when SOC is weak but not negligible. Then, the $2S + 1$ lowest eigenstates of $\hat{H}$ are split and become weakly mixed with higher-lying spin states. The spin $\mathbf{S}$ is not conserved, and $\mathcal{P}'$ cannot be fully spanned by the set $\{|SM_S\rangle\}$. $\mathcal{P}'$ is also no longer closed under the operations $\hat{\mathbf{S}}^2$ and $\hat{S}_z$, but now the operators connect the states in $\mathcal{P}'$ to those in its orthogonal complement $\mathcal{P} - \mathcal{P}'$.[97,155,175] We can, however, still construct a spin Hamiltonian in such a way that

$$\hat{H}|\psi_I\rangle = E_I|\psi_I\rangle \Longleftrightarrow \hat{H}_{\text{spin}}|\xi_I\rangle = E_I|\xi_I\rangle, \tag{54}$$

where the eigenstates $\{|\xi_I\rangle\}$ of $\hat{H}_{\text{spin}}$ are expanded in the basis states of $\mathcal{P}_0$:

$$|\xi_I\rangle = \sum_{M_{S1}, M_{S2}, \cdots} C_{M_{S1} M_{S2} \cdots} |S_1 M_{S1}\rangle \otimes |S_2 M_{S2}\rangle \otimes \cdots \tag{55}$$

At this point, it is clear that the spin operators $\hat{\mathbf{S}}_1, \hat{\mathbf{S}}_2, \cdots$ used in the construction of $\hat{H}_{\text{spin}}$ can no longer be physical spin operators, but instead should be considered as convenient fiction, which is used to obtain the eigenvalues $\{E_I\}$ from the states spanning $\mathcal{P}_0$. $\hat{H}_{\text{spin}}$ can be derived from $\hat{H}$ by using the theory of effective Hamiltonians introduced in section 3.3.2. Here, it suffices to say that as long as one can establish a mapping between $\{|\psi_I\rangle\}$ in $\mathcal{P}'$ and $\{|\xi_I\rangle\}$, a spin

Hamiltonian can, in principle, be constructed in such a way that equation (54) holds *exactly*.

Choosing the manifold of states defining the spin Hamiltonian is easy when SOC is weak and the $(2S+1)$-dimensional manifold of states is clearly separated from the other states. The situation is also similar when SOC is very strong and other interactions are weak so that the lower manifold is $(2J+1)$-dimensional and the spin Hamiltonian can be constructed in terms of $\hat{\mathbf{J}}$ operators. In other cases of strong SOC, the N lowest energy eigenstates of the full Hamiltonian cannot necessarily be attributed to any set of spin operators. A very common example of this is a trivalent lanthanide ion, which splits under SOC and crystal-field interaction into Kramers doublets. The two components of the lowest doublet do not coincide with any real angular momentum, spin or orbital, of the system except in special accidental cases. Such a system cannot then be described by any spin Hamiltonian. It is however, possible to define a pseudospin $\tilde{\mathbf{S}}$ so that $2\tilde{S}+1=N$. The total pseudospin can then be decomposed into contributions from pseudospins $\tilde{\mathbf{S}}_1, \tilde{\mathbf{S}}_2, \cdots$ of individual spin sites. The corresponding pseudospin operators behave like normal spin operators and obey all the same commutation relations. The pseudospin operators are, however, only defined by the matrices representing them. Thus, no general form can be given to any pseudospin operator. To emphasize this, we are not using the hat symbol for pseudospin operators but opt for the tilde symbol both for the pseudospins and the respective operators. In the literature, pseudospin is sometimes referred to as effective spin (which has other meanings as well), fictitious spin, or simply as spin.[176]

The difference between spin and pseudospin Hamiltonians is most obvious when the ground manifold of electronic states cannot be assigned to the set of eigenstates of any real angular momentum operator. The spin and pseudospin formalism may differ, however, also in the case when $\tilde{S}=S$. This results from the fact that pseudospin Hamiltonians are defined in such a way that they can always be put in correspondence with the phenomenological Hamiltonians used to describe experimental results,[20] which is not always possible with spin Hamiltonians (see section 3.4.3).[100] In such a case, the spin operator entering the definition of the spin Hamiltonian is related to the respective pseudospin operator by a rotation in the Cartesian space.[97] The spin Hamiltonian formalism can be related to experiment in the most general case only when SOC is completely absent. The deviations between the spin and pseudospin, when present, arise already at the first order of perturbation theory when SOC is included.[97] In real systems, SOC is always present, but quantum chemical calculations can be (and often are) carried out without any SOC, and in such cases, the calculated Hamiltonian can be put in correspondence with the spin Hamiltonians in a meaningful and, in principle, exact way in all situations.

Explicit forms of spin and pseudospin Hamiltonians will be discussed in sections 3.4 and 3.5.

3.3.2 Effective Hamiltonian theory

Spin and pseudospin Hamiltonians can be constructed on purely phenomenological grounds as they were first introduced.[170,171] They can, however, also be rigorously derived from the full Hamiltonian $\hat{H}$ (or some reasonably general approximation of the full Hamiltonian) using the theory of effective Hamiltonians.[153–155,175,177] Similar to the spin and pseudospin Hamiltonians introduced in section 3.3.1, an effective Hamiltonian $\hat{H}_{\text{eff}}$ spans an N-dimensional model space $\mathcal{P}_0$ which is put into correspondence with the isodimensional target space $\mathcal{P}'$ spanned by the N lowest eigenstates $\{|\psi_I\rangle\}$ of $\hat{H}$:

$$\hat{H}|\psi_I\rangle = E_I|\psi_I\rangle \Longleftrightarrow \hat{H}_{\text{eff}}|\xi_I\rangle = E_I|\xi_I\rangle, \tag{56}$$

where $I = 1, \cdots, N$ and $\{|\xi_I\rangle\}$ are the eigenstates of the effective Hamiltonian.

An effective Hamiltonian can be constructed from the eigenstates $\{|\xi_I\rangle\}$ using the spectral decomposition

$$\hat{H}_{\text{eff}} = \sum_I |\xi_I\rangle E_I \langle\xi_I|. \tag{57}$$

In order to use equation (57), we need to know the projections of $\{|\xi_I\rangle\}$ onto $\{|\psi_I\rangle\}$ and the eigenvalues $\{E_I\}$. The former can be easily evaluated, but the latter can only be obtained by diagonalizing the full Hamiltonian. This is certainly feasible if we have already calculated the eigenvalues using some *ab initio* method and want to put the calculated Hamiltonian in correspondence with some effective Hamiltonian. If we, however, simply want to know the form of the effective Hamiltonian without carrying out the diagonalization, equation (57) is not very useful. Furthermore, Hamiltonian (57) is not necessarily Hermitian as the projection $P_0 = \sum_I |\xi_I\rangle\langle\xi_I|$ acting on the states in the target space $\mathcal{P}'$ does not necessarily yield a complete basis. Exact Hermicity can be enforced by orthogonalization of the basis,[178] but the Hamiltonian is then no longer unique.[77] This problem of non-Hermicity can be avoided by constructing the effective Hamiltonian using the theory of unitary transformations.[154,155,179] The full Hamiltonian is first decomposed to $\hat{H} = \hat{H}_0 + \hat{V}$, where $\hat{H}_0$ connects states within the target space $\mathcal{P}'$ or within its orthogonal complement $\mathcal{P} - \mathcal{P}'$. The operator $\hat{V}$ connects these two blocks in the Hamiltonian. Once the Hamiltonian has been partitioned, the full Hamiltonian can be transformed to the effective Hamiltonian by

$$\hat{H}_{\text{eff}} = e^{\hat{W}} \hat{H} e^{-\hat{W}}, \tag{58}$$

where $\hat{W}$ is an anti-Hermitian operator defined as

$$\hat{W} = \sum_{I,J} \frac{\langle\psi_I^{(0)}|\hat{V}|\psi_J^{(0)}\rangle}{E_J - E_I} |\psi_I^{(0)}\rangle\langle\psi_J^{(0)}|. \tag{59}$$

$\{|\psi_I^{(0)}\rangle\}$ are eigenstates of $\hat{H}_0$. In practice, the exponential is expanded as a Taylor series, and the expansion is terminated at some pre-determined order. If

the states in $\mathcal{P}'$ are only weakly coupled to those in $\mathcal{P} - \mathcal{P}'$, the series should converge rapidly. If the coupling is strong, the physical sense of the chosen form of the effective Hamiltonian can be questioned. The transformation (58) can be interpreted as "decoupling" the states in $\mathcal{P}'$ from those of its orthogonal complement so that they can be related to the states in the model space $\mathcal{P}_0$. The interaction coupling $\mathcal{P}'$ and $\mathcal{P} - \mathcal{P}'$ is constructed into the effective Hamiltonian in a perturbative manner.

3.4 Electronic structure of metal ions in molecular complexes

3.4.1 Classification of metal ions

The building blocks of molecular systems with magnetic properties are either transition metal ions, lanthanide ions, actinide ions, or radicals. Radicals are the simplest to treat as the ground state is usually a spin-doublet with no angular momentum, and usually SOC effects can be largely neglected, although exceptions do exist.[180] The electronic structure of metal ions of the d and f blocks is usually much more complicated, and the single-ion electronic states are often discussed by starting from the free-ion approximation and then introducing various interactions, including SOC and interaction with the CF, in a step-wise manner. In the literature, the ions are often classified into two or three separate classes depending on the relative strength of the intra-ionic interactions and the interaction with the crystal-field.[20,152,181] We will use a somewhat different (although largely analogous) classification system, which is compatible with the pseudospin description introduced in section 3.3. In this approach the systems are classified according to the quantum numbers, which can be used to approximately classify manifolds of electronic states.[97]

In *S*-type systems, the CF is much stronger than SOC and splits any spatially degenerate states quenching the angular momentum to such an extent that no orbital angular momentum can be coupled to the spin at the lowest order of (quasi-degenerate) perturbation theory. Such systems are said to have no first-order angular momentum. The ground spin-multiplet is then well-separated from any excited state. The $2S + 1$-fold degeneracy of the ground spin-multiplet is slightly lifted by SOC due to mixing of higher-lying states into the ground spin-multiplet at higher orders of perturbation theory, but the ground manifold is still characterized by a manifold of $2S + 1$ state clearly separated from other states, and the system can be described by a pseudospin quantum number $\tilde{S} = S$. In systems with an odd number of electrons, at least double degeneracy in each spin-orbit split multiplet state is retained. Most complexes of the 3d transition-metal elements are *S*-type systems (with some exceptions, such as the Co(II) ion in a CF of octahedral symmetry), and practically all organic and main-group radical systems fall into this category as well.[20,23]

In *J*-type systems, SOC is much stronger than the CF splitting, and the

ground manifold consists of $2J + 1$ states, which are weakly split by the CF. This situation is encountered in trivalent lanthanide complexes, where the 4f orbitals housing the unpaired electrons are strongly shielded by the occupied 5s and 5p orbitals with larger spatial extents. This leads to very weak CF splitting. In lanthanide ions, the splitting of different J multiplets is of the order $\sim 10^3\,\mathrm{cm}^{-1}$, whereas the CF splitting is of the order $\sim 10^2\,\mathrm{cm}^{-1}$. Thus, all of the electronic states can be clearly assigned to some J manifold described by the pseudospin quantum number $\tilde{J} = J$. Exceptions to this are Sm(III) and Eu(III) systems, where the splitting due to SOC is relatively weak.[182–184] In the case of Kramers systems, the $2J + 1$ states of the ground manifold are split into Kramers doublets. Higher degeneracy is possible in cubic or higher point-group symmetries, but such are extremely rare in lanthanide complexes. Non-kramers systems do not necessarily retain any degeneracies, but usually the energy spectrum is such that some quasi-doublet structure is retained. In trigonal or higher point-group symmetries some doublets can be exactly degenerate due to spatial symmetry and are called Ising doublets.

Γ-type systems are complexes of high symmetry (usually cubic), where the SOC and CF are of the same order of magnitude. In such cases, the number of states in the ground manifold does not correspond to $2S + 1$ nor to $2J + 1$. However, in sufficiently high symmetry, the number of states corresponds to $2\Gamma + 1$, where Γ is the dimension of the representation of the molecular point group corresponding to the ground state. It should be noted that since SOC is included, one should use relativistic double groups instead of the non-relativistic point groups usually encountered in chemistry. Examples of Γ-type systems include most high-symmetry paramagnetic complexes of 4d and 5d transition-metals, actinides, and some systems of 3d transition-metals, such as complexes of Co(II) in octahedral CFs.[97] An important special case of Γ-type systems with no spatial point group symmetry beyond C_1 are all systems with an odd number of electrons. The ground electronic state of such systems consists of a Kramers doublet and the two states of the doublet related by the operation of time-reversal transform as a two-dimensional representation of SU(2)[167] (special unitary group in two dimensions[158]); therefore, the manifold defined by the doublet can be described using a $\tilde{\Gamma} = 1/2$ pseudospin.

The last class of systems is all systems that cannot be classified as *S*-, *J*-, or Γ-type systems and contains low-symmetry systems with SOC and CF of comparable strength. In such cases, the molecular electronic structure cannot be related to the electronic structure of the respective free ion in a meaningful way and has to be treated on a case-by-case basis.

It is important to note that in some cases the classification depends on the available thermal energy. For example, in coordination complexes of trivalent lanthanide ions, the overall CF splitting is usually of the same order of magnitude as the thermal energy at room temperature (although in some case it can be considerably higher). Thus, in ambient conditions all states in the multiplet are populated, and the system can be described as a *J*-type system. When the temperature is lowered to that of liquid helium, usually only the lowest doublet

is occupied, and the magnetic properties are better described by categorizing the system as a Γ-type system. It is common that the optical spectrum of a lanthanide complex is treated using a $\tilde{J}$-pseudospin, whereas the low-energy EPR spectrum is rationalized in terms of a $\tilde{\Gamma} = 1/2$ pseudospin.

3.4.2 The microscopic Hamiltonian

The electronic structure of a metal ion in a complex can be described by the electronic Hamiltonian

$$\hat{H}_{\text{complex}} = \hat{H}_{\text{el}} + \hat{H}_{\text{CF}} + \hat{H}_{\text{SOC}} + \hat{H}_{\text{Zee}}, \tag{60}$$

where the first terms includes all the electrostatic interactions within the metal ion (including the kinetic energy, electrostatic interactions, and exchange interaction), the second describes the interaction between the ion and the CF, the third describes the SOC, and the last is the Zeeman operator. The eigenstates of $\hat{H}_{\text{complex}}$ are expanded in terms of angular momentum states

$$|\psi_I\rangle = \sum_{\nu} \sum_{J,M_J} C_{\nu J M_J} |\nu J M_J\rangle \quad \text{or} \quad |\psi_I\rangle = \sum_{\nu} \sum_{S,M_S} \sum_{L,M_L} C_{\nu S M_S L M_L} |S M_S\rangle \otimes |\nu L M_L\rangle \tag{61}$$

depending on whether we choose a coupled or uncoupled basis. The former is the natural choice for J-type systems, whereas the latter is a better choice for S-type systems. The index ν contains all other quantum numbers required to define the electronic state beyond the angular momentum quantum numbers. $\hat{H}_{\text{el}}$ is the only part of (60) that acts on the part of the state defined by ν, whereas $\hat{H}_{\text{CF}}$, $\hat{H}_{\text{SOC}}$, and $\hat{H}_{\text{Zee}}$ all act on the angular momentum part of the state.

The form of the SOC operator is discussed in section 4.4.5 in more detail, and it suffices to state here that it mixes states that differ in spin by $\Delta S = \pm 1, 0$ and in orbital angular momentum by $\Delta L = \mp 1, 0$. The Zeeman interaction is given by equation (52). The CF is an electrostatic potential, which can be expanded in spherical tensor operators using the method of equivalent operators[20] (see section 3.2.3):

$$\hat{H}_{\text{CF}} = \sum_{k=0}^{\infty} \sum_{q=-k}^{k} B_{kq} \hat{O}_{kq}(\hat{\mathbf{J}}), \tag{62}$$

where B_{kq} are the CF parameters and $\hat{O}_{kq}(\hat{\mathbf{J}})$ is a Stevens operator named after Stevens who first introduced the concept of equivalent operators in 1952.[165] The original definition by Stevens has been extended to the so-called extended Stevens operators introduced by Rudowicz.[185–187] The operators are proportional to the Cartesian spherical harmonics: $\hat{O}_{kq}(\hat{\mathbf{J}}) \propto Y_{kq}(\hat{\mathbf{J}})$. The normalization constants of the spherical harmonics have been dropped and can be considered as being absorbed into the CF parameters B_{kq}. This means that the CF parameters of high ranks may have very small values but can still contribute significantly. Also, the Stevens operators are not Hermitian: $\hat{O}_{kq}^{\dagger}(\hat{\mathbf{J}}) = (-1)^q \hat{O}_{k-q}(\hat{\mathbf{J}})$. These inconvenient properties along with the lack of any general expression for matrix elements

of the operators has lead to alternative definitions.[95,119] Some of the Stevens operators are tabulated, for example, in the appendices of ref. 20, but it should be noted that the tabulated forms of Stevens operators in various sources have some notorious typos.[187]

In the basis $\{|JM_J\rangle\}$, the operators with $q = 0$ only induce splitting between states corresponding to different values of M_J but do not induce any mixing. Thus, they are usually referred to as the diagonal operators. The operators with $q \neq 0$ are referred to as off-diagonal operators and mix states belonging to different values of M_J differing at maximum by q. The CF parameters B_{kq} should be interpreted as phenomenological parameters that reproduce the experimentally observed splitting of the states. The parameters do not have any simple explicit relation to the integrals defining the energy levels of the real system. When CF theory was first introduced, the CF was considered as a purely electrostatic potential acting on the free ion.[184,188–191] It quickly became apparent that metal–ligand covalency plays an important role in the CF splitting;[152,171,181,192–195] this has been confirmed both by spectroscopic measurements[196] and high-level *ab initio* calculations.[101,103] Several attempts have since been made to calculate the CF parameters from first principles by approximating the electrostatic potential or from models introducing effects of the metal–ligand covalency in some empirical manner,[152,181,195,197] but none of these methods have been able to reproduce the relevant splittings on a quantitative level without making some reference to parameters determined by a fit to experiment. Thus, the CF Hamiltonian should be interpreted as an effective Hamiltonian, not as an approximation to the full microscopic Hamiltonian.

The highest rank of operators giving non-zero matrix elements is $2J$. Time-reversal symmetry further dictates that only operators with even ranks enter the expansion. The CF operator must also transform as the totally symmetric representation of the molecular point group. In high-symmetry systems this greatly reduces the number of operators. The non-zero CF parameters for various crystallographic point groups are listed, for example, in Benelli and Gatteschi.[26] It is rather common in the literature to encounter the so-called electrostatic approximation, where all covalent interactions between the metal ion and the ligands are neglected. In this case, the highest rank entering the CF operator is $2l$, where l is the orbital angular momentum of the orbitals occupied by the unpaired electrons. Thus, for transition metal ions only ranks $k = 0, 2$ enter the expansion, and for trivalent lanthanides only ranks $k = 0, 2, 4, 6$ are retained. The zeroth rank operator is a scalar, and it only constitutes a constants shift in the energy spectrum and is therefore usually neglected. The electrostatic approximation has, however, been show to be rarely valid for molecular systems.[101] It nonetheless remains widely used in the literature.

In S-type systems, the operator $\hat{H}_{\mathrm{el}} + \hat{H}_{\mathrm{CF}}$ determines the main features of the electronic structure, and $\hat{H}_{\mathrm{SOC}}$ and $\hat{H}_{\mathrm{Zee}}$ can be treated as a perturbation, which lifts the degeneracy of various manifolds. In such systems, the effect of $\hat{H}_{\mathrm{SOC}}$ is called zero-field splitting (ZFS), as it lifts the $(2S + 1)$-fold degeneracy of spin states in the absence of an external field. In J-type systems, the main

manifolds of the electronic states are determined by the operator $\hat{H}_{\mathrm{el}} + \hat{H}_{\mathrm{SOC}}$ (i. e., the free-ion Hamiltonian), and the operators $\hat{H}_{\mathrm{CF}}$ and $\hat{H}_{\mathrm{Zee}}$ act as a perturbation, which lifts the $(2J+1)$-fold degeneracy of the manifolds. Equation (62) can be applied in the $\{|SM_S\rangle \otimes |LM_L\rangle\}$ basis by the simple replacement $\hat{\mathbf{J}} \to \hat{\mathbf{L}}$.

3.4.3 Spin and pseudospin Hamiltonians for monometallic complexes

Before proceeding to the pseudospin description, we will first discuss the spin Hamiltonians describing the Zeeman interaction and ZFS. In S-type systems, we can partition the Hamiltonian into $\hat{H} = \hat{H}_0 + \hat{V}$ in such a way that $\hat{H}_0 = \hat{H}_{\mathrm{el}} + \hat{H}_{\mathrm{CF}}$ and $\hat{V} = \hat{H}_{\mathrm{SOC}} + \hat{H}_{\mathrm{Zee}}$. The form of the spin Hamiltonians is then obtained using the transformation (58) as

$$\hat{H}^{\mathrm{spin}}_{\mathrm{Zee}} = e^{\hat{W}} \hat{H}_{\mathrm{Zee}} e^{-\hat{W}} = \mu_B \mathbf{B} \cdot \mathbf{g} \cdot \hat{\mathbf{S}} \quad \text{and} \tag{63}$$

$$\hat{H}^{\mathrm{spin}}_{\mathrm{ZFS}} = e^{\hat{W}} \hat{H}_{\mathrm{SOC}} e^{-\hat{W}} = \hat{\mathbf{S}} \cdot \mathbf{D} \cdot \hat{\mathbf{S}}, \tag{64}$$

where the transformation of $\hat{H}_{\mathrm{Zee}}$ has been carried out to the first order and the transformation of $\hat{H}_{\mathrm{SOC}}$ to the second order.[97] $\mathbf{g}$ is the so-called Zeeman $\mathbf{g}$-tensor, also sometimes known as the gyromagnetic tensor, and $\mathbf{D}$ is known as the ZFS tensor.

The elements of the $\mathbf{g}$-tensor are given as[87,89,97,198,199]

$$g_{\alpha\beta} = g_e \delta_{\alpha\beta} + \frac{N}{2S} \sum_{\nu} \frac{\langle \psi^{(0)}_{0SS} | \hat{L}_\alpha | \psi^{(0)}_{\nu SS} \rangle \langle \psi^{(0)}_{\nu SS} | \hat{z}_\beta | \psi^{(0)}_{0SS} \rangle + \langle \psi^{(0)}_{0SS} | \hat{z}_\beta | \psi^{(0)}_{\nu SS} \rangle \langle \psi^{(0)}_{\nu SS} | \hat{L}_\alpha | \psi^{(0)}_{0SS} \rangle}{E^{(0)}_{0S} - E^{(0)}_{\nu S}}, \tag{65}$$

where $\alpha, \beta \in x, y, z$, N is the number of electrons, ν contains other indices used to define the electronic states beyond the spin indices, $\hat{z}_\beta$ are spatial operators arising in the mean field treatment of SOC (see section 4.4.5). The states $|\psi^{(0)}_{\nu SS}\rangle$ are eigenstates of $\hat{H}_0$ with specific spin S and spin projection $M_S = S$. It is easy to see from (65) that in the absence of terms arising from the SOC operator, the $\mathbf{g}$-tensor reduces to the isotropic form $\mathbf{g} = g_e \mathbb{1}$.

The elements of the ZFS tensor have somewhat more complicated forms. By defining the operator

$$\hat{H}^{(2)}_{\alpha\beta} = \sum_{p,q} \hat{s}_{\alpha p} \hat{z}_{\alpha p} \hat{W} \hat{s}_{\alpha q} \hat{z}_{\alpha q}, \tag{66}$$

where $\hat{s}_{\alpha p}$ are one-particle spin operators and the summation in $\hat{W}$ (equation (59)) runs over the index ν defining the electronic states, the elements of $\mathbf{D}$ can be

given as[60,87,89,97]

$$
\begin{aligned}
D_{\alpha\alpha} &= -\frac{2}{2S-1}\left(\langle\psi^{(0)}_{0SS}|\hat{H}^{(2)}_{\alpha\alpha}|\psi^{(0)}_{0SS}\rangle - \langle\psi^{(0)}_{0SS-1}|\hat{H}^{(2)}_{\alpha\alpha}|\psi^{(0)}_{0SS-1}\rangle\right) \\
D_{xy} &= D_{yx} = -i\frac{2}{S}\left(\langle\psi^{(0)}_{0SS-1}|\hat{H}^{(2)}_{xy}|\psi^{(0)}_{0SS}\rangle\right) \\
D_{xz} &= D_{zx} = \frac{\sqrt{2}}{S\sqrt{S}}\left(\langle\psi^{(0)}_{0SS-1}|\hat{H}^{(2)}_{xz}|\psi^{(0)}_{0SS}\rangle\right) \\
D_{yz} &= D_{zy} = -i\frac{\sqrt{2}}{S\sqrt{S}}\left(\langle\psi^{(0)}_{0SS-1}|\hat{H}^{(2)}_{yz}|\psi^{(0)}_{0SS}\rangle\right).
\end{aligned}
\tag{67}
$$

The ZFS tensor is usually discussed in terms of the ZFS parameters D and E. The parameters are obtained by diagonalization of $\mathbf{D}$ to yield the eigenvalues D_x, D_y, and D_z and then assigning the eigenvalues to D and E so that[24]

$$
D = \frac{3D_z}{2} \quad \text{and} \quad E = \frac{D_x - D_y}{2}. \tag{68}
$$

The eigenvalues are assigned to D_x, D_y, and D_z in such a way that D_z is the one most clearly distinct from the two others and that $D_x - D_y$ is positive. Or, in other words, $|D| > 3E$ and $E \geq 0$.[175] A negative value of the D parameter indicates an easy-axis (or uniaxial) type anisotropy, where the magnetic moment of the ground state favors alignment along the main anisotropy axis. Easy-axis anisotropy is usually a requirement for an S-type SMM[25] although some exceptions are known.[200,201] The opposite situation to easy-axis anisotropy is easy-plane anisotropy.

The experimentally observed Zeeman splitting and ZFS can be described using phenomenological model pseudospin Hamiltonians of the form

$$
\tilde{H}_{\text{Zee}} = \mu_B \mathbf{B}\cdot\tilde{\mathbf{g}}\cdot\tilde{\mathbf{S}} \quad \text{and} \quad \tilde{H}_{\text{ZFS}} = \tilde{\mathbf{S}}\cdot\mathbf{D}\cdot\tilde{\mathbf{S}}, \tag{69}
$$

where $\tilde{\mathbf{g}}$ is the pseudospin $\mathbf{g}$-tensor. The $\mathbf{D}$ tensors in the pseudospin and spin description at the weak SOC limit are equivalent; therefore, ZFS can be described by both spin and pseudospin Hamiltonian formalism. The $\mathbf{g}$- and $\tilde{\mathbf{g}}$ tensors are not, in general, equivalent. This results from the fact that in experiments the main magnetic axes (defined as eigenvectors of $\tilde{\mathbf{g}}$) of the system are defined in such a way that the Zeeman splitting has an extremum value when the magnetic field is applied along these directions. The Hamiltonian (69) can then be made diagonal in the coordinate frame defined by the magnetic axes by applying the magnetic field along one of these axes:

$$
\tilde{H}_{\text{Zee}} = \mu_B B_\alpha \tilde{g}_\alpha \tilde{S}_\alpha, \tag{70}
$$

where α labels the Cartesian axes. $\hat{H}^{\text{spin}}_{\text{Zee}}$ cannot, in general, be brought to the form (70) for any direction of the magnetic field. The operators $\hat{\mathbf{S}}$ and $\tilde{\mathbf{S}}$ are related by a rotation

$$
\tilde{S}_\alpha = \hat{S}_\alpha + \sum_\beta \frac{g_{\alpha\beta} - g_{\beta\alpha}}{g_e}\hat{S}_\beta. \tag{71}
$$

If the system has a three-fold rotation axis or higher (trigonal point group symmetry or higher), the main magnetic axis of the system (usually chosen as the z axis) is oriented along the main rotational axis. When all of the axes are determined by symmetry, the spin and pseudospin descriptions become equivalent for S-type systems.

In the case of arbitrarily strong SOC we are only interested in the $\tilde{S} = 1/2$ pseudospin in the present work. ZFS is effective only when $\tilde{S} \geq 1$; therefore, we only need to consider the Zeeman splitting. Let us denote the two components of the doublet as $|\psi_1\rangle$ and $|\psi_2\rangle$. If the system has an odd number of electrons, the two components are degenerate due to Kramers theorem and are related by the operation of time-reversal. The matrix element of the α component of the magnetic moment in the basis of these states is given as

$$(\mu_\alpha)_{IJ} = \langle \psi_I | \hat{S}_\alpha + g_e \hat{L}_\alpha | \psi_J \rangle, \quad I, J \in 1, 2. \tag{72}$$

If the doublet is subjected to a homogeneous magnetic field of the form $(\xi_x B, \xi_y B, \xi_z B)$, where $\{\xi_x, \xi_y, \xi_z\}$ are the directional cosines and B is the field strength, the doublet splits into states with eigenvalues[20,95,97]

$$E = \pm B \sqrt{\sum_{\alpha,\beta} \xi_\alpha A_{\alpha\beta} \xi_\beta}, \tag{73}$$

where $A_{\alpha\beta}$ are components of a tensor $\mathbf{A}$ given as

$$A_{\alpha\beta} = -\frac{1}{2} \left(\begin{vmatrix} (\mu_\alpha)_{11} & (\mu_\alpha)_{12} \\ (\mu_\beta)_{21} & (\mu_\beta)_{22} \end{vmatrix} + \begin{vmatrix} (\mu_\beta)_{11} & (\mu_\beta)_{12} \\ (\mu_\alpha)_{21} & (\mu_\alpha)_{22} \end{vmatrix} \right) \tag{74}$$

The $\mathbf{A}$ tensor is proportional to the Abragam–Bleaney tensor[20] $\mathbf{G} = \tilde{\mathbf{g}} \cdot \tilde{\mathbf{g}}^{\mathrm{T}}$: ${\mu_B}^2 \mathbf{G}/4 = \mathbf{A}$. Both tensors can be brought to their diagonal forms $\mathbf{G}'$ and $\mathbf{A}'$ by the same transformation, and the diagonal elements of the $\tilde{\mathbf{g}}'$ and $\mathbf{A}'$ tensor can then be related as[95,97]

$$\tilde{g}'_{\alpha\alpha} = \pm \frac{2}{\mu_B} \sqrt{A'_{\alpha\alpha}}. \tag{75}$$

The back transformation to the original coordinate system can be determined from the eigenvectors of $\mathbf{A}$, and $\tilde{\mathbf{g}}'$ can then be transformed to $\tilde{\mathbf{g}}$. It should be noted that due to the square root operation in (75), the signs of the individual components of the $\tilde{\mathbf{g}}$-tensor cannot be determined. In Ising and quasi doublets, only the eigenvalue of $\tilde{\mathbf{g}}$-tensor corresponding to main magnetic axis has a non-zero value due to the Griffith's theorem.[202]

General expressions for the elements of the $\tilde{\mathbf{g}}$ and $\mathbf{D}$ tensors at arbitrarily strong SOC and arbitrary magnitude of pseudospin have been derived by Chibotaru and Ungur using ITO techniques[95,97] but will not be discussed here.

3.5 Exchange interaction

3.5.1 Direct exchange mechanism

In systems with multiple magnetic sites, such as polymetallic complexes, the way the spin angular momenta of the sites are coupled to yield the total spin **S** of the system is determined by exchange interactions. In most cases, the exchange interaction is a two-site process (although some exceptions do exist[177,203–206]), and the exchange interactions in polymetallic systems can be constructed from pairwise two-site exchange interactions. We will first consider the case of exchange interaction known as direct exchange, where the magnetic sites interact directly. We will further limit our initial treatment to the simplest case, which considers two sites a and b, each with one unpaired electron and zero orbital angular momentum. Such a case is encountered, for example, when considering organic diradicals, radical dimers, or bimetallic Cu(II) systems, where the metal ions interact directly. More complicated situations are discussed in terms of spin Hamiltonians in section 3.5. The electrons occupy magnetic orbitals[76,177] $\phi_a(\mathbf{r})$ and $\phi_b(\mathbf{r})$, which are Wannier type functions,[207–209] maximally localized at sites a and b while still maintaining their mutual orthogonality. A useful starting point for the description of this system is the generalized Hubbard model[177,179,210]

$$\begin{aligned}\hat{H}^{\text{direct}}_{\text{Hubbard}} =& U_a \hat{n}_{a\alpha}\hat{n}_{a\beta} + U_b \hat{n}_{b\alpha}\hat{n}_{b\beta} + U_{ab}\sum_{\sigma,\sigma'}\hat{n}_{a\sigma}\hat{n}_{b\sigma'} \\ &+ K_{ab}\sum_{\sigma,\sigma'}\hat{a}^\dagger_{a\sigma}a^\dagger_{b\sigma'}\hat{a}_{a\sigma'}a_{b\sigma} + t_{ab}\sum_{\sigma}\left(\hat{a}^\dagger_{a\sigma}\hat{a}_{b\sigma} + \hat{a}^\dagger_{b\sigma}\hat{a}_{a\sigma}\right),\end{aligned} \tag{76}$$

where $U_a = (aa|aa)$ and $U_b = (bb|bb)$ describe the on-site Coulomb repulsion between two electrons occupying orbitals ϕ_a and ϕ_b, respectively, $U_{ab} = (aa|bb)$ describes the inter-site repulsion between electrons in different orbitals, $K_{ab} = (ab|ba)$ is the exchange integral between the electrons in the different orbitals, and $t_{ab} = \langle\phi_a|\hat{h}|\phi_b\rangle$ is the transfer integral describing the resonance of the electrons between the two orbitals ($\hat{h}$ is the one-electron part of the full Hamiltonian). The indices $\sigma, \sigma' \in \alpha, \beta$ run over the spin indices. The mechanism is schematically represented in Figure 5a.

The magnetic orbitals $\phi_a(\mathbf{r})$ and $\phi_a(\mathbf{r})$ can be occupied in four different ways to give four ON vectors with $M_S = 0$: $|a\bar{b}\rangle$, $|\bar{a}b\rangle$, $|a\bar{a}\rangle$, and $|b\bar{b}\rangle$; one ON vector with $M_S = 1$: $|ab\rangle$; and one with $M_S = -1$: $|\bar{a}\bar{b}\rangle$. $|a\bar{b}\rangle$ and $|\bar{a}b\rangle$ are called neutral states, and $|a\bar{a}\rangle$ and $|b\bar{b}\rangle$ are called ionic states, as they have an excess electron on one site and an electron hole in the other state. The configurations are given in a pictorial form in Figure 5b. The two neutral states are mixed to each other and the two ionic states to each other by the exchange term in (76). The neutral and ionic states are separated from each other by the electron promotion energies $U_a - U_{ab}$ and $U_b - U_{ab}$. The neutral and ionic states are mixed into each by the transfer term in (76) and the off-diagonal element connecting the states is t_{ab}. In magnetic insulators (of which we are mostly interested

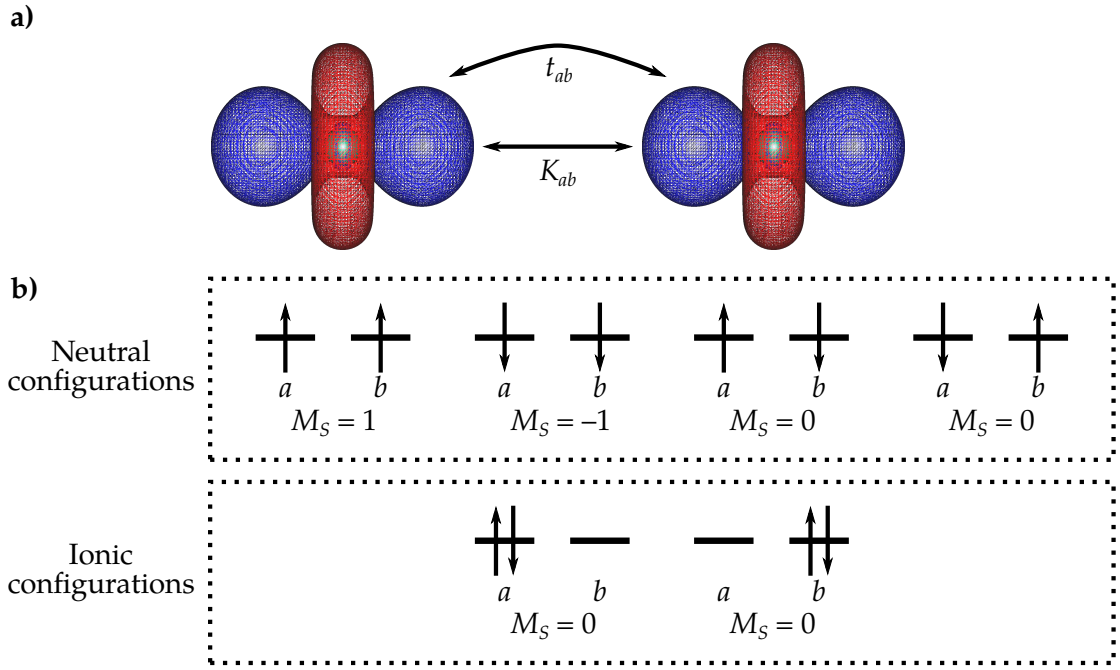

FIGURE 5 **a)** A schematic representation of the direct exchange mechanism involving two electrons in two orbitals and **b)** the electron configurations involved in the mechanism.

in molecular magnetism), the Coulombic repulsion is much stronger than the transfer interaction: $t_{ab} \ll U_a - U_{ab}$, $t_{ab} \ll U_b - U_{ab}$. This means that the ionic states can be considered as a perturbation mixed into the neutral states by the transfer term.[179] Since we are assuming there is no orbital angular momentum, SOC has no effect and the spin projection M_S is conserved. Thus, the $M_S = \pm 1$ ON vectors will not mix with any other state, and the Hamiltonian can be diagonalized in the basis of the two neutral $M_S = 0$ states; the mixing with the ionic states can be introduced later as a perturbation.[179,211,212]

The energy difference between the $M_S = 0$ singlet and triplet states is

$$\Delta E_{\mathrm{ST}} = E(S_0) - E(T_0) = 2K_{ab} - {t_{ab}}^2 \left(\frac{2}{U_a - U_{ab}} + \frac{2}{U_b - U_{ab}} \right). \qquad (77)$$

The other two components of the triplet are the $M_S = \pm 1$ basis states, which are degenerate with $|T_0\rangle$. The exchange integral K_{ab} is always positive and, therefore, stabilizes the triplet state which favors FM interaction. We refer to this form of exchange as Coulomb exchange as it originates from the Coulomb operator in the Hamiltonian. This interaction is sometimes also called direct exchange on its own. The Coulomb repulsion integrals U_a, U_b, and U_{ab} in the denominator are always positive, and the on-site repulsion is always larger than the inter-site repulsion; hence, the latter term in (77) stabilized the singlet state and favors anti-ferromagnetic (AFM) interaction. It is known as kinetic exchange,[212] as its magnitude is determined by the transfer integral, which largely depends on how strongly the kinetic energy operator mixes the two magnetic orbitals. The kinetic exchange is usually much stronger than the direct exchange unless the transfer

integral is zero or nearly zero by some symmetry condition. Consequently, AFM interaction is much more common in Nature than FM interaction.

When discussing exchange interaction, we usually mean all interactions that determine the relative ordering of the coupled spin states. Therefore, the direct exchange interaction contains in addition to the Coulomb exchange, which is exchange in its purest form, also the kinetic exchange contribution, which originates from electron delocalization or resonance. It is also worth noting here that the kinetic exchange formally originates from the mixture of the ionic states into the neutral states, and magnetic interaction occurs when this mixing is weak. The opposing limit, when t_{ab} is of the same order as U, is known as the covalent or Hückel limit and corresponds to the formation of a covalent bond between the magnetic orbitals. Thus, the exchange interaction between two electrons in two orbitals can also be interpreted as an extremely weak covalent bond. The exact limit between strong AFM exchange and weak covalent bonding is not well-defined, and organic diradicals, where this situation is often encountered, can be essentially described as either of the cases.

3.5.2 Superexchange mechanism

In the previous section, exchange interaction was introduced as a two-orbital process where the two electrons in those two orbitals interact directly. This is the case in radical–radical or metal–radical systems and is known as direct exchange. In polynuclear transition metal complexes, however, the exchange interaction usually takes place through some diamagnetic ligand, and the metal orbitals do not directly interact. Such a process is known as superexchange. The concept was first considered by Kramers,[213] formulated by Anderson,[211,212] and elaborated by Goodenough[214–216] and Kanamori.[217] We will demonstrate here the simplest possible case with two unpaired electrons in two equivalent magnetic orbitals $\phi_a(\mathbf{r})$ and $\phi_b(\mathbf{r})$, and one doubly occupied ligand orbital $\phi_l(\mathbf{r})$. Even in this relatively simple situation, the number of relevant interactions is fairly large, and in order to obtain a simple closed-form expression for the singlet–triplet splitting comparable to (77), only the major interactions can be introduced to the Hamiltonian. Thus, we will only consider the on-site Coulomb repulsion at the two metal sites (U_m), the metal–ligand transfer parameter (t_{ml}), and the splitting between the metal and ligand orbital energies (Δ_{ml}). All intersite interactions beyond electron transfer will be neglected as well as the Coulombic on-site repulsion at the ligand. Direct metal–metal transfer will also be neglected. This simple models provides a qualitatively correct picture, and the effect of the various parameters neglected here on quantitative estimates has been discussed in great detail by Van den Heuvel and Chibotaru.[218] The generalized Hubbard Hamiltonian is given as

$$\begin{aligned}\hat{H}^{\text{super}}_{\text{Hubbard}} =& U_m\left(\hat{n}_{a\alpha}\hat{n}_{a\beta}+\hat{n}_{b\alpha}\hat{n}_{b\beta}\right)+\Delta_{ml}\left(\hat{n}_{l\alpha}+\hat{n}_{l\beta}\right)\\ &+t_{ml}\sum_{\sigma}\left(\hat{a}^{\dagger}_{a\sigma}\hat{a}_{l\sigma}+\hat{a}^{\dagger}_{l\sigma}\hat{a}_{a\sigma}+\hat{a}^{\dagger}_{b\sigma}\hat{a}_{l\sigma}+\hat{a}^{\dagger}_{l\sigma}\hat{a}_{b\sigma}\right).\end{aligned} \tag{78}$$

A schematic representation of the superexchange mechanism is given in Figure 6a. The basis for the diagonalization of this Hamiltonian consists of three $M_S = 1$, three $M_S = -1$, and eight $M_S = 0$ configurations given in Figure 6b. Treating the ionic states as a perturbation and following the same procedure as in section 3.5.1 gives the singlet–triplet splitting as

$$\Delta E_{\mathrm{ST}} = \frac{4{t_{ml}}^4}{(U_m + \Delta_{ml})^2}\left(\frac{1}{U_m} + \frac{1}{U_m + \Delta_{ml}}\right) \tag{79}$$

It is worth noting that the superexchange mechanism as described by Hamiltonian (78) will always stabilize the AFM state. Stabilization of the FM state requires either a mechanism involving additional mutually orthogonal orbitals in the bridging ligand (the so-called ferromagnetic superexchange), a competing direct exchange mechanism between the metal orbitals, or more than one orbital per metal site (the so-called Goodenough's mechanism). Usually the ferromagnetic superexchange mechanism is the only FM mechanism strong enough to affect the energetic ordering of spin states. More detailed account of the different kinetic exchange terms in the case of higher number of orbitals and/or electrons is given in Goodenough's book.[216]

3.5.3 Double-exchange mechanism

A third form of exchange interaction we will consider is the so-called double-exchange introduced by Zener,[219] Anderson and Hasegawa,[220] and de Gennes.[221] In this model, we again consider two sites a and b, but now both sites have two orbitals $\phi_a(\mathbf{r})$, $\phi'_a(\mathbf{r})$ and $\phi_b(\mathbf{r})$, $\phi'_b(\mathbf{r})$. The orbitals $\phi_a(\mathbf{r})$ and $\phi_b(\mathbf{r})$ are both occupied by one electron each in the ground state. The system has one additional electron, which resonates between the orbitals $\phi'_a(\mathbf{r})$ and $\phi'_b(\mathbf{r})$. We will assume that the orbitals $\phi_a(\mathbf{r})$ and $\phi_b(\mathbf{r})$ do not interact directly; therefore the only inter-site interaction is the $a' \leftrightarrow b'$ transfer interaction described by the transfer parameter $t_{a'b'}$. At site a, the resonating electron occupying $\phi_{a'}$ is coupled to the electron in ϕ_a by the Hund's rule coupling described by the parameter $K_{aa'}$ and likewise for site b. The systems is then described by a Hamiltonian

$$\begin{aligned}\hat{H}^{\mathrm{double}}_{\mathrm{Hubbard}} = {} & (U_a + U_{ab})\left(\hat{n}_{a'\alpha} + \hat{n}_{a'\beta}\right) + (U_b + U_{ab})\left(\hat{n}_{b'\alpha} + \hat{n}_{b'\beta}\right) \\ & + K_{aa'}\sum_{\sigma,\sigma'}\hat{a}^\dagger_{a\sigma}a^\dagger_{a'\sigma'}\hat{a}_{a\sigma'}a_{a'\sigma} + K_{bb'}\sum_{\sigma,\sigma'}\hat{a}^\dagger_{b\sigma}a^\dagger_{b'\sigma'}\hat{a}_{b\sigma'}a_{b'\sigma} \\ & + t_{a'b'}\sum_{\sigma}\left(\hat{a}^\dagger_{a'\sigma}\hat{a}_{b'\sigma} + \hat{a}^\dagger_{b'\sigma}\hat{a}_{a'\sigma}\right).\end{aligned} \tag{80}$$

A schematic representation of the mechanism is given in Figure 7a.

The basis consists of two $M_S = {}^3/_2$ states, two $M_S = -{}^3/_2$ states, six $M_S = {}^1/_2$ states, and six $M_S = -{}^1/_2$ states. Each basis state represents a localized state, where the resonating electron is localized at either site a or site b. The configurations are given in pictorial form in Figure 7b. It should be noted that in all states, either $\phi'_a(\mathbf{r})$ or $\phi'_b(\mathbf{r})$ is occupied; hence, the on-site repulsion U_a

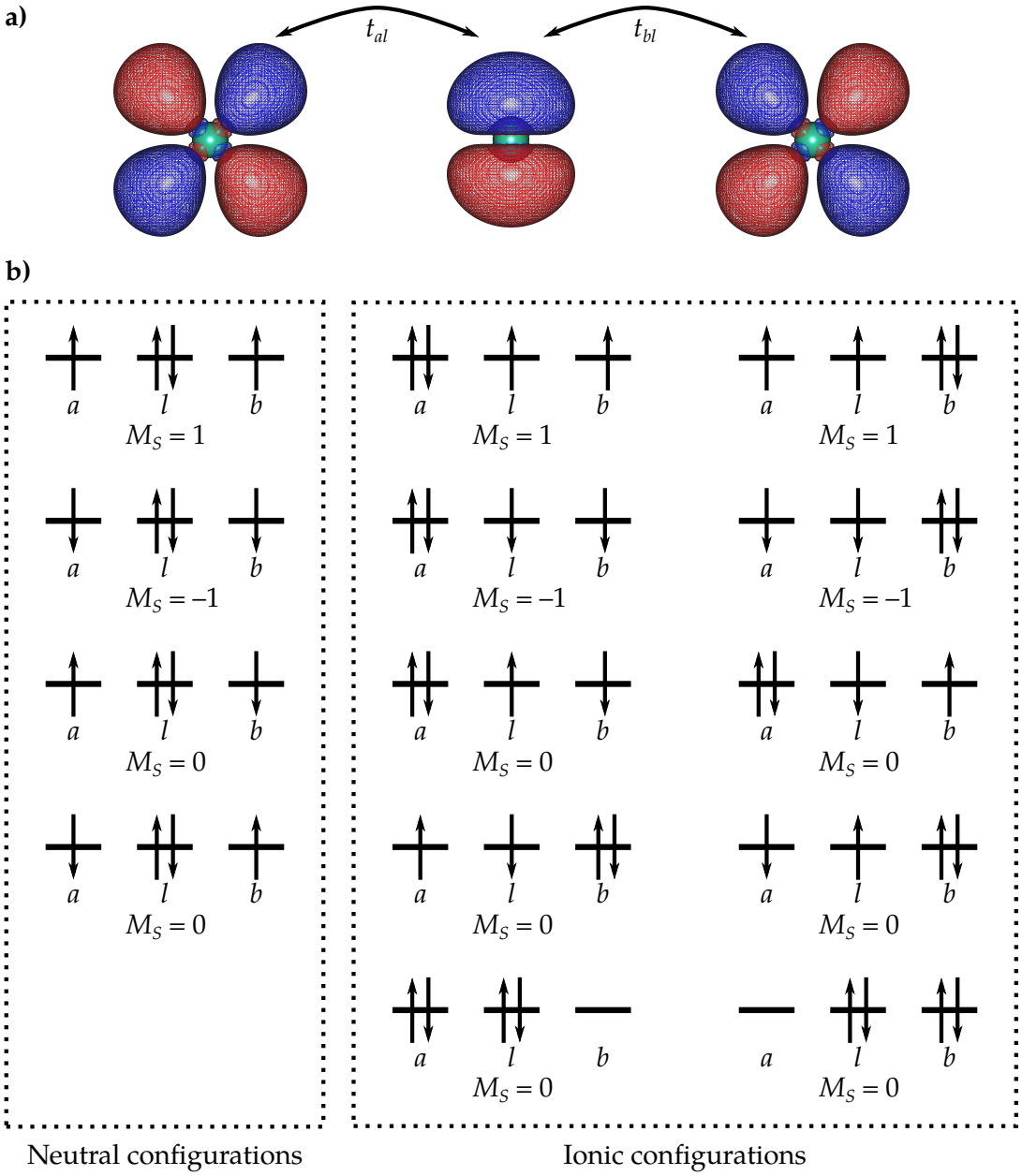

FIGURE 6 **a)** A schematic representation of the superexchange mechanism involving four electrons in three orbitals and **b)** the electron configurations involved in the mechanism.

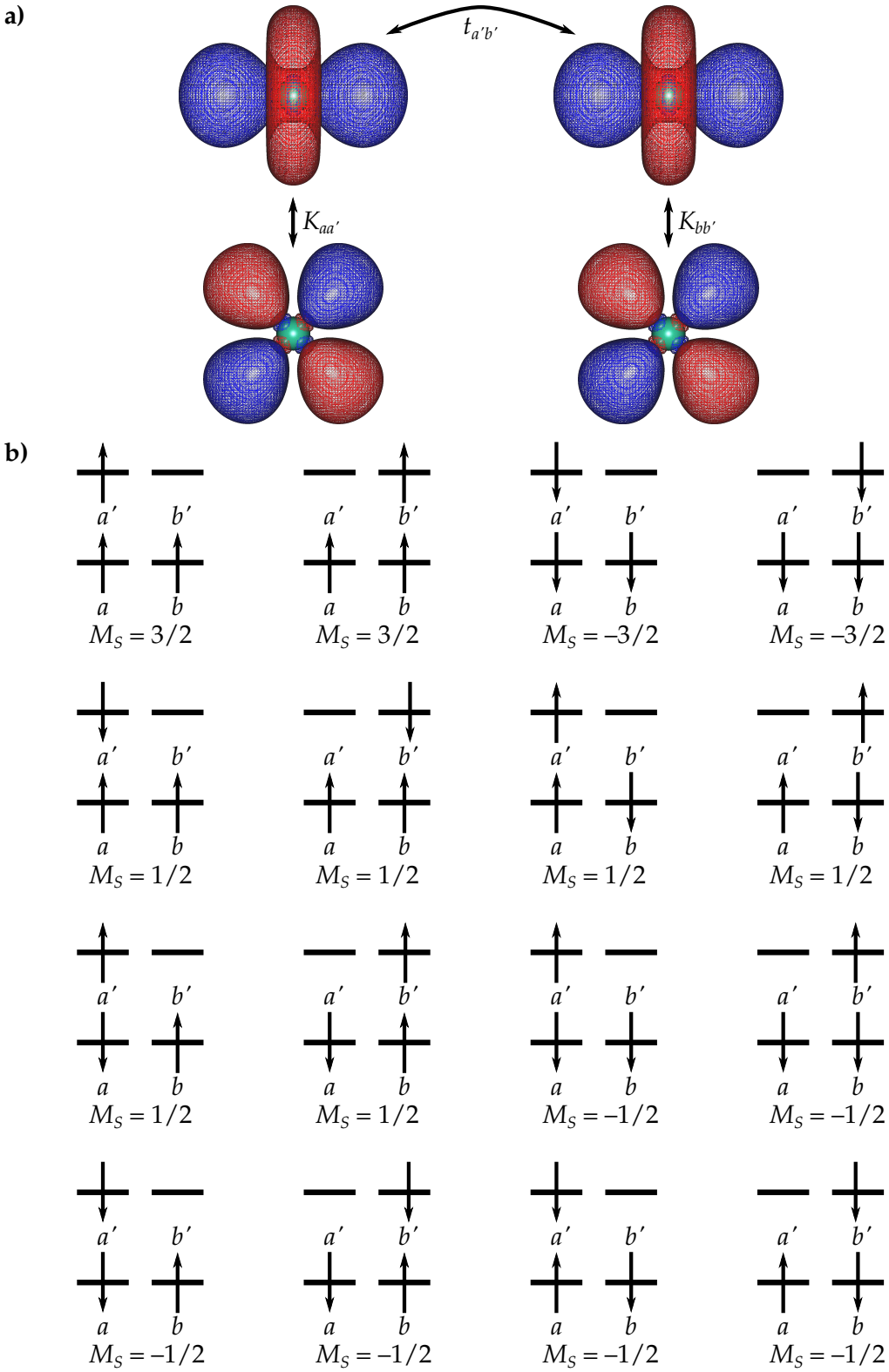

FIGURE 7 **a)** A schematic representation of the double-exchange mechanism involving three electrons in four orbitals and **b)** the electron configurations involved in the mechanism.

or U_b contributes to the energy of all basis states and the energy penalty for electron transfer is $|U_a - U_b|$, which is usually a small quantity. This situation is commonly encountered in conducting materials. If we further assume that the two sites are equivalent (i. e., related by a symmetry operation), $|U_a - U_b| = 0$, and the energy of the localized states is completely defined by the Hund's rule coupling $K_{aa'} = K_{bb'} \equiv K$. In the case when $t_{a'b'} \ll K$, which is considered a requirement for the double-exchange mechanism to be operational, the electron transfer can be considered as a perturbation. To first order, the eigenvalues of the quartet states of (80) are

$$-K \pm t_{a'b'} \tag{81}$$

and those of the four doublet states are

$$-K \pm \frac{t_{a'b'}}{2} \quad \text{and} \quad K \pm \frac{t_{a'b'}}{2} \tag{82}$$

Thus, energies of all the states are centered around the Hund's rule coupling with splitting $\pm t_{a'b'}$ or $\pm t_{a'b'}/2$ for the quartets and doublets, respectively. The energy difference between the lowest quartet state and the lowest doublet state is

$$\Delta E_{\mathrm{ST}} = \frac{|t_{a'b'}|}{2}, \tag{83}$$

which is always positive; thus, double-exchange always stabilizes the high-spin state. This result also holds in the case when the system has higher number of unpaired electrons or when the electrons in the orbitals $\phi_a(\mathbf{r})$ and $\phi_b(\mathbf{r})$ interact weakly via a direct or superexchange mechanism. The more general case will be discussed in section 3.5.4 in terms of spin Hamiltonians.

3.5.4 Spin Hamiltonians for isotropic exchange

The simplest exchange coupled systems consisting of two electron in two orbitals can be described by the Heisenberg–Dirac–van Vleck spin Hamiltonian

$$\hat{H}_{\mathrm{HDvV}} = -J_{ab}\hat{\mathbf{S}}_a \cdot \hat{\mathbf{S}}_b \tag{84}$$

first introduced by Heisenberg[15] and later refined by Dirac,[8] van Vleck,[184,222] and Slater.[223] J_{ab} is an exchange coupling constant, and $\hat{\mathbf{S}}_a$ and $\hat{\mathbf{S}}_b$ are spin operators acting on sites a and b. The product of spin operators has two unique eigenvalues, one corresponding to a singlet state and the other triply degenerate and corresponding to a triplet state. The main purpose of the bilinear operator $\hat{\mathbf{S}}_a \cdot \hat{\mathbf{S}}_b$ is, therefore, to separate the different spin states from each other. The operators $\hat{\mathbf{S}}_a$ and $\hat{\mathbf{S}}_b$ on their own do not serve any physical meaning, and they could equally well be replaced by an operator in orbital space, which interchanges the sites a and b without any effect on the interpretation of the final results.[179] The energy difference between the singlet and triplet states is $J_{ab} = \Delta E_{\mathrm{ST}} = E_{\mathrm{S}} - E_{\mathrm{T}}$. Therefore, a positive exchange coupling constant favors FM interaction and a negative value favors AFM interaction. Comparing this result with equations (77)

and (79) immediately yields the results

$$J_{ab} = 2K_{ab} - {t_{ab}}^2 \left(\frac{2}{U_a - U_{ab}} + \frac{2}{U_b - U_{ab}} \right) \quad \text{and} \tag{85}$$

$$J_{ab} = \frac{4{t_{ml}}^4}{(U_m + \Delta_{ml})^2} \left(\frac{1}{U_m} + \frac{1}{U_m + \Delta_{ml}} \right) \tag{86}$$

for the direct and superexchange mechanisms, respectively, under the approximation discussed in sections 3.5.1 and 3.5.2. $\hat{H}_{\mathrm{HDvV}}$ can be derived from the Hubbard Hamiltonian using the effective Hamiltonian theory.[177,179,224] It should be noted that several forms of $\hat{H}_{\mathrm{HDvV}}$ are used in the literature, where $2J$ might be used instead of J or where the negative sign might be dropped.

The HDvV Hamiltonian can be generalized to the case when $S_a > 1/2$ and/or $S_b > 1/2$. This is most often carried out by simply using the form (84) with no modification other than applying the operators $\hat{\mathbf{S}}_a$ and $\hat{\mathbf{S}}_b$ on larger spins.[24] In this case, the value of the exchange coupling constant can be related to the energy difference between the $S = S_a + S_b$ (high-spin, HS) and $S = |S_a - S_b|$ (low-spin, LS) states as[225]

$$J_{ab} = \frac{E_{\mathrm{LS}} - E_{\mathrm{HS}}}{2S_aS_b + S_b}, \tag{87}$$

where we have assumed (without loss of generality) that $S_a \geq S_b$. If the exchange Hamiltonian in the $S_a, S_b > 1/2$ case is derived from the Hubbard Hamiltonian using effective Hamiltonian theory, in addition to the bilinear term of equation (84), also biquadratic terms of the type $(\hat{\mathbf{S}}_a \cdot \hat{\mathbf{S}}_b)^2$ and possibly higher-order terms can arise,[177,226] which are not necessarily negligible.[227] These terms are usually only considered in the context of *ab initio* calculations, as extracting them from experiment is usually difficult due to correlations between the parameters, which make obtaining a unique fit impossible.

An isotropic spin Hamiltonian has also been derived for double-exchange by Girerd, Münck (GM), and co-workers:[24,224,228]

$$\hat{H}_{\mathrm{GM}} = \left(E_a - J_a\hat{\mathbf{S}}_a \cdot \hat{\mathbf{s}}_a\right) \hat{n}_a + \left(E_b - J_b\hat{\mathbf{S}}_b \cdot \hat{\mathbf{s}}_b\right) \hat{n}_b + d\hat{T}_{ab}. \tag{88}$$

The operator acts in a basis of states $\{|SM_S\rangle_a, |SM_S\rangle_b\}$, where the subscript a or b indicates that the resonating electron is localized at site a or b. The fixed spins at the two sites can have any magnitude but the resonating electron will have $s = 1/2$. The operators $\hat{\mathbf{S}}_a$ and $\hat{\mathbf{s}}_a$ act on the total spin of the fixed electron and the spin of the resonating electron when it is located on site a, and the operators $\hat{\mathbf{S}}_b$ and $\hat{\mathbf{s}}_b$ act analogously at site b. The operators $\hat{n}_a$ and $\hat{n}_b$ return one if the resonating electron is at site a or b, respectively, and zero otherwise. The operator $\hat{T}_{ab}$ connects the two localized states:

$$\hat{T}_{ab}|SM_S\rangle_a = (S + s)\,|SM_S\rangle_b \quad \text{and} \quad \hat{T}_{ab}|SM_S\rangle_b = (S + s)\,|SM_S\rangle_a. \tag{89}$$

E_a and E_b are the zeroth-order energies of sites a and b in the absence of the resonating electron, and d is the effective transfer parameter. If the two sites are identical, d is given as

$$d = \frac{t_{ab}}{2S_0 + 1}, \tag{90}$$

where S_0 is the total spin of the fixed electrons.

3.5.5 Spin Hamiltonians for weak anisotropic exchange

When SOC is weak enough for the spin Hamiltonian approach still to make physical sense but strong enough not be neglected, the exchange coupling is given by the spin Hamiltonian

$$\hat{H}_{\text{aniso}} = -\hat{\mathbf{S}}_a \cdot \mathbf{J}_{ab} \cdot \hat{\mathbf{S}}_b, \tag{91}$$

where $\mathbf{J}_{ab}$ is the exchange tensor and relates the two spin sites in a non-collinear manner. It is convenient to decompose $\mathbf{J}_{ab}$ into contributions from various interactions:[24,175,229,230]

$$\hat{H}_{\text{aniso}} = -J_{ab}\hat{\mathbf{S}}_a \cdot \hat{\mathbf{S}}_b + \hat{\mathbf{S}}_a \cdot \mathbf{D}_{ab} \cdot \hat{\mathbf{S}}_b + \mathbf{d}_{ab} \cdot \hat{\mathbf{S}}_a \times \hat{\mathbf{S}}_b, \tag{92}$$

where the first term is the isotropic part of the exchange interaction described by (84), the middle term is the symmetric anisotropic exchange, and the last is the antisymmetric or Dzyaloshinsky–Moriya (DM) interaction.[229,231] The DM interaction is strictly zero if the spin sites are related by inversion symmetry.

In the case of $S_a, S_b \geq 1$, biquadratic symmetric exchange interaction

$$\hat{\mathbf{S}}_a \otimes \hat{\mathbf{S}}_a \cdot \mathbf{D}_{aabb} \cdot \hat{\mathbf{S}}_b \otimes \hat{\mathbf{S}}_b, \tag{93}$$

where $\mathbf{D}_{aabb}$ is a rank four tensor, should be included into $\hat{H}_{\text{aniso}}$ as well.[230] Higher-order terms for the antisymmetric exchange have also been derived,[232] but will not be discussed here.

3.5.6 Pseudospin Hamiltonians for strongly anisotropic exchange

In the case of strong SOC, no general form of a pseudospin Hamiltonian applicable in all cases has been derived. In such cases each situation has to be considered separately, and the form of the Hamiltonians can be extremely complicated.[179,233,234] In certain special cases, however, general Hamiltonians are available. The first situation is Ising exchange interaction, which takes place under special conditions and can be described by a pseudospin Hamiltonian of the form[235]

$$\tilde{H}^{\text{Ising}}_{\text{aniso}} = -J_{ab}\tilde{S}_{za}\tilde{S}_{zb}, \tag{94}$$

where the pseudospin operators act only on the projection of the pseudospin.

Another case where the Hamiltonian has been derived is the situation where the *LS* coupling is a reasonable approximation to the electronic structure at the two interacting sites and, the angular momentum at the sites can be described by $\hat{\mathbf{J}}$ operators. Within the *LS* coupling, the target space is closed relative to the operator $\hat{\mathbf{J}}$, and the descriptions according to the real angular momentum operators $\hat{\mathbf{J}}$ and the respective pseudospin operators $\tilde{\mathbf{J}}$ are equivalent. The Hamiltonian describing the exchange interaction is then[119]

$$\hat{H}^{\text{LS}}_{\text{aniso}} = \sum_{k,q}\sum_{k',q'} J_{kqk'q'} \frac{\hat{O}_{kq}(\hat{\mathbf{J}}_a)\hat{O}_{k'q'}(\hat{\mathbf{J}}_b)}{O_{k0}(J_a)O_{k'0}(J_b)}, \tag{95}$$

where $O_{kq}(\hat{\mathbf{J}}_a)$ and $\hat{O}_{k'q'}(\hat{\mathbf{J}}_b)$ are Stevens operators. Due to time-reversal symmetry, the sum of the ranks of operators $k + k'$ must be even for all terms. The highest value of the rank k is determined either by $2l_a + 1$, where l_a is the orbital angular momentum of the orbital occupied by the unpaired electrons at site a, or by $2J_a$, depending on which is larger. The highest rank k' is determined in an analogous manner for site b. The number of terms entering the expansion can also be limited by symmetry, but it should be clear that in low-symmetry systems, the number of exchange coupling constants $J_{kqk'q'}$ required to describe the interaction is very large. Expressions for the $J_{kqk'q'}$ parameters in terms of quantities of the generalized Hubbard Hamiltonian is given in ref. 119.

3.6 Dynamic magnetic properties

Slow relaxation of magnetization is the most important characteristic feature of SMMs. The term "slow relaxation" implies non-equilibrium dynamics. Although the features of the electronic structure required for achieving slow relaxation are well-known, especially in the case of monometallic systems, there are serious gaps in the quantitative understanding of the actual dynamics of the relaxation process at a microscopic level. The relaxation is a consequence of the interaction of the magnetic system with the lattice vibrations described as phonons. The widely used theory is based on the seminal work of Orbach published in 1962,[236] which assumes validity of the so-called Debye model[237] and assigns all relaxation interactions to the low-energy acoustic phonons. In the words of Lunghi *et al.*: "Despite its first formulation is more than fifty years old and the fact that a proof of its validity has never been provided, the Debye model remains the basis for the interpretation of every experiment to date."[123] Some very recent work in the field has been carried out to improve our understanding of the models and to relate the model parameters to microscopic or *ab initio* quantities.[122,123,238–241] As the present work is mostly focused on static properties, we will introduce the dynamic properties on a superficial manner and using the widely used qualitative theory. More in-depth discussion is available on a general level in Abragam and Bleaney,[20] focusing on transition-metals in Gatteschi *et al.*[25] and the review published by Atanasov, Neese, and co-workers,[89] and on a more introductory level in the tutorial review by Liddle and van Slageren.[242]

The ZFS (in S-type systems) or the CF splitting (in J-type systems) leads to the splitting of the lowest $(2S + 1)$- or $(2J + 1)$-fold degeneracy of the states, which under optimal conditions form a barrier-like structure of energy levels in terms of the magnitude of the magnetic moment (Figure 8a). The lowest states on the opposite side of the barrier have opposite signs of magnetic moment leading to opposite signs of microscopic, and eventually macroscopic, magnetization. When an external field is applied along one of these magnetization directions, the state with a magnetic moment opposite to the field will have the lowest energy. The system will then relax in such a way that only this side of the

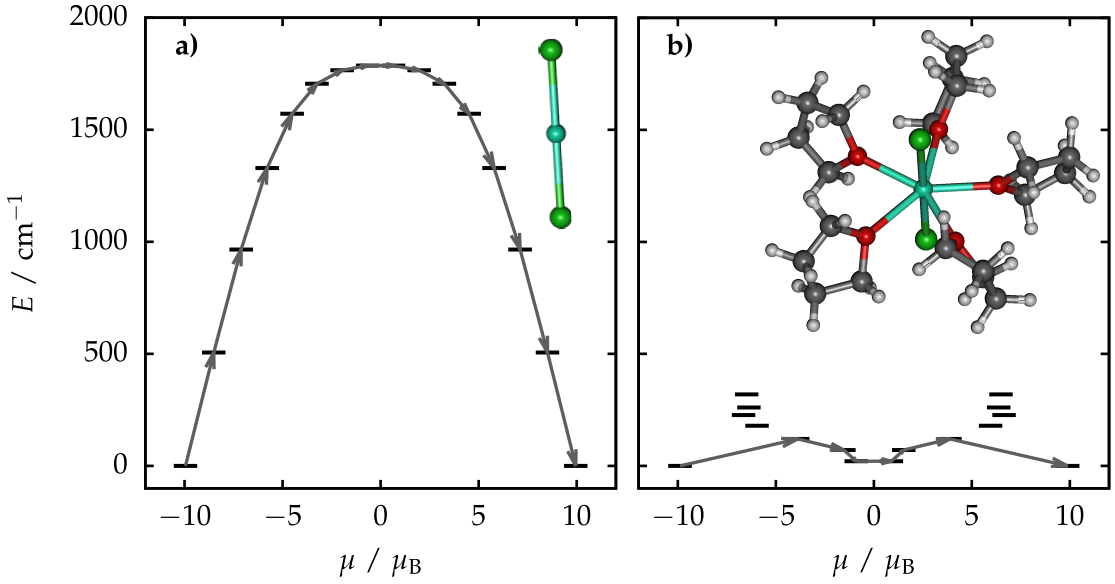

FIGURE 8 Examples of the relaxation of magnetization in SMMs: **a)** the relaxation pathway in an ideal $D_{\infty h}$ symmetric $[DyCl_2]^+$ ion and **b)** a more realistic pathway in a pseudo-D_{5h} symmetric complex. The energetics and the calculated relaxation pathway are unpublished results of the present author. The geometry in **b)** is taken from ref. 243.

barrier has significant population. Once the external field is switched off, the systems will still have an excess magnetization in one direction, creating a non-equilibrium situation that will eventually evolve into an equilibrium where both sides of the barrier have equal populations. In an ideal situation, the relaxation of magnetization would require transitions over the barrier leading to an Arrhenius-like temperature-dependence of the relaxation rate with an "activation energy" corresponding to the barrier height. In reality, however, there is no reason why the magnetization should traverse the entire barrier, but transition between any electronic states are, in principle, possible (Figure 8b). Any transition between the components of the ground doublet (whether it takes place directly or via some intermediate state) requires some magnetic interaction. This can originate from dipolar or weak exchange coupling between neighboring ions, from the hyperfine coupling between nuclear spins, or from the modulation of the CF by lattice vibrations, which through SOC translate into an oscillating magnetic field. The actual transitions imply exchange of energy with the phonons of the crystal through spin–phonon coupling or quantum tunneling of magnetization (QTM).

QTM takes place when a transverse (i. e., perpendicular to the magnetic z axis) external magnetic field, usually originating from dipolar or hyperfine coupling, couples the two components of the ground doublet.[25,244] In the case of Kramers systems, this can only take place if the $\tilde{\mathbf{g}}$-tensor describing the Zeeman interaction with the doublet has non-zero transverse components g_x and g_y in the coordinate frame of the magnetic axis.[105,109] In low-symmetry systems, this is usually the case. The $g_{x,y}$ values of all doublets are strictly zero in the axial point group symmetries $D_{\infty h}$ and $C_{\infty v}$, and some of them will be strictly zero when

the point group has a threefold or higher rotational axis.[105] If no point group symmetry is present but the system has a very axial CF, usually the values of $g_{x,y}$ in the lowest doublets are negligibly small.[V, VI, 111–114] The mixing of the doublets by magnetic field induces a weak splitting, and QTM between the states can occur. In non-Kramers systems, QTM is possible always when the doublets are not exactly degenerate (i. e., not Ising doublets). This is the case in all low-symmetry systems. Again, in point group symmetries $D_{\infty h}$ and $C_{\infty v}$, all doublets are exactly degenerate and no QTM takes place, and in point group symmetries with a threefold or higher rotational axis, some doublets may be Ising doublets.[245] The QTM process can in many cases be suppressed by applying a static external field in the z direction, which decouples the states.

Spin–phonon transitions can take place either directly between the two components of the doublet (direct process), via an excited doublet (Orbach process) or via a virtual state (first- and second-order Raman processes). The spin–phonon factor in the direct process is proportional to the third power of the energy gap between the two states[20] and is therefore not present in Kramers systems due to the so-called van Vleck cancellation[246] unless the components of the lowest doublet are split by an external magnetic field. In non-Kramers systems, the direct process is operative, but usually the density of phonons in the relevant energy range is so low that this process is not competitive with the other relaxation mechanisms. In the Orbach process, one phonon first excites the systems to an excited state, which is then relaxed to the ground doublet via an emission of another phonon. The Orbach relaxation process from one component of the ground doublet to the other can include several elementary excitation and de-excitation steps (i. e., climbing the barrier). This type of transition can be interpreted as several consecutive direct transitions. In the first-order Raman process, the magnetic system interacts with a superposition of two lattice waves with an energy difference which matches that of the electronic transition. The electronic transition can be interpreted as taking place via a virtual state similar to the Raman mechanism in optical spectroscopy. In the second-order Raman process, both the electronic system and the phonon system undergo a transition via a virtual state. Due to the presence of the virtual state, the transition does not require the energy of the interacting phonons to match the energy difference between some real electronic states. The different spin-phonon relaxation mechanisms are summarized schematically in Figure 9.

The dominant relaxation process in *S*-type 3d transition-metal SMMs is the Orbach process, and the relaxation usually takes place over the full barrier. In lanthanide systems, QTM is usually very strong and needs to be suppressed by correct design of the CF environment or by applying an external field. Depending on the system, various mechanisms might become dominant.[247] In actinide SMMs, the relaxation mechanisms are largely unknown.[248]

The temperature-dependence of the time constant τ of the total relaxation process arising from different relaxation mechanisms can be written as

$$\tau^{-1} = \tau_{\mathrm{QTM}}^{-1} + AB^{n_1}T + CT^{n_2} + {\tau_0}^{-1} \exp\left(-\frac{U_{\mathrm{eff}}}{k_B T}\right), \tag{96}$$

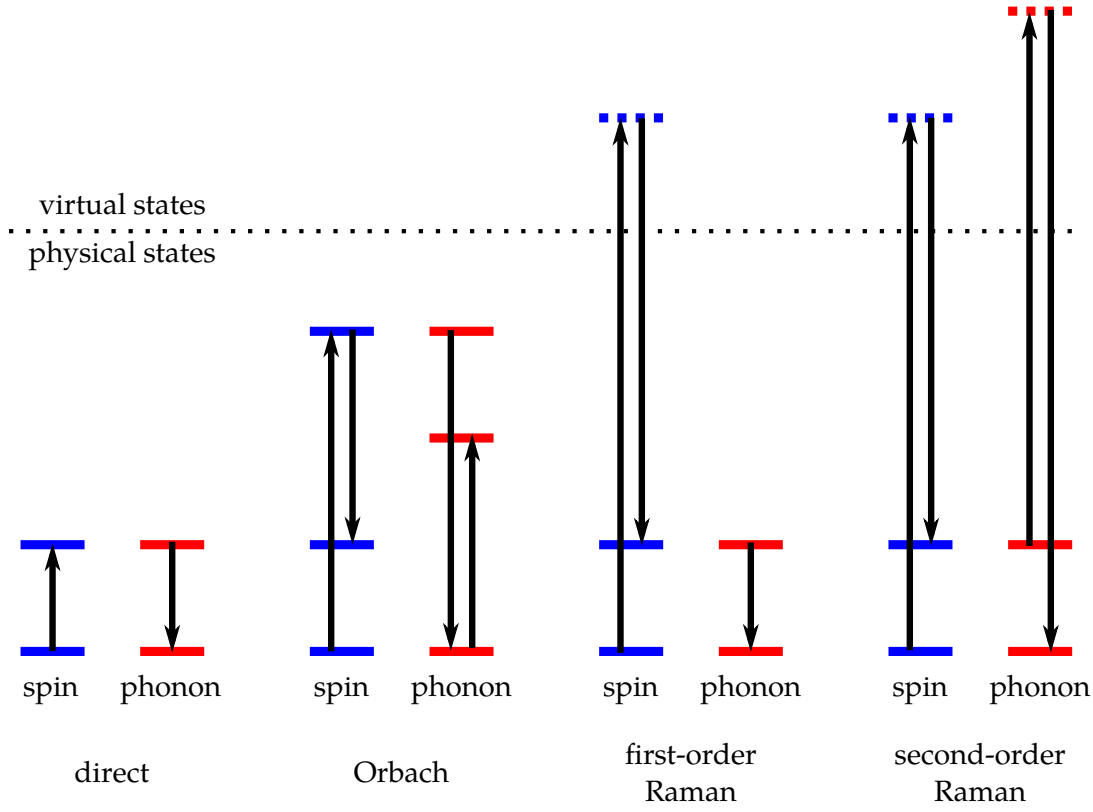

FIGURE 9 A schematic representation of the different spin-phonon relaxation mechanism operational in SMMs. Blue levels show transitions in the spin system, whereas red levels indicate transitions in the phonon system.

where T is the temperature, U_{eff} is the effective barrier height determining the Arrhenius-like behavior, B is the field strength, and τ_{QTM}, A, C, n_1, n_2, and τ_0 are parameters of the model. The powers n_1 and n_2 can be given predefined integer values under certain conditions,[20] or they can be considered as adjustable parameters. The parameters are not, in general, mutually independent. The first term in (96) describes the QTM, the second term describes the direct relaxation processes, the third term describes the Raman processes, and the last term describes the Orbach processes. In polymetallic systems, each magnetic site has an individual set of relaxation processes along with the relaxation processes of the coupled system.[249] The temperature-dependence of the relaxation is usually studied by constructing a $\log \tau$ vs. T^{-1} plot based on experimental results. In monometallic systems, if the direct and Raman processes are negligible, which is usually the case for Kramers or Ising doublets and relatively low temperatures, the plot will have a linear region at higher temperatures due to the Orbach term and a temperature-independent term at low temperatures due to the QTM term. A linear Arrhenius-type fit to the linear region yields the exponential prefactor τ_0 and the effective barrier height U_{eff}. In polynuclear systems, the plot may have several different linear regions due to the different sites. In the case when Raman processes are active, the plot will deviate from linearity. It is in principle possible to extract the full set of parameters τ_{QTM}, A, C, n_1, n_2, and τ_0 by fitting the data,

but the risk of a non-unique fit due to cross-correlations is very high. Therefore, usually attempts are made to suppress some of the processes by the experimental conditions (i. e., specific temperature range or magnetic dilution).

The value of U_{eff} is the characteristic property of SMMs most often reported in the literature. Effective barrier heights have been reproduced, at least at a semi-quantitative level, by modeling the dynamics of the system based on quantities calculated from first principles.[114] The effective barrier height is, however, usually considerably higher than the actual magnetic blocking temperature. For example, the current record for blocking is 60 K, whereas the respective barrier height is 1837 K (given in here in units kelvin for comparison),[VI,114] which differ by a factor of 30. The magnetic blocking temperature has *never* been calculated, qualitatively or otherwise, from first principles nor derived from theory at any level of approximation. This indicates that the theory related to the magnetic relaxation of SMMs still remains rather incomplete.

3.7 On experimental techniques

Although the present work is purely focused on theory, the aim of any theory is to explain experimentally observed phenomena; therefore, the theory will always be discussed in the context of experiment. Thus, we will very briefly describe the experimental techniques, which provide the data that are to be explained by the theory. The emphasis is placed on the types of data these experiments provide and the actual experimental procedures will not be described in any detail. Further information is available, for example, in Benelli and Gatteschi,[26] Gatteschi *et al.*,[25] in the book chapter by Pedersen *et al.*[250] and the references therein.

The two most widely used experimental techniques in the study of the magnetic properties of molecular systems are SQUID magnetometry and EPR spectroscopy, although other methods are used as well.[250] The first is perhaps the most widely used technique in molecular magnetism. SQUID, or a superconducting quantum interference device, is a magnetometer capable of detecting extremely weak magnetic fields. The experiments usually measure the magnetization either as a function of temperature or as a function of the magnetic field strength. The most often reported data are the temperature-dependent χT product (calculated from the magnetization by $\chi = {}^{M}/_{B}$) and the isothermal field-dependent magnetization. The χT data is usually measured in a temperature range from liquid helium temperature to ambient conditions, and the magnetization is measured in temperatures of a few kelvins above absolute zero. The χT plot can be fitted to a model to obtain various pseudospin Hamiltonian parameters. In highly anisotropic systems, the problem is that the number of parameters is large and the models becomes overparameterized very easily. Fitting the χT product is the main method for obtaining experimental values for isotropic exchange coupling constants when the number of unique parameters is

reasonably small. Additional information from optical spectra, NMR spectra, and elastic neutron scattering measurements can also be used to reduce the number of free parameters. The isothermal magnetization at high fields can be used to extract the ground state (pseudo)spin.

Dynamics of the relaxation of magnetization can also be examined by SQUID magnetometry. In the case of sufficiently slow relaxation, the two most often used experiments measure the magnetic hysteresis and the divergence of the field-cooled (FC) and zero-field-cooled (ZFS) magnetization. In a hysteresis measurement, the magnetization is measured as a function of the field strength at some fixed ramping speed by first bringing the field to the point of magnetic saturation and then ramping the field down to the opposite direction. In the case of slow relaxation, the sample should remain magnetized once the field is ramped down to zero and show some coercivity to magnetization in the opposite direction when the field is further ramped down. This experiment gives values of the remnant magnetization (the value of magnetization once the field is brought down to zero) and the coercive field (the strength of the magnetic field required to reverse the magnetization). In the FC/ZFC experiment, the magnetization is measured twice, first by lowering the temperature with an external magnetic field and then repeating the measurement without the field. At some temperature the two curves will diverge from each other, indicating a point where the relaxation of the magnetization becomes blocked. Both the divergence temperature in the FC/ZFC experiment and the highest temperature where hysteresis is observed are used as values for the blocking temperature of an SMM. One should be careful to note that the results of both experiments depend on some arbitrarily defined ramping speed of the field strength and the values measured for two different systems are therefore not necessarily comparable.

In the case when the slow relaxation dynamics are too fast compared to the ramping speed of the measurement device, the dynamics can be probed by alternating current (ac) SQUID magnetometry. The alternating current creates an oscillating magnetic field, and the frequency of these oscillations can be varied. If the magnetization relaxes more slowly than the field oscillates, the magnetization starts to "lag behind" the field oscillations, and this can be observed in the so-called out-of-phase component of the susceptibility. Data extracted from these measurements can also be fitted to empirical models of the relaxation to obtained the effective barrier height (U_{eff}) and the parameters describing the QTM and Raman relaxation processes. It should also be noted that a temperature-dependent frequency shift in the ac susceptibility measurement cannot be attributed to the formation or deformation of domain walls in a bulk magnetic (which also lead to magnetic hysteresis and divergence of FC/ZFC plots), but is an indication of SMM or spin glass behavior.

EPR spectroscopy measures the transition between different states split by the Zeeman interaction.[20] If sufficiently well resolved, the EPR spectrum of a given complex shows a large number of peaks and, in principle, contains more information than a χT plot, which is often just a single slope with a varying gradient. Simulation of the observed EPR spectra with a model Hamiltonian,

therefore, allows the extraction of a much larger number of parameters than can be reliably obtained from a χT plot. EPR spectra are also considerably more sensitive to anisotropy effects than susceptibility measurements are even in the presence of strong isotropic exchange coupling. In solid-state measurements, it is possible to extract all elements of the $\tilde{\mathbf{g}}$ and $\mathbf{D}$ tensors of the ground state. In magnetically diluted samples, such as in solvated systems or complexes doped into a diamagnetic lattice, it is possible to also deduce the hyperfine structure of the spectrum that results from the coupling of electron spin with the nuclear spin. This gives valuable information on the delocalization of the electron spin over the molecule and is especially useful in the analysis of organic radical systems. In the context of organic systems, EPR is sometimes referred to as electron spin resonance (ESR).

4 WAVE-FUNCTION-BASED QUANTUM CHEMISTRY OF STRONGLY CORRELATED SYSTEMS

The purpose of the present chapter is to introduce wave-function-based (as opposed to density-functional-based) computational methods, which are widely used in the field of molecular magnetism. Practically all molecular magnetic systems studied by quantum chemistry have very strong electron correlation effects and are hence called strongly correlated. This means that the systems cannot be described by mean-field independent particle models, and the necessary treatment even at zeroth order is rather complicated. Emphasis is based on introducing quantum chemical methods used in the present work, and other methods are simply mentioned in passing. The emphasis is also placed on the implementations (and especially on the differences in the implementations) in ORCA[251,252] and MOLCAS[253,254] codes, which are the two most commonly used sets of programs in the field of molecular magnetism. Much of the methodology is available in other computer codes as well, most notably in MOLPRO,[255] possibly with some variations, but these will not be discussed. The aim of the text is to provide the reader with sufficient understanding on why a certain method might be favored over another and what challenges one faces when applying these methods in practice.

In molecular electronic structure theory, the quantum system of interest consists of N electrons interacting with each other, with atomic nuclei, and possibly with some external fields. Usually we make the so-called Born–Oppenheimer approximation[129,256,a] where we assume that the nuclear and electronic degrees of freedom are not coupled and we can, therefore, solve the Schrödinger equation of the interacting electrons independent of the motion of the nuclei. Once the electronic problem has been solved, derivatives of the electronic energy

[a] The standard citation for Born–Oppenheimer approximation is the 1927 paper by Born and Oppenheimer. The approximation is implied in the paper, but it is neither purposefully derived nor clearly apparent in the equations. A clear derivation is available, for example, in Jensen's book.[129]

and nuclear–nuclear repulsion energy relative to displacements of the nuclei can be calculated, and the nuclear wave function can then be constructed in a semi-classical manner, which is usually sufficiently accurate for chemical problems.[129,257] Furthermore, we usually either neglect relativistic effects completely, or, assume that they can be sufficiently well reintroduced as some simple correction to the non-relativistic equations. Thus, the molecular electronic structure problem consists of analyzing a system of N electrons interacting with each other and some local multiplicative external potential V_{ext}. In the present work, we are only interested in time-independent properties and will therefore only consider systems where V_{ext} is independent of time. External magnetic field will be considered separately, and we will therefore further assume that V_{ext} contains only electric fields.

4.1 Basics of electronic structure calculations

4.1.1 Variation of energy

The essence of electronic structure calculations lies in the variational principle,[144,145,258,259] which states that the energy expectation value of any approximate wave function must be greater than or equal to the ground state energy of the system and that the equality only holds if the approximate wave function is the ground state wave function. Therefore, the ground state energy and wave function of a given system for which the Hamiltonian is known, can be approximated by minimizing the energy expectation value in terms of some variation in the wave function. The parameters that are obviously suitable for variation are the CI coefficients in (8), but another important set of parameters, which we have not discussed so for, are found in the spatial orbitals $\{\phi_i(\mathbf{r})\}$.

Exact expressions for the spatial orbitals are not, in general, available, and they are usually expanded in some predetermined basis set:

$$\phi_p(\mathbf{r}) = \sum_m c_{mp}\chi_m(\mathbf{r}), \tag{97}$$

where the expansion coefficients c_{mp} are usually referred to as the MO coefficients. In molecular calculations, a good compromise between accuracy, computational efficiency, and conceptual simplicity can be obtained by using atomic orbital (AO) like basis functions as the one-particle basis set. It is well-known that the atomic orbitals of a hydrogen-like atom consist of a spherical harmonic and a radial function with exponential decay. In the context of atomic calculations, Slater suggested the use of radial functions with exponential decay.[260] Such functions, however, are rarely used in molecular calculations (with some very notable exceptions[261,262]) due to the unfavorable mathematical properties of the exponential functions when considering computational efficiency. Boys first suggested using a Gaussian functions instead of an exponential one,[263] and these ideas were greatly developed by Pople in the following decades.[264–277] Gaussian

functions have much more favorable mathematical properties than exponential functions; namely, the product of two Gaussian functions is a single Gaussian centered between the two original functions. Even though usually a much larger number of Gaussian functions are needed to sufficiently converge the results in terms of the basis set expansion in (97),[133] the availability of analytical expressions for Gaussian products leads to better scaling in terms of overall cpu time. In modern calculations, the set of basis functions for a given atom is considerably larger than the number of corresponding atomic orbitals. The valence orbitals are usually split into so-called double-ζ, triple-ζ, etc. sets of orbitals, which indicate that there are two, three, etc. sets of valence orbitals for each atom. Usually higher angular momentum functions, known as polarization functions, are also added to the basis sets to afford more variational freedom in terms of polarization and electron correlation (see section 4.1.3 *vide infra*). Sometimes, functions with slowly decaying tails, known as augmentation functions, are also added to the basis if molecular properties related to diffuse electron densities are of interest.[129] Usually, preoptimized basis sets are used, and each basis function consists of several Gaussian functions contracted with predetermined coefficients.

The ground state energy can be determined by minimizing the energy functional

$$E = \min_{\mathbf{C},\mathbf{c}} E[\psi(\mathbf{C},\mathbf{c})] = \min_{\mathbf{C},\mathbf{c}} \frac{\langle \psi(\mathbf{C},\mathbf{c})|\hat{H}|\psi(\mathbf{C},\mathbf{c})\rangle}{\langle \psi(\mathbf{C},\mathbf{c})|\psi(\mathbf{C},\mathbf{c})\rangle}. \tag{98}$$

Vector $\mathbf{C}$ and matrix $\mathbf{c}$ contain the CI expansion coefficients of equation (8) and the MO orbital expansion coefficients of equation (97), respectively. Considering the Hamiltonian within the Born–Oppenheimer approximation ($\hat{H} = \hat{H}_{\mathrm{BO}}$), neglecting relativistic terms, and using (18) and (19), the energy functional can be written as

$$E = \min_{\mathbf{C},\mathbf{c}} \left[\sum_{p,q} h_{pq}\gamma_{pq} + \frac{1}{2} \sum_{p,q,r,s} (pq|rs)\Gamma_{pqrs} \right], \tag{99}$$

where

$$h_{pq} = \int \phi_p^*(\mathbf{r}) \left(-\frac{1}{2}\nabla_p^T \cdot \nabla_q + V_{\mathrm{ext}}(\mathbf{r}) \right) \phi_q^*(\mathbf{r}) \mathrm{d}\mathbf{r}. \tag{100}$$

In the minimization, the density matrices γ_{pq} and Γ_{pqrs} depend only on the CI coefficients, whereas the one- and two-particle integrals depend only on the MO coefficient matrix $\mathbf{c}$.

The energy expression (99) can be minimized by making it stationary with respect to the MO and CI coefficients. The latter is straightforward, as the CI coefficients enter the energy expression in a linear fashion and the problem can be cast into a simple eigenvalue problem:[127,133,278]

$$\mathbf{H}_{\mathrm{BO}}\mathbf{C}_A = E_A\mathbf{C}_A, \tag{101}$$

where $\mathbf{H}_{\mathrm{BO}}$ is a matrix representing the Born–Oppenheimer Hamiltonian in configuration basis, and the index A runs over different pairs of eigenvalues (E_A) and eigenvectors ($\mathbf{C}_A$). Optimization of the MO coefficients is less straightforward as

they enter the equations in a non-linear manner and can only be solved iteratively. Furthermore, the orbitals must be kept orthogonal during the optimization procedure, which can be achieved either by introducing a Lagrange multiplier[127,129,278] or by carrying out the optimization in terms of unitary rotations.[133,134,150] Making (99) stationary with respect to the MO coefficients leads to effective one-particle equations known as the self-consistent field (SCF) equations:

$$\sum_p \hat{F}_{pq}\phi_q(\mathrm{r}) = \sum_p \epsilon_{pq}\phi_q(\mathrm{r}), \tag{102}$$

where $\hat{F}_{pq}$ is the Fock operator and the ϵ_{pq} are Lagrange multipliers. The Fock operator is defined as

$$\hat{F}_{pq} = \gamma_{pq}\hat{h}_C + \sum_{r,s}\Gamma_{pqrs}\left(\hat{J}_{rs} - \hat{K}_{rs}\right). \tag{103}$$

The operators

$$\hat{J}_{rs}\phi_q(\mathbf{r}_1) = \int \frac{\phi_r^*(\mathbf{r}_2)\phi_s(\mathbf{r}_2)\mathrm{d}\mathbf{r}_2}{|\mathbf{r}_1 - \mathbf{r}_2|}\phi_q(\mathbf{r}_1) \tag{104}$$

$$\hat{K}_{rs}\phi_q(\mathbf{r}_1) = \int \frac{\phi_r^*(\mathbf{r}_2)\phi_q(\mathbf{r}_2)\mathrm{d}\mathbf{r}_2}{|\mathbf{r}_1 - \mathbf{r}_2|}\phi_s(\mathbf{r}_1) \tag{105}$$

are the Coulomb and the exchange operators, respectively. The letter J used for the Coulomb operator should not be confused with an exchange coupling constant. The Fock operator only contains one-electron operators, but as can be seen from (104) and (105), all of the orbitals are required to construct the Coulomb and exchange operators; thus, the effective one-particle equations must be solved iteratively. This means that some initial guess of the orbitals is first made, and then all one-particle equations are solved to produce a new set of orbitals. The new Fock operator is then constructed from these orbitals, and the procedure is repeated until the orbitals no longer change (i. e., the equations become self-consistent). In practice, such a naïve SCF procedure rarely leads to convergence, and a convergence acceleration scheme or more complex SCF algorithm is required to bring the equations into self-consistency.[129,133]

If the expansions in both (8) and (97) are complete (i. e., infinitely long), E is the exact lowest eigenvalue of $\hat{H}_{\mathrm{BO}}$, and this is called the full CI (FCI) limit. Such a calculation is impossible to perform in practice as we are always constricted to a finite expansion of the MOs in (97), and this then results in a finite number of one-particle states. Thus, only a finite number of configurations can be constructed, and the CI expansion (8) will also be finite. If the full CI expansion is constructed in this finite one-particle basis, the limit is called the complete CI limit (CCI). CCI can be considered as FCI in a subspace of the complete Fock space. It should be noted that in the literature, the term FCI is often used for CCI. Although the CCI method offers the most accurate results in any given finite one-particle basis, the length of the CI expansion becomes untractable for all but the smallest of molecular systems, such as diatomics or the water molecule. Some approximation to the CI expansion is, therefore, necessary to perform calculations on larger molecular systems.

4.1.2 The Hartree–Fock method

The simplest approximation to the CCI problem is to only include one state in the CI expansion. This state corresponds to the ground electron configuration constructed by occupying the orbitals according to the *aufbau* principle, and the resulting approximation is called the Hartree–Fock method[13,124,126–128,279,280,b]. A single configuration is the exact solution for an ensemble of non-interacting fermions; therefore, if the one-particle interactions are much stronger than the electron–electron repulsion, this single-configuration approximation should be reasonable. Indeed, the HF method is remarkably successful, and for many chemical problems, it provides qualitatively correct results.[129,133,257] The HF method is most accurate in cases where the ground configuration is well-separated in energy from any excited configuration. In the presence of degenerate electronic states, the model fails completely. Since the field of molecular magnetism almost exclusively works with systems with near-degenerate electronic states, the HF model is all but useless in the present work. The theory, however, provides a useful reference for the discussion on DFT-based methods in Chapter 5; therefore, the HF method will be briefly introduced here.

The reference state consists of only a single configuration; thus, the possible orbital ONs are $n_{p\sigma} = 0$ or $n_{p\sigma} = 1$. The unoccupied orbitals are usually referred to as virtual orbitals in the context of quantum chemistry. It turns out that all density matrix elements with virtual indices are zero; consequently, the summations in the energy expression (99) only need to run over the occupied orbitals.[133] The single-configuration approximation greatly simplifies the structure of the density matrices, and the ground state HF energy is given as

$$E_{\mathrm{HF}} = \min_{\mathbf{c}} \left(\sum_{p}^{N^\alpha} h_{pp} + \sum_{p}^{N^\beta} h_{\bar{p}\bar{p}} + \frac{1}{2} \sum_{p,r}^{N^\alpha} [(pp|rr) - (pr|rp)] \right. \\ \left. + \frac{1}{2} \sum_{p,r}^{N^\beta} [(\bar{p}\bar{p}|\bar{r}\bar{r}) - (\bar{p}\bar{r}|\bar{r}\bar{p})] + \frac{1}{2} \sum_{p,r}^{N^\alpha, N^\beta} (pp|\bar{r}\bar{r}) \right), \tag{106}$$

where N_α and N_β are the number of α and β electrons, respectively. The orbitals are considered as unrestricted, and the bar over the orbital indices in the two-electron integrals indicates a β orbital and the lack of a bar an α orbital. The two types of two-electron integrals appearing in (106), $(pp|rr)$ and $(pr|rp)$, are known as the Coulomb and exchange integrals according to the operators (104) and (105) used to generate them.

The minimization leads to two sets of effective one-particle equations, one

[b] We are citing here, in addition to the papers of Hartee and Fock, also the papers by Slater. By all fairness, the method should be called Hartree–Slater–Fock method as John C. Slater contributed to the development of the theory *at least* as much as Douglas Hartree did. A summary of the contributions from various authors into the development of the HF method in the late 1920's is given in the section "History of the determinental method" in Slater's MIT technical report from 1953.[14]

for the α orbitals and another for the β orbitals:

$$\hat{F}^{\alpha}_{pp}\phi_{p\alpha}(\mathbf{r}) = \epsilon_{p\alpha}\phi_{p\alpha}(\mathbf{r}) \quad \text{and} \quad \hat{F}^{\beta}_{pp}\phi_{p\alpha}(\mathbf{r}) = \epsilon_{p\beta}\phi_{p\alpha}(\mathbf{r}), \tag{107}$$

which are written here in the so-called canonical form where the orbitals are transformed in such a way that they are eigenfunctions of the Fock operator.[127,129] The eigenvalues $\epsilon_{p\sigma}$ can be interpreted as the orbital energies. The Fock operators $\hat{F}^{\alpha}_{pp}$ and $\hat{F}^{\beta}_{pp}$ can be written as:

$$\hat{F}^{\alpha}_{pp} = \hat{h}_C + \sum_{r}^{N^{\alpha}} \left[\hat{J}^{\alpha\alpha}_{rr} - \hat{K}^{\alpha\alpha}_{rr}\right] + \sum_{r}^{N^{\beta}} \hat{J}^{\beta\beta}_{rr} \quad \text{and} \tag{108}$$

$$\hat{F}^{\beta}_{pp} = \hat{h}_C + \sum_{r}^{N^{\beta}} \left[\hat{J}^{\beta\beta}_{rr} - \hat{K}^{\beta\beta}_{rr}\right] + \sum_{r}^{N^{\alpha}} \hat{J}^{\alpha\alpha}_{rr}. \tag{109}$$

Inserting the MO expansion in (97) into (107) gives two coupled matrix equations

$$\mathbf{F}^{\alpha}\mathbf{c}^{\alpha} = \mathbf{S}\mathbf{c}^{\alpha}\boldsymbol{\epsilon}^{\alpha} \quad \text{and} \quad \mathbf{F}^{\beta}\mathbf{c}^{\beta} = \mathbf{S}\mathbf{c}^{\beta}\boldsymbol{\epsilon}^{\beta}, \tag{110}$$

where $\mathbf{F}^{\alpha}$ and $\mathbf{F}^{\beta}$ are matrix representation of the α and β Fock operators in the AO basis, $\mathbf{c}^{\alpha}$ and $\mathbf{c}^{\beta}$ are matrices of the MO expansion coefficients c_{mp} in (97), $\mathbf{S}$ is an overlap matrix of the AO basis functions ($S_{mn} = \langle\chi_m(\mathbf{r})|\chi_n(\mathbf{r})\rangle$), and $\boldsymbol{\epsilon}^{\alpha}$ and $\boldsymbol{\epsilon}^{\beta}$ are diagonal matrices containing the eigenvalues $\epsilon_{p\alpha}$ and $\epsilon_{p\beta}$. Equations (110) are known as the Pople–Nesbet equations[281] and are essentially a generalized eigenvalue problem, which can be solved using standard linear algebra techniques.[127]

In the literature, the HF method is most often given in its restricted formulation, where the system has an equal number of α and β electrons and each pair of electrons shares a spatial orbital. The formulation of the theory is very similar. The main difference is that the summation runs over the electron pairs and, therefore, only runs up to $N/2$, where N is the total number of electrons. The ground state energy is given as

$$E_{\mathrm{HF}} = \min_{\mathbf{c}} \left(\sum_{p}^{N/2} h_{pp} + \sum_{p,q}^{N/2} [2(pp|qq) - (pq|qp)] \right) \tag{111}$$

The minimization leads to a set of $N/2$ one-particle equations with the Fock operator

$$\hat{F}^{\mathrm{RHF}}_{pp} = \hat{h}_C + \sum_{r}^{N/2} \left[2\hat{J}_{rr} - K_{rr}\right]. \tag{112}$$

We have used here the superscript RHF to explicitly state that this is the HF Fock operator in the closed-shell or restricted case. Expansion of the MOs leads to a single matrix equation

$$\mathbf{F}\mathbf{c} = \mathbf{S}\mathbf{c}\boldsymbol{\epsilon}, \tag{113}$$

which is known as the Roothan–Hall equation.[282,283]

The most computationally expensive part of a HF calculations is the generation of the two-electron integrals, and the method formally scales as $\mathcal{O}({N_{\text{basis}}}^4)$, where N_{basis} is the number of basis functions. The number of integrals is so large that for moderate or large systems, it is not usually feasible to store them on disk, and they are evaluated as they are needed. The Fock operator is usually constructed in an incremental manner, which means that not all integrals need to be calculated at every iteration,[133] which brings the scaling down. The Coulomb integrals can also be evaluated more efficiently using the so-called density fitting[284–289] or resolution of identity (RI)[290–296] approximations, which can significantly reduce the computational costs. The exchange integrals are more difficult to evaluate in an efficient manner, but Weigends RI-JK approximation[297] and the chain of spheres exchange (COSX) method of Neese and co-workers[298,299] can make the evaluation of integrals very efficient. The RI approximation can be considered a special case of the Cholesky decomposition (CD) method of integral evaluation, which can also be used to hasten the integral evaluation.[300–302] CD employs a single parameter to determine the level of approximation, whereas the RI approximation is based on preconstructed density fitting (or auxiliary) basis sets.

4.1.3 Electron correlation

The single-configuration approximation in the HF method leads to a model where N electrons move in a mean-field potential formed by the other electrons. The movement of same-spin electrons is correlated due to the Pauli principle, which has been enforced on the Fock space state by the antisymmetrizing operator. The opposite-spin electrons are not correlated in any way. Thus, the HF model includes the Fermi correlation, resulting from antisymmetry, but does not take into account the Coulomb correlation, resulting from electrostatic interaction, in any way.[129,151,303] The energy not accounted by the HF method is accordingly called the correlation energy (E_{corr}) and is defined as

$$E_{\text{corr}} = E_0 - E_{\text{HF}}, \tag{114}$$

where E_0 is the ground state energy corresponding to the Born–Oppenheimer Hamiltonian (with some relativistic correction possibly included). The definition of E_{corr} in (114) was originally proposed by Löwdin[141] and is the one most often used in the context of wave-function-based quantum chemistry, although it is not the only one;[304] in DFT a different definition is used. The correlation energy is always negative and according to the variational principle accounting for E_{corr} will always bring the model closer to the exact solution. In the Fock space, the correlation can be interpreted as the mixing of different ON vectors (i. e., configurations) and in the Cartesian space as the reduction of electron density in the vicinity of a given electron.

Molecular systems can be very roughly divided into two categories: single-reference systems and multireference systems. If a system is a single-reference system, it means that the HF method provides a qualitatively correct picture

of the relevant physics, and the electrons can be considered to a very good approximation as independent particles interacting with some mean-field potential. In the case of a multireference system, the independent particle picture breaks down, and the HF approximation often provides results that are incorrect even at a qualitative level. Thus, the importance of electron correlation is much greater in multireference systems, and such systems are said to be strongly correlated. Likewise, single-reference systems are said to be weakly correlated. Of course, no distinct border can be drawn between single- and multireference systems, and this division is always somewhat arbitrary; it nonetheless provides a very useful picture. Most of molecular systems fall into the category of single-reference systems. The system has multireference character only when several electronic configurations lie close in energy. Such a situation can occur, for example, in transition metal complexes due to close-lying d or f orbitals or in bond dissociation processes where bonding and anti-bonding orbital combinations lie close in energy and occupying either one of these orbitals leads to similar energy. The simplest diagnostic for the evaluation of multireference character in a given state is by calculating its NOONs (see equation (29)). In a single-reference system for the lowest N single-particle states $\omega_p \sim 1$, and for the rest of the states $\omega_p \sim 0$; in multireference systems, significant deviations are observed.

In quantum chemistry electron correlation is often divided into two categories: static correlation and dynamic correlation. Static correlation is associated to multireference character, whereas dynamic correlation is present in all electronic systems. In the Fock space picture, dynamic correlation can be considered as the weak mixing of high-lying configurations into the ground configuration, whereas static correlation is the strong mixing of a relatively small number of low-lying configurations. The mixing due to static correlation can be so strong that the system no longer has a single dominant configuration.

Weak or dynamic electron correlation can be systematically introduced into the model by starting with the HF model and then including more ON vectors into the approximate state. The Fock space can be spanned by generating singly, doublet, triply, etc. excited ON vectors from a HF reference state:[127,133]

$$|\psi\rangle = \left(C_0 + \sum_{p,t} C_p^t \hat{a}_t^\dagger \hat{a}_p + \sum_{\substack{p,q,\\ t,u}} C_{pq}^{tu} \hat{a}_t^\dagger \hat{a}_u^\dagger \hat{a}_p \hat{a}_q + \sum_{\substack{p,q,r,\\ t,u,v}} C_{pqr}^{tuv} \hat{a}_t^\dagger \hat{a}_u^\dagger \hat{a}_v^\dagger \hat{a}_p \hat{a}_q \hat{a}_r + \cdots \right) |\mathrm{HF}\rangle, \tag{115}$$

where p, q and r are indices of orbitals that are occupied in the HF reference and t, u and v are indices of virtual orbitals. In practice, usually only single and double excitations can be included into the model to keep the problem computationally tractable. Such a model is called CI singles, doubles, or CISD.[305–307] Higher excitations can be included into the model, but this limits the size of the system to a few atoms. The reference state can also be generated using more complicated methods. In coupled cluster theory, the reference state is constructed using an exponential excitation operator.[133,308] Such a reference state has more favorable physical properties but will not be of interest to us here. The CISD model can

provide very good results for single-reference systems, where $|C_0|^2 \sim 1$. However, in the case of multireference systems, the single and double excitations are not sufficient to account for the electron correlation, and CISD can often be almost as inaccurate as HF is. A more useful approach is the so-called complete active space SCF method, which will be introduced in the next section.

4.2 The complete active space self-consistent field method

The general idea in the complete active space self-consistent field (CASSCF) method[133,150,309–312] is to choose a relatively small orbital space, usually consisting of two to sixteen orbitals, and generate all possible CI states withing this space. This orbital space is known as the active space. The doubly occupied orbitals are known as inactive orbitals, and, like in HF theory, the unoccupied orbitals are called virtual orbitals. The active space corresponds to a subspace of the complete one-particle Hilbert space $\mathcal{H}$ and will be referred to as $\mathcal{H}_{\text{active}}$. All possible configurations within the active space are constructed and used as the variational state. This is known as the complete active space (CAS) expansion. The CAS expansion is equivalent to fully spanning the Fock space constructed from $\mathcal{H}_{\text{active}}$, referred to as $\mathcal{F}_{\text{CAS}}$. The CI problem in the CAS (usually referred to as the complete active space CI, CASCI) is equivalent to the CCI problem in $\mathcal{F}_{\text{CAS}}$. Once the active space is chosen and the CAS is constructed, the CI and MO coefficients are simultaneously optimized. Thus, the CASSCF method is a special case of the more general multiconfigurational SCF (MCSCF) theory.[313,314] Limiting the CI expansion to the CAS means that only a relatively small portion of the electron correlation is recovered. The trick here is to choose the active space using chemical intuition so that the properties of interest are reasonably well described. For example, if one is studying the properties of a transition metal complex, the active space should include the valence d orbitals and some ligand orbitals. Some useful rules for the choice of active space can be formulated, but ultimately the correct choice depends on intuition, trial and error, and sometimes on pure luck.[150]

The MCSCF approach to the electronic structure problem was formulated a decade after the HF theory was brought to a complete form.[315,316] Over the following decades the MCSCF theory developed slowly along with advances in computational algorithms and availability of better computational hardware.[313,314,317] A brief historical outline on the development of the theory is given in Roos *et al.*[150] The modern approach to solving the CASSCF problem is based on unitary rotations expressed as an exponential of an anti-Hermitian operator[133,134,150] and was initially formulated by Dalgaard and Jørgensen.[318] The actual theory is rather involved and will not be reviewed in great detail here. We will only give the main results. Detailed account of the derivations is available, for example, in Helgaker, Jørgensen, and Olsen[133] and in Jørgensen and Simons.[134] Before proceeding to the minimization of the CASSCF energy, we need to define unitary

operators $e^{\hat{T}}$ and $e^{\hat{S}}$, which conduct unitary transformations on the orbitals and the CI vector, respectively. We follow the usual convention of using the character S for the CI rotations, even though the symbol has already been used for spin and orbital overlap. The operators $\hat{T}$ and $\hat{S}$ are defined as

$$\hat{T} = \sum_{p>q} T_{pq} \left(\hat{E}_{pq} - \hat{E}_{qp} \right) \tag{116}$$

$$\hat{S} = \sum_{K \neq 0} S_{K0} \left(|\psi_K\rangle\langle\psi_0| - |\psi_0\rangle\langle\psi_K| \right), \tag{117}$$

where the matrix elements T_{pq} and S_{K0} are parameters for the unitary transformation and describe the mixing of orbitals p and q, and the mixing of the CI vectors 0 and K. The CASSCF reference state (i. e., the zeroth CI vector) is defined as

$$|\psi_0\rangle = \sum_{\mathbf{k}} C_{\mathbf{k}0} |\mathbf{k}\rangle, \tag{118}$$

where $\{|\mathbf{k}\rangle\}$ are the ON vectors or CSFs spanning $\mathcal{F}_{\mathrm{CAS}}$. We can also define $\dim(\mathcal{F}_{\mathrm{CAS}}) - 1$ other CI vectors, which are orthonormal to $|\psi_0\rangle$:

$$|\psi_K\rangle = \sum_{\mathbf{k}} C_{\mathbf{k}K} |\mathbf{k}\rangle. \tag{119}$$

The operators $e^{\hat{T}}$ and $e^{\hat{S}}$ can be used to generate a new CASSCF state $|\psi_0'\rangle$ from the CASSCF reference state $|\psi_0\rangle$ by unitary transformations of the orbitals and the CI vector:

$$|\psi_0'\rangle = e^{\hat{T}} e^{\hat{S}} |\psi_0\rangle. \tag{120}$$

The energy expectation value of $|\psi_0'\rangle$ can then be expressed as a function of the matrices $\mathbf{T}$ and $\mathbf{S}$ containing the transformation parameters T_{pq} and S_{K0}:

$$E_{\mathrm{CASSCF}}(\mathbf{T}, \mathbf{S}) = \langle\psi_0| e^{-\hat{S}} e^{-\hat{T}} \hat{H} e^{\hat{T}} e^{\hat{S}} |\psi_0\rangle. \tag{121}$$

The CASSCF energy is invariant under inactive–inactive, active–active, and virtual–virtual rotations; therefore, only rotations between the different orbital subspaces need to be considered in the construction of (116).

The main reason behind this rather complicated re-parameterization is that the optimization problem in terms of the matrices $\mathbf{c}$ and $\mathbf{C}$ can be cast into an optimization problem in terms of the matrices $\mathbf{T}$ and $\mathbf{S}$:

$$E_{\mathrm{CASSCF}} = \min_{\mathbf{C},\mathbf{c}} E(\mathbf{C}, \mathbf{c}) \rightarrow \min_{\mathbf{T},\mathbf{S}} E(\mathbf{T}, \mathbf{S}). \tag{122}$$

The energy $E(\mathbf{T}, \mathbf{S})$ can be expanded up to second order as

$$E(\mathbf{T}, \mathbf{S}) = E(\mathbf{0}, \mathbf{0}) - 2 \begin{pmatrix} \mathbf{T} & \mathbf{S} \end{pmatrix} \begin{pmatrix} \mathbf{W} \\ \mathbf{V} \end{pmatrix} + \begin{pmatrix} \mathbf{T} & \mathbf{S} \end{pmatrix} \underbrace{\begin{pmatrix} \mathbf{H}_{TT} & \mathbf{H}_{TS} \\ \mathbf{H}_{ST} & \mathbf{H}_{SS} \end{pmatrix}}_{=\mathbf{H}} \begin{pmatrix} \mathbf{T} \\ \mathbf{S} \end{pmatrix} + \cdots, \tag{123}$$

where $E(\mathbf{0}, \mathbf{0})$ is the energy expectation value of $|\psi_0\rangle$, $\mathbf{W}$ is the orbital gradient matrix, $\mathbf{V}$ is the CI gradient vector, and $\mathbf{H}$ is the electronic Hessian matrix. Thus,

the CASSCF energy can be minimized by finding the parameters T_{pq} and S_{K0}, which minimize (123), and then by using these parameters and equation (120) to construct a new CI vector and orbitals, and subsequently repeating this process until the gradients fall below certain predetermined threshold. Making the energy stationary with respect to variations in **T** and **S** gives

$$\begin{pmatrix} \mathbf{T} \\ \mathbf{S} \end{pmatrix} = \begin{pmatrix} \mathbf{H}_{TT} & \mathbf{H}_{TS} \\ \mathbf{H}_{ST} & \mathbf{H}_{SS} \end{pmatrix}^{-1} \begin{pmatrix} \mathbf{W} \\ \mathbf{V} \end{pmatrix}. \tag{124}$$

The elements of the gradient matrix **W** and vector **V** are relatively straightforward to evaluate. The orbital gradient elements are given as

$$W_{pq} = \langle \psi_0 | [\hat{H}, \hat{E}_{pq} - \hat{E}_{qp}] | \psi_0 \rangle, \tag{125}$$

which is known as the generalized Brillouin theorem (also known as the Brillouin–Lévy–Bethier theorem), and it states that at a stationary state, the Hamiltonian matrix elements between the optimized ground state and a singly excited state are zero.[319] The CI gradients are given as

$$V_K = 2\langle \psi_0 | \hat{H} | \psi_K \rangle, \tag{126}$$

which implies that $|\psi_0\rangle$ is a solution to the eigenvalue equation (101) as should be expected. Evaluation of the Hessian matrix elements is less straightforward and will not be discussed here. More detailed description is available in references 133 and 134. What is worth noting here is that if one is optimizing the HF state (i. e., the active space has zero orbitals), only the orbital–orbital matrix $\mathbf{H}_{TT}$ is non-zero and if one is optimizing the CI state with no orbital optimization, only the $\mathbf{H}_{SS}$ matrix is non-zero. In principle, the CASSCF problem can be solved without ever constructing the Hessian matrix by only considering the linear term (the first term on the right-hand side of (123)) in the energy minimization. In practical calculations, this can be a feasible approach to the first few iterations when the MCSCF is far from convergence but full convergence is extremely difficult to achieve without including the quadratic term in (123) in some manner.

One of the main advantages of the CASSCF method is that it can be used to solve the energy, CI vectors, and orbitals of not just the ground state but of several low-lying states. In principle, each of these states have their own sets of CI coefficients and orbitals. However, it is usually advantageous to use a single set of orbitals, which are optimized as the averaged optimal orbitals of each state considered. This method is known as state-averaged (SA) CASSCF. The opposite case is known as state-specific CASSCF. Using state-specific orbitals is in principle more accurate than using the SA orbitals. However, if a large number of states are considered, the convergence can become practically impossible in the state-specific case. Also, if qualitatively different orbitals are optimized for the different states, energy differences between the states can be difficult to assign to any physical energy difference. The state-specific density matrices of state K are

$$\gamma^K_{pq} = \langle \psi_K | \hat{E}_{pq} | \psi_K \rangle \quad \text{and} \quad \Gamma^K_{pqrs} = \langle \psi_K | \hat{E}_{pq,rs} | \psi_K \rangle, \tag{127}$$

and the state-averaged densities are obtained as

$$\gamma_{pq}^{\mathrm{SA}} = \sum_K \nu_K \gamma_{pq}^K \quad \text{and} \quad \Gamma_{pqrs}^{\mathrm{SA}} = \sum_K \nu_K \Gamma_{pqrs}^K, \tag{128}$$

where $\sum \nu_K = 1$. The coefficients $\{\nu_K\}$ are usually chosen to be equal for all states.

By far the most serious computational limit in a CASSCF calculation is the number of orbitals included in the active space. The dimension of the CAS is given as

$$\dim(\mathcal{F}_{\mathrm{CAS}}) = \frac{2S+1}{n_{\mathrm{orb}}+1} \binom{n_{\mathrm{orb}}+1}{N_{\mathrm{CAS}}/2 - S} \binom{n_{\mathrm{orb}}+1}{N_{\mathrm{CAS}}/2 + S + 1}, \tag{129}$$

where S is the total spin, n_{orb} is the number of orbitals, and N_{CAS} is the number of electrons in the active space. The quantities in parenthesis are binomial coefficients, and their presence in (129) means that the complexity of the CI problem grows essentially factorially with the size of the active orbital space. For example, if we consider singlet states constructed in a two-electron-two-orbital active space (commonly denoted as a (2,2) space), there are three configurations. When we start increasing the active space to (4,4), (6,6), or (8,8) spaces, we have 20, 175, and 1764 configurations respectively. In a (16,16) space there are 34 *million* configurations. The number of orbitals that can today be included in the active space is roughly fourteen to sixteen orbitals depending on the spin state, or around one million ON vectors.[150]

New theories have been developed to address the steep computational scaling relative to the size of the active space. The oldest of these is probably the restricted active space SCF (RASSCF) method, in which the active orbitals are divided into three subspaces and when excited configurations are constructed, only limited excitations between different subspaces are allowed.[150,320] The RASSCF model has been extended to an arbitrary number of subspaces in the generalized active space SCF (GASSCF) of Gagliardi and co-workers.[321,322] In addition to the development of methods to limit the number of configurations constructed in the active space, other methods have been developed to approximately solve the full CASSCF problem. Arguably, the most successful of these methods are the ones based on the density matrix renormalization group (DMRG), which allows calculations on active spaces including more than fifty orbitals.[323–330] Other novel CASSCF methods include the very recent iterative configuration expansion CI (ICE-CI)[331] which provides performance comparable to the DMRG and the variational two-particle reduced density matrix calculations of Mazziotti.[332,333] All of these approximate CASSCF methods represent state-of-the-art methods that are still under development and are lacking in certain key properties, such as unique solutions and invariance with respect to orbital rotations in a given orbital subspace.[150] Furthermore, inclusion of dynamic correlation on top of the reference wave functions produced by these methods is usually not trivial, although in recent years, some promising methods have been developed in the context of DMRG.[334–339] None of these methods have yet found widespread use in the field of molecular magnetism, and they have not been used in the present work.

4.3 Multireference perturbation methods

4.3.1 General remarks

As mentioned above, the CASSCF method only accounts for a small part of the electron correlation energy. If the active space is chosen in a reasonable way, the method does account for enough correlation to provide a qualitatively correct wave functions for multireference systems. However, in order to provide quantitative results, the CASSCF wave functions need to be augmented with dynamic electron correlation. The most popular way of achieving this in systems of moderate to large size is to utilize second-order multireference perturbation methods. The most widespread ones are the complete active space perturbation theory at the second order (CASPT2) of Roos and co-workers[340–342] and the N-electron valence state perturbation theory at the second order (NEVPT2) of Angeli *et al*.[343–345] The former is implemented in the Molcas code and the latter in the Orca code. CASPT2 and NEVPT2 are the most popular multireference perturbation theories and are the ones used in the present work, but they are by no means the only formulations of the multireference perturbation problem.

One of the main problems in any perturbation approach is the choice of the zeroth-order Hamiltonian $\hat{H}_0$. In the case of a closed-shell single-reference systems and a HF reference state, this is rather straightforward, as the Fock operator is diagonal and $\hat{H}_0$ can be chosen as the Fock operator. The first-order correction to energy is simply the HF energy, and the second-order correction includes some electron correlation. This approach is known as the Møller–Plesset perturbation theory[346] and is most often used up to the second order, giving the MP2 method. In the case of multireference wave functions, the choice of $\hat{H}_0$ is less straightforward as the general Fock operator given by (103) is no longer diagonal and the CASSCF eigenstates are not eigenstates of the Fock operator. The main difference between the CASPT2 and NEVPT2 theories lies in the choice of the zeroth-order Hamiltonian. Another important choice for practical application of perturbation theory in electronic structure calculations is the first-order interacting space (FOIS) containing the states that are mixed with the reference state $|\psi^{(0)}\rangle$ through the perturbation $\hat{H}_1$. In principle, this space could consist of all states generated as single or doublet excitations from the reference CASSCF state as ON vectors differing by one or two occupations interact through the one- and two-electron operators of the Hamiltonian. In practice, however, such a space would be unmanageably large even for relative small system. Therefore, a process called internal contraction is applied to the FOIS as first suggested by Siegbahn[347,348] and Meyer.[349] In this approach, the FOIS states $\{|\psi'_{pqrs}\rangle\}$ are generated from a CASSCF reference state $|\psi_0\rangle$ as

$$|\psi'_{ijat}\rangle = \hat{E}_{ai}\hat{E}_{tj}|\psi_0\rangle = \sum_{\mathbf{k}} C^{(0)}_{\mathbf{k}} \hat{E}_{ai}\hat{E}_{tj}|\mathbf{k}\rangle, \tag{130}$$

where $C^{(0)}_{\mathbf{k}}$ are the zeroth-order CI coefficients determined by the preceding

CASSCF calculation. The indices i and j refer to inactive orbitals in the CASSCF reference, a to orbitals in the active space, and t to virtual orbitals. To simplify notation, we define an overall index I for the states in the FOIS $\{|\psi'_{ijat}\rangle\} \equiv \{|\psi'_I\rangle\}$. Not all of the states in the FOIS generated in (130) are needed. There are eight different classes of excitations depending on whether the excitation indices belong to the inactive, active, or virtual orbital subspaces. The different classes are given in ref. 341. The internal contraction greatly complicates the structure of the FOIS, and the states $\{|\psi'_I\rangle\}$ are, in general, neither orthogonal nor linearly independent. We can, therefore, define an overlap integral $S_{IJ} = \langle\psi'_I|\psi'_J\rangle$. Furthermore, the contraction introduces more excitation operators into the matrix elements requiring the evaluation of higher-order density matrices. The construction of higher-order density matrices can be avoided by keeping certain subspaces of the FOIS uncontracted.[350] In either case, the internal contraction procedure does, however, considerably reduce the size of the FOIS; thus, regardless of all the computational complications that arise in the theory, it still greatly reduces the overall computational costs. The number of states in the FOIS is larger than in the corresponding MP2 case, where the active space is empty but still of the same order of magnitude.[150]

4.3.2 The CASPT2 method

In the CASPT2, following the Møller–Plesset theory, the Fock operator

$$\hat{F} = \sum_{p,q} F_{pq}\hat{E}_{pq} \tag{131}$$

is chosen as $\hat{H}_0$. In general, $|\psi_0\rangle$ is not an eigenstate of the Fock operator, and it interacts with the states in the FOIS via $\hat{H}_0$. Therefore, $\hat{H}_0^{\text{CASPT2}}$ must be constructed using projection operators.[133,341] The interacting space is divided into the reference space $\mathcal{P}$ containing the single reference CASSCF state and the complementary space $\mathcal{Q} = \mathcal{F} - \mathcal{P}$, which includes the other CASSCF states and the states in the FOIS. The projectors onto these spaces are

$$\hat{P} = |\psi_0\rangle\langle\psi_0| \quad \text{and} \quad \hat{Q} = \sum_{K\neq 0} |\psi_K\rangle\langle\psi_K| + \sum_I |\psi'_I\rangle\langle\psi'_I|, \tag{132}$$

where K runs over all states in the CAS and I over all states in the FOIS. The zeroth-order Hamiltonian can then be defined as

$$\hat{H}_0^{\text{CASPT2}} = \hat{P}\hat{F}\hat{P} + \hat{Q}\hat{F}\hat{Q}. \tag{133}$$

The first-order correction to the CI coefficients can be obtained from the matrix equation[133]

$$\begin{aligned} \mathbf{C}^{(1)} &= -\mathbf{P}\left(\mathbf{H}_0 - E^{(0)}\mathbf{S}\right)^{-1}\mathbf{P}\mathbf{H}_1\mathbf{C}^{(0)} \\ \mathbf{P} &= \mathbb{1} - \mathbf{C}^{(0)}\mathbf{C}^{(0)^{\mathrm{T}}}, \end{aligned} \tag{134}$$

where $S_{IJ} = \langle \psi'_I | \psi'_J \rangle$. This set of linear equations is known as the CASPT2 equations, and their solution is the computational bottleneck of a CASPT2 calculation. The solution procedure is not trivial due to linear dependencies in the FOIS and has to be solved by a symmetric orthonormalization.[150] Once the first-order CI coefficients are obtained, the first and second-order corrections to the energy can be calculated as:[133]

$$E^{(1)} = \mathbf{C}^{(0)^{\mathrm{T}}} \mathbf{H}_1 \mathbf{C}^{(0)} \quad \text{and} \quad E^{(2)} = \mathbf{C}^{(1)^{\mathrm{T}}} \mathbf{H}_1 \mathbf{C}^{(0)}. \tag{135}$$

The one-electron operator used as $\hat{H}_0^{\mathrm{CASPT2}}$ introduces the problem that, at the zeroth order, there may be states in the FOIS with energies similar to or below the CASSCF reference state. In practice, this can cause denominators in the expression used for solving the CASPT2 equations to become zero or very nearly so, which then leads to singularities in the energy and spurious results. The common solution to this so-called intruder state problem is to shift the zeroth-order energies of all the states in the FOIS.[351–353] Such a level shift affects the results, and although the results are corrected for this afterwards, the level shift still makes the results dependent on a user-defined number. Another user-defined parameter, which is often used in CASPT2 calculations, is the so-called IPEA shift (IPEA stands for ionization potential electron affinity), which modifies the diagonal elements of the Fock operator. The shift leads to improved results (but see the discussion by Zobel *et al.*[354]), and an IPEA shift of 0.25 is used as default in newer versions of the Molcas code.

The CASPT2 theory as presented so far is state-specific in the sense that the CASPT2 correction is calculated for an individual CASSCF state. Each CASSCF state has a state-specific zeroth-order Hamiltonian due to the projector $\hat{P}$ in (133), which only projects onto the reference state. Such a treatment is, however, insufficient if the dynamic correlation introduces a strong mixing of closely packed CASSCF states. The closely related multistate CASPT2 (MS-CASPT2)[355] and extended multistate CASPT2 (XMS-CASPT2)[356] methods use multidimensional reference spaces. The reference space consists of the set of states $\{|\psi_A\rangle\}$, which is a subset of the CASSCF states obtained from a SA-CASSCF calculation. The projector into this reference space is

$$\hat{P} = \sum_A |\psi_A\rangle\langle\psi_A| \tag{136}$$

and, like in the conventional CASPT2, the zeroth-order Hamiltonian is

$$\hat{H}_0^{(\mathrm{X})\mathrm{MS\text{-}CASPT2}} = \hat{P}\hat{F}^{\mathrm{SA}}\hat{P} + \hat{Q}\hat{F}^{\mathrm{SA}}\hat{Q}. \tag{137}$$

The Fock operator $\hat{F}^{\mathrm{SA}}$ is constructed using a SA density:

$$\hat{F}^{\mathrm{SA}} = \sum_{p,q} F_{pq}^{\mathrm{SA}} \hat{E}_{pq}, \quad F_{pq}^{\mathrm{SA}} = h_{pq} + \sum_{r,s} \gamma_{rs}^{\mathrm{SA}} \left[(rs|pq) - \frac{1}{2}(rp|sq) \right] \tag{138}$$

and is, in general, not diagonal in the basis of the reference states:

$$F_{AB} = \langle \psi_A | \hat{F} | \psi_B \rangle = \sum_{p,q} \sum_{\mathbf{k},\mathbf{k}'} F_{pq} C^*_{\mathbf{k}A} C_{\mathbf{k}'B} \langle \mathbf{k} | \hat{E}_{pq} | \mathbf{k}' \rangle. \tag{139}$$

The difference between the MS-CASPT2 and XMS-CASPT2 methods lies in the construction of the operator $\hat{P}\hat{F}^{\mathrm{SA}}\hat{P}$ in (137). In MS-CASPT2, only the diagonal elements of the Fock operator in the reference state basis, $|\psi_A\rangle F_{AA}\langle\psi_A|$, are included, whereas in XMS-CASPT2, the off-diagonal elements $|\psi_A\rangle F_{AB}\langle\psi_B|$ are also taken into account. In XMS-CASPT2 theory, the reference states are rotated by a suitable unitary operator into basis $\{|\tilde{\psi}_A\rangle\}$, which diagonalizes $\hat{P}\hat{F}^{\mathrm{SA}}\hat{P}$. The only difference in the zeroth-order Hamiltonian in MS-CASPT2 and XMS-CASPT2 theories is then the basis used for the representation of the first operator in the right-hand side of (137).

The (X)MS-CASPT2 problem is solved for each reference state following the same procedure of solving linear equations (134) as in the conventional CASPT2 to yield the first-order states $\{|\psi_A^{(1)}\rangle\}$. These states are used to construct an effective Hamiltonian $\hat{H}_{\mathrm{eff}}^{\text{MS-CASPT2}}$ with matrix elements

$$\left(\hat{H}_{\mathrm{eff}}^{\text{MS-CASPT2}}\right)_{AB} = \frac{1}{2}\left(\langle\psi_A + \psi_A^{(1)}|\hat{H}|\psi_B\rangle + \langle\psi_A|\hat{H}|\psi_B + \psi_B^{(1)}\rangle\right), \tag{140}$$

where $|\psi_A + \psi_A^{(1)}\rangle$ is the reference state corrected to first order. This effective Hamiltonian is then diagonalized to yield the final second-order MS-CASPT2 energies. In case of XMS-CASPT2, exactly the same procedure is used but in the transformed reference state basis. Construction of the effective Hamiltonian (140) requires the calculation of the off-diagonal elements between different first-order corrected states. This becomes increasingly expensive in terms of computational resources as the number of states included in the reference space grows. Great savings in cpu time can be achieved by neglecting the off-diagonal terms, which considerably simplifies the calculation. This approximation essentially means that the (X)MS calculation does not mix any of the reference states but simply calculates corrections to diagonal elements of the CASSCF Hamiltonian using the state-averaged Fock operator. This is the method that is most often used in SOC calculations utilizing CASPT2 corrections discussed in section 4.4.5.

It is very important to note that when performing calculations on metal ions with an orbitally degenerate ground state, only XMS-CASPT2 will correctly reproduce the degeneracy.[V,101] In trivalent lanthanide ions (with the exception of Gd), the artificial splitting produced in a CASPT2 or MS-CASPT2 calculations can be several hundreds of wave numbers. Similar serious problems have been reported in calculations of potential energy surfaces in the vicinities of conical intersections and avoided crossings.[357] It is currently not known how severe the artificial splitting problem is in molecular lanthanide complexes, where the spatial degeneracies of the ions are broken. In a recent study on the CF energy

levels of some lanthanide complexes Ruiz, Coronado, and co-workers,[358,c] using the conventional CASPT2 method, noticed no significant improvement in the results compared to CASSCF, whereas in a study by Ungur and Chibotaru[101] a significant improvement over CASSCF was observed using the XMS-CASPT2 method. In any case, until these issues have been fully investigated, the XMS-CASPT2 method should be the method of choice for treating lanthanide systems. The same problems also appear in lighter transition metal systems, but the artificial splittings are usually not as severe as in the case of lanthanides.

4.3.3 The NEVPT2 method

NEVPT2 has been formulated in three different variations: uncontracted, partially contracted, and strongly contracted.[343–345] The first features no internal contraction, and the middle one uses the same contraction as CASPT2. The last is the one we are interested in as it is computationally fastest and the most widely used variant. The wide use is most likely a result of the fact that it was the only variant implemented in ORCA 3.0.X codes, which popularized the method, and the other two variants were only implemented in the newer ORCA 4.0.0 code. The strongly contracted variant takes the internal contraction scheme one step further than equation (130) and also contracts the excitation operators using two-electron integrals:

$$|\psi'_{ija}\rangle = \sum_t \left[(aj|ti)\hat{E}_{aj}\hat{E}_{ti} + (ai|tj)\hat{E}_{ai}\hat{E}_{tj}\right]|\psi_0\rangle, \tag{141}$$

where we have used the same indexing scheme as in (130). The states defined in (141) are mutually orthogonal: $\langle\psi'_I|\psi'_J\rangle = \delta_{IJ}$ where we have again used a general indices I and J for states in the FOIS. It has been shown that the strong contraction (141) introduces only a negligible error compared to the contraction in (130).[343]

The choice of zeroth-order Hamiltonian in NEVPT2 is based on the rather elaborate operator $\hat{H}^{\mathrm{D}}$ known as the Dyall Hamiltonian:[359]

$$\hat{H}^{\mathrm{D}} = \sum_i F_{ii}\hat{E}_{ii} + \sum_a F_{aa}\hat{E}_{aa} + \sum_{p,q} h^{\mathrm{eff}}_{pq}\hat{E}_{pq} + \frac{1}{2}\sum_{p,q,r,s}(pq|rs)\left[\hat{E}_{pq}\hat{E}_{rs} - \delta_{qr}\hat{E}_{ps}\right] + C, \tag{142}$$

[c] It should be noted that there are some very notable misunderstandings of the theory in the work of Ruiz, Coronado, and co-workers.[358] For example, sentences "...apply perturbations in the wrong order, in CASPT2 both dynamic correlation and spin-orbit effect are included perturbatively..." and "...the fact that the SINGLE_ANISO procedure applies spin-orbit coupling after, rather than before, the ligand-field, has fundamental..." are clearly incorrect as the spin-orbit coupling is not treated as a perturbation and the SINGLE_ANISO procedure does not add any SOC, but rather uses *ab initio* results calculated earlier. Overall, they present a lot of criticism of the fact that the *ab initio* methodology does not treat the effects of SOC, CF, etc. in the same manner as is done in conventional pen-on-paper treatments of the electronic structure problem of transition metal complexes, where one starts with an isolated ion and then adds interactions in consecutive manner. Such criticism is rather unfounded, as treating the electronic structure of the entire complex in one calculation is certainly more accurate than introducing various interactions in a step-wise manner.

where

$$F_{mn} = h_{mn} + \sum_i [2(ii|mn) - (im|in)] + \sum_{p,q} \gamma_{pq}^{\mathrm{SA}} \left[2(mn|pq) - \frac{1}{2}(mp|nq) \right], \quad (143)$$

$$h_{pq}^{\mathrm{eff}} = h_{pq} + \sum_i [(ii|pq) - (ip|iq)], \text{ and} \quad (144)$$

$$C = 2\sum_i h_{ii} + \sum_{i,j} [2(ii|jj) - (ij|ij)] - 2\sum_i F_{ii}. \quad (145)$$

Indices i and j indicate inactive orbitals, t and u indicate active orbitals, a and b indicate virtual orbitals, and p, q, r, and s run over all orbitals. m and n are dummy indices, which can mean either inactive, active, or virtual orbitals depending on the context. $\hat{H}^{\mathrm{D}}$ is much more complicated in form than the simple Fock operators used in CASPT2, but it has many advantages. Most notably, the CASSCF reference is an eigenstate of $\hat{H}^{\mathrm{D}}$ (this is ensured by addition of the constants C to the Hamiltonian), and the two-electron terms included in the operator account for all electron correlation within the CAS and ensure that no intruder states are present. Therefore, no empirical parameters are needed in a NEVPT2 calculation.

The NEVPT2 zeroth-order Hamiltonian can be expressed in a spectral decomposition form as

$$\hat{H}_0^{\mathrm{NEVPT2}} = |\psi_0\rangle E^{(0)} \langle\psi_0| + \sum_I |\psi_I'\rangle E_I' \langle\psi_I'|, \quad (146)$$

where $E_I' = \langle\psi_I'|\hat{H}^{\mathrm{D}}|\psi_I'\rangle$. The states in the FOIS are eigenstates of $\hat{H}_0^{\mathrm{NEVPT2}}$; thus, unlike in CASPT2, no system of linear equations needs to be solved and the calculations are very efficient. The first-order correction to the CI coefficients is given as

$$|\psi_0^{(1)}\rangle = \sum_I \frac{\sqrt{\langle\psi_I'|\psi_I'\rangle}}{E^{(0)} - E_I'} |\psi_I'\rangle \quad (147)$$

and the second-order energy as

$$E^{(2)} = \sum_I \frac{\langle\psi_I'|\psi_I'\rangle}{E^{(0)} - E_I'}. \quad (148)$$

The NEVPT2 method is state-specific, similar to CASPT2. A multistate version of the NEVPT2 method known as quasi-degenerate NEVPT2 (QD-NEVPT2) has also been formulated.[360] A more recent development is the domain-based local pair-natural orbital NEVPT2 (DLPNO-NEVPT2), which scales linearly for large systems in terms of computational effort and can, therefore, be used for very large systems, which are not accessible using conventional NEVPT2 or CASPT2. Similar to CASPT2, NEVPT2 and QD-NEVPT2 also fail to reproduce exact spatial degeneracies. However, at least in the case of strongly contracted NEVPT2, the artificial splitting in the case of lanthanide ions is much weaker than in CASPT2 or MS-CASPT2 and is usually in the range of a few wave numbers. The exact reason

for this has not yet been clarified, but it seems that unless one is interested in very accurate results, NEVPT2 should be a viable method for lanthanide systems as well.

The NEVPT2 method has not been as thoroughly tested by time as CASPT2, but it has been demonstrated to show very good performance in variety of problems, usually comparable to CASPT2.[89,361–363] A recent study by Pierloot *et al.* found surprisingly large deviations between CASPT2 and NEVPT2 results when calculating excitation energies of transition metal complexes.[364] It should, however, be noted that in that study, the IPEA shift was employed in the CASPT2 calculations, whereas NEVPT2 is parameter-free; hence, the results essentially compare semi-empirical CASPT2 results to purely *ab initio* NEVPT2 results.

4.3.4 Beyond perturbation theory

The CASPT2 and NEVPT2 methods are popular as the computational costs are low enough for them to be applied to moderate size systems. They often provide good results, but the perturbation series is still truncated at the second order, and there is, therefore, no reason to assume that they would provide quantitative results in every case. Usually, the quality of the results is largely dependent on the quality of the CASSCF reference wave function. The next logical step in improving the results would be to include the interaction with the FOIS in a variational manner, as opposed to second-order perturbation theory by diagonalizing the CI Hamiltonian constructed in the basis of the states in the CAS and FOIS. Such a treatment is known as multireference CI (MRCI). In principle, higher-order excitations could also be added to the treatment as the triple and quadruple excitations interact with the reference state indirectly through the singles and doubles block of the Hamiltonian. Such a treatment would, however, be untractable and is never done in practice. The acronym MRCISD is sometimes used to highlight the fact that the method includes only the single and double excitations, but MRCISD is largely synonymous to MRCI in the literature.

The earliest MRCI calculations were carried out by Buenker and Peyerimhoff[365–367] and precede multireference perturbation treatments but were severely limited in scope by the computational hardware. These methods were based on individual selection of configurations rather than on internal contraction of the interacting space. More efficient MRCI approaches have been developed using internal contraction schemes. The most widely used method (based on the number of citations on the original paper) is the MRCI approach proposed by Werner and Knowles,[368–370] which is implemented in the Molpro code. Even with the internal contraction, the method has rather strong limits on the number of inactive orbitals, which makes it inapplicable to most molecular magnetic systems. The most efficient MRCI code to date is the mrcic code in Molpro based on the newer internal contraction scheme by Werner and co-workers.[350,371] Unfortunately, the method is currently limited to only the lowest state in a given multiplicity and representation of the molecular point-group, and, therefore, has limited applicability in molecular magnetism. Another very recent internally

contracted MRCI approach is that of Sivalingam *et al*.[372] implemented in the ORCA 4.0.0 code. The implementations, is however, still not complete enough to apply it to molecular magnetic problems.

The only MRCI method that has seen wide application in the field of molecular magnetism is the so-called difference-dedicated CI (DDCI) method by Caballol and co-workers.[373–375] DDCI is based on individual selection, and the general idea in the method is that the interacting space is generated with single and double excitations, where at least one of the indices is an active orbital. This eliminates all "doubly external" excitations and offers considerable computational savings while still describing the relative energy differences within a given geometry reasonably accurately. A more detailed account of the DDCI method and its applications to molecular magnetism is available in the review by Guihéry and co-workers[177] and in the references therein.

4.4 Relativistic corrections and properties

4.4.1 Four- two- and one-component theories

The electronic structure theory as described so far is a one-component theory; that is, the one-particle states can be represented as functions in the three-dimensional Cartesian space with one additional spin index. On the other hand, Dirac's theory of the electron,[9,376,377] which unifies one-particle quantum theory and special relativity, leads to the result that the mathematical entity representing the electron must be a four-component quantity. In a wave function representation, the state can be represented by the Dirac four-component spinor (a spinor can be considered as a relativistic generalization of a spinorbital) consisting of the one-component wave functions functions $\Psi_{+\alpha}$, $\Psi_{+\beta}$, $\Psi_{-\alpha}$, and $\Psi_{-\beta}$. The former two are the α and β components of the large component, and the latter two are α and β components of the small component. This notation can be expressed as

$$\begin{pmatrix} \Psi_{+\alpha} \\ \Psi_{+\beta} \\ \Psi_{-\alpha} \\ \Psi_{-\beta} \end{pmatrix} = \begin{pmatrix} \Psi_{+} \\ \Psi_{-} \end{pmatrix}. \tag{149}$$

The large component represents the electronic (or positive energy) states and the small component the positronic (or negative energy) states. The Dirac equation in this representation for a stationary system in a stationary frame of reference[378] and in the absence of external magnetic fields is given as

$$\begin{pmatrix} m_e c^2 + \hat{V}_{\text{ext}} & c\boldsymbol{\sigma}\cdot\hat{\mathbf{p}} \\ c\boldsymbol{\sigma}\cdot\hat{\mathbf{p}} & -m_e c^2 + \hat{V}_{\text{ext}} \end{pmatrix} \begin{pmatrix} \Psi_{+} \\ \Psi_{-} \end{pmatrix} = E \begin{pmatrix} \Psi_{+} \\ \Psi_{-} \end{pmatrix}. \tag{150}$$

$\boldsymbol{\sigma}$ is a vector of the Pauli spin matrices

$$\sigma_1 = \begin{pmatrix} 0 & 1 \\ 1 & 0 \end{pmatrix}, \quad \sigma_2 = \begin{pmatrix} 0 & -i \\ i & 0 \end{pmatrix}, \quad \text{and} \quad \sigma_3 = \begin{pmatrix} 1 & 0 \\ 0 & -1 \end{pmatrix}, \tag{151}$$

where $\hat{\mathbf{p}}$ is the momentum operator and V_{ext} is an external electric potential. It should be noted here that we are adhering to the convention in relativistic quantum chemistry to explicitly write the electron mass m_e even though in Hartee atomic units $m_e \equiv 1$.

All commonly used quantum chemical methods have been generalized to a four-component form even though this has faced considerable difficulties in many cases.[278,378] The positronic states themselves, however, have little relevance in chemistry, and it would, therefore, be useful to decouple the large and small components of the Hamiltonian:

$$\begin{pmatrix} m_e c^2 + \hat{V}_{\text{ext}} & c\boldsymbol{\sigma} \cdot \hat{\mathbf{p}} \\ c\boldsymbol{\sigma} \cdot \hat{\mathbf{p}} & -m_e c^2 + \hat{V}_{\text{ext}} \end{pmatrix} \begin{pmatrix} \Psi_+ \\ \Psi_- \end{pmatrix} \rightarrow \begin{pmatrix} \hat{H}_+ & 0 \\ 0 & \hat{H}_- \end{pmatrix} \begin{pmatrix} \Psi_+ \\ \Psi_- \end{pmatrix}. \tag{152}$$

Such decoupling would then allow one to solve the eigenvalue problem of the electronic states and simply neglect the positronic states. This also avoids all physical ambiguities in interpretation of the negative energy states, which is a source of numerous complications in four-component quantum chemistry.[278,378]

Two approaches to the decoupling have been successfully used: the elimination of the small component and unitary transformations.[278] The most popular approach to the former is the zeroth-order regular approximation (ZORA)[379–382] and to the latter is the Douglas–Kroll–Heß (DKH) theory[383,384] as well as the so-called exact decoupling methods.[385] Once the eigenvalue equation has been reduced to a two-component form, the Hamiltonian can be further divided into a scalar term and a spin-orbit term[380] although such a division is usually somewhat arbitrary.[386] In scalar relativistic approximations, the spin-orbit terms are simply neglected, and only the scalar term is considered. As the name suggests, the scalar term only contains a scalar potential, and the two-component eigenvalue problem can then be further decoupled into two eigenvalue problems of α and β spins, which in the absence of magnetic fields are equivalent to a one-electron problem; thus, the one-component form of non-relativistic quantum mechanics is recovered. Scalar relativistic terms are the simplest relativistic corrections to introduce in a quantum chemical calculation as they only require modification of the one-electron operator. This will be discussed in more detail in sections 4.4.2, 4.4.3, and 4.4.4. Calculation of properties that depend on the one-electron operator usually requires some modification of the property integrals known as picture-change effects. The spin-orbit interaction can be treated either by not neglecting the spin-orbit term in the two-component Hamiltonian, which leads to a two-component formalism (which is widely used in the context of DFT), or by first solving the electronic structure problem with only scalar relativistic effects included and then accounting for SOC *a posteriori*.[378] In the present work, we are only interested of the latter, and this approach will be discussed in section 4.4.5.

So far, we have discussed relativity only in the context of a one-electron theory. Generalization to a many-particle problem requires introduction of the Coulomb operator into the Hamiltonian. The simplest approximation is to simply use the non-relativistic form $|\mathbf{r}_1 - \mathbf{r}_2|^{-1}$ together with the Dirac one-electron operator to give the Dirac–Coulomb Hamiltonian. The non-relativistic Coulomb

operator, however, suggests immediate interaction across any distance in space and is clearly not Lorentz-invariant and, therefore, not compatible with any theory based on special relativity. The practical SOC calculations discussed in section 4.4.5 are based on the Breit–Pauli Hamiltonian.[137,278,387,388,d]

4.4.2 Zeroth-order regular approximation

The ZORA Hamiltonian was first derived by Chang, Pelissier, and Durand[379] in 1986 using the theory of effective Hamiltonians. It is, therefore, sometimes, although rarely, referred to as the CPD Hamiltonian. The name zeroth-order regular approximation (ZORA) was given to it by van Lenthe *et al*. in a series of papers published during the 1990's.[380–382,389] ZORA was first implemented in the Amsterdam Density Functional (ADF) code[261] and due to its conceptual simplicity, it is now available in numerous quantum chemistry programs. The ZORA Hamiltonian reads[379,380]

$$\hat{H}^{\mathrm{ZORA}} = \frac{(c\boldsymbol{\sigma}\cdot\hat{\mathbf{p}})^2}{2m_e c^2 - V} + \hat{V} \tag{153}$$

and it can be separated into a scalar and spin-orbit parts as[380]

$$\hat{H}^{\mathrm{ZORA}} = \underbrace{\frac{c^2\hat{\mathbf{p}}^2}{2m_e c^2 - V} + \hat{V}}_{=\hat{H}^{\mathrm{ZORA}}_{\mathrm{scalar}}} + \underbrace{\frac{c^2\boldsymbol{\sigma}\cdot(\nabla\hat{V}\times\hat{\mathbf{p}})}{(2m_e c^2 - V)^2}}_{=\hat{H}^{\mathrm{ZORA}}_{\mathrm{SO}}}. \tag{154}$$

The ZORA method has been extended to the so-called infinite-order regular approximation (IORA).[390]

The obvious problem in application of $\hat{H}^{\mathrm{ZORA}}$ is the presence of the potential in the denominator. First, this introduces considerable difficulties in evaluation of the matrix elements, and if the real potential is explicitly introduced into the denominator, the operator in most cases has to be integrated numerically over a grid. The second and much more serious problem is that the potential enters the Hamiltonian in a non-linear manner. This means that a constant shift in the potential does not translate to a constant shift in the eigenvalues and $\hat{H}^{\mathrm{ZORA}}$ is not energy-gauge-independent. In practice, this problem can be circumvented by using some model potential constructed, for example, as a superposition of pre-defined atomic densities.[391,392] The numerical integration and the construction of a model-potential are both easier to implement in the context of DFT; thus, ZORA is mostly utilized in density functional calculations. Since in DFT calculations, the computational bottleneck is usually the evaluation of two-electron integrals, the inclusion of scalar ZORA often leads to a negligible increase in the overall computational costs (assuming that a model potential in $\hat{H}^{\mathrm{ZORA}}_{\mathrm{scalar}}$ is used) and

[d] We are citing here the papers by Pauli[137] and Breit,[387,388] which along with the papers by Dirac,[376,377] constitute the citation for the Dirac–Coulomb–Breit Hamiltonian. The actual Breit–Pauli Hamiltonian can be derived from the Dirac–Coulomb–Breit Hamiltonian by applying the so-called Foldy–Wouthuysen transformation. A detailed account of this process along with the related references are given in Reiher and Wolf.[278]

is, therefore, a very viable way of treating scalar relativity. In the present work, ZORA is applied only in DFT calculations, whereas wave function calculations are carried out using the methods introduced in the next sections.

4.4.3 Douglas–Kroll–Heß transformation

The Douglas–Kroll–Heß (DKH) transformation was first suggested by Douglas and Kroll in 1974[383] and formulated to a practically applicable form by Heß in 1986.[384] The general idea in DKH theory is that a unitary transformation, which exactly decouples the Dirac Hamiltonian, is expanded in a sequence of specific unitary transformations:

$$\hat{U}^\dagger \hat{H}_{\text{Dirac}} \hat{U} = \hat{U}_\infty^\dagger \cdots \hat{U}_2^\dagger \hat{U}_1^\dagger \hat{U}_0 \hat{H}_{\text{Dirac}} \hat{U}_0 \hat{U}_1 \hat{U}_2 \cdots \hat{U}_\infty = \begin{pmatrix} \hat{H}_+ & 0 \\ 0 & \hat{H}_- \end{pmatrix}. \tag{155}$$

A given transformation $\hat{U}_i$ is constructed in such a way that it removes the off-diagonal elements of (150) up to a given order in the potential V. The approximately decoupled hamiltonian to order K can be written as

$$\hat{H}^{\text{DKH}K} = \sum_k^K h_k^{\text{DKH}} = \begin{pmatrix} h_{K+}^{\text{DKH}} & 0 \\ 0 & h_{K-}^{\text{DKH}} \end{pmatrix}. \tag{156}$$

The explicit expressions of the unitary transformations and h_k^{DKH} up to DKH5 are given in the book of Reiher and Wolf[278] and will not be repeated here. The theory is most often used in the scalar relativistic form (the scalar form is again obtained by neglecting the non-scalar terms) up to second-order giving the scalar DKH2 method. The necessary expressions for arbitrary-order DKHK can be generated symbolically.[393]

A complication that arises in the DKH theory is that exact expressions of the specific unitary transformations can only be given in a basis that diagonalizes $\hat{\mathbf{p}}^2$. This requires that the operators must first be transformed into the $\hat{\mathbf{p}}^2$ basis and then back-transformed once the DKH Hamiltonian of a given order is calculated. This transformation does add notable computational costs, but in most cases, the calculation of two-electron integrals still dominates over the DKH transformation; therefore, inclusion of the DKH correction does not introduce any bottlenecks to the calculation.

4.4.4 Exact decoupling methods

A decoupling scheme that has gained popularity over recent years is the so-called exact two-component (X2C) approach[385,394–399,e] which is based on a one-step decoupling of the large and small component as opposed to the sequential DKH approach. Also, as opposed to any finite-order DKH approach, the decoupling of one-particle Hamiltonians in X2C theory is, in principle, *exact*. The starting point of the X2C method is the modified Dirac equation[400]

$$\begin{pmatrix} \mathbf{V} & \mathbf{T} \\ \mathbf{T} & \frac{1}{4m_e^2c^2}\mathbf{W} - \mathbf{T} \end{pmatrix} \begin{pmatrix} \mathbf{c}_+ \\ \mathbf{c}_- \end{pmatrix} = \begin{pmatrix} \mathbf{S} & 0 \\ 0 & \frac{1}{2m_ec^2}\mathbf{T} \end{pmatrix} \begin{pmatrix} \mathbf{c}_+ \\ \mathbf{c}_- \end{pmatrix} \mathbf{E} \tag{157}$$

which can be considered as the matrix representation of the Dirac equation (150) transformed to a spin-restricted kinetically balanced basis.[278,397] $\mathbf{V}$, $\mathbf{T}$, and $\mathbf{S}$ are matrix representations of the external electrostatic potential $\hat{V}_{\text{ext}}$, non-relativistic kinetic energy, and basis overlap, respectively. $\mathbf{E}$ is a diagonal matrix containing the eigenvalues, and $\mathbf{W}$ is the matrix representation of the operator $(\boldsymbol{\sigma}\cdot\hat{\mathbf{p}})\hat{V}_{\text{ext}}(\boldsymbol{\sigma}\cdot\hat{\mathbf{p}})$. The matrices $\mathbf{c}_+$ and $\mathbf{c}_-$ contain the expansion coefficients of the two-component spinors of the large and small component in the same basis. Equation (157) presents a generalized eigenvalue problem, which can be solved to yield the coefficients $\mathbf{c}_+$ and $\mathbf{c}_-$. This allows one to construct an operator $\hat{X}$, which relates the large and small components:[278]

$$\Psi_- = \hat{X}\Psi_+, \tag{158}$$

which in the spinor basis reads $\mathbf{c}_- = \mathbf{X}\mathbf{c}_+$ and can be trivially solved to yield

$$\mathbf{X} = \mathbf{c}_- \left(\mathbf{c}_+\right)^{-1}. \tag{159}$$

This result is highly significant, as the operator $\mathbf{X}$ can be used to construct the transformation matrix

$$\mathbf{U}_{\text{X2C}} = \begin{pmatrix} \frac{1}{\sqrt{1+\mathbf{X}^\dagger\mathbf{X}}} & -\frac{\mathbf{X}^\dagger}{\sqrt{1+\mathbf{X}\mathbf{X}^\dagger}} \\ \frac{\mathbf{X}}{\sqrt{1+\mathbf{X}^\dagger\mathbf{X}}} & \frac{1}{\sqrt{1+\mathbf{X}\mathbf{X}^\dagger}} \end{pmatrix}, \tag{160}$$

which exactly decouples the Dirac equation to yield a two-component operator. A scalar version of the X2C method can be achieved by the replacement

$$(\boldsymbol{\sigma}\cdot\hat{\mathbf{p}})\hat{V}_{\text{ext}}(\boldsymbol{\sigma}\cdot\hat{\mathbf{p}}) \rightarrow \hat{\mathbf{p}}\cdot\hat{V}_{\text{ext}}\hat{\mathbf{p}} \tag{161}$$

in the elements of the $\mathbf{W}$ matrix in the modified Dirac equation (157).[278]

[e] A citation for the X2C method is somewhat complicated. We are citing here the theoretical work by Kutzelnigg and Liu,[394–396] and the practical implementations by Liu and Peng[397,398] and by Iliaš and Saue.[399] It should be noted that the work by Kutzelnigg and Liu is based on a conference presentation "Douglas–Kroll the easy way" by Jensen presented at the REHE2005 conference as discussed by Reiher.[385] The review by Reiher,[385] which we are also including in the citation, does not contribute to the development of the theory but does contain a very useful historical narrative of the development along with several more references. The review also discusses other (more or less) equivalent methods developed simultaneously with the work of Kutzelnigg and Liu. The essentially same discussion is also available in ref. 278.

4.4.5 Spin-orbit coupling

In the context of CASSCF calculations, SOC can be introduced in a two-step process. First, a state-averaged CASSCF calculation is carried out to produce a large number CASSCF states. If the active space is chosen as the d- or f-orbital space, usually all possible roots are solved at least in the highest multiplicities. The SOC Hamiltonian matrix is then constructed using these states as a basis and diagonalized to yield the spin-orbit coupled states.[88,89,94,378] This approach to SOC has been shown to be extremely accurate if the preceding *ab initio* calculations are accurate enough.[89,401] If the set of CASSCF states is $\{|\psi_{\nu,S,M_S}\rangle\}$, (where ν contains all other quantum numbers beyond S and M_S required to defined the state), matrix elements of the full Hamiltonian can be written as

$$\begin{aligned}\langle\psi_{\nu,S,M_S}|\hat{H}_{\mathrm{BO}}+\hat{H}_{\mathrm{SOC}}|\psi_{\nu',S',M'_S}\rangle \\ =\delta_{\nu\nu'}\delta_{SS'}\delta_{M_SM'_S}E^{\mathrm{CASSCF}}_{\nu,S,M_S}+\langle\psi_{\nu,S,M_S}|\hat{H}_{\mathrm{SOC}}|\psi_{\nu',S',M'_S}\rangle,\end{aligned} \tag{162}$$

where $\hat{H}_{\mathrm{BO}}$ is the Born–Oppenheimer Hamiltonian including scalar relativistic effects in the one-electron operator. The SOC eigenstates are then given as

$$|\psi^{\mathrm{SOC}}_I\rangle=\sum_{\nu,S,M_S}C^I_{\nu,S,M_S}|\psi_{\nu,S,M_S}\rangle, \tag{163}$$

where the expansion coefficients $\{C^I_{\nu,S,M_S}\}$ are, in general, complex. Before the inclusion of SOC the M_S components of states with the same values of ν and S are degenerate, and this degeneracy is, in general, lifted by SOC. Dynamic correlation corrections calculated with CASPT2 or NEVPT2 methods can be included as simple corrections to the diagonal values of (162). In the context of molecular magnetism, the method in equation (162) is most often used with the Orca and Molcas codes. In the former, the method is called quasi-degenerate perturbation theory (QDPT) approach to SOC, and in the latter the methods is called spin-orbit restricted active space state-interaction (SO-RASSI).[f] The implementations in Orca and Molcas differ in some details but produce very similar results.

The main problem in diagonalizing (162) is the evaluation of the matrix elements of the SOC Hamiltonian. In both Orca and Molcas implementations, the SOC operator is based on the SOC part of the Breit–Pauli Hamiltonian:[137,278,387]

$$\hat{H}^{\mathrm{BP}}_{\mathrm{SOC}}=\frac{\alpha^2}{2}\left(\sum_{i,A}\frac{Z_A}{|\mathbf{r}_i-\mathbf{R}_A|^3}\hat{\mathbf{l}}_{iA}\cdot\hat{\mathbf{s}}_i-\sum_{i,j}\frac{1}{|\mathbf{r}_i-\mathbf{r}_j|^3}\hat{\mathbf{l}}_{ij}\cdot\left(\hat{\mathbf{s}}_i+2\hat{\mathbf{s}}_j\right)\right), \tag{164}$$

where $\alpha=c^{-1}$ is the fine structure constant, A indexes nuclei, i and j index electrons, Z_A is a nuclear charge, $\mathbf{r}_i$ is an electron coordinate, and $\mathbf{R}_A$ is a nuclear

[f] The method could also be SO-CASSI for spin-orbit complete active space state-interaction, but the rassi program in Molcas is general enough to treat states calculated with the RASSCF method. Sometimes, the abbreviation RASSI is used instead of SO-RASSI to denote the method, but this should be avoided, as the RASSI methodology and the rassi program in Molcas can be used to calculate numerous other properties and neither the method nor the program is in any way specific to SOC.

coordinate. The orbital angular momenta are given as

$$\hat{\mathbf{l}}_{iA} = \left(\hat{\mathbf{r}}_i - \hat{\mathbf{R}}_A\right) \times \hat{\mathbf{p}}_i \quad \text{and} \quad \hat{\mathbf{l}}_{ij} = \left(\hat{\mathbf{r}}_i - \hat{\mathbf{r}}_j\right) \times \hat{\mathbf{p}}_j. \tag{165}$$

The first term in the parentheses in (164) is a one-electron SOC operator, whereas the second term is a two-electron operator and contains a contribution from spin-same-orbit and spin-other-orbit couplings. The two-electron terms are rather complicated to evaluate and introduce a substantial bottleneck in the computational times. It would, therefore, be useful to somehow recast $\hat{H}_{\text{SOC}}^{\text{BP}}$ into the form of an effective one-electron operator. The simplest approximation would be to simply neglect the two-electron term and scale the one-electron operator in an empirical manner by, for example, using effective nuclear charges. Such an approach has indeed been attempted, but it produces unreliable results. Heß suggested[402] that the Breit–Pauli SOC operator could be treated with a mean-field approximation, which allows it to be written in the form

$$\hat{H}_{\text{SOC}}^{\text{SOMF}} = \sum_i \hat{\mathbf{z}}_i \cdot \hat{\mathbf{s}}_i, \tag{166}$$

where $\hat{\mathbf{z}}_i$ is a vector operator that only acts on the spatial orbital of electron i, and SOMF stands for spin-orbit mean-field. The SOMF operator can be written as an ITO:[88]

$$\hat{H}_{\text{SOC}}^{\text{SOMF}} = \sum_{q=-k}^{k} (-1)^q \sum_i \hat{z}_{i,q} \hat{s}_{i,-q}, \tag{167}$$

where $k = 1$ is the rank of the operator. It is easy to see from (167) that the SOMF operator transfers 0 or ± 1 quanta of angular momentum projection from the orbital part to the spin part. The problem that remains now is evaluation of the matrix elements $(z_{i,m_k})_{pq} = \langle \phi_p | \hat{z}_{i,m_k} | \phi_q \rangle$. The matrix elements of (164) and (166) between two ON vectors that differ by a single one-electron excitation are equivalent. Thus, in the SOMF approximation, all matrix elements are constructed as if they were evaluated between two CASSCF states differing by a one-electron excitation.[401,402] If a CI expansion is generated that contains only single excitations, the SOMF treatment is equivalent to the use of the full $\hat{H}_{\text{SOC}}^{\text{BP}}$ operator, but the inclusion of higher excitations (as is the case in all problems considered in the present study), it constitutes an approximation. Based on numerical results, however, the approximation is very good.[401]

Following Neese[401] and Berning *et al.*,[403] the matrix elements of $\hat{\mathbf{z}}_p$ are given as

$$\begin{aligned} \langle \phi_p | \hat{\mathbf{z}} | \phi_q \rangle = & \langle \phi_p | \hat{\mathbf{h}}_{\text{SOC}}^{\text{BP}} | \phi_q \rangle + \sum_r n_r \Bigg(\iint \phi_p^*(\mathbf{r}_1) \phi_r^*(\mathbf{r}_2) \hat{\mathbf{g}}_{\text{SOC}}^{\text{BP}} \phi_q(\mathbf{r}_1) \phi_r(\mathbf{r}_2) \mathrm{d}\mathbf{r}_1 \mathrm{d}\mathbf{r}_2 \\ & - \frac{3}{2} \iint \phi_p^*(\mathbf{r}_1) \phi_r^*(\mathbf{r}_2) \hat{\mathbf{g}}_{\text{SOC}}^{\text{BP}} \phi_r(\mathbf{r}_1) \phi_q(\mathbf{r}_2) \mathrm{d}\mathbf{r}_1 \mathrm{d}\mathbf{r}_2 \\ & - \frac{3}{2} \iint \phi_r^*(\mathbf{r}_1) \phi_q^*(\mathbf{r}_2) \hat{\mathbf{g}}_{\text{SOC}}^{\text{BP}} \phi_p(\mathbf{r}_1) \phi_r(\mathbf{r}_2) \mathrm{d}\mathbf{r}_1 \mathrm{d}\mathbf{r}_2 \Bigg), \end{aligned} \tag{168}$$

where

$$\hat{\mathbf{h}}_{\mathrm{SOC}}^{\mathrm{BP}} = \frac{\alpha^2}{2}\sum_{t,T}\frac{Z_T}{|\mathbf{r}_t - \mathbf{R}_T|^3}\hat{\mathbf{l}}_{mM}, \quad \hat{\mathbf{g}}_{\mathrm{SOC}}^{\mathrm{BP}} = \frac{\alpha^2}{2}\sum_{t,u}\frac{1}{|\mathbf{r}_t - \mathbf{r}_u|^3}, \tag{169}$$

and n_p is the occupation number of orbital p. First of the two-electron integrals in the parenthesis in (168) is the Coulomb integral, and the other two are exchange integrals, analogous to HF theory. Two exchange integrals are needed as the matrix elements of the two-electron SOC operator have lower permutational symmetry than the respective elements of the Coulomb operator. The matrix elements of individual Cartesian or spherical components of the operator $\hat{\mathbf{z}}$ can be obtained by simply replacing the angular momentum vector operator with the operator of the corresponding component. Equation (168) constitutes the "full" SOMF approximation, which is widely used in the Orca code. A further approximation to the SOMF treatment is the atomic mean-field integral (AMFI) operator, where only one-center integrals are kept in all expressions and the other integrals are simply neglected; moreover, instead of the full molecular density, pre-determined spherical atomic densities are used in the Coulomb and exchange terms.[402,404] One-center integrals implies here the integrals in AO basis, where all the AOs entering the expression are centered on the same nucleus. The AMFI operator is used in the Molcas code and numerous other programs. The SOMF and AMFI operators give very similar results.[89,401]

In order to diagonalize (162), the matrix element between the CI states $\{|\psi_{\nu,S,M_S}\rangle\}$ need to be evaluated. This can be greatly simplified by application of the Wigner–Eckart theorem, as $\hat{H}_{\mathrm{SOC}}^{\mathrm{SOMF}}$ can be written as an ITO, and the spin-states are eigenstates of the $\hat{S}^2$ operator. The matrix elements can be written in terms of a reduced matrix element as

$$\langle\psi_{\nu,S,M_S}|\hat{H}_{\mathrm{SOC}}^{\mathrm{SOMF}}|\psi_{\nu',S',M'_S}\rangle = \sum_{m_k=-k}^{k}(-1)^{m_k}C_{S'M'_S,km_k}^{SM_S}\langle\psi_{\nu,S}||\sum_i\hat{z}_{i,m_k}\hat{s}_{i,-m_k}||\psi_{\nu',S'}\rangle, \tag{170}$$

where $C_{S'M'_S,km_k}^{SM_S}$ is a CG coefficient and $k = 1$ is the rank of the SOMF operator. The only non-zero reduced matrix elements are

$$\langle\psi_{\nu,S}||\sum_i\hat{z}_{i,0}\hat{s}_{i,0}||\psi_{\nu',S}\rangle = \frac{\sqrt{S(S+1)}}{S}\langle\psi_{\nu,S,M_S}|\sum_i\hat{z}_{i,0}\hat{s}_{i,0}|\psi_{\nu',S,M_S}\rangle, \tag{171}$$

$$\langle\psi_{\nu,S}||\sum_i\hat{z}_{i,+1}\hat{s}_{i,-1}||\psi_{\nu',S+1}\rangle = \sqrt{\frac{2S+3}{2S+1}}\langle\psi_{\nu,S,M_S}|\sum_i\hat{z}_{i,+1}\hat{s}_{i,-1}|\psi_{\nu',S+1,M_S}\rangle, \text{ and} \tag{172}$$

$$\langle\psi_{\nu,S}||\sum_i\hat{z}_{i,-1}\hat{s}_{i,+1}||\psi_{\nu',S-1}\rangle = \langle\psi_{\nu,S,M_S}|\sum_i\hat{z}_{i,-1}\hat{s}_{i,+1}|\psi_{\nu',S-1,M_S}\rangle, \tag{173}$$

where M_S can be any of the allowed values and is usually chosen as $M_S = S$ which is the simplest to evaluate as usually the $M_S = \pm S$ CASSCF states have the shortest CI expansions. Thus, only a single matrix element for each value of M_S corresponding to some S, ν need to be evaluated. The only problem

then remaining is the diagonalization of (162). This is rather trivial as the number of states solved in a state-averaged CASSCF calculation is rarely over a thousand; therefore, the matrix can be completely stored in memory and diagonalized by any standard linear algebra library. In ORCA, the limit of the number of states to include is essentially set by the hardware limits on how large a CASSCF calculation can be carried out. In MOLCAS, the RASSI method is implemented in such a way that it writes large arrays of scratch data on disk during evaluation of the SOC operator matrix, and the size of the scratch disk usually limits the number of states that can be included in the SOC treatment. A further complication that arises in the SO-RASSI treatment of MOLCAS is that the CASSCF states for each multiplicity have their own set of optimized orbitals. This means that if CASSCF states of several multiplicities are mixed by SOC, they are not necessarily orthogonal. Thus, overlap matrices between the CASSCF states need to be evaluated, and the states are then transformed using a method known as a biorthogonal transformation to a form where they can be used as if they had been constructed in the same orbital basis.[94,150,405]

4.4.6 Zeeman interaction

Zeeman interaction between the electron angular momentum and the magnetic field is not strictly a relativistic effect, but it will be mentioned in this section, as the evaluation is based on the same formalism as the spin-orbit coupling treatment discussed in section 4.4.5. The Zeeman interaction can be included by simply adding the Zeeman term ($\hat{H}_{\text{Zee}}$) into equation (162):

$$\delta_{\nu\nu'}\delta_{SS'}\delta_{M_S M_S'} E^{\text{CASSCF}}_{\nu,S,M_S} + \langle \psi_{\nu,S,M_S} | \hat{H}_{\text{SOC}} + \hat{H}_{\text{Zee}} | \psi_{\nu',S',M_S'} \rangle, \tag{174}$$

where $\hat{H}_{\text{Zee}}$ is

$$\hat{H}_{\text{Zee}} = \mu_B \mathbf{B} \cdot \sum_p \left(\hat{\mathbf{l}}_{pO} + g_e \hat{\mathbf{s}}_p \right). \tag{175}$$

The index pO indicates the angular momentum of electron p relative to some user-defined origin O.

4.5 Extraction of spin Hamiltonian parameters from *ab initio* calculations

4.5.1 g-, g̃-, and D-tensors

The one-site anisotropy tensors **g** and **D** are usually calculated by performing a state-averaged CASSCF calculations on a monometallic systems by correlating all electrons in the open atomic shell usually consisting of d or f orbitals. In polymetallic-systems all ions except the one of interest are usually replaced by the closest matching diamagnetic ion. For example, in trivalent lanthanide systems, this is usually achieved by replacing the other ions with Y(III) or Lu(III)

depending on the ionic radius. Dynamic correlation can be accounted for with the NEPVT2, CASPT2, or XMS-CASPT2 methods and/or by extending the active space beyond the minimal CAS.

In the weak SOC case, the elements of the **g** and **D** tensors can be evaluated directly by using expressions in equations (65) and (67). This approach is implemented in ORCA and works well when SOC is weak. Once the SOC starts to grow stronger, the second-order treatment will fail. In such a case, one can use the effective Hamiltonian approach of Maurice, Guihéry, and co-workers.[406] In this approach, a numerical effective Hamiltonian is constructed from spin-orbit coupled orthogonalized *ab intio* eigenvalues and eigenvectors using the spectral decomposition in equation (57). This numerical Hamiltonian is then put in correspondence with an analytical Hamiltonian written in the model space basis of $\{|SM_S\rangle\}$. The elements of the **g** and **D** tensors enter the Hamiltonian matrix elements in a linear manner, and a system of linear equations can be formed by equating the elements of the numerical and analytical matrices. This approach does not rely on any expansion terminated at some finite order and, therefore, works better when SOC is moderately strong. The method does assume that the forms (63) and (64) of the Zeeman and ZFS operators are valid and that the coupling between the target space $\mathcal{P}'$ and its orthogonal complement $\mathcal{P} - \mathcal{P}'$ is weak. The latter conditions breaks down for sufficiently strong SOC. The effective Hamiltonian approach is also implemented in ORCA.

In the case of strong SOC and $\tilde{S} = 1/2$, the $\tilde{\mathbf{g}}$-tensor can be obtained by directly applying equations (72)–(75). The elements of the $\tilde{\mathbf{g}}$-tensor are completely defined by the values of the magnetic moments (72), which are produced by the *ab initio* calculation. Evaluation of the pseudospin tensors is implemented in the SINGLE_ANISO routine of MOLCAS for arbitrarily high values of $\tilde{S}$.[95–97]

4.5.2 Isotropic exchange coupling constants

In systems with just a few spin sites, isotropic exchange coupling constants are usually extracted from energy differences between different spin states. In the simplest case of just two sites, the exchange coupling constant can be evaluated using equation (87). In more complicated cases, especially when one is also interested in the biquadratic terms, effective Hamiltonian methods can be used in a similar manner as described in section 4.5.1.[177,407]

The exchange coupling constants are usually extracted from state-averaged CASSCF calculations performed on a bimetallic system. The values depend very strongly on the amount of dynamic correlation included in the calculation. Performing a CASSCF calculation using just the minimal active space (i. e., the ten d orbitals in transition metal dimer or just the HOMO and LUMO of an organic diradical) can lead to values that are only 20% of the actual exchange coupling constants.[177] In order to produce quantitative values, dynamic correlation must be explicitly treated. Methods based on second-order perturbation theory (such as NEVPT2 or CASPT2) are insufficient if only the minimal active space is used in the preceding CASSCF calculation.[76,77,177,408–413] Better results can be obtained either

by variational treatment of dynamic correlation using multireference CI methods or by enlarging the active space beyond the minimum. The problems arising from insufficient treatment of dynamic correlation are usually more severe in organic radical systems, where the magnetic orbitals are highly delocalized.[414–416]

4.5.3 Parameters for anisotropic exchange

No general implementation for the evaluation of anisotropic exchange parameters is available in any commonly available quantum chemistry code. In the case of weak SOC, Maurice, Guihéry, and co-workers have derived the elements of the tensors describing the anisotropic exchange interaction in simple bimetallic high-symmetry model systems.[230,417] The extraction is based on comparison of analytical and numerical effective Hamiltonians. The approach is not general nor can it be used when the systems have low symmetry. In the case of strong SOC, to the best of our knowledge, no fully *ab initio* calculations have ever been carried out on bimetallic systems. The largest strongly spin-orbit coupled systems that have been treated in a fully *ab initio* manner to date consist of lanthanide–radical systems[418] and without any treatment of dynamic correlation.

The most commonly applied computational method for the treatment of weak exchange interactions in trivalent lanthanide systems is based on a model proposed by Lines[118] and used in an empirical manner. The idea is that one carries out calculations on each magnetic site in the system while all other sites are replaced by diamagnetic ions. Then a basis $\{|\psi_I^{(a)}\rangle \otimes |\psi_J^{(b)}\rangle \otimes \cdots\}$ is constructed from the one-site states as a direct product of the electronic states $I, J = 1, 2, \cdots$ of each site $a, b, \cdots$. For polymetallic systems, the dimension of the basis grows very quickly, and it is common to only include a few states from each site, usually either the lowest Kramers, Ising, or quasi doublet, or all doublets originating from a J-multiplet. A model exchange operator of the form

$$\hat{H}_{\text{Lines}} = -\sum_{i,j} J_{ij} \hat{\mathbf{S}}_i \cdot \hat{\mathbf{S}}_j, \tag{176}$$

where $i, j \in a, b, \cdots$ is then introduced. $\hat{H}_{\text{Lines}}$ only acts on the spin parts of the states. The Lines parameters J_{ij} are empirical parameters, and their value is chosen by fitting the χT product and/or magnetization obtained from the *ab initio* calculation to experiment. In the limit of vanishing SOC or Ising-type exchange interaction,[235] the J_{ij} parameters can be related to physical quantities by the effective Hamiltonian theory. In other cases (which entails practically all cases where the model is used), the J_{ij} parameters are purely empirical; they cannot be related to physical quantities, and they cannot be, even in principle, explicitly calculated from *ab intio* results. The Lines model is widely used in the POLY_ANISO routine of MOLCAS.[96,98,99]

Beyond the use of the Lines model, there are very few examples of the calculation of exchange parameters in lanthanide systems. The exchange Hamiltonian for the coupling between LS multiplets given in equation (95) has been applied to molecular systems. In these calculations, the various parameters necessary for the

evaluation of the exchange parameters have been extracted from various *ab initio* calculations on free ions and DFT calculation on the full systems.[119–121] A similar approach has been used in the present work for the description of anisotropic spin-dependent delocalization.[VIII]

4.5.4 *Ab initio* crystal-field for lanthanides

In addition to methods for the evaluation of pseudospin Hamiltonian parameters, a method for the extraction of the CF parameters (equation (62)) has been implemented in Molcas.[101] The formalism is based on the assumption that the $2J+1$ lowest eigenstates of the SO-RASSI calculation can be put in direct correspondence to states expanded in the basis $\{|JM_J\rangle\}$ with one specific value of J, i. e., one assumes that the coupling between $\mathcal{P}'$ and $\mathcal{P}-\mathcal{P}'$ is negligible. In the case of trivalent lanthanides (with the exception of Sm(III) and Eu(III), see section 3.4.1), this is usually a very good approximation. The magnetic moment operator $\hat{\boldsymbol{\mu}} = \hat{\mathbf{L}} + g_e\hat{\mathbf{S}} = g_J\hat{\mathbf{J}}$ is diagonal in the states $\{|JM_J\rangle\}$ spanning the model space. g_J is the so-called Landé g-factor[20,419] given by

$$g_J = \frac{(g_e+1)J(J+1) - (g_e-1)[L(L+1) - S(S+1)]}{2J(J+1)}. \tag{177}$$

The operator $\hat{\boldsymbol{\mu}}$ can be constructed from the integrals produced by the *ab initio* calculation. Diagonalization of this operator in the target space gives the transformation matrix from the basis of the *ab initio* eigenstates to the mode space basis $\{|JM_J\rangle\}$. Thus, the numerical matrix elements from obtained from the *ab initio* calculation can be put in correspondence with the analytical matrix elements of the CF Hamiltonian (62) in the $\{|JM_J\rangle\}$ basis. The CF parameters B_{kq} enter matrix elements in a linear manner allowing one to write down a system of linear equations for the values of the CF parameters. The set of equations is usually overdetermined, so the parameters are solved by a least-squares fit.

A related but in principle more general method implemented in Orca is the *ab initio* ligand-field theory (AILFT) of Atanasov, Neese and co-workers.[102,103] The theory as, presented above, is restricted to J-type systems, where LS coupling is reasonably well realized. The AILFT has no such restrictions but has not been used in this work.

4.5.5 Qualitative relaxation barrier

As discussed in section 3.6, the calculation (or more precisely, simulation) of the dynamic magnetic relaxation in SMMs is a field still largely in its infancy. A method based on the construction of a qualitative relaxation barrier is, however, implemented in the single_aniso and poly_aniso modules of Molcas.[100] The idea is to plot the energy of the electronic states as a function of the magnetic moment, which gives the barrier-like structure. The electronic states are then connected by matrix elements of the transition magnetic moment, and the path laid by the largest matrix elements defines the relaxation pathway. The results are

conceptually easy to interpret and, although inevitably qualitative, give ample insight into the relaxation process.[249]

The spin–phonon coupling is caused by dynamical distortions of the CF potential.[25] The matrix elements of the spin–phonon coupling are then constructed from factors depending on the lattice vibrations (which possibly include temperature- and field-dependent terms depending on the mechanism) and from an electronic matrix element resulting from the distorted CF. The electronic matrix element consists of the two states coupled by the CF distortion operator, which can be expanded as powers of the operators $\hat{S}_\alpha$ (for S-type systems) or $\hat{J}_\alpha$ (for J-type systems), where $\alpha \in x, y, z$. In S-type systems, the most important contributions to the relaxation mechanisms arise from the rotational contributions of the CF distortions, which are given by operators proportional to the anti-commutator $[\hat{S}_\alpha, \hat{S}_z]_+, \alpha \in x, y$.[25,109,420,421] Assuming that this is also the case for J-type systems, the transition matrix elements are taken over operators of the form $[\hat{J}_\alpha, \hat{J}_z]_+, \alpha \in x, y$.[109,422,423] Let us further assume that the LS-coupling scheme is valid so that the state can be expanded as $|\psi\rangle = \sum_{M_J} C_{M_J} |JM_J\rangle$. Since the basis states are eigenstates of $\hat{J}_z$, only the $\hat{J}_\alpha$ operators in $[\hat{J}_\alpha, \hat{J}_z]$ induce mixing between the states. Then, the electronic contribution to the transition can be reduced to elements of the transition magnetic moment

$$(\boldsymbol{\mu}_{IJ})_\alpha = g_J \mu_B \langle \psi_I | \hat{J}_\alpha | \psi_J \rangle, \tag{178}$$

where $|\psi_I\rangle$ and $|\psi_J\rangle$ are the initial and final states in the transition and $\alpha \in x, y, z$. The transition probability can then be estimated from the average

$$\mu_{IJ} = \frac{|(\boldsymbol{\mu}_{IJ})_x| + |(\boldsymbol{\mu}_{IJ})_y| + |(\boldsymbol{\mu}_{IJ})_z|}{3}. \tag{179}$$

The relaxation barrier calculated using the values of μ_{IJ} is qualitative at best, as all factors governing the lattice part of the spin–phonon transition rates are assumed to be of relatively the same order in all matrix elements so that the transition rate is determined purely by the magnitude of the electronic factors, and because only the lowest ranks of angular momentum operators (the rotational contributions) are considered. Therefore, there is no reason to assume that the qualitative barrier should in all cases coincide with experimental observations.

5 DENSITY FUNCTIONAL THEORY OF STRONGLY CORRELATED SYSTEMS

The quantum chemical methods introduced in Chapter 4 were based on calculations where the state vector $|\psi\rangle$ was approximate but the exact form of the energy functional $E[\psi]$ was known at least to a very good approximation. The main challenge that then arose was the minimization of the energy in terms of the massively complex state vector. An alternate formulation to the theory is to, instead of the state vector, use the three-dimensional electron density $\rho(\mathbf{r})$ (see section 2.3) as the variational entity and approximate the energy functional $E[\rho(\mathbf{r})]$. In approaches based on the exact Hamiltonian, the exact form of the state vector is known (i. e., the FCI treatment) although it must be approximated in practice. In density functional approaches, we know very little of the exact energy functional. It, nonetheless, turns out that fairly simple approximations of the functional can actually lead to very accurate results, which are obtained in density functional approaches at a fraction of the computational costs associated with CI treatments.

Density functional theory (DFT) in its Kohn–Sham incarnation[151,303,424–429] is in many ways an unrivaled success story in the annals of theoretical chemistry, and it can be used to describe a multitude of molecular properties to very high accuracy.[61,78,303] However, in the case of strongly correlated systems (as introduced in Chapter 4) all commonly used density functional approximations will fail in one way or the other.[430–433] DFT can, however, be used to describe strongly correlated systems within the so-called broken symmetry formalism initially proposed by Noodleman.[70–73] The general theory and features of DFT are only briefly introduced here as a great wealth of literature on DFT is available that can describe these aspects at any desired level of detail.[151,209,303,429,434] We will further consider only calculations on finite molecular systems that are carried out using atomic orbital basis sets in the spirit of HF calculation introduced in section 4.1.2. The main focus is placed on introducing the broken-symmetry approach and the many theoretical and practical complications associated to it. We will also briefly address the calculation of **g**- and **D** tensors using DFT.

5.1 Density functional theory

5.1.1 Fundamental proofs

Methods to evaluate the energy as a functional of the electron density emerged already at the same time as the HF theory was being developed.[435–438] However, the first formal proof for the existence of $E[\rho(\mathbf{r})]$ was not given until 1964 when Hohenberg and Kohn published their famous theorems.[424] The first theorem proves the existence of $E[\rho(\mathbf{r})]$ for non-degenerate ground states of an N-particle system of interacting fermions with the density $\rho(\mathbf{r})$, which can be associated with local and multiplicative external electric potential $V_{\text{ext}}(\mathbf{r})$. This association with a potential is called the V-representability condition. The density $\rho(\mathbf{r})$ is completely defined by the external potential $V_{\text{ext}}(\mathbf{r})$ up to an arbitrary constant, and since the external potential $V_{\text{ext}}(\mathbf{r})$ along with the number of particles N (which can be obtained by integrating the density) completely defines the Hamiltonian, the density $\rho(\mathbf{r})$ implicitly determines all properties of the system. The second theorem states that for any trial density $\tilde{\rho}(\mathbf{r})$, $E[\tilde{\rho}(\mathbf{r})] > E_0$, meaning that the ground state energy can be determined in a variational manner:

$$E_0 = \min_{\rho(\mathbf{r})} E[\rho(\mathbf{r})]. \tag{180}$$

The general form of the energy functional is

$$E = \min_{\rho(\mathbf{r})} E[\rho(\mathbf{r})] = \min_{\rho(\mathbf{r})} \left\{ F_{\text{LL}}[\rho(\mathbf{r})] + \int \rho(\mathbf{r}) V_{\text{ext}}(\mathbf{r}) \mathrm{d}\mathbf{r} \right\}, \tag{181}$$

where $F_{\text{LL}}[\rho(\mathbf{r})]$ is the so-called Levy–Lieb (LL) functional. We are following here the constrained search formulation of DFT formulated by Levy[439,440] and Lieb.[441] In the original theory by Hohenberg and Kohn, the Hohenberg–Kohn (HK) functional $F_{\text{HK}}[\rho(\mathbf{r})]$ was used, which has a very similar mathematical form as $F_{\text{LL}}[\rho(\mathbf{r})]$ but is constrained to densities that are V-representable. The most general approach to DFT is given by the Lieb functional $F_{\text{L}}[\rho(\mathbf{r})]$.[426,441] The Lieb functional is convex and has very favorable properties, such as it is guaranteed to produce a unique solution and the convexity of the functional is closely related to its differentiability.[442,443] The derivation and properties of the Lieb functional are related to convex analysis and will not be discussed here.

The LL functional is given as

$$F_{\text{LL}}[\rho(\mathbf{r})] = \min_{\psi \to \rho(\mathbf{r})} \langle \psi | \hat{T} + \hat{V}_{\text{ee}} | \psi \rangle, \tag{182}$$

where $\hat{T}$ is a kinetic energy operator, $\hat{V}_{\text{ee}}$ is the Coulomb operator for the electron–electron repulsion, and the minimization runs over all states $|\psi\rangle$ represented by a wave function $\psi(\{\mathbf{r_i}, m_{si}\})$, which produces the density $\rho(\mathbf{r})$ through equation (23). The LL functional is defined for any density $\rho(\mathbf{r})$, which can be generated from some N-particle wave function $\psi(\{\mathbf{r_i}, m_{si}\})$ (the so-called N-representability

condition), and the existence of such a wave function for a set of simple and reasonable conditions has been proven.[444] It should be noted that in the strictest mathematical sense, the minimum in (182) should be replaced with an infimum.

The proof of Hohenberg and Kohn considers purely electrostatic external potentials $V_{\text{ext}}(\mathbf{r})$, which are time-independent. Generalization to time-dependent potential is possible[445] but is of no interest to us here. When considering the magnetic properties of materials, much more relevant generalization is to consider external potentials with magnetic fields. In a non-relativistic framework, the practical generalization to the case of magnetic fields is fairly simple if we neglect the effects of the magnetic field on orbital degrees of freedom. This is a rather good approximation for S-type systems in weak fields, and this is the situation we are mostly interested in here. The generalization entails the replacement of the total density with spin densities:[151,446–448] $\rho(\mathbf{r}) \rightarrow \rho^{\alpha}(\mathbf{r}), \rho^{\beta}(\mathbf{r})$. An equivalent formulation is to consider the density and the spin-polarization density defined as $Q(\mathbf{r}) = \rho^{\alpha}(\mathbf{r}) - \rho^{\beta}(\mathbf{r})$. Both the density and the spin-polarization density are actual observables. The spin-dependent generalization of DFT is known as the spin-density functional theory, which is the theory we are interested in here, and we will refer to it simply as DFT. A strict derivation of spin DFT starting from the relativistic theory is rather complicated and cannot be presented in a satisfactory way without considering quantum field theory.[278,429,449] In the present work, we will only consider the spin-dependent generalization by the substitution $\rho(\mathbf{r}) \rightarrow \rho^{\alpha}(\mathbf{r}), \rho^{\beta}(\mathbf{r})$.

The application of $F_{\text{LL}}[\rho(\mathbf{r})]$ is in practice equivalent to carrying out a full CI calculation on *all* conceivable wave functions describing the system. It is obvious that such an approach is neither feasible even for a fairly small set of wave functions of a very simple system of chemical interest nor would such an approach make any sense since if this was possible we could simply carry out the FCI calculation and be content with it. The unfortunate feature of HK, and LL, and Lieb theories for that matter, is that they do not suggest any useful way of approximating $F_{\text{HK}}[\rho(\mathbf{r})]$, $F_{\text{LL}}[\rho(\mathbf{r})]$, or $F_{\text{L}}[\rho(\mathbf{r})]$. It can be rather easily shown that the value of the energy depends on the value of the density at *every point in space* and that the functional will vary in terms of the particle number N in a *non-analytic* manner.[209] The idea of developing a simple, or even highly complicated, approximation to the LL functional, therefore, seems rather hopeless. The theory can, however, be turned into a useful form by the approach proposed by Kohn and Sham by the introduction of a non-interacting reference system.[425]

5.1.2 The Kohn–Sham theory

In 1965, the year following the publication of the celebrated HK theorems, Kohn and Sham published another seminal paper, which formulated a practical approach to DFT.[425] The Kohn–Sham (KS) formulation is so widely used today that the term DFT is by all intents and purposes synonymous with KS DFT. The idea in KS theory is that the density $\rho(\mathbf{r})$ has an energy $E = E[\rho(\mathbf{r})]$ regardless of how the density is produced as long as it and the energy functional are exact.

Therefore, they introduced a non-interacting KS reference system $\Phi_{\mathrm{KS}}(\{\mathbf{r}_p, m_{sp}\})$, which is represented by a single Slater determinant constructed from orbitals $\{\phi_{p\sigma}(\mathbf{r})\}$ so that

$$\rho(\mathbf{r}) = \sum_{p,\sigma} \phi^*_{p\sigma}(\mathbf{r})\phi_{p\sigma}(\mathbf{r}). \tag{183}$$

The LL functional is then divided into

$$F_{\mathrm{LL}}[\rho(\mathbf{r})] = T[\{\phi_{p\sigma}(\mathbf{r})\}] + J[\rho(\mathbf{r})] + E_{\mathrm{XC}}[\rho_\alpha(\mathbf{r}), \rho_\alpha(\mathbf{r})], \tag{184}$$

where the first term on the right-hand side is the kinetic energy of the non-interacting reference system, the second term is the classic electrostatic interaction between the electrons (usually known as the Hartree energy), and the last term is the so-called exchange–correlation (XC) functional. The kinetic and Hartree energies are given by the well-known expressions

$$T[\{\phi_{p\sigma}(\mathbf{r})\}] = -\frac{1}{2}\sum_{i,\sigma} \phi^*_{p\sigma}(\mathbf{r})\nabla^2\phi_{p\sigma}(\mathbf{r})\mathrm{d}\mathbf{r} \quad \text{and} \quad J[\rho(\mathbf{r})] = \iint \frac{\rho(\mathbf{r}_1)\rho(\mathbf{r}_2)}{|\mathbf{r}_1 - \mathbf{r}_2|}\mathrm{d}\mathbf{r}_1\mathrm{d}\mathbf{r}_2. \tag{185}$$

The explicit form of the XC functional is not known, but assuming that we can approximate it reasonably well using some simple expression (and it turns out we can), we should be able to approximate the full energy of the system reasonably well since most of the energy is already accounted for by the $T[\{\phi_{p\sigma}(\mathbf{r})\}]$ and $J[\rho(\mathbf{r})]$ terms. It should be noted that $T[\{\phi_{p\sigma}(\mathbf{r})\}]$ is an explicit functional of the orbitals, and implicit functional of the density as the density indirectly determines the orbitals. In spin-polarized systems, the XC functional is a functional of the spin densities or, equivalently, a functional of the density and the spin-polarization density.

Minimization of (181) using (184), similar to HF theory, yields N effective one-particle equations known as the KS equations

$$\left(-\frac{1}{2}\nabla^2 + \hat{V}^\sigma_{\mathrm{KS}}(\mathbf{r})\right)\phi_{i\sigma}(\mathbf{r}) = \epsilon_{i\sigma}\phi_{i\sigma}(\mathbf{r}). \tag{186}$$

The KS potential $\hat{V}^\sigma_{\mathrm{KS}}(\mathbf{r})$ is defined as

$$\hat{V}^\sigma_{\mathrm{KS}}(\mathbf{r}) = \hat{V}_{\mathrm{ext}}(\mathbf{r}) + \hat{V}_{\mathrm{Hartree}}(\mathbf{r}) + \hat{V}^\sigma_{\mathrm{XC}}(\mathbf{r}), \tag{187}$$

where $\hat{V}_{\mathrm{Hartree}}(\mathbf{r})$ and $\hat{V}^\sigma_{\mathrm{XC}}(\mathbf{r})$ are the functional derivatives of the Hartree and XC functionals with respect to the density:

$$\hat{V}_{\mathrm{Hartree}}(\mathbf{r}) = \int \frac{\rho(\mathbf{r})'}{|\mathbf{r} - \mathbf{r}'|}\mathrm{d}\mathbf{r}' \quad \text{and} \quad \hat{V}^\sigma_{\mathrm{XC}}(\mathbf{r}) = \frac{\delta E_{\mathrm{XC}}[\rho^\alpha(\mathbf{r}), \rho^\beta(\mathbf{r})]}{\delta\rho^\sigma(\mathbf{r})}. \tag{188}$$

It should be noted that compared to the HF theory, the energy minimization has an additional constraint that the XC potential must be local and multiplicative.[429]

Solving the KS equations is very similar to solving the HF equations, and most quantum chemistry codes capable of carrying out HF calculations are also

capable of carrying out KS DFT calculations. The most problematic term is the XC potential, which usually cannot be integrated analytically and, therefore, has to be evaluated on a grid. The grid introduces a new approximation to the calculation, but the actual numerical integration is rarely a computational bottleneck. A further advantage in DFT calculations is that the energy does not necessarily depend on any non-local potential, and RI and density-fitting techniques can be used very efficiently. The formal scaling of DFT methods is of the same order as HF but can be brought significantly down using linear scaling techniques.[450] Like HF calculations, DFT calculations can also be formulated in restricted and unrestricted formalism. We will here focus only on the unrestricted case as the restricted case is not relevant for magnetic systems.

5.1.3 The exchange-correlation functional

The main choice for the user of a DFT code is the approximation to the XC functional, or equivalently, the XC potential. The quality of the approximation is ultimately what the success of a DFT calculation thrives or dies with. The XC energy is usually divided to contributions from the exchange energy $E_X = E_X[\rho^\alpha(\mathbf{r}), \rho^\beta(\mathbf{r})]$ and the correlation energy $E_C = E_C[\rho^\alpha(\mathbf{r}), \rho^\beta(\mathbf{r})]$. The XC potential can then be divided in a similar manner. The exchange energy is usually (at least in single-reference systems) an order of magnitude larger than the correlation energy.

DFT was originally founded as a theory to describe materials; therefore, the simplest starting point for the description of exchange and correlation is the homogeneous electron gas (HEG), which is a hypothetical model system consisting of constant electron density over all space balanced by a uniform positive charge. The exact expression for the exchange energy of HEG is known, and the correlation energy can be approximated to very high accuracy.[151] The simplest approximation to the XC functional is the local spin density approximation (LSDA), where the electron density is assumed to act locally like the HEG and to vary slowly over space. The LSDA was the initial approximation to the XC functional proposed in the paper of Kohn and Sham.[425] The LSDA exchange and correlation functionals are given as

$$E_X^{\mathrm{LSDA}}[\rho^\alpha(\mathbf{r}), \rho^\beta(\mathbf{r})] = \int \rho(\mathbf{r}) \epsilon_X^{\mathrm{HEG}}(\rho^\alpha(\mathbf{r}), \rho^\beta(\mathbf{r})) \mathrm{d}\mathbf{r} \tag{189}$$

$$E_C^{\mathrm{LSDA}}[\rho^\alpha(\mathbf{r}), \rho^\beta(\mathbf{r})] = \int \rho(\mathbf{r}) \epsilon_C^{\mathrm{HEG}}(\rho^\alpha(\mathbf{r}), \rho^\beta(\mathbf{r})) \mathrm{d}\mathbf{r}, \tag{190}$$

where $\epsilon_X^{\mathrm{HEG}}(\rho^\alpha(\mathbf{r}), \rho^\beta(\mathbf{r}))$ and $\epsilon_C^{\mathrm{HEG}}(\rho^\alpha(\mathbf{r}), \rho^\beta(\mathbf{r}))$ are the exchange and correlation energy densities of the HEG, which are *functions* of the spin densities. The explicit form of the former is known, and it is called the Slater exchange, and the latter is usually approximated by an empirical form fitted to high-accuracy *ab initio* data. The most common approximations to the correlation energy density are the VWN and VWN5 approximation of Vosko, Wilk and Nusair.[451]

While the homogeneous electron gas is a reasonable approximation to certain metallic materials, such as the alkali metals where the electron density

is rather uniform, this is certainly not the case for atoms or molecules where the density can vary from high values near atomic nuclei to zero in the vacuum surrounding the system. The generalized gradient approximation (GGA) is an improvement over the LSDA in the cases of non-homogeneous electron gas. The GGA exchange functional is written as

$$E_{\mathrm{X}}^{\mathrm{GGA}}[\rho^{\alpha}(\mathbf{r}),\rho^{\beta}(\mathbf{r}),\nabla\rho(\mathbf{r})] = \int \rho(\mathbf{r})F_{\mathrm{X}}(\xi)\epsilon_{\mathrm{X}}^{\mathrm{HEG}}(\rho^{\alpha}(\mathbf{r}),\rho^{\beta}(\mathbf{r}))\mathrm{d}\mathbf{r}, \tag{191}$$

where we have introduced the enhancement factor $F(\xi)$, which is a function of the reduced density gradient

$$\xi = \left(\frac{\nabla\rho(\mathbf{r})}{2\left[3\pi^2\rho(\mathbf{r})\right]^{1/3}\rho(\mathbf{r})}\right)^2. \tag{192}$$

A more generalized approximation can be achieved in the so-called meta-GGA functionals, where the enhancement factor is, in addition to ξ, also a function of the "reduced density Laplacian" η written as a function of the kinetic energy density

$$\tau(\mathbf{r}) = \frac{1}{2}\sum_{p,\sigma}|\nabla\phi_p(\mathbf{r})|^2, \tag{193}$$

where the summation runs over occupied orbitals.

While certain properties of $F(\xi)$ and $F(\xi,\eta)$ are known, the enhancement factors are usually constructed in a somewhat empirical way by either enforcing known limits and constraints and/or by fitting parameters to experimental or high-level *ab initio* data. Popular early approximations to the exchange functional that still remain in wide use are the 1986 approximation by Perdew and Wang (PW86)[452] and the improved version developed in 1991 (PW91),[453,454] the 1988 approximation by Becke (B88),[455] and the 1996 functional by Perdew, Burker, and Ernzerhof (PBE).[456,457] The GGA and meta-GGA correlation functionals have somewhat complicated forms and will not be discussed in detail here. The most popular early approximations include the 1986 approximation by Perdew (P86)[458,459] the 1988 functional by Lee, Yang, and Par (LYP),[460] the correlation part of the PW91 functional,[453,454] and the correlation part of the 1996 PBE functional.[456,457] All of these early functionals were developed by satisfaction of known constraints and limits. A general form of a GGA with parameters that can be fitted to experiment was developed by Becke in 1997 (B97).[461] Several other parameterizations, including the B97-1, B97-2, B98 functionals, have since been published by several authors.[462–464] Ideas borrowed from the B97 model have also been used in the development of the HCTH family of functionals by Handy and co-workers,[465–467] the meta-GGA kinetics functional by Bose and Martin (BMK),[468] the meta-GGA functional by Tao, Perdew, Staroverov, and Scuseria (TPSS),[469,470] and the M06-L[471,472] and SOGGA11[473] meta-GGA functionals by Truhlar and co-workers.

GGA and meta-GGA functionals are accurate enough to have practical use in quantum chemistry. It was not, however, until a class of functionals known as

hybrid functionals were introduced that DFT became an overwhelming success in computational chemistry. The idea in hybrid functionals is to introduce a percentage of exchange energy calculated using HF theory. The exchange energy is given by the expectation value of the operator (105) taken over all orbitals of the reference system. This exchange is usually referred to either as exact exchange or Fock exchange. We will adopt the latter term, as the Fock exchange is not exact in the broadest sense of the word. HF theory is capable of treating exchange effects of a non-interacting many-particle system of fermions *exactly*. In KS DFT, we are already introducing the majority of the kinetic energy by simply evaluating the kinetic energy of the non-interacting reference system; it would, therefore, seem reasonable that we could also introduce the majority of exchange energy by considering the exchange energy of the reference system. This is, however, not the case. Fock exchange is a non-local property, whereas the GGA correlation is a local in the sense that it only depends on local gradients. It can be shown that the sum of exact exchange and exact correlation is also a local property.[430] Therefore, the correlation functional should be able to compensate for the non-locality of the Fock exchange, which cannot be achieved by any local or semi-local approximation, such as LSDA or GGA. The locality/non-locality of exchange and correlation is usually discussed in terms of the exchange and correlation holes, which make the concepts much more intuitive (see, for example, references 303 and 430). To avoid the problems related to the non-locality, Becke suggested that a predetermined percentage of Fock exchange should be introduced, while the rest of the exchange would be described by the LSDA and GGA exchanges.[474,475] A formal justification for this approach lies in the so-called adiabatic connection.[429,475–478]

Hybrid functionals are usually constructed in an empirical manner. Initially, Becke suggested a fifty-fifty mixing of Fock and LSDA exchanges.[474] The initial form was not highly successful, but it was later refined to the the so-called B-half-and-half-LYP, which utilizes B88 exchange and LYP correlation and is often abbreviated as BHHLYP. The first truly successful hybrid was introduced by Becke in the general form[475]

$$E_{\mathrm{X}}^{3-\mathrm{hyb}} = a_0 E_{\mathrm{X}}^{\mathrm{Fock}} + a_1 \Delta E_{\mathrm{X}}^{\mathrm{GGA}} + (1 - a_0 - a_1) E_{\mathrm{X}}^{\mathrm{LSDA}} \tag{194}$$

$$E_{\mathrm{C}}^{3-\mathrm{hyb}} = b_1 \Delta E_{\mathrm{C}}^{\mathrm{GGA}} + (1 - b_1) E_{\mathrm{C}}^{\mathrm{LSDA}}, \tag{195}$$

where $\Delta E_{\mathrm{X}}^{\mathrm{GGA}}$ and $\Delta E_{\mathrm{C}}^{\mathrm{GGA}}$ are the GGA corrections to the LSDA exchange and correlation energies. The original parameterization used the standard Slater exchange in the LSDA part, the B88 GGA functional for exchange, the VWN correlation in the LSDA part, and the PW91 GGA correlation.[474] Several forms of the VWN functional were introduced in the original paper by Vosko, Wilk, and Nusair[451] and the version used in the hybrid functional depends on the implementation in a specific quantum chemistry code. The parameters were optimized by fitting to experimental thermochemical data to give $a_0 = 0.20$, $a_1 = 0.72$, and $b_1 = 0.81$. This combination of functionals and parameters is known as the B3PW91 hybrid. The same functional form and set of parameters

were also employed by Stephens *et al.* in the B3LYP functional, where the PW91 GGA correlation is replaced by the LYP correlation.[479] B3LYP is possibly the most widely used hybrid functional, and in fields, such as organic thermochemistry, its use is so widespread that the terms B3LYP and DFT are largely synonymous.

Later, a simpler one-parameter form

$$E_{\mathrm{X}}^{1-\mathrm{hyb}} = a_0 E_{\mathrm{X}}^{\mathrm{Fock}} + (1 - a_0) E_{\mathrm{X}}^{\mathrm{GGA}} \tag{196}$$

$$E_{\mathrm{C}}^{1-\mathrm{hyb}} = E_{\mathrm{C}}^{\mathrm{GGA}} \tag{197}$$

has been introduced,[478] where $E_{\mathrm{X}}^{\mathrm{GGA}}$ and $E_{\mathrm{C}}^{\mathrm{GGA}}$ are total GGA energies including the contribution from the underlying LSDA. The most notable example of this functional form is the PBE0 functional, where $a_0 = 0.25$ and the PBE exchange and correlation GGA functionals have been used.[480,481,a] The parameter has been determined in a non-empirical manner by perturbation arguments.[478] A similar functional form was also used in Becke's B1B95 functional, which employs the B88 exchange functional and the rarely used 1995 correlation functional by Becke.[482] Numerous other hybrid functionals have been developed with more complicated parameterization including hybrid versions of the B97, B97-1, B97-2, B98, HCTH, BMK, and TPSS (known as TPSSh) functionals discussed above. Some of the most complicated functionals have been developed by Truhlar and co-workers and are usually referred to as the Minnesota family of functionals. These functionals come in a number of different incarnations and modifications, and include the M05,[483] M05-2X,[484] M06,[471,472] M06-2X,[471,472] M06-HF,[471,472,485] M08-HX,[486] M08-SO,[486] and SOGGA11-X.[487]

It should be noted that the the energy minimization in KS DFT is constrained in such a way that the KS potential (187) must be local and multiplicative; the exchange potential in HF theory constructed using the operator (105) is neither. The non-local nature of the potential introduces an explicit dependence on the "off-diagonal" elements of the spin-density matrices in the energy expression. This means that if the HF exchange potential is used in a DFT calculation, as it usually is, the calculation is no longer strictly a DFT calculation but instead a reduced density matrix functional theory calculation.[444,488] Usually, this problem is, however, simply ignored as a theoretical formality with little practical relevance. A potential that is both local and multiplicative and corresponds to the HF

[a] The first results using the PBE0 functional were simultaneously and independently published by Ernzerhof and Scuseria[480] and by Adamo and Barone.[481] The papers were submitted to the Journal of Chemical Physics on consecutive days and both accepted in December 1998. Ernzerhof and Scuseria called the functional PBE1PBE standing for "PBE exchange one-parameter hybrid PBE correlation" following the same naming convention as Becke. Adamo and Barone used the name PBE0, which stands for "PBE zero-parameter hybrid". The term 'zero parameter' implies that the functional has no parameters, which have been fitted to experimental data although it does have one parameter determined from first principles. The name PBE1PBE is used in the GAUSSIAN code, whereas the name PBE0 is more common in other codes. In the literature, sometimes only one of the papers is cited, usually in a manner related to the naming convention of the functional. The PBE0 and PBE1PBE functionals are, however, equivalent and in our opinion, the standard citation should include both papers.

exchange energy functional can be constructed using the optimized effective potential (OEP) methods,[209,429] but this will not be discussed here.

The hybrids defined by equations (194)–(195) introduce the Fock exchange through global scaling, meaning that the same set of parameters for the Fock/GGA exchange division is used in every point in space. An alternative approach is to use range-separation, where the Fock exchange is introduced as a function of $\mathbf{r}$ in the exchange potential $V_X^\sigma(\mathbf{r})$.[489] The idea was first introduced into quantum chemistry by Savin and co-workers in various approaches to combine wave-function-based methods with DFT[490–492] and was later applied to the separation of the exchange potential by Tsuneda and co-workers.[493] The general idea in range-separated functionals is to separate the Coulomb operator into a short and a long range part. This is most often achieved by use of the error function:

$$\frac{1}{\mathbf{r}} = \frac{1 - \mathrm{erf}(\omega \mathbf{r})}{\mathbf{r}} + \frac{\mathrm{erf}(\omega \mathbf{r})}{\mathbf{r}}, \tag{198}$$

where $\mathbf{r} = |\mathbf{r}_1 - \mathbf{r}_2|$ and ω is the range separation parameter. In solid state calculations on periodic systems, the long-range part in (198) is usually treated with GGA exchange due to complications which arise from the slow decay of the Fock potential, and the short-range exchange is treated with Fock exchange. In molecular systems, which we are mostly interested in the present work, the short range part is treated with GGA exchange and the long-range part using Fock exchange. This results into the correct asymptotic decay of the exchange potential and also allows one to include higher amounts of Fock exchange into the approximation as compared to conventional global hybrids, which is useful in the context of the calculation of exchange coupling constants as discussed in section 5.2.4. In such approximations, at the limits $|\mathbf{r}| = 0$ and $|\mathbf{r}| \to \infty$, all of the exchange is described by the GGA and Fock exchange, respectively. The range-separation parameter ω determines how rapidly the transition between these two types of exchange potentials takes place when $\mathbf{r}$ increases. The ω parameter is in principle a functional of the density and, therefore, system-specific,[494] but in practice, a single value is usually determined from a fit to experimental data and used in the functional definition. Another approach is the so-called optimal tuning, where ω is chosen for each system in such a way that it equates the energy of the highest occupied orbital with the ionization potential.[495,496] This approach is often used in the calculation of charge-transfer excitation energies[497–499] but leads to undesired consequences, such as loss of size-consistency.[500] The error function is chosen due to its favorable mathematical properties when used in conjunction with Gaussian basis sets, but other functions are possible and have been used.[501–503]

A more general parameterization of the range-separation (198) was introduced later by Yanai *et al.*, which allows one to have finite amounts of GGA and Fock exchange at both limits $|\mathbf{r}| = 0$ and $|\mathbf{r}| \to \infty$:[504]

$$\frac{1}{\mathbf{r}} = \frac{1 - [a + b\,\mathrm{erf}(\omega \mathbf{r})]}{\mathbf{r}} + \frac{a + b\,\mathrm{erf}(\omega \mathbf{r})}{\mathbf{r}}, \tag{199}$$

The original paper by Yanai *et al*. applied the general form (199) with the B88 and LYP GGA functionals and parameters $\omega = 0.33$, $a = 0.23$ and $b = 0.57$ giving the CAM-B3LYP functional (CAM stands for Coulomb-attenuating method). Other widely used parameterization is the ωB97X functional of Head-Gordon and co-workers based on the B97 GGA.[505] Range-separation has also been used in the context of highly paremterized pure meta-GGA functionals, such as the M11-L,[506] MN12-L,[507] N12,[508] and MN15-L[509] to introduce the GGA exchange in different forms for different ranges. These meta-GGA functionals have been further employed in the construction of the state-of-the-art range-separated hybrids M11,[510] N12-SX,[511] MN12-SX[511] and the global hybrid MN15[512] with range-separated GGA exchange.

In the original approach suggested by Tsuneda, the range-separation enters the density functional approximation only in the LSDA part. This means that any GGA functional can be used in conjunction with the range-separation as the enhancement factor $F(\xi, \eta)$ in equation (191) remains unaltered. Another approach has been introduced by various authors in conjunction with the PBE functional, where the range-separation is carried out on the full GGA functional and not just on the LSDA part giving the functional ωPBE.[513–515] This approach is, in principle, more accurate, but the derivation has so far only been possible on the PBE functional due to its simple analytical form. The ωPBE functional is used in the LC-ωPBE[515–518] and HSE[515,517,519–523] functionals of Heyd, Scuseria, Ernzerhof, Vydrov, Henderson, and co-workers.[b] The former uses Fock exchange in the long-range part, whereas the latter is designed for periodic calculations and uses Fock exchange in the short-range part.

5.2 The broken symmetry method for strongly correlated systems

5.2.1 Energy difference between spin states in the context of DFT

In order to calculate exchange coupling constants between two sites with spins S_1 and S_2, one needs to evaluate the energy difference between the HS state, where $S = S_1 + S_2$ and the LS state with $S = |S_1 - S_2|$. Assuming the two sites are orbitally non-degenerate (i. e., *S*-type systems), the HS state is described

[b] When comparing data calculated with HSE and LC-ωPBE functionals, one should be careful as both functionals have several incarnations. The first forms of ωPBE and HSE were published in 2003[513,514] and a slight improvement in the derivation of the ωPBE functional was carried out in 2004.[519] Both of these first two incarnations or just the latter one are sometimes referred to as HSE03 in the literature. The LC-ωPBE functional was introduced in 2006 using the 2004 definition of ωPBE.[516] In 2006, the value of the range-separation parameter in HSE was slightly modified, and the improved version of the functional is usually referred to as HSE06.[523] In 2009, Henderson *et al*. suggested a further improvement in the ωPBE functional derivation.[515] The resulting improved version of HSE is still usually referred to as HSE06, whereas the improved version of LC-ωPBE is sometimes referred to as LC-ωHPBE, where the H stands for Henderson. It should be noted that the notations HSE03, HSE06, and LC-ωHPBE are in no way standardized.

qualitatively correctly using just a single Slater determinant. The LS state is, however, intrinsically multiconfigurational and cannot be described by a single determinant. In principle, this should not matter in DFT as the KS reference system is just mathematical fiction and is not required to represent the true many-particle wave function of the system. In practice, however, all commonly applied approximation to the XC functional will fail if the KS reference wave function is qualitatively different from the real wave function; or, in other words, the XC energy is large.[430–433] The KS approach is able to account for some of the static electron correlation arising from the multireference nature of the state, but does this in a spurious manner. The "static correlation" is mostly errors in the functional approximation mimicking static correlation effects. The concept of static electron correlation in the context of DFT has been extensively discussed by Cremer and co-workers in a number of articles.[524–533]

A further problem in the calculation of energy differences between spin states arises because one cannot strictly enforce a spin-state on a system in KS DFT. It has been shown by Gunnarsson and Lundqvist[476] that the energy minimization can be carried out in principle by confining the solution to a specific spin state assuming that SOC can be neglected. The total spin of the system is a functional of the electron density, but no explicit expression is available. Therefore, in practice, one usually only fixes the projection of the spin M_S, which can be simply calculated from the number of α and β electrons in the system and is known if the spin densities are known, which is usually the case. Thus, when addressing the HS and LS states in the context of DFT, the HS state is taken as the one where $M_S = M_{S1} + M_{S2}$ and the LS state as the one where $M_S = |M_{S1} - M_{S2}|$. The single-determinental state with $S = S_1 + S_2$ is the lowest energy state with $M_S = M_{S1} + M_{S2}$; thus, fixing the spin projection to $M_S = M_{S1} + M_{S2}$ usually yields a good approximation to the actual $S = S_1 + S_2$ state. The situation is quite different in the case of the LS solution, where the $M_S = |M_{S1} - M_{S2}|$ solution usually converges to a state that is neither the $M_S = |M_{S1} - M_{S2}|$ component of the $S = S_1 + S_2$ state nor the $S = |S_1 - S_2|$ state. If the two magnetic sites are related by a symmetry operation, the LS solution usually has lower symmetry than the nuclear framework and is therefore referred to as the broken symmetry (BS) solution. The symmetry breaking results from the inability of the XC functional to introduce enough static correlation energy to optimize the LS solution to the correct spin state. In the following, we will use the term BS state for the $M_S = |M_{S1} - M_{S2}|$ state and the term HS state for both the $S = S_1 + S_2$ and $M_S = M_{S1} + M_{S2}$ states.

DFT approaches to avoid this unphysical symmetry breaking by introducing the missing static electron correlation have been developed. Some notable successes have been achieved by using the random phase approximation (RPA)[534–537] or by replacing the single-determinental reference wave function with an ensemble density in the ensemble KS referenced (REKS) approach of Filatov and co-workers.[538–543] Some success in describing the static correlation has also been achieved in the conventional KS scheme by Becke[544–548] and, based on Becke's work, by Kong and co-workers.[549–552] A completely different approach is to cal-

culate the energy difference between the HS and LS states as a response property of the HS state and avoid making any explicit reference to problematic BS state altogether. Such approaches include methods based on spin-flip time-dependent DFT,[553–556] constrained DFT,[557,558] non-collinear spin DFT perturbation theory,[559] non-collinear couple-perturbed spin DFT,[560–563] non-collinear time-dependent spin DFT,[564] and Green's functions.[565]

The most popular approach to the evaluation of the energy difference, however, is the BS formalism. In the BS approach, the idea is to construct the energy difference between the HS and LS states from the energy difference between the HS and BS states. The BS approach was initially introduced in the context of unrestricted HF theory and Slater's $X\alpha$ theory[303,566] also known as the Hartree–Fock–Slater method. The $X\alpha$ theory can be considered as both an approximate HF approach and rudimentary density functional method. The difference between DFT and the HF methods is that in the latter we have an approximate wave function, whereas in the former we only have the wave function of the reference state, which serves no physical meaning. We will first discuss the BS approach in the context of approximate wave functions, as it was originally formulated, in section 5.2.2 and then discuss the generalization to DFT framework in section 5.2.3.

5.2.2 Broken symmetry method in the context of Hartree–Fock theory

Let us again consider a system with two spin sites a and b. The HS state is described reasonably well at unrestricted HF (UHF) level by constraining the spin projection to $M_S = M_{Sa} + M_{Sb}$. The calculation produces a single determinant with a number of approximately closed shell orbitals corresponding to the metal core and ligand orbitals and a set of singly occupied molecular orbitals (SOMOs) localized at the spin sites a and b. This is a reasonable approximation to the true HS state with $S = S_a + S_b$, and the SOMOs can be put into direct correspondence with the orthogonal magnetic orbitals. If the SOMOs are delocalized, they might first have to be transformed by some unitary transformation. The LS state with $S = |S_a - S_b|$ is inherently multideterminental and cannot be described at HF level. Constraining the spin projection to $M_S = |M_{Sa} - M_{Sb}|$ and lifting any spatial symmetry constraints leads to the BS state. The BS state can be thought of as the HS state but with the spins at one site flipped and the orbitals re-optimized. In UHF, the α and β orbitals are orthogonal with each other only through the spin functions, and the spatial orbitals can have finite overlap. This means, that unlike the orthogonal magnetic orbitals, the SOMOs in the BS solution are not orthogonal and are conceptually more closely related to the valence bond description of magnetic interaction than the strictly orthogonal MO description.[70,567] The two limits, zero overlap and perfect overlap, are known as the Ising limit and the covalent limit, respectively. At the covalent limit, the orbitals at the two sites interact strongly, and the situation is better described as covalent bonding than AFM interaction. At this limit, the system can be reasonably well described by a single determinant and is of no interest to us. In molecular magnetic systems, the

Ising limit is usually realized at least approximately. The nature of the BS state can be investigated by the $\langle \hat{S}^2 \rangle_{\mathrm{BS}}$ expectation value, which is produced after the UHF calculation. $\langle \hat{S}^2 \rangle_{\mathrm{UHF}}$ is given by[127]

$$\langle \hat{S}^2 \rangle_{\mathrm{UHF}} = M_S(M_S+1) + N_\beta - \sum_p^{N_\alpha} \sum_q^{N_\beta} \underbrace{\left| \int \phi^*_{p\alpha}(\mathbf{r}) \phi_{q\beta}(\mathbf{r}) \mathrm{d}\mathbf{r} \right|^2}_{=S_{ab}^{\alpha\beta}}, \tag{200}$$

where we have, without loss of generality, assumed that $N_\alpha \geq N_\beta$. When $S_a = S_b$, at the covalent limit, all overlap integrals $S_{ab}^{\alpha\beta}$ between the magnetic orbitals are equal to unity and $\langle \hat{S}^2 \rangle_{\mathrm{BS}} = 0$ (i. e., the BS state is the pure singlet state). At the Ising limit, the integrals $S_{ab}^{\alpha\beta}$ between the magnetic orbitals are all zero and $\langle \hat{S}^2 \rangle_{\mathrm{BS}} = 2N_{\mathrm{up}}$, where N_{up} is the number of unpaired electrons (i. e., electrons occupying the SOMOs).

In the simplest case, when $S_a = S_b = 1/2$, the space spanned by the two SOMOs and the orthogonal magnetic orbitals is the same, and the BS and HS states constructed in this space can be related to the CI states constructed in this same orbital space in a complete manner. This means that within this highly truncated orbital space, the *exact* energy difference between the HS and LS states can be mapped to the energy difference between the HS and BS states. The derivation of the exchange coupling constant in this case can be carried out at the Ising and covalent limits and any intermediate situation (see, for example, references 80 and 568). Once the interactions between the magnetic orbital space and the other orbitals are taken into account, additional energy contributions will arise from spin and charge polarization effects, and the treatment is no longer exact. Nor is the treatment exact in the more general case when $S_a = S_b > 1/2$. At the Ising limit, an approximate expression for the exchange coupling constant in the $S_a = S_b > 1/2$ case is given by

$$J_{ab} = \frac{2(E_{\mathrm{BS}} - E_{\mathrm{HS}})}{(S_a + S_b)^2}, \tag{201}$$

which is the form initially proposed by Noodleman.[70] Equation (201) is usually referred to as a spin projection or Noodleman's projection. The most general case in the Ising limit when $S_a \neq S_b$ is discussed in terms of the Ising Hamiltonian in the next section.

The intermediate situations between the Ising and covalent limits are more difficult to treat and usually one simply assumes one of the limits based on whichever limit the value of $\langle \hat{S}^2 \rangle_{\mathrm{BS}}$ is closer to. Yamaguchi and co-workers have developed an approximate projection method in the intermediate $S_a = S_b$ case given as[569–572]

$$J_{ab} = \frac{2(E_{\mathrm{BS}} - E_{\mathrm{HS}})}{\langle \hat{S}^2 \rangle_{\mathrm{HS}} - \langle \hat{S}^2 \rangle_{\mathrm{BS}}}. \tag{202}$$

The Yamaguchi projection reduces to the form (201) at the Ising limit and to (87) at the covalent limit and offers some approximation in the intermediate situations.

It has been recently shown that the Yamaguchi projection can produce spurious results if the system becomes highly spin-polarized.[573]

It should be noted that the derivation of equation (201) in the form presented here assumes that contributions from spin-polarization of the non-magnetic orbitals can be neglected. Spin-polarization is definitely present in both the BS and HS states, but the assumption is realized if the extent of spin-polarization is similar in the two states so that it does not contribute to the energy difference $E_{\mathrm{BS}} - E_{\mathrm{HS}}$. It has been shown, however, that the energy contribution from spin-polarization can be rather sizable in certain cases,[574,575] which inevitably introduces spurious energy components into the exchange coupling constant.

5.2.3 Broken symmetry method in the context of DFT

In practice, the BS formalism can be applied to DFT calculations in the exact same manner as to HF calculations. However, application in a theoretically rigorous manner is much less straightforward. The problem arises because one needs to interpret the BS state and its energy in some way in the context of DFT. In HF theory, an approximate wave function is available, and the interpretation is unambiguous. If we had the exact XC functional, a calculation constrained to some value of M_S should produce the lowest energy solution with that spin projection. For a system with a triplet ground state, the $M_S = 0$ and $M_S = 1$ components should then be degenerate, but it is very easy to show by calculation that this is not case for *any* known XC functional within the KS framework. On the other hand, the XC functional does introduce some static correlation[524,527–529,533] and the energy difference between the BS and HS states is then not strictly equivalent to the UHF formulation of the BS approach. If one wishes to use equations (201) or (87), one needs to first make an assumption whether the energy of the BS state is a closer approximation to that of the Ising state or the LS state. Use of equation (202) further requires that one must take the $\langle \hat{S}^2 \rangle$ expectation values of the KS reference system as an approximation to the $\langle \hat{S}^2 \rangle$ values calculated from the approximate true wave function, producing the same density as the KS reference system.

The assumption that the energy of the BS state is a reasonable approximation to the energy of the LS state was made in some early $X\alpha$ calculations[576,577] and later by Ruiz and co-workers in the context of KS DFT.[225,578–581] The original justification for this assumption was that DFT tends to produce more delocalized densities; therefore, the covalent limit is a more appropriate model, and on numerical success of the calculations, as pointed out by Illas and co-workers.[80] Later studies showed that neither of these arguments holds to scrutiny. A more formal rationalization was given in terms of the self-interaction error (SIE)[447,582,583] which is an inherent problem in all approximate XC functionals and arises from the incomplete cancellation of the self-interaction terms in the Hartree potential by the XC functional. The SIE is closely related to the delocalization error,[432,584,585] and these terms are sometimes used interchangeably. The SIE mimics static correlation,[529] and Ruiz and co-workers argued in a notoriously

controversial paper that the use of equation (201) leads to double-counting of static electron correlation, and based on this reasoning, equation (87) should be favored.[84,86,586] Perdew *et al*. have also argued that there is no fundamental reason in KS DFT why spin symmetry needs to be enforced on the BS solutions.[587]

The later advances in the field, however, turned strongly towards favoring the spin projected approach. This was partially due to improvements in the XC functional approximations, which allowed one to reduce SIE and the double-counting of electron correlation (see section 5.2.4). The need to correctly enforce spin symmetry on the BS solution by projecting the exchange coupling constant from the $E_{\mathrm{BS}} - E_{\mathrm{HS}}$ energy difference has been strongly emphasized by Illas and co-workers.[80–82,85,588,589] They have suggested that the HS and BS states in the context of DFT should be interpreted as Ising states. The Ising states are eigenstates of the Ising Hamiltonian

$$\hat{H}_{\mathrm{Ising}} = -J_{ab}\hat{S}_{za}\hat{S}_{zb}, \tag{203}$$

which only operates on the z component of the local spins. In a basis of the orthogonal magnetic orbitals, the diagonal elements of the Ising Hamiltonian are equivalent to the diagonal elements of the HDvV Hamiltonian (84).[590,591] If the HS and BS states are interpreted as eigenstates of (203), the energies of these states can then be interpreted as the diagonal elements of the HDvV Hamiltonian, and the exchange coupling constant can be easily extracted from their energy differences. The equivalence between the diagonal elements of (203) and (84) further guarantees that the exchange coupling constants in the two operators are equivalent.[85,590,591] The great advantage of using (203) is that it only contains operators acting on the individual spin sites, and its practical application and extension to polymetallic systems with three or more magnetic sites is straightforward. The exchange coupling constant in a two-site system is then given as

$$J_{ab} = \frac{E_{\mathrm{BS}} - E_{\mathrm{HS}}}{2S_aS_b}, \tag{204}$$

which is also valid in the case when $S_a \neq S_b$ (but see ref. 592). In the case of $S_a = S_b$, equation (204) is equivalent to equation (201) and to equation (202) in the Ising limit.

The underlying assumption for the validity of equation (204), as already mentioned, is that the HS and BS states can be interpreted as Ising states. This assumption is only really founded on the homomorphicity between the set of eigenstates of (203) and the set of BS states, which can be generated within the same set of orbitals. Furthermore, the two sets are truly homomorphic only when $S_a = S_b$.[592] Equation (204) is strictly valid only when i) all electron correlation outside the magnetic orbital space is accounted for; ii) all dynamic electron correlation within the magnetic orbital space is accounted for; iii) all static correlation within each site a and b in the magnetic orbital space is accounted for; iv) *no* static correlation between the magnetic orbitals on sites a and b is included; and v) none of the spin and/or charge polarization effects of the doubly occupied orbitals due to changes in the magnetic orbitals contributes to

the energy difference between the HS and BS states. This list of assumptions also makes the further assumptions that dynamic and static correlation can be distinguished from each other in an unambiguous manner and that the concept of magnetic orbitals can be rigorously defined in the framework of DFT. It is rather safe to say that these conditions are never rigorously realized, except perhaps for the simplest of model systems, such as two weakly interacting hydrogen atoms. A study by the author of the present work is currently underway to better understand to what extent these assumptions are broken and what types of spurious energy contributions the violations introduce to the exchange coupling constants. As of now, the main justification for the validity of the BS methodology in the context of DFT lies in the numerical success of the recipe.

5.2.4 On the choice of exchange-correlation functional

It has been well established in a number of benchmarking studies that the magnitudes of exchange coupling constants calculated using BS DFT have a very strong dependence on the choice of the XC functional.[84,225,578,592–607] The errors can range in the order of hundreds of percents, and errors of the order of 50% are rather common. This means that it is, in principle, possible to reproduce any predefined value, which causes significant problems if BS DFT is used to predict exchange couplings. Usually, the sign of J_{ab} is produced correctly except when the value is very small, such as a few wave numbers.

The majority of the experimentally characterized systems used for benchmarking different XC functionals for the calculation of exchange coupling constants consist of bimetallic Cu(II) complexes although other 3d transition-metals complexes have been included in some studies.[84,225,592,594,602] A H–He–H model system has also been extensively studied, as the system is simple enough so that reference values can be calculated at the CCI level.[84,225,595,596,601] The general conclusion from all of these studies is that range-separated functionals, such as the LC-ωPBE, global hybrids with larger-than-average percentage of Fock exchange, such as BHHLYP and double hybrid functionals such as B2PLYP,[608] give the best results. In a detailed study on the effect of Fock exchange in BS DFT calculations, Phillips and Peralta showed that good results are obtained if a large enough percentage of Fock exchange is introduced regardless of whether it is introduced through global scaling or through range-separation.[609] The improvement of results upon increasing the percentage of Fock exchange can be rationalized by reduced SIE. In magnetic coupling calculations, SIE has a tendency to exaggerate the covalent interactions between spin sites and, therefore, overestimate the magnitude of AFM interaction.

The results obtained for transition-metal complexes do not, however, usually apply to π conjugated organic radical systems. In a detailed study of the *meta*-xylylene diradical, Illas and co-workers observed that the LC-ωPBE functional produced unacceptably bad estimates of the exchange coupling, whereas reasonable values were obtained with M06-2X and B3LYP. For transition-metal systems the exact opposite is observed: LC-ωPBE produces consistently good results, and

M06-2X and B3LYP may have relative errors larger than 50%.[592,596,599] Related discrepancy is also observed when tuning the percentage of Fock exchange in the B3LYP functional to optimally reproduce experimental values. In the case of ionic transition-metal salts, the best results are obtained by using a value of 35%.[610,611] Similarly, 35% of Fock exchange in the PBE0 functional produce the best results for a series of transition-metal complexes.[609] For a series of organic diradicals, Cho *et al.* obtained the best estimates with a value of 5%.[612]

The system-specific dependence of the values of exchange coupling constants on the choice of the XC functional and the arbitrariness related to the interpretation of the BS state as discussed in section 5.2.3 all highlight the importance that BS DFT should never be applied in a black box manner.

5.3 Calculation of g- and D-tensors using DFT

Several approaches to the DFT calculation of **g**-tensors were introduced starting from the late 1990s.[50–57,65,613] The elements of the **g**-tensor are given by the derivative

$$g_{\alpha\beta} = \frac{1}{\mu_{\mathrm{B}}} \frac{\partial^2 E}{\partial B_\alpha \partial S_\beta}, \tag{205}$$

where $\alpha, \beta \in x, y, z$. Technical details of the application of (205) are given, for example, in the review by Autschbach[56] and in the various papers on the practical implementations.[51,55,57] Usually the DFT-based approaches to the **g**-tensor provide rather accurate results if the effects from SOC are very weak, such as in organic systems, and the system is reasonably well described by a single determinant. In multireference systems, the DFT treatment breaks down, and the correct way to approach the problem is through multireference *ab initio* calculations as described in section 4.5.1.

Two DFT methods have been developed for the calculation of the ZFS tensor, or more precisely, the D and E parameters. The first method was proposed by Pederson and Khanna[58] and another was introduced by Neese.[59,60] The Pederson–Khanna method was later studied and improved by van Wüllen and co-workers.[62–64,614] It should be noted that the approach proposed by Neese and the approach of Pederson, Khanna, van Wüllen, and co-workers are not strictly equal at any limit.[64] This is a rather serious problem, but even more severe is the fact that none of the methods are highly reliable and can fail rather dramatically in an inconsistent manner.[615,616] The predictive power of the methods is qualitative at best. This makes the DFT approaches to ZFS rather useless in practical problems. In the present work,[VIII] we developed a method for extracting the ZFS parameters from DFT calculations using the so-called DFT/ROCIS method, which introduces SOC in a similar manner as described in section 4.4.5 but using orbitals and eigenvalues calculated at DFT level and some empirical scaling parameters.[617–619] Although the method provided better results than the common DFT-based methods, no actual validation studies on its

performance have been carried out.

Part II

Results

6 COMPUTATIONAL MODELING OF ISOTROPIC EXCHANGE INTERACTIONS AND WEAK ANISOTROPY

The field of molecular magnetism was founded on the systematic design of isotropic exchange interactions in molecular systems by modification of the chemical structure of the constituting molecules. Whereas intramolecular magnetic interactions can be relatively easily related to the chemical structure through the so-called magneto-structural correlations,[24,27] the systematic design of intermolecular interactions proved a much tougher challenge and remains as such to this date. In transition metal systems, it is extremely difficult to construct intermolecular superexchange pathways in such a way that sufficiently strong magnetic interaction is retained. An alternative approach to superexchange is the so-called metal-radical approach, where the coupling between metal ions is mediated by paramagnetic radical ligands.[29] Organic or organo-main-group radicals usually have much more delocalized spin densities and intermolecular magnetic interactions are then much more likely. Papers **I** and **II** included in the present work investigate the magnetic interactions in molecular complexes constructed using the metal-radical approach. Although this approach allows one to construct intermolecular exchange interactions, the problem of controlling the type (i. e., FM or AFM) of interaction still remains unsolved. Nature has a strong tendency towards favoring AFM interaction, which ultimately leads to diamagnetic (or ferrimagnetic) solids. In Paper **IV**, rational design of mixed radical systems with ferromagnetic interaction is examined. The focus is placed on purely organic radical systems, but the results are also generalizable to more complicated systems, such as transition-metal–radical complexes. The calculations in Paper **III** focus on analysis of the exchange interactions in a polymetallic Ni(I) complex.

In addition to the analysis of isotropic exchange coupling, the ZFS parameters of some of the complexes introduced in Paper **I** will also be calculated. The system studied in Paper **II** has a strongly anisotropic Dy(III) ion and displays slow relaxation of magnetization under an applied dc field, but the focus in the study

is placed on the exchange interactions and not on the anisotropic properties.

6.1 Computational details

The BS DFT calculations in Paper **I** were carried out in a non-relativistic DFT framework with the Gaussian 09 program revision D.01[620] using the 2006 version of the range-separated LC-ωPBE hybrid XC functional in conjunction with Ahlrichs' older polarized triple-ζ quality basis sets (TZVP, sometimes known as def-TZVP).[621] The calculations utilized geometries extracted from the crystal structures, and no additional geometry optimizations were carried out. No constraints were placed on spin or spatial symmetries, and stability analyses[622,623] were carried out to ensure that all optimized reference wave functions corresponded to minima in the variational space. The same computational approach was also used for the BS DFT calculations in Paper **III**.

In Paper **II**, the BS DFT calculations were carried out using scalar relativistic DFT with the Orca 3.0.3 code.[251] The scalar relativistic effects were treated using ZORA as implemented in Orca.[392] The range-separated CAM-B3LYP hybrid XC functional was used in conjunction with the polarized triple-ζ quality ZORA-def2-TZVP basis sets[624] for the lighter elements and the polarized quadruple-ζ quality SARC2-ZORA-QZVP for the Gd ions.[625] Both basis sets are specifically designed for scalar relativistic ZORA calculations; the former is a re-contracted version of the widely used def2-TZVP basis sets,[294,626] and the latter is a 2016 upgrade of the segmented all-electron relativistically contracted (SARC) basis sets of Pantazis *et al.*, which are purpose-specifically designed for ZORA calculations on heavy elements.[627]

Wave-function-based multireference calculations in Papers **I** and **III** were carried out with the Orca 3.0.3 code using standard CASSCF techniques and the strongly contracted variant of the NEVPT2 method for the treatment of electron correlation outside the CAS. In Paper **I**, two different active spaces were employed. The first CAS consisted of the five 3d orbitals and the radical SOMO. All states that can be constructed in this CAS were solved in a single SA-CASSCF calculation. This entails 6 sextets, 84 quartets, and 210 doublets for Fe(II); 15 quintets, 105 triplets, and 105 singlets for Co(II); and 20 quartets and 70 doublets for Ni(II). The second active space, used in conjunction with a diamagnetic ligand, contained only the five 3d orbitals. Again, all states that can be constructed in this space were solved: 5 quintets, 45 triplets, and 50 singlets for Fe(II); 10 quartets and 40 doublets for Co(II); and 10 triplets and 15 singlets for Ni(II). In Paper **III**, a four-electron-four-orbital active space containing the four different $3d_{x^2-y^2}$ orbital combinations was used. Larger active spaces were also tested, but these did not lead to visible improvement in the results. One quintet, three triplets, and one singlet corresponding to the lowest manifold of states were solved in the SA-CASSCF calculation. Scalar relativistic effects were treated using the second-order DKH transformation. DKH-def2-TZVP basis sets[624] (analogous to

ZORA-def2-TZVP put optimized for DKH2) were used along with corresponding auxiliary basis sets for the RI approximation used in the integral transformations. SOC was treated using the SOMF operator and the QDPT formalism as described in section 4.4.5 and as implemented in ORCA.[88] The ZFS D and E parameters in Paper **I** were extracted using the effective Hamiltonian approach of Maurice *et al*.[406]

In Paper **IV**, a comprehensive validation study of various functionals was carried out (*vide infra*). The tested functionals included the global hybrids B3LYP, PBE0, M06, M06-2X and the range-separated hybrids LC-ωPBE, CAM-B3LYP, and ωB97XD.[628] The latter has the same functional form as ωB97X but has been optimized with an empirical dispersion correction. The validation calculations were carried out both by completely neglecting dispersion effects not accounted for by the XC functional and by treating them using the DFT-D3 correction of Grimme and co-workers.[629] Both the original zero damping function and the newer Becke–Johnson (BJ) damping[630] were used in the DFT-D3 calculations. The DFT-D3 correction has only been parameterized for the M06 and M06-2X functionals using the zero damping function as the functional included some short-range dispersion interaction, and using a non-zero damping in the short range would lead to double-counting of dispersion energy. The ωB97X functional already includes the dispersion correction in its definition and was, therefore, not augmented with any additional correction. The LC-ωPBE functional with the DFT-D3 correction and BJ damping was chosen for all further calculations. The DFT calculations were carried out in a non-relativistic framework using the GAUSSIAN 09 code revision D.01[620] and def2-TZVP basis sets.[294] The geometries were fully optimized with no constraints on spatial or spin symmetries, and frequency calculations were carried out to ensure that the optimized stationary points corresponded to true minima on the potential energy surface and to generate the vibrational frequencies used in the evaluation of thermochemical quantities. The thermochemical data were evaluated using standard methods[257] at 298 K. The geometry optimizations were started from crystal structures where available and from scratch in other cases. Basis set superposition error (BSSE)[133] was corrected with the counterpoise method.[631] All calculated reference wave functions were subjected to stability analysis before and after the geometry optimizations to ensure that no lower energy minima were obtainable in the variational space. Additional energy evaluations of the HS states using the LC-ωPBE/def2-TZVP optimized geometries were carried out employing the domain-based local pair-natural orbital (DLPNO) coupled cluster theory with single, double, and perturbative triple excitations (DLPNO-CCSD(T)).[632–636] The CCSD(T) method[129,133,308] offers highly accurate energies for single reference systems, and the DLPNO approach[627,637–639] makes the scaling of the computational costs relative to system size effectively linear, thus greatly reducing the computational costs.[640–642] The DLPNO-CCSD(T) calculations were carried out using the ORCA 4.0.1 code.[252]

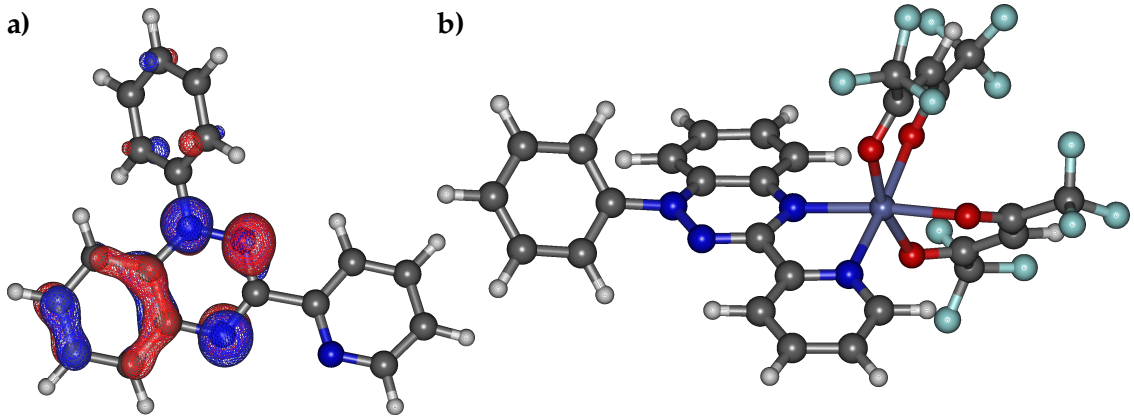

FIGURE 10 **a)** The structure and SOMO of the radical **1** and **b)** the structure of the **1**–Co(II) complex **4**. The structures of complexes **2**, **3**, and **5** are qualitatively similar.

6.2 Computational analysis of exchange interactions in transition-metal, lanthanide, and radical systems

6.2.1 3d metal complexes of a 1,2,4-benzotriazinyl radical

Papers **I** and **II** study the coordination complexes of a 1-phenyl-3-(pyrid-2-yl)benzo[*e*][1,2,4]triazinyl radical ligand (**1**, Figure 10a) based on a radical framework initially synthesized by Blatter in the 1960s.[643] The ligand is air- and moisture-stable and has highly delocalized spin density. Properties of the ligand and its Cu(II) coordination complex were studied in an initial communication.[644] The experimental work in Paper **I** extended the coordination complexes of **1** to the rest of the latter 3d transition metals, and the complexes Mn(**1**)(hfac)$_2$ (**2**, hfac = hexafluoroacetylacetonate), Fe(**1**)(hfac)$_2$ (**3**), Co(**1**)(hfac)$_2$ (**4**), and Ni(**1**)(hfac)$_2$ (**5**) were characterized. In all cases, the coordination geometry around the metal ion is pseudo-octahedral. Structure of **4** is presented in Figure 10b and the geometries of the other complexes are qualitatively similar. In the crystal phase, the complexes **2** and **3** form dimers with some short, intradimeric, radical–radical contacts. The unit cell of complex **4** contains a large number of complexes with a number of short radical–radical contacts. Complex **5** also forms dimers with intradimeric radical–radical contacts as well as short radical–radical contacts between neighboring dimers giving a chain-like structure.

The most general HDvV-type Hamiltonian describing the magnetic interaction within a given dimer of complexes can be written as

$$\begin{aligned}\hat{H}_{\mathrm{HDvV}} = &- J_{\mathrm{MR}}\hat{\mathbf{S}}_{\mathrm{M}}\cdot\hat{\mathbf{S}}_{\mathrm{R}} - J_{\mathrm{M'R'}}\hat{\mathbf{S}}_{\mathrm{M'}}\cdot\hat{\mathbf{S}}_{\mathrm{R'}} - J_{\mathrm{RR'}}\hat{\mathbf{S}}_{\mathrm{R}}\cdot\hat{\mathbf{S}}_{\mathrm{R'}} \\ &- J_{\mathrm{MR'}}\hat{\mathbf{S}}_{\mathrm{M}}\cdot\hat{\mathbf{S}}_{\mathrm{R'}} - J_{\mathrm{M'R}}\hat{\mathbf{S}}_{\mathrm{M'}}\cdot\hat{\mathbf{S}}_{\mathrm{R}} - J_{\mathrm{MM'}}\hat{\mathbf{S}}_{\mathrm{M}}\cdot\hat{\mathbf{S}}_{\mathrm{M'}},\end{aligned} \tag{206}$$

where the indices M and R refer to the metal and the radical, respectively, and the indices in the first complex of the dimer are unprimed, whereas the indices in the second complex are primed. The Hamiltonian thus considers the metal–radical

interactions within both complexes, the radical–radical interaction, the interaction between the metal-ion in one complex and the radical in the other complex, and the interaction between the two metal ions. The metal–radical interactions in both complexes can be considered equivalent as can the interactions between the metal ion and the radical of the other complex, thus setting $J_{\mathrm{MR}} \equiv J_{\mathrm{M'R'}}$ and $J_{\mathrm{MR'}} \equiv J_{\mathrm{M'R}}$. With these simplifications, it is possible to form six different states in the BS DFT calculations with unique energies. Let us label these states as $|\alpha\alpha\alpha\alpha\rangle$, $|\alpha\alpha\alpha\beta\rangle$, $|\alpha\alpha\beta\alpha\rangle$, $|\alpha\alpha\beta\beta\rangle$, $|\alpha\beta\alpha\beta\rangle$, $|\alpha\beta\beta\alpha\rangle$, where the spin indices are ordered as M, R, R′, M′, and we only consider the local states at the metal ions where all unpaired electron have the same spin. Interpreting these states as Ising states allows one to extract the exchange coupling constants from the energy differences as

$$J_{\mathrm{MR}} = -\frac{1}{14}E_{\alpha\alpha\alpha\alpha} - \frac{1}{14}E_{\alpha\alpha\beta\beta} + \frac{1}{14}E_{\alpha\beta\alpha\beta} + \frac{1}{14}E_{\alpha\beta\beta\alpha} \tag{207}$$

$$J_{\mathrm{RR}} = -\frac{1}{2}E_{\alpha\alpha\alpha\alpha} - E_{\alpha\alpha\alpha\beta} + E_{\alpha\alpha\beta\alpha} + \frac{1}{2}E_{\alpha\alpha\beta\beta} + \frac{1}{2}E_{\alpha\beta\alpha\beta} - \frac{1}{2}E_{\alpha\beta\beta\alpha} \tag{208}$$

$$J_{\mathrm{MR'}} = -\frac{1}{14}E_{\alpha\alpha\alpha\alpha} + \frac{1}{14}E_{\alpha\alpha\beta\beta} - \frac{1}{14}E_{\alpha\beta\alpha\beta} + \frac{1}{14}E_{\alpha\beta\beta\alpha} \tag{209}$$

$$J_{\mathrm{MM'}} = -\frac{1}{98}E_{\alpha\alpha\alpha\alpha} + \frac{1}{49}E_{\alpha\alpha\alpha\beta} + \frac{1}{49}E_{\alpha\alpha\beta\alpha} + \frac{1}{98}E_{\alpha\alpha\beta\beta} + \frac{1}{98}E_{\alpha\beta\alpha\beta} - \frac{1}{98}E_{\alpha\beta\beta\alpha}. \tag{210}$$

In the case of complexes **2**, **3**, and **5**, the exchange coupling constants $J_{\mathrm{MR'}}$ and $J_{\mathrm{MM'}}$ have negligibly small values that cannot be reliably distinguished from numerical noise, and these exchange couplings are, therefore, neglected in all subsequent considerations. The exchange couplings J_{MR} and J_{RR} were determined for **2**, **3**, and **5** using BS DFT calculations and are listed in Table 1 along with the experimental values obtained by fitting experimentally observed temperature-dependent χT plots. In the case of **4**, the ZFS is of the same order of magnitude as the exchange coupling (*vide infra*), and the exchange interaction, therefore, cannot be described by any simple model with a single effective parameter. The exchange coupling constants could, in practice, be determined from the BS DFT calculations but would not correspond to any parameter of a physically relevant model. Obtaining the necessary parameters from a fit to experimental data would also lead to severe overparameterization of the model and was not carried out. The agreement with the calculated and experimental values of J_{MR} in the case of complexes **2** and **3** is good. In the fit to experimental data, the intermolecular interactions were modeled by the so-called molecular mean-field operator, which reduces the intermolecular interactions into a single effective parameter. This parameter also indirectly contains all the effects arising from the weak ZFS. Thus, the parameter cannot be related to the calculated values in a meaningful way, but the parameters do indicate weak intermolecular AFM exchange. In the case of **3**, this is correctly reproduced by the calculations, but the calculations for **2** indicate weak FM exchange. The origin of this discrepancy is difficult to explain, but it should be noted that the the value of $1.3\,\mathrm{cm}^{-1}$ is an extremely small energy difference and well beyond the numerical accuracy of DFT calculations. It is, therefore, likely that the difference in the sign arises simply from inaccuracies in

TABLE 1 Values of exchange coupling constants of complexes **2** to **5** as calculated at BS DFT level and as obtained by fitting experimental data

	Calculated		Experimental	
Complex	J_{MR} / cm^{-1}	$J_{RR'}$ / cm^{-1}	J_{MR} / cm^{-1}	$J_{RR'}$ / cm^{-1}
2 (Mn)	−142	1.3	−129	weak, AFM
3 (Fe)	−175	−0.6	−143	weak, AFM
4 (Co)				
5 (Ni)	222	−3.9, −45.3	111 to 222	−76 to −60

the underlying DFT calculation.

The experimental determination of the metal–metal and metal–radical couplings in complex **4** was problematic, as the two coupling constants had very strong cross-correlation. The temperature-dependent χT product could be equally well reproduced with J_{MR} values ranging from 111 cm^{-1} to 222 cm^{-1} and $J_{RR'}$ values ranging from $-76\,cm^{-1}$ to $-60\,cm^{-1}$. A slightly worse fit could be obtained with an even wider range of values. The calculation predicts a metal–radical exchange coupling of $222\,cm^{-1}$, which matches exactly the largest value obtainable from the fit. Analysis of the crystal structure and further calculations show that there exists two radical–radical couplings: one within the dimer and another between neighboring dimers. The calculated values are $-45.3\,cm^{-1}$ and $-3.9\,cm^{-1}$ for the intra- and inter-dimeric interactions, respectively. Neither value fits into the range of values obtained from the fit, but the order of magnitude is correct. Furthermore, the fit only considered a single radical–radical exchange parameter and, therefore, in principle, neglected the weak intra-dimeric exchange. This will inevitably have an effect on the quality of the experimental radical–radical couplings but adding another parameter into the model, which is already strongly cross-correlated, would add further ambiguity into the experimental parameters. Thus, in this particular case, the calculated parameters cannot be reliably compared with the experimentally obtained ones.

The ZFS parameters D and E were also determined for complexes **3**, **4**, and **5** at CASSCF/NEVPT2/QDPT level. The Mn(II) complex **2** has a $3d^5$ configuration giving rise to a ${}^6A_{1g}$ term in an octahedral field, which has no first-order angular momentum and which is well-separated from any higher-lying configurations in an octahedral field; this, and the relatively small SOC constant of the Mn(II) ion,[23] means that ZFS can be assumed to be extremely weak and the ZFS parameters for **2** were, therefore, not calculated. The ZFS was treated using the giant spin approach, where it is assumed that the exchange coupling is much stronger than the ZFS; the radical and metal spins in a given complex are coupled to give some total spin S; the resulting $(2S + 1)$-fold degenerate manifold is then weakly split by SOC.[175,230] The calculated values are $D = 8.5\,cm^{-1}$ and $E = 2.0\,cm^{-1}$ for **3**, $D = 17.0\,cm^{-1}$ and $E = 2.5\,cm^{-1}$ for **4**, and $D = -2.2\,cm^{-1}$ and $E = 0.6\,cm^{-1}$ for **5**. The ZFS is of easy-plane type in **3** and **4**; hence no SMM behavior should be expected for these systems. The anisotropy in **5** is of easy-axis type but very weak; thus, the system should not display any pronounced SMM behavior. The values adhere very well to what can be expected based on the electronic ground

states of the relevant ions in an ideal octahedral field. The ground configurations of Fe(II) and Co(II) ions give rise to $^5T_{2g}$ and $^4T_{1g}$ terms with first-order angular momentum;[23] thus, both **3** and **4** show moderately strong ZFS when compared to other pseudo-octahedral 3d transition metal complexes. The ground term of Ni(II) is $^3A_{2g}$, which has no first-order angular momentum.[23] **5** shows the weakest ZFS of the systems considered and results from the mixing of higher states into the ground term by the SOC.

The validity of the assumption behind the giant spin approach to the evaluation of the ZFS parameters can be tested by calculating the ZFS parameters for analogous systems with diamagnetic ligands. This can be achieved by replacing one of the non-coordinated nitrogen atoms in **1** by a carbon. Such a change inevitably also changes the CF potential experienced by the metal ions, and the calculated ZFS parameters are thus only approximations of the real single-ion parameters. If the parameters are much smaller than the respective exchange coupling constants, the giant spin approach should be well justified. The calculated values are $D = 5.8\,\mathrm{cm}^{-1}$ and $E = 1.4\,\mathrm{cm}^{-1}$ for **3**, $D = 43.1\,\mathrm{cm}^{-1}$ and $E = 9.7\,\mathrm{cm}^{-1}$ for **4**, and $D = -2.2\,\mathrm{cm}^{-1}$ and $E = 1.2\,\mathrm{cm}^{-1}$ for **5**. Thus, the giant spin approach is a reasonable approximation for the anisotropy in **3** and **5**. In **4**, however, the D parameter is fairly large and starts to become comparable to the exchange coupling constants. Thus, the electronic structure of **4** is no longer properly described as an S-type system nor can it be described as a Γ-type system due to deviations of the pseudo-octahedral coordination geometry from an ideal octahedron. The electronic structure can then only be described using spin Hamiltonians by introducing a very large number of parameters, which would destroy the interpretive qualities of the model.

6.2.2 Dy(III) complexes of a 1,2,4-benzotriazinyl radical

After completing the series of 3d transition-metal complexes of the radical ligand **1**, the possibility to coordinate it to trivalent lanthanide ions was studied next. Paper **II** describes the characterization of the Dy(III) complex Dy(**1**)(tbacac)$_3$ (**6**, tbacac = 2,2,6,6-tetramethyl-3,5-heptane-dionato). The Dy(III) ion has a distorted square anti-prismatic or, roughly equivalently, a distorted triangular dodecahedral coordination geometry. The complex **6** form dimers in the solid state with short intradimeric contacts and also with some short contacts between neighboring dimers in a column-like structure along the crystal c axis. The structure of the complex dimer is shown in Figure 11.

The coordination geometry around the Dy(III) ion is not ideal when considering possible SMM properties as Dy(III) ion is known to show strong anisotropy in axial CFs.[106] The low axiality and low overall symmetry of the CF in **6** mean that the QTM process should be very efficient. Indeed, ac susceptibility measurements at zero dc field do not show any out-of-phase component in the susceptibility meaning that any relaxation of magnetization is faster than the oscillating magnetic field in the ac experiments. In principle, the exchange interaction between the Dy(III) ion and the radical ligand could suppress the QTM due to decoupling

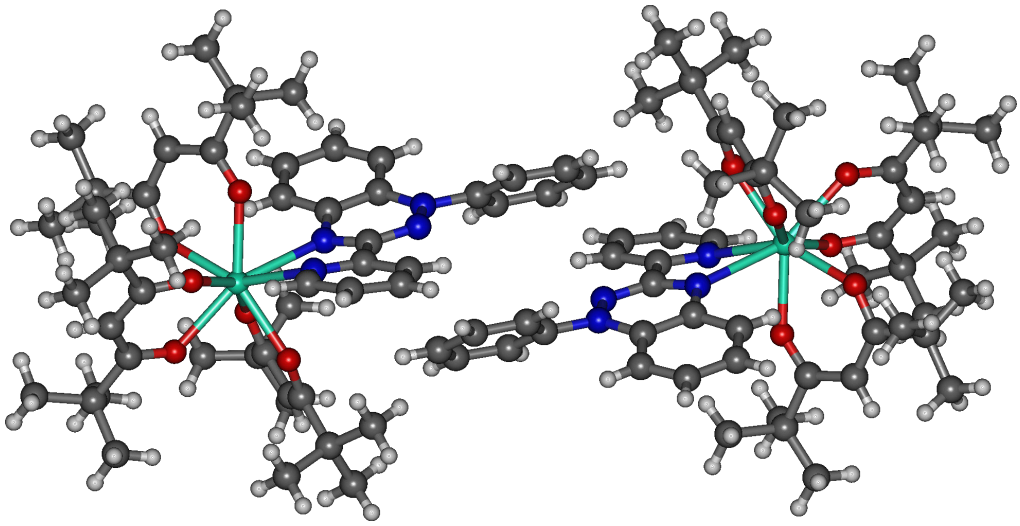

FIGURE 11 The structure of a dimer of complexes **6**.

of the two components of the ground Kramers doublet of the Dy(III) ion, but this is not the case for **6**. The $S_M = 5/2$ spin on the Dy(III) ion and the $S_R = 1/2$ spin of the radical give an integer total spin, and this means that the exact degeneracy of the ground doublet is no longer enforced by Kramers theorem. Given the low symmetry of the distorted square anti-prismatic coordination environment, the exchange interaction is more likely to enhance QTM than to suppress it.

A much more interesting feature revealed by magnetization measurements is that the system orders anti-ferromagnetically below 8.6 K at zero field. This ordering can be lifted by an external magnetic field. The external field can also be used to suppress the QTM to show some slow relaxation of magnetization. Application of a 9100 G field at 1.85 K, which lies at the border between the AFM and paramagnetic phases in a H vs. T plot, led to the observation of slow relaxation of magnetization with an Arrhenius-type profile. This decoupling of the dynamic properties of the individual magnetic sites from the long-range magnetic properties of the crystalline solid has been utilized before in long-range ordered single-chain magnet systems.[645–647] A fit to the relaxation data yielded an effective barrier height of $U_{eff} = 8.2\,cm^{-1}$, which is fairly low for a Dy(III) system. Thus, the dynamic magnetic properties of **6** were not studied any further, and the main focus was placed on the origin of the AFM ordering.

In order to study the system without the theoretical complications arising from the strong SOC of the Dy(III) ion, calculations were carried out on an isostructural model system, where the Dy(III) ions were replaced by Gd(III). The $^8S_{7/2}$ ground multiplet of the Gd(III) ion has no first-order angular momentum and can be treated by simply considering the $S_M = 7/2$ spin. The *tert*-butyl groups in the auxiliary tbacac ligands were replaced by methyl groups in the calculations to reduce computational costs. The alkyl groups in the ligands do not carry any spin density, and thus their neglection should have a negligible effect on the relative energies of the different spin states. Two structures were considered in the calculations: the complex dimer in Figure 11 and a dimer constructed from two neighboring complexes along the crystal c axis with short

intermolecular radical–radical contacts. The exchange coupling constants can then be extracted by applying equations (207)–(210). The evaluated intramolecular exchange coupling constants $J_{MR'}$ and $J_{MM'}$ were again so small ($< 0.1\,cm^{-1}$) that they are either zero or cannot be reliably distinguished from numerical noise. The intramolecular coupling constant is $J_{MR} = -9.4\,cm^{-1}$. This can be re-scaled from the $S_M = 7/2$ spin of the Gd(III) ion to the $S_M = 5/2$ spin of the Dy(III) ion to give an approximate Dy(III)–radical coupling of $J_{MR} = -6.7\,cm^{-1}$. Similar re-scaling approach has been used in several papers.[648–650] The resulting exchange parameter estimates the coupling strength, but it is purely fictional in the sense that in the real physical system SOC will play a considerable role and the interaction cannot be reduced to a single parameter. The intradimeric radical–radical coupling constant is $J_{RR'} = -16\,cm^{-1}$, which is rather strong for an intermolecular interaction. These two exchange coupling constants explain the interactions within the complex dimer, but not the long-range AFM ordering. A radical–radical coupling constant between neighboring complexes along the crystal c axis is $J_{RR''} = -0.4\,cm^{-1}$. This would, however, still only explain long-range ordering in one dimension, and the value is too small to support AFM ordering at 8.6 K. Other possible exchange pathways were also studied, but none showed exchange coupling constants with values larger than $0.1\,cm^{-1}$. Values below this threshold cannot be reliably evaluate at BS DFT level. Thus, the long range ordering must be addressed to dipolar coupling between the magnetic moments of the Dy(III) ions. Further theoretical studies are still needed to elucidate the details of the interactions leading to the AFM ordering.

6.2.3 $[Ni\{N(SiMe_3)_2\}]_4$ tetramer

The Ni(I) tetramer $[Ni\{N(SiMe_3)_2\}]_4$ (**7**, Figure 12a) was characterized as a decomposition product during the preparation of the linear Ni(II) silylamide complex $Ni\{N(SiMe_3)_2\}_2$.[III] The characterization of two-coordinate complexes $M\{N(SiMe_3)_2\}_2$ where M = Mn(II), Fe(II), Co(II), and Ni(II) were first reported several decades ago.[651–653] It was later shown that the reported Co(II) and Ni(II) complexes were in fact the THF adducts $M\{N(SiMe_3)_2\}_2(THF)$.[III,654] All of the complexes except $Ni\{N(SiMe_3)_2\}_2$ are thermally stable, but $Ni\{N(SiMe_3)_2\}_2$ decomposes at room temperature. The early work reported the decomposition product as a black solid, but it was not structurally characterized.[652] In 2015, during the preparation of the THF-free complex $Ni\{N(SiMe_3)_2\}_2$, the black solid was isolated, characterized by X-ray crystallography, and shown to contain the tetramer **7**. The THF-free $Ni\{N(SiMe_3)_2\}_2$ was characterized in solution but did not yield crystals suitable for further structural characterization by X-ray crystallography.[III] A structurally similar cobalt tetramer with highly pronounced SMM properties has been very recently characterized.[655]

The effective magnetic moment of **7**, determined using the Evans method[656] at 300 K, is $\mu_{eff} = 2.70\,\mu_B$. This number should be taken as the Boltzmann-averaged magnetic moment of the different spin states thermally populated at 300 K each having an effective magnetic moment of $\mu_{eff} = 2\sqrt{S(S+1)}\mu_B$, where

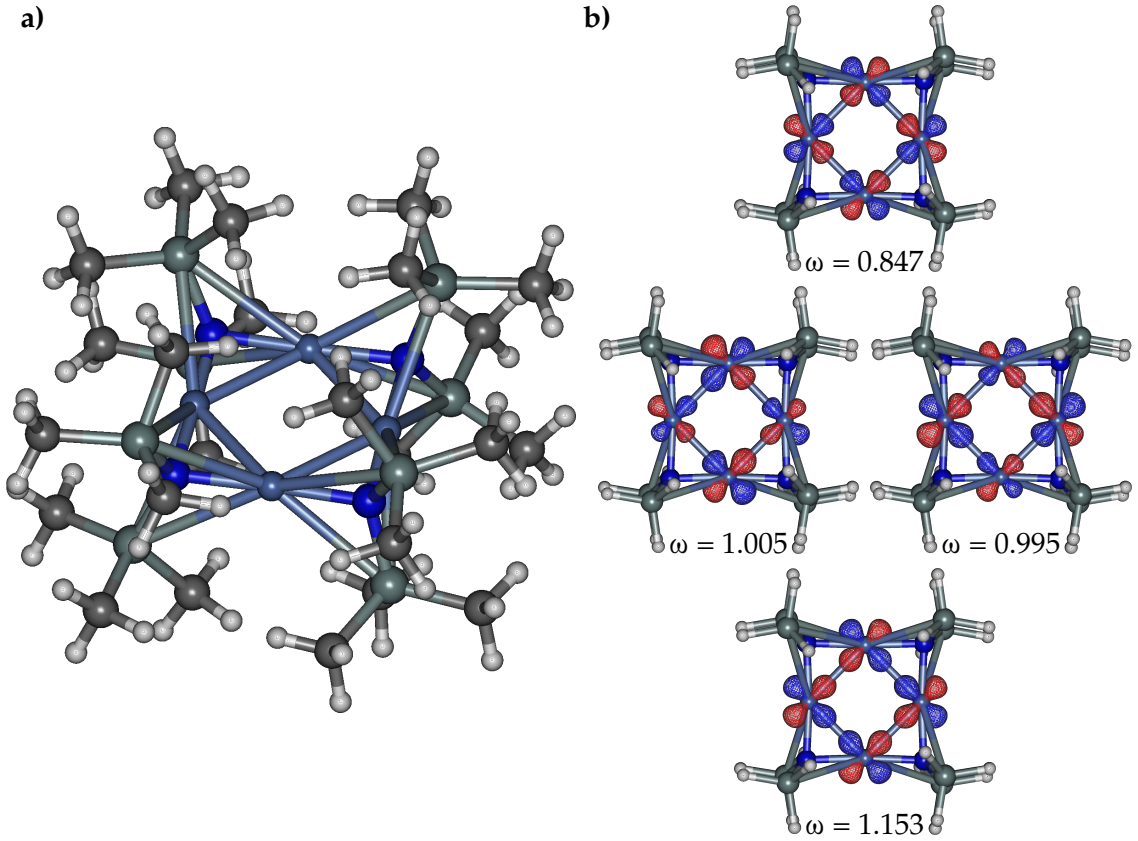

FIGURE 12 **a)** Structure of the complex **7** and **b)** the four valence orbitals describing the intermolecular exchange interactions along with the respective natural orbital occupation numbers.

S is the total spin of the electronic state. The temperature-dependent χT product was also measured. The interpretation of the susceptibility data was, however, greatly complicated by the presence of some paramagnetic impurity or impurities. This impurity was taken into account in the simulation of the data as a constant shift in the χT values independent of temperature. The constant shift corresponds to a spin system with some total spin S with no orbital angular momentum at any order, and where all M_S states are equally populated. This is equivalent to the Curie law.[24,184] No real system strictly adheres to these conditions, but they are rather well realized in 3d transition-metal ions with no first-order angular momentum, except for very low temperatures. The spin system in **7** was modeled by the HDvV-type Hamiltonian

$$\hat{H}_{\mathrm{HDvV}} = -J\left(\hat{\mathbf{S}}_1 \cdot \hat{\mathbf{S}}_2 + \hat{\mathbf{S}}_2 \cdot \hat{\mathbf{S}}_3 + \hat{\mathbf{S}}_3 \cdot \hat{\mathbf{S}}_4 + \hat{\mathbf{S}}_4 \cdot \hat{\mathbf{S}}_1\right), \tag{211}$$

where the indices on the spin operators index the four Ni(II) ions in a consecutive manner and $S_1 = S_2 = S_3 = S_4 = 1/2$. The model only included the exchange coupling between nearest-neighbor ions. A fit to the χT plot yielded a value of $J = -204\,\mathrm{cm}^{-1}$ for the exchange coupling constant, although the quality of the fit was not very good. The low-quality fit, the simplistic treatment of the paramagnetic impurity, and the neglection of exchange coupling beyond the nearest neighboring ions mean that the experimental exchange coupling constant

is neither reliable nor is the model used to characterize the experimental data necessarily capable of accounting for all magnetic properties of the system.

The energies of the different spin states were calculated at CASSCF/NEVPT2 level. The (4,4) active space included the four possible combinations of the $3d_{x^2-y^2}$ orbitals (Figure 12b). Several test calculations with larger active spaces were carried out but with no visible change in the energetics or NOONs. This is somewhat surprising considering the minimal size of the (4,4)CAS used but can be rationalized by the fact that all valence orbitals in **7** except the ones in the (4,4) CAS are fully occupied. This considerably reduces the number of excitations in the valence space, which could be used to account for the electron correlation. Thus, the correlation effects mainly arise from interactions with configurations, which are considerably higher in energy and reasonably well described at NEVPT2 level. The calculations predict the ground state of **7** as a singlet with the first excited singlet $1160\,\mathrm{cm}^{-1}$ above the ground state. The three triplets lie $587\,\mathrm{cm}^{-1}$, $1186\,\mathrm{cm}^{-1}$, and $1188\,\mathrm{cm}^{-1}$ above the singlet and one quintet lies at $1735\,\mathrm{cm}^{-1}$. The effective magnetic moments of the singlet, triplet, and quintet states are $0.00\,\mu_\mathrm{B}$, $2.83\,\mu_\mathrm{B}$, and $4.90\,\mu_\mathrm{B}$, respectively. The room temperature effective magnetic moment of $2.70\,\mu_\mathrm{B}$ indicates significant thermal populations of the triplet and quintet states, which is somewhat at odds with the relatively high energies. Calculating μ_eff at 300 K using the energy values listed above would yield a value of $\mu_\mathrm{eff} = 0.44\,\mu_\mathrm{B}$, which is considerably smaller than the experimentally observed value. It should, however, be noted that the experimental measurement has been carried out on the solvated system, whereas the calculated values are evaluated on geometry extracted from the crystal structure. Thus, any chemical interaction with the solvent is neglected from the calculations, and it has been well established that small geometric variations can lead to large differences in the spin state energetics.

At the time of publication of Paper **III**, no further computational analysis of the spin state energetics had been carried out. BS DFT calculations on **7** were, however, carried out later and are reported here. It has been shown both by experimental measurements and theoretical calculations that in the case of rectangular spin arrangements in Cu(II) salts, both next-nearest-neighbor and four-body exchange terms are important in the quantitative description of spin state energetics.[177,203–206,657,658] The four-body terms describe ring currents in the four-site system. Assuming that the same interactions are also operational in **7**, the HDvV-type Hamiltonian describing the system is then

$$\begin{aligned}\hat{H}_\mathrm{HDvV} = &- J\left(\hat{\mathbf{S}}_1\cdot\hat{\mathbf{S}}_2 + \hat{\mathbf{S}}_2\cdot\hat{\mathbf{S}}_3 + \hat{\mathbf{S}}_3\cdot\hat{\mathbf{S}}_4 + \hat{\mathbf{S}}_4\cdot\hat{\mathbf{S}}_1\right) - J'\left(\hat{\mathbf{S}}_1\cdot\hat{\mathbf{S}}_3 + \hat{\mathbf{S}}_2\cdot\hat{\mathbf{S}}_4\right) \\ &- J''\left[\left(\hat{\mathbf{S}}_1\cdot\hat{\mathbf{S}}_2\right)\left(\hat{\mathbf{S}}_3\cdot\hat{\mathbf{S}}_4\right) + \left(\hat{\mathbf{S}}_1\cdot\hat{\mathbf{S}}_4\right)\left(\hat{\mathbf{S}}_2\cdot\hat{\mathbf{S}}_3\right) - \left(\hat{\mathbf{S}}_1\cdot\hat{\mathbf{S}}_3\right)\left(\hat{\mathbf{S}}_2\cdot\hat{\mathbf{S}}_4\right)\right],\end{aligned} \tag{212}$$

where J' is the next-nearest-neighbor exchange coupling constant and J'' is the exchange coupling constant for the ring current or, in other words, for the cyclic permutation of all four spins. We are neglecting some of the cyclic permutation terms considered in ref. 206 (the h_2 and h_3 terms) as the number of unique energy differences only allows for the extraction of three independent parameters. Assuming that all four sites are chemically equivalent, four different states with

unique energies can be formed in the BS DFT calculations: $|\alpha\alpha\alpha\alpha\rangle$, $|\alpha\alpha\alpha\beta$, $|\alpha\alpha\beta\beta\rangle$, and $|\alpha\beta\alpha\beta\rangle$, where the spin indices are in numerical order. Following Calzado and Malrieu, the exchange coupling constants can be extracted from the BS DFT energies by interpreting them as the expectation values of (212) acting on the respective Ising states as:[206,a]

$$J = \frac{1}{2}\left(E_{\alpha\beta\alpha\beta} - E_{\alpha\alpha\alpha\alpha}\right) \tag{213}$$

$$J' = E_{\alpha\alpha\beta\beta} - \frac{1}{2}E_{\alpha\beta\alpha\beta} - \frac{1}{2}E_{\alpha\alpha\alpha\alpha} \tag{214}$$

$$J'' = 8E_{\alpha\alpha\alpha\beta} - 2E_{\alpha\beta\alpha\beta} - 4E_{\alpha\alpha\beta\beta} - 2E_{\alpha\alpha\alpha\alpha}. \tag{215}$$

The calculated values are $J = -619\,\mathrm{cm}^{-1}$, $J' = -51\,\mathrm{cm}^{-1}$, and $J'' = -22\,\mathrm{cm}^{-1}$. Hence, it is immediately clear that the exchange couplings J' and J'' are certainly not negligible and that the Hamiltonian (212) is insufficient to describe all the relevant magnetic properties of **7**. The calculated nearest-neighbor exchange parameter J is roughly three times larger in magnitude than the value extracted from the experimental fit, but the calculated values should be considered as more reliable due to the reasons discussed above. All of the exchange couplings are AFM, meaning that the system is spin-frustrated. The nearest-neighbor exchange, however, is an order of magnitude larger than the two other couplings, meaning that the ground state should be singlet as predicted by the CASSCF/NEVPT2 calculations.

6.3 Design of organic radical systems with ferromagnetic interaction

6.3.1 Theoretical framework

The complex **6** orders antiferromagnetically and complexes **2**, **3**, and **5** show some intermolecular AFM interaction. Design of molecular ferromagnets requires that the intramolecular interactions must be ferromagnetic. This is usually very difficult to realize as the kinetic exchange in equation (77) almost always surpasses the Coulomb exchange contribution resulting in AFM interaction. The interaction is FM only when the transfer integral t_{ab} in (77) vanishes. In organic magnets, such as the *para*-nitrophenyl nitronyl nitroxide,[31] this results from what was referred to by Kahn as "accidental orthogonality" of the radical SOMOs.[28] In the same paper, Kahn and co-workers synthesized a hetero-bimetallic transition-metal complex, where the transfer integrals between the metal SOMOs is exactly zero due to symmetry. In Paper **IV**, we extended Kahn's approach to organic radical dimers. Although our paper focuses on specific organic systems as a proof-of-concept, the approach is general enough that it can also be applied to radical–metal complexes

[a] If comparing the expressions presented here and those in ref. 206, one should note that we use a different sign for the exchange coupling constants here.

and other systems with sufficiently high symmetry or, possibly, pseudo-symmetry. We are not the first ones to consider the extension of Kahn's approach to radical systems.[659,660] However, we present quantitative calculations on real-life radical systems, which could, in principle, be experimentally characterized.

In their original work, Kahn and co-workers formulated the theory for the enforcement of FM interaction in hetero-bimetallic transition metal complexes within the framework of valence bond theory,[28,661] and this same approach has been used in other works in the field.[659,660] We will describe the theory here in terms of orthogonal magnetic orbitals, which are easier to relate to the point group symmetry of the system. We will consider a system with two spin sites a and b with one electron each occupying the orthogonal magnetic orbitals $\phi_a(\mathbf{r})$ and $\phi_b(\mathbf{r})$ localized at the two sites. All orbital angular momentum is assumed to be absent, which is usually a reasonable assumption in radical systems. The transfer integral t_{ab} is given as the Fock matrix element between the two orbitals: $t_{ab} = \langle\phi_a|\hat{F}|\phi_b\rangle$.[177] If the two sites are identical and related by a symmetry operation, say inversion, neither $\phi_a(\mathbf{r})$ nor $\phi_b(\mathbf{r})$ forms a basis for a representation of the molecular point group. A HF calculation on the system produces two canonical symmetry-adapted orbitals of *gerade* (g) and *ungerade* (u) symmetry:

$$\phi_g(\mathbf{r}) = \frac{1}{\sqrt{2}}\left[\phi_a(\mathbf{r}) + \phi_b(\mathbf{r})\right] \quad \text{and} \quad \phi_u(\mathbf{r}) = \frac{1}{\sqrt{2}}\left[\phi_a(\mathbf{r}) - \phi_b(\mathbf{r})\right]. \tag{216}$$

The transfer integral is then given by

$$\begin{aligned} t_{ab} = \langle\phi_a|\hat{F}|\phi_b\rangle &= \frac{1}{2}\left(\underbrace{\langle\phi_g|\hat{F}|\phi_g\rangle}_{=\epsilon_g} - \underbrace{\langle\phi_g|\hat{F}|\phi_u\rangle}_{=0} + \underbrace{\langle\phi_u|\hat{F}|\phi_g\rangle}_{=0} - \underbrace{\langle\phi_u|\hat{F}|\phi_u\rangle}_{=\epsilon_u}\right) \\ &= \frac{1}{2}\left(\epsilon_g - \epsilon_u\right), \end{aligned} \tag{217}$$

where we have used the fact that $\hat{F}$ is diagonal in the canonical orbitals with the orbital energies ϵ_g and ϵ_u as eigenvalues. Thus, the transfer integral is simply half the negative of the HOMO–LUMO gap. If the interaction between the two sites is non-vanishing, the HOMO–LUMO gap will be non-zero, and kinetic exchange will be present.

Now, let us consider another situation where the molecule has a point group symmetry, which is higher than C_1, but the two sites a and b are *not* related by any symmetry operation. In practice, this means that the system has a mirror plane, which dissects the two spin sites. Let us then further consider the situation where a and b are not equivalent and transform differently under the symmetry operations of the point group. In this situation, the magnetic orbitals $\phi_a(\mathbf{r})$ and $\phi_b(\mathbf{r})$ both form a basis for a different representation of the point group, and no linear combination of them can give a symmetry-adapted canonical orbital. Thus, a HF calculation on this system produces the orbitals $\phi_a(\mathbf{r})$ and $\phi_b(\mathbf{r})$ as solutions, and the magnetic orbitals are eigenfunctions of the Fock operator. In other words:

$$t_{ab} = \langle\phi_a|\hat{F}|\phi_b\rangle = 0, \tag{218}$$

and the interaction between the sites must be FM. The conditions for this are that i) each magnetic orbital forms a basis for a representation of the point group on its own, and ii) the magnetic orbitals form bases for different representations.

6.3.2 Model systems for a proof-of-concept study

When applying Kahn's approach to organic radical dimers, the natural starting point is to consider radicals with sufficiently high symmetry or pseudo-symmetry and with highly predictable dimerization geometry. Preferably, the chosen radical framework should also be chemically modifiable to fine tune the necessary interactions for the radical dimerization. These conditions are fulfilled by systems based on the phenalenyl radical (Figure 13a),[662–665] and systems of this type were used in Paper **IV**. Phenalenyl is an odd-alternate π-conjugated hydrocarbon, which can be considered as three fused benzene rings or, equivalent, as a small piece of graphene.[666] A more detailed account on the properties of phenalenyl and a more comprehensive bibliography is given in the book chapter by Morita and Nishida.[667] Phenalenyl cannot be isolated in the solid state, but in 1999, Goto *et al*. synthesized the *tert*-butyl substituted 2,5,8-tri-*tert*-butyl-phenalenyl (**8**, Figure 13c) and obtained crystals suitable for X-ray diffraction.[668] **8** forms staggered **8–8** dimers (Figure 13b) with short intermolecular carbon–carbon contacts ranging from 320.1 pm to 332.3 pm. The radical spins are strongly coupled to give an AFM ground state. The exchange coupling constant has been estimated as $J = -1390\,\mathrm{cm}^{-1}$ based on SQUID measurements[668–670] carried out in the presence of paramagnetic impurities and as $J = -2910\,\mathrm{cm}^{-1}$ based on signal intensities in EPR measurements.[671] The radical–radical interaction in **8–8** has been the subject of several spectroscopic and computational studies and is often described as a two-electron-twelve-center covalent bond.[672–685]

The 2,5,7-tri-*tert*-butyl-6-oxophenalenoxyl radical (**9**, Figure 13c) is structurally similar to **8** but has oxygen substituents on the phenalenyl skeleton at 1 and 6 positions.[686] **9** also forms a staggered **9–9** dimer with AFM interaction.[687] Visual examination of the SOMOs of **8** and **9** (Figures 13d and 13e) shows that they transform differently relative to a reflection through a plane perpendicular to the molecular plane. Considering the staggered geometry, which retains this reflection pseudo-symmetry also in the dimer means that according to Kahn's approach, the interaction in a **8–9** heterodimer should be ferromagnetic. In Paper **IV**, the exchange interactions and dimerization enthalpies of **8–8**, **9–9**, and **8–9** were calculated. Paper **IV** only discusses the dimers constructed from **8** and **9**, but we also studied dimers constructed from other experimentally characterized phenalenyl derivatives 2,5,8-triphenyl-phenalenyl (**10**)[682] and 2,5,8-tris(perfluorophenyl)-phenalenyl (**12**),[688] as well as from their hypothetical oxophenalenoxyl analogues 2,5,8-triphenyl-6-oxophenalenoxyl (**11**) and 2,5,8-tris(perfluorophenyl)-6-oxophenalenoxyl (**13**). The results of these calculations will be reported here.

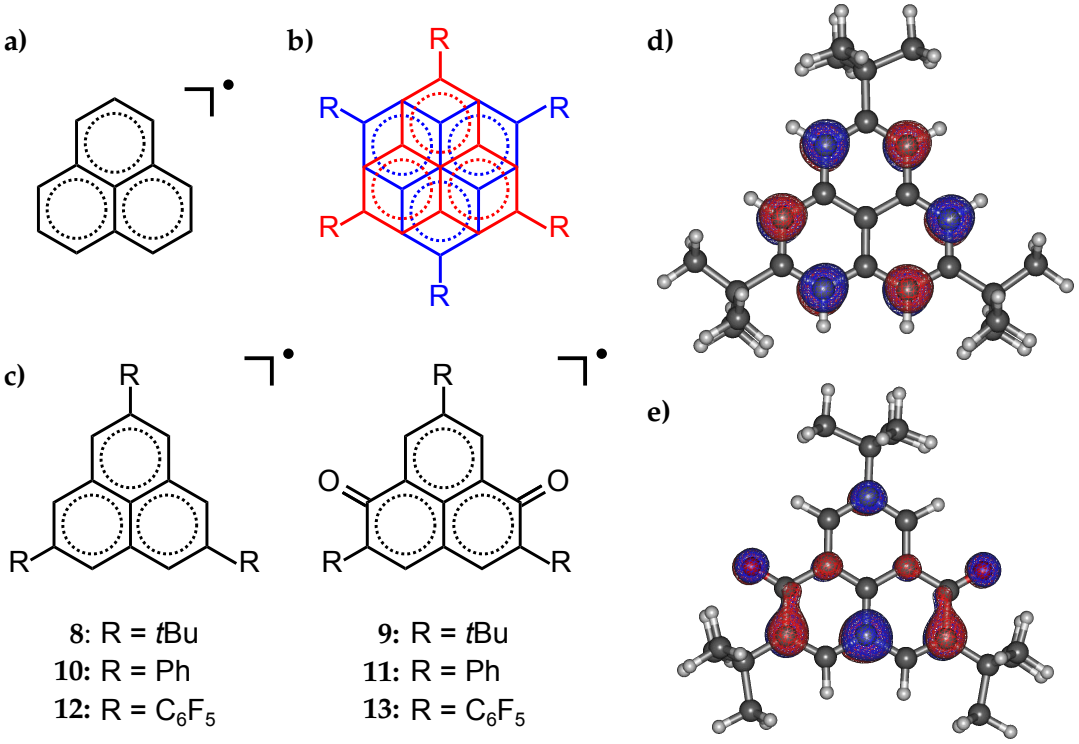

FIGURE 13 **a)** The structure of phenalenyl radical, **b)** a phenalenyl-based radical dimer, **c)** structures of phenalenyl derivatives **8** to **13**, **d)** the optimized structure and SOMO of **8**, and **e)** the optimized structure and SOMO of **9**.

6.3.3 Validation studies

Before the actual calculations were carried out, the DFT methods used in the computations were subjected to a validation study to ensure reliability of the final results. Since we were mostly dealing with dimers for which there are no experimental structures available, the geometries had to be optimized from scratch. This proved somewhat challenging as the formation of the dimers is strongly stabilized by long-range dispersion interactions. Although some functionals can treat short-range dispersion in a phenomenological manner (such as the Minnesota functionals), long-range dispersion must be treated by some empirical dispersion correction. Furthermore, in order to evaluate the dimerization enthalpies, the calculations must be corrected for BSSE, and the energy of the ground singlet state must be projected from the energies of the BS and HS states. Assuming that the geometry optimized for the BS state is a reasonable approximation to the geometry of the LS state, which is an unavoidable approximation, the energy of the LS state can be evaluated by adding the value of the exchange coupling constant to the HS energy evaluated at the LS geometry:[598]

$$E_{\mathrm{LS}}^{\mathrm{LS}} \approx E_{\mathrm{LS}}^{\mathrm{BS}} = E_{\mathrm{HS}}^{\mathrm{BS}} + \frac{2(E_{\mathrm{BS}}^{\mathrm{BS}} - E_{\mathrm{HS}}^{\mathrm{BS}})}{\langle \hat{S}^2 \rangle_{\mathrm{HS}}^{\mathrm{BS}} + \langle \hat{S}^2 \rangle_{\mathrm{BS}}^{\mathrm{BS}}}, \tag{219}$$

where the subscript refers to the state being evaluated and the superscript refers to the state the geometry has been optimized in, and we have used equation (202)

TABLE 2 Exchange coupling constants calculated for the **8–8** dimer using various functionals and geometry extracted from the crystal structure.

Functional	J_{crystal} / cm^{-1}
B3LYP	−3669
PBE0	−3531
M06	−3787
M06-2X	−4239
LC-ωPBE	−2754
CAM-B3LYP	−3323
ωB97XD	−3431
Experimental	−1390[a], −2910[b]

[a] Based on SQUID measurements.[668–670]

[b] Based EPR measurements[671]

for the evaluation of the exchange coupling constant. In a similar approximation, it is assumed that the vibrational frequencies calculated for the BS state are a reasonable approximation those of the LS state.

The validation calculations were carried out on the **8–8** dimer in two phases. In the first series of calculations, the exchange coupling constants were calculated using the geometry extracted from the crystal structure to separate the effects of the XC functional on the exchange interaction from those on the geometry optimization and the dimerization energetics. In the second phase, the dimerization enthalpy was calculated using fully optimized geometries. The exchange coupling constants calculated using the crystal structure geometry are listed in Table 2. All calculated XC functionals exaggerate the AFM coupling when compared to the experimental values. However, as discussed above, the experimental values have been determined in the presence of paramagnetic impurities and should be taken as qualitative. Thus, direct comparison with experiment is difficult. The best agreement is made with the LC-ωPBE functional. All functionals do predict strong AFM coupling and are in qualitative agreement with the experiment.

The results of the dimerization enthalpy calculations listed in Table 3 show that with the exception of the Minnesota functionals, a dispersion correction is required to make the dimerization energetically favorable. The cases where the monomer–monomer interaction is repulsive, were not studied any further. The dimerization enthalpy has been determined experimentally using different methods, all giving roughly similar values (see Table 3). The results show that in all cases, the magnitude of the dimerization enthalpy is exaggerated by the calculations. This systematic overestimation makes direct comparison with experiment again rather difficult. The best estimate of the experimental value is given by CAM-B3LYP-D3, although with a considerably overestimated distance between the monomers. Based on this observation, the dimerization enthalpies of the HS states in the final calculations were evaluated at DLPNO-CCSD(T) level using the DFT optimized geometries. The main criteria for the choice of the XC functional was then made the ability of the chosen functional to correctly reproduce the experimental geometry. The crystallographically

TABLE 3 Exchange coupling constants, dimerization enthalpies, and central carbon distances in the **8–8** dimer as calculated with various functionals using optimized geometries

Functional	J_{opt} / cm^{-1}	ΔH_{dimer} / $kJ\,mol^{-1}$	$d(C-C)$ / pm[a]
B3LYP		Repulsive	
B3LYP-D3	−4524	−78	315.1
B3LYP-D3BJ	−5345	−88	308.2
PBE0		Repulsive	
PBE0-D3	−3246	−81	327.0
PBE0-D3BJ	−4347	−80	313.7
M06	−3327	−89	331.3
M06-D3	−3434	−143	331.0
M06-2X	−5110	−74	312.7
M06-2X-D3	−5120	−98	312.7
LC-ωPBE		Repulsive	
LC-ωPBE-D3	−2016	−83	329.9
LC-ωPBE-D3BJ	−2140	−92	327.6
CAM-B3LYP		Repulsive	
CAM-B3LYP-D3	−1864	−73	344.6
CAM-B3LYP-D3BJ	−1829	−81	345.0
ωB97XD	−2828	−105	331.0
Experimental	−1390[b], −2190[c]	−31[d], −37[e], −40[f]	320.1[g]

[a] Distance between the central carbons of the two radicals.
[b] Based on SQUID measurements.[668–670]
[c] Based EPR measurements[671]
[d] Based on UV-Vis measurements.[676]
[e] Based on UV-Vis measurements.[675]
[f] Based on EPR measurements.[675]
[g] From crystal structure.[668]

determined $d(C-C)$ distance between the central carbons of the two radicals is best reproduced with the B3LYP-D3 functional. The functionals LC-ωPBE-D3, LC-ωPBE-D3BJ, M06-2X, M06-2X-D3, PBE0-D3, and PBE0-D3BJ also produce geometries with the value of $d(C-C)$ deviating from experiment by less than 1 pm. Based on these results and the calculated exchange coupling constants, the LC-ωPBE-D3BJ functional was chosen for further calculations. It should be noted, however, that any of the tested functionals should produce qualitatively correct results.

The dimerization energy of **8–8** has been calculated previously from first principles only in the paper of Kertesz and co-workers,[679] and the same results have been later used in ref.[682] Kertesz used the M05-2X functional without any dispersion correction and obtained a dimerization energy (including zeropoint and BSSE corrections) of $-33\,kJ\,mol^{-1}$ and a distance of 320.9 pm between the central carbons of the two radicals. Both values are in very good agreement with experiment. In our calculations, the dimerization enthalpy calculated using the M06-2X functional (which is an improved version of M05-2X) without any

TABLE 4 Exchange coupling constants, dimerization enthalpies, and central carbon distances calculated for dimers of various phenalenyl-based radicals

Dimer	J_{opt} / cm^{-1}	ΔH_{dimer} / $kJ\,mol^{-1}$	$d(C-C)$ / pm[a]
8–8	−2141	−69 (−103)[b]	327.6
9–9	−75	−59 (−93)[b]	359.5
8–9	435	−00 (−105)[b]	330.6
10–10	−4234	−146	321.6
11–11	−130	−130	356.0
12–12	−117	−98	711.2
13–13	−35	−101	337.7
10–11	−227	−128	335.4
10–13	−898	−131	343.7
11–12	−274	−115	274.3
12–13	−201	−98	337.7

[a] Distance between the central carbons of the two radicals.
[b] The first value is evaluated using DLPNO-CCSD(T) energies and the value in parenthesis uses only DFT energies.

dispersion correction is $-74\,kJ\,mol^{-1}$, which is considerably larger than that calculated by Kertesz and co-workers. We attribute these differences to the use of spin-projection in our calculations and the use of a considerably larger basis set. In preliminary calculations, we noted that using the smaller def2-SVP basis sets[626] lead to qualitatively different results in some cases as compared to calculations carried out using the def2-TZVP basis. Thus, our calculations should be taken as more accurate than those of Kertesz and co-workers.

6.3.4 Results

In order to demonstrate the validity of the theoretical framework presented in section 6.3.1, calculations were carried out on the dimers **8–8**, **9–9**, and **8–9**. The dimerization enthalpies were evaluated by using DLPNO-CCSD(T) energies for the HS states and by evaluating the first E_{HS}^{BS} term on the right-hand side of equation (219) at DLPNO-CCSD(T) level in the case of the LS states. The results are listed in Table 4 and show that in the case of **8–8** and **9–9**, the exchange interaction is AFM, whereas in the case of the mixed dimer **8–9**, the interaction is FM and in full agreement with the theoretical reasoning. It is also notable that formation of the mixed **8–9** dimer is energetically more favorable than the formation of the respective homodimers **8–8** and **9–9**; the enthalpy difference for the formation of **8–8** and **9–9** from two equivalents of **8** and **9** is $-128\,kJ\,mol^{-1}$, whereas the enthalpy difference for the formation of two equivalents of **8–9** is $-145\,kJ\,mol^{-1}$. This results is very encouraging when considering the practical application of this approach.

Next, we studied whether FM interaction could also be enforced in dimers constructed from the phenyl and perfluorophenyl subsituted phenalenyl radicals **10**, **11**, **12**, and **13**. The calculated results for these systems are also listed in Table 4. None of the dimers, however, show any FM coupling. The reason for

this is that the phenyl or perfluorophenyl substituents are not bulky enough to prevent the rotation of the two radicals relative to each other in the dimer. Such a rotation breaks the pseudo-reflection symmetry of the radical SOMOs in the dimer geometry and allows non-zero overlap between the orbitals, which then leads to AFM interaction. The use of different substituents does lead to varying dimerization enthalpies, which means that the interaction between the two radicals can be made more or less favorable by the introduction of specific substituents. If these substituents are bulky enough to prevent the relative rotation of the radicals, the substituents can be tuned to favor the formation of the mixed dimer over the homodimers.

7 COMPUTATIONAL MODELING OF STRONGLY ANISOTROPIC MAGNETIC PROPERTIES

The main challenge in the study of SMMs is to synthesize new systems with higher operational temperatures. In the case of monometallic systems, general conditions for high-temperature SMMs have been established.[106,108,109] The most important of these is the design of CFs in such a way that it stabilizes the largest $|M_J|$ projections of the ground J-multiplet of the respective trivalent lanthanide ion. This can be achieved either by constructing strongly axial CFs[**V**, **VI**, 111–114, 689–692] or strongly equatorial CFs.[693–696] So far, the latter has not been as successful an approach as the former. Papers **V** and **VI** included in this work focus on the characterization of SMMs with highly axial CFs. One of the complexes synthesized in Paper **VI** holds the record of the highest blocking temperature ever observed in a molecular lanthanide SMM: 60 K. Paper **VII** focuses on the other main approach to designing high-temperature SMMs: the construction of exchange coupled lanthanide systems, where the exchange interactions blocks the ground state QTM.

7.1 Computational details

All multireference calculations in this chapter were carried out using the Molcas code.[254] The 8.1 development version was used for XMS-CASPT2 calculations in Paper **V**, the 8.2. release version was used for some of the calculations in Paper **VII**, and the 8.0 release version was used for all other calculations. Scalar relativistic effects were treated with the X2C method. The relativistically contracted atomic natural orbital (ANO-RCC) basis sets where used throughout.[697–699] In papers **VI** and **VII**, a polarized triple-ζ quality basis (ANO-RCC-VTZP) was used for the Dy(III) ions[699] and polarized double-ζ quality basis sets (ANO-RCC-VDZP) were used for the other atoms.[697,698] In Paper **V**, a slightly larger basis was used, which consisted of a polarized quadruple-ζ quality basis (ANO-RCC-VQZP) for the Dy(III) ion, ANO-RCC-VTZP for the atoms in the first coordination sphere,

and ANO-RCC-VDZP for atoms in the outer coordination spheres. CD with a threshold of 10^{-8} atomic units was used in all two-electron integral calculations. In papers **VI** and **VII**, the calculations were standard CASSCF calculations with no consideration of dynamic electron correlation. In Paper **V**, CASSCF calculations were carried out using the full geometry, whereas XMS-CASPT2 calculations were performed on a simple model geometry. In all papers, all 21 sextet, 224 quartet, and 490 doublet roots were solved in three separate SA-CASSCF calculations, one for each multiplicity. The XMS-CASPT2 corrections were only calculated for the sextet states.

SOC was included using the SO-RASSI methodology and the AMFI operator. In the pure CASSCF calculations, all 21 sextets, 128 quartets, and 130 doublets were included in the SO-RASSI treatment corresponding to an energy cut-off of $50\,000\,\mathrm{cm}^{-1}$. Magnetic properties were calculated using the SINGLE_ANISO[95–97,100,101] and POLY_ANISO[96,98,99] programs of the MOLCAS code. The Lines exchange parameter in Paper **VII** was determined by fitting *ab initio* values to experimental χT data. The fit was carried out by scanning the parameter with $0.001\,\mathrm{cm}^{-1}$ increments.

In papers **V** and **VI**, the positions of the hydrogen atoms were optimized, while the coordinates of all heavier atoms were kept frozen to their respective crystal structure geometries. This was carried out because the hydrogen positions extracted from crystal structures are not reliable and the close proximity of the hydrogen atoms to the lanthanide ions could have an effect on the magnetic properties. In Paper **VII**, the geometry was used as obtained from the crystal structure. The hydrogen optimizations were carried out at DFT level using the BP86 GGA XC functional in Paper **V** and the PBE GGA XC functional in **VI**. In **V**, polarized double-ζ quality ZORA-def2-SVP basis sets[624] were used for lighter atoms, ZORA-SARC-TZVP[627] for the Dy(III) ion, and corresponding auxiliary basis sets[624,627] for the RI approximation. Scalar relativistic effects were taken into account in the geometry optimization using the ZORA as implemented in ORCA.[392] In **VII**, the geometry optimization was carried out in a non-relativistic framework using the polarized double-ζ def2-SVP basis sets[626,700] and a corresponding auxiliary basis.[292,293] The Dy(III) ion was replaced by a diamagnetic Y(III) ion to avoid problems related to static electron correlation. The core electrons of the Y(III) ion were treated using an 28-electron effective core potential (ECP). All DFT optimization were carried out using ORCA 3.0.3 code[251] and the RI approximation for the Coulomb potential.

The CF-correction procedure introduced in Paper **V** used the EASYSPIN module[701] in MATLAB[702] to carry out the diagonalization of the CF Hamiltonian.

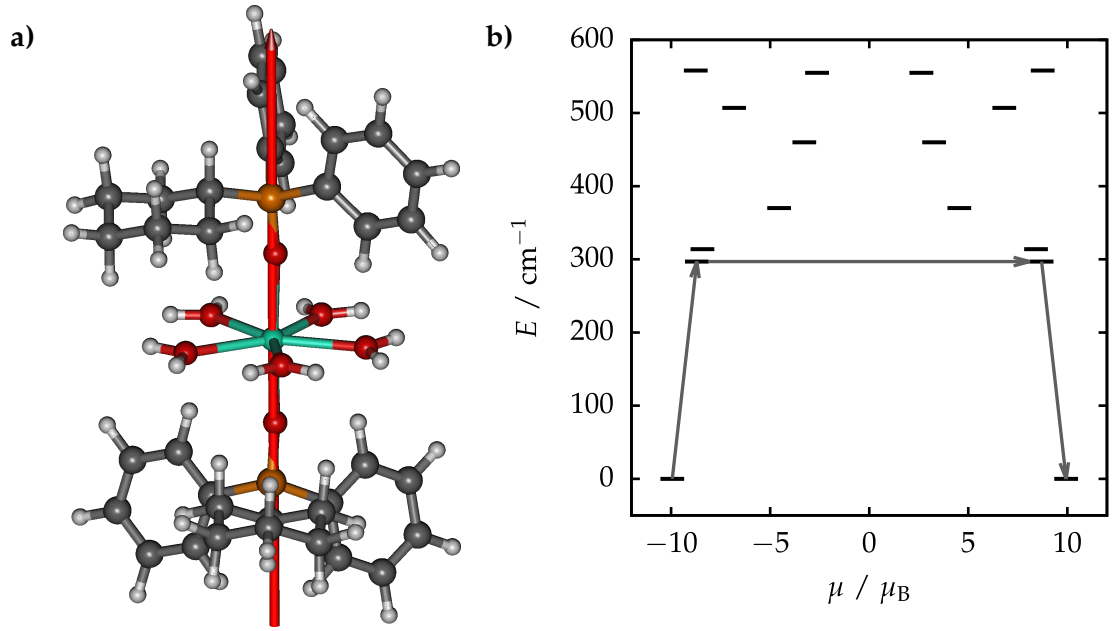

FIGURE 14 **a)** The structure and principal magnetic axis of the ground Kramers doublet of **14** and **b)** the qualitative barrier for the relaxation of magnetization in **14**.

7.2 Monometallic Dy(III) complexes

7.2.1 $Dy[(CyPh_2PO)_2(H_2O)_5]Br_3$ complex

Paper **V** studied the magnetic properties of the complex $Dy[(CyPh_2PO)_2(H_2O)_5]Br_3 \cdot 2(CyPh_2PO) \cdot EtOH \cdot 3H_2O$ (**14**, Figure 14a, $CyPh_2PO$ = cyclohexyl-(diphenyl) phosphine oxide). The structure is very similar to other high-performing SMMs published by Tong and co-workers.[111,689] The equatorial coordination positions around the Dy(III) ion in **14** are taken by five water molecules in an almost ideal D_{5h} geometry. The axial positions are coordinated by two $CyPh_2PO$ ligands. The overall coordination geometry is pentagonal bipyramidal with some deviations from ideal D_{5h} symmetry already in the first coordination sphere. The second coordination sphere around the water ligands consists of two free $CyPh_2PO$ ligands and three bromide ions. The neutral water molecules are weak ligands, whereas the coordinated oxygen atoms in the $CyPh_2PO$ ligands have formally negative charge, giving an overall axial coordination environment around the Dy(III) ion. The pseudo-D_{5h} coordination environment makes the CF even more preferable for a Dy(III) SMM, as in an ideal pentagonal bipyramidal field all Stevens operators with $q \neq 0$ in expansion (62) up to rank $k = 10$ vanish due to symmetry.[26] The off-diagonal $q \neq 0$ operators introduce non-vanishing transition matrix elements between the different states. Thus, in an ideal D_{5h} symmetry, all relaxation processes in the lowest doublets should be suppressed to a high order. Pentagonal bipyramidal SIMs have indeed proven to be some of the best characterized so far.[111–113,689]

The magnetic properties of **14** were studied by dc and ac susceptibility

TABLE 5 The energies, principal components of the $\tilde{\mathbf{g}}$ tensors, and directions of the principal magnetic axes of the eight lowest Kramers doublets (KDs) corresponding to the CF-split components of the Dy(III) ground $^6H_{15/2}$ multiplet in **14**

KD	E / cm^{-1}	$\tilde{g}_x$	$\tilde{g}_y$	$\tilde{g}_z$	θ[a]
1	0	0.000	0.000	19.881	0.0°
2	297	0.957	3.427	16.696	90.0°
3	314	0.088	0.127	16.923	0.3°
4	370	3.303	4.546	8.707	90.0°
5	460	1.401	3.777	6.525	0.3°
6	507	0.247	0.387	13.627	0.4°
7	555	0.296	1.214	11.228	26.4°
8	588	0.504	1.011	13.170	28.5°

[a] The angle between the principal magnetic axis of the doublet and that of the ground doublet.

measurements. The system shows hysteresis with open loops up to 19 K with a scan speed of 200 G s^{-1}. The FC and ZFC susceptibilities diverge below 11 K with a ramping speed of 2 K min^{-1}. Based on the ac susceptibility measurements, the relaxation behavior was modeled as an Arrhenius-type process yielding an effective barrier height of $U_{\text{eff}} = 353\,\text{cm}^{-1}$. The presence of the aromatic substituents in the $CyPh_2PO$ ligands leads to a well-resolved luminescence spectrum with sharp peaks corresponding to the energy levels of the individual Kramers doublets. The peaks were assigned to give energies 322 cm^{-1} and 396 cm^{-1} for the first and second excited Kramers doublet relative to the ground doublet. The energy of the first excited state is in good agreement with the effective barrier height obtained from the ac susceptibility measurements strongly supporting the Arrhenius-type model for the relaxation of the magnetization.

The energies and principal components of the $\tilde{\mathbf{g}}$-tensors of the eight lowest Kramers doublets corresponding to the CF-split components of the ground $^6H_{15/2}$ multiplet of the Dy(III) ion were calculated. The results are listed in Table 5. The $\tilde{\mathbf{g}}$-tensor of the ground doublet is strongly axial ($\tilde{g}_x, \tilde{g}_y \sim 0$), explaining the lack of QTM in the ground doublet. The angle between the principle magnetic axes (the eigenvector of $\tilde{\mathbf{g}}$ corresponding to the eigenvalue $\tilde{g}_z$) of the ground and first excited state is almost exactly 90°. This relative rotation of the magnetic axis leads to strong transition matrix elements between the components of the ground and first excited doublets.[105,109] The qualitative relaxation pathway of **14** is given in Figure 14b.

Although the magnetic relaxation via the first excited doublet is well explained by the calculations, reproducing the energy of the said doublet proved much more difficult. A simple CASSCF/SO-RASSI calculation yielded the value 206 cm^{-1}, which is only 64% of the experimental value. It has been well established that pure CASSCF calculations, which completely neglect the electron correlation outside the active space are, in many cases, incapable of quantitatively reproducing the energies of the lowest excited states, although in the case of

trivalent lanthanides, the results are usually qualitatively correct.[101] The problem in the case of **14** is that the free ligands in the second coordination sphere affect the energies of the Kramers doublets; therefore, the geometry that needs to be treated in the *ab initio* calculations is rather large. An XMS-CASPT2 calculation on the full geometry is not possible due to the high computational costs. In order to introduce the missing correlation energy into the CASSCF calculations, at least approximately, a CF-correction scheme was developed. This was carried out by first performing a CASSCF/SO-RASSI calculation on the full geometry. Then, CASSCF/SO-RASSI and CASSCF/XMS-CASPT2/SO-RASSI calculations were carried out on a truncated geometry, where all of the phenyl and cyclohexyl groups in the ligands had beed replaced by methyl groups. The *ab initio* CF parameters were extracted from each calculation as described in section 4.5.4. The difference in the CF Hamiltonians as calculated at CASSCF/SO-RASSI and CASSCF/XMS-CASPT2/SO-RASSI levels on the truncated geometry is

$$\Delta\hat{H}_{\mathrm{CF}} = \hat{H}_{\mathrm{CF}}^{\text{XMS-CASPT2,truncated}} - \hat{H}_{\mathrm{CF}}^{\text{CASSCF,truncated}}, \tag{220}$$

and this "CF-correction" was added to the CF Hamiltonian extracted from the CASSCF/SO-RASSI calculation on the full geometry to yield the corrected CF Hamiltonian:

$$\hat{H}_{\mathrm{CF}}^{\text{corrected}} = \hat{H}_{\mathrm{CF}}^{\text{CASSCF,full}} + \Delta\hat{H}_{\mathrm{CF}}. \tag{221}$$

This Hamiltonian should, in a highly approximate manner, include the electron correlation effects outside the CAS within the immediate coordination sphere around the Dy(III) ion. The final energies of the Kramers doublets were obtained by diagonalizing this Hamiltonian. The CF-corrected energy of the first excited doublet is 297 cm^{-1}, which still does not perfectly match the experimental value, but is much closer than the pure CASSCF/SO-RASSI value and considering the heuristic nature of the approximation, the result is fairly good. The energies of the eight lowest Kramers doublets calculated with the different approximations are listed in Table 6.

TABLE 6 The energies (in cm^{-1}) of the eight lowest Kramers doublets (KDs) corresponding to the CF-split components of the Dy(III) ground $^{6}H_{15/2}$ multiplet in **14** as calculated with various approximations as well as the available experimental values

	full geometry	truncated geometry			
KD	CASSCF	CASSCF	CASPT2	CF-correction	Experimental
1	0	0	0	0	0
2	206	130	223	297	322
3	242	180	284	314	396
4	267	214	288	370	
5	342	250	371	460	
6	389	321	451	507	
7	425	338	467	555	
8	454	365	506	588	

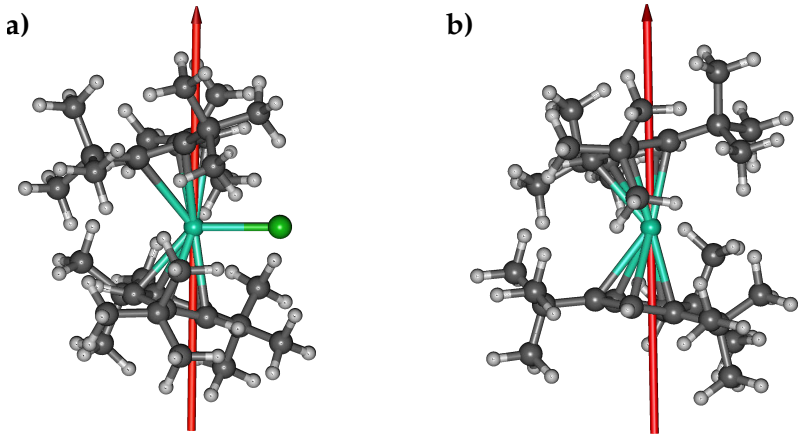

FIGURE 15 **a)** The structures and principal magnetic axes of the ground Kramers doublet of **15** and **b)** the structures and principal magnetic axes of the ground Kramers doublet of **16**.

7.2.2 Dysprocenium complexes

In the previous section, it was shown that the strong axial donor ligands in **14** lead to very pronounced SMM behavior. It had already been shown by earlier theoretical work on a related system that removing the equatorial ligands altogether would most likely lead to even higher blocking temperatures.[111] The large ionic radius of the Dy(III) ion makes low-coordinate complexes extremely unstable, and it would be very unlikely that the $CyPh_2PO$ ligands would be able to offer enough steric protection to stabilize the Dy(III) ion in the absence of the equatorial coordination sphere. Much better steric protection is offered by cyclopentadienyl ligands with some alkyl substituents coordinated to give metallocene-type sandwich complexes of Dy(III). Various experimental works have established that the cyclopentadienyl ligands produce a strongly axial CF and introducing only weakly coordinating ligands into equatorial positions leads to very pronounced SMM behavior.[110,703–709] Like in the case of complexes analogous to **14**, it has been pointed out that removing the equatorial ligands should lead to slower relaxation of magnetization and higher blocking temperatures.[110,705] Paper **VI** discusses the characterization of two dysprocenium complexes $[(Cp^{ttt})_2DyCl]$ (**15**, Figure 15a) and $[(Cp^{ttt})_2Dy]^+$ (**16**, Figure 15b), where Cp^{ttt} = 1,2,4-tri(*tert*-butyl)cyclopentadienide. The latter has no equatorial ligands and is the best SMM known to date. It should be pointed out that the same exact complexes were simultaneously and independently characterized and published by Chilton, Mills, and co-workers.[114] During the preparation of this dissertation also the Gd, Ho, Er, Tm, Yb, and Lu analogues of **16** were characterized by Chilton, Mills and co-workers.[710]

The magnetic properties of the chloride salt **15** are not very interesting. The complex does not show any out-of-phase signal in ac susceptibility measurements at zero dc field and is therefore not a SMM. The energies, principal components of the $\tilde{\mathbf{g}}$-tensors, and the relative angles of the principal magnetic axes of the eight lowest Kramers doublet corresponding to the CF-split components of the

TABLE 7 The energies, principal components of the $\tilde{\mathbf{g}}$ tensors, and directions of the principal magnetic axes of the eight lowest Kramers doublets (KDs) corresponding to the CF-split components of the Dy(III) ground $^6H_{15/2}$ multiplet in **15**

KD	E / cm^{-1}	$\tilde{g}_x$	$\tilde{g}_y$	$\tilde{g}_z$	θ[a]
1	0	0.036	0.073	19.318	0.0°
2	198	1.325	3.374	13.918	2.1°
3	289	2.735	4.848	10.155	95.4°
4	397	2.175	3.272	8.838	94.7°
5	523	0.787	0.878	11.962	89.8°
6	661	0.008	0.043	14.751	84.4°
7	833	0.022	0.023	17.208	87.5°
8	1084	0.002	0.003	19.725	90.7°

[a] The angle between the principal magnetic axis of the doublet and that of the ground doublet.

TABLE 8 The energies, principal components of the $\tilde{\mathbf{g}}$-tensors, and directions of the principal magnetic axes of the eight lowest Kramers doublets (KDs) corresponding to the CF-split components of the Dy(III) ground $^6H_{15/2}$ multiplet in **16**

KD	E / cm^{-1}	$\tilde{g}_x$	$\tilde{g}_y$	$\tilde{g}_z$	θ[a]
1	0	0.000	0.000	19.884	0.0°
2	457	0.000	0.000	17.041	2.4°
3	705	0.001	0.001	14.393	3.9°
4	864	0.002	0.005	11.749	4.9°
5	1012	0.075	0.078	9.123	5.6°
6	1156	0.750	0.962	6.508	4.0°
7	1270	0.165	1.941	3.881	4.0°
8	1334	11.556	9.420	1.284	0.6°

[a] The angle between the principal magnetic axis of the doublet and that of the ground doublet.

Dy(III) ground $^6H_{15/2}$ multiplet were calculated at CASSCF/SO-RASSI level and are listed in Table 7. The ground doublet has a largely axial $\tilde{\mathbf{g}}$-tensor, but the transverse components $\tilde{g}_x$ and $\tilde{g}_y$ are not small enough to fully suppress the QTM. This is the most likely reason for the absence of slow relaxation in **15**. If the ground doublet QTM was blocked by an external field, the relaxation would take place via the first excited doublet giving rise to a barrier of $U_{\text{eff}} = 198\,\text{cm}^{-1}$. The relaxation pathway is illustrated in Figure 16a.

The dysprocenium cation **16** was crystallized with the non-coordinating $B(C_6F_5)_4]^-$ anion and displays very notable SMM behavior. The hysteresis loops remain open up to 60 K using a scan speed of $39\,\text{G}\,\text{s}^{-1}$. The FC and ZFC susceptibilities diverge also at 60 K using a ramping speed of $2\,\text{K}\,\text{min}^{-1}$. The blocking temperature is more than four times higher than in any other system characterized earlier. The relaxation data were fitted using an Arrhenius-type

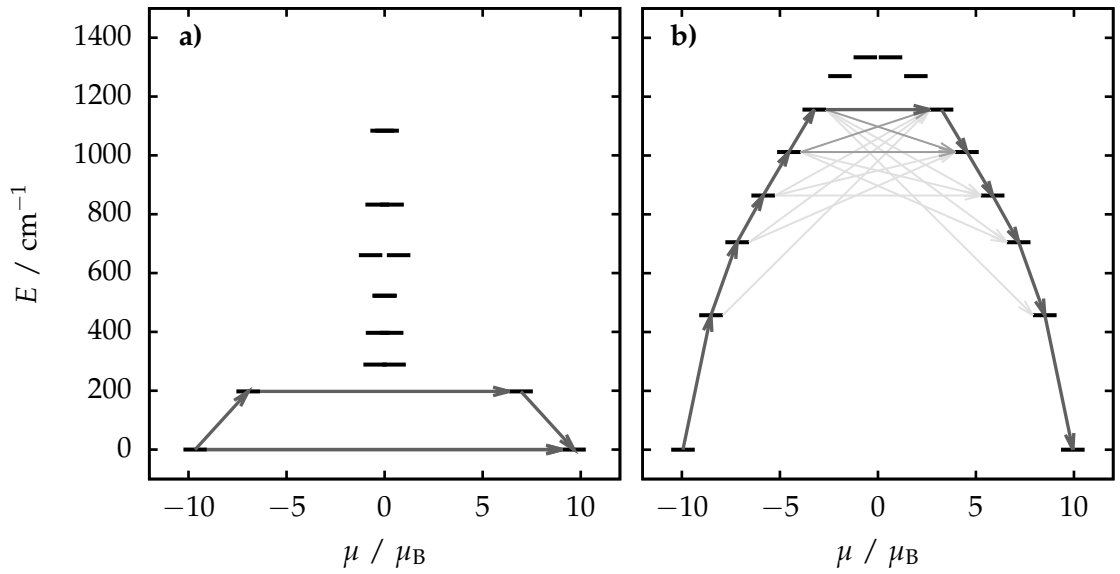

FIGURE 16 **a)** The qualitative barriers for the relaxation of magnetization in **15** and **b)** the qualitative barriers for the relaxation of magnetization in **16**.

model giving an effective barrier height of $U_{\text{eff}} = 1277\,\text{cm}^{-1}$. Properties of the eight lowest Kramers doublets were calculated at CASSCF/SO-RASSI level and are listed in Table 8. The two lowest doublets have practically perfectly axial $\tilde{\mathbf{g}}$-tensors. The transverse components $\tilde{g}_x$ and $\tilde{g}_y$ grow roughly an order of magnitude each time when one moves to higher energy doublets. The principal magnetic axes of all doublets are almost perfectly aligned; the largest angle between the ground doublet and an excited doublet is the 4.9° angle between the ground and fourth excited doublets. The calculated transition matrix elements predict that the relaxation pathway takes place via the fifth excited doublet (Figure 16b) predicting an effective barrier of $1156\,\text{cm}^{-1}$, which is in fairly good agreement with the experimental value. The small deviation most likely results from the neglection of electron correlation effects outside the active space.

The *ab initio* CF calculations allow one to decompose the *ab initio* SO-RASSI eigenstates into projections onto the states $\{|JM_J\rangle\}$. It is rather common in the case of Dy(III) SMMs that the lowest doublets have very large projection onto a state characterized by a single value of J and of M_J. In the higher energy doublets, the different M_J components become increasingly mixed. In the case of **16**, however, *all* states have very large projection on some single state $|JM_J\rangle$. The smallest squared modulus of a projection onto some $|JM_J\rangle$ state is 0.964 in the fifth excited Kramers doublet. This is also the doublet where the energy barrier is crossed in the qualitative relaxation pathway. In an ideally axial system with a $D_{\infty h}$ or $C_{\infty v}$ symmetry, none of the $|JM_J\rangle$ states are mixed by the CF. Based on the CF decomposition and to the best of our knowledge, **16** is the closest to an ideally axial system ever observed in a molecular lanthanide system. This further highlights the importance of designing strong axial CFs with *no* ligands in the equatorial coordination positions. It should also be noted that the axiality could still be improved leading to an even more pronounced SMM behavior and higher

blocking temperature.

7.3 Bimetallic [BQ{$DyCl_2(THF)_3$}$_2$] complex

In the design of lanthanide SMMs with higher operational temperatures, the first step is always suppression of the QTM in the ground doublet. In complexes **14** and **16** discussed in the previous sections, this was achieved by a highly axial CF. Another approach to suppress QTM is to couple lanthanide ions to each other, to transition-metal ions, or to radical ligands to introduce exchange interactions. The exchange interaction has a similar decoupling effect on the components of the ground Kramers doublet as does an external magnetic field. Several important hallmarks have been achieved by this strategy in the case of polymetallic Dy(III) complexes.[711–715] The exchange interactions between trivalent lanthanide ions mediated by some superexchange mechanism are usually rather weak, as the unpaired electrons of the lanthanide ions occupy the 4f shell, which is strongly shielded by the doubly occupied 5d and 5p orbitals with larger spatial extents. The strongest exchange coupling so far has been achieved in N_2^{3-} radical-bridged lanthanide complexes.[115,116,716] The systems shows magnetic blocking up to 20 K demonstrating that strong direct exchange interactions (when compared to lanthanide–lanthanide superexchange) can be utilized to design systems with highly pronounced SMM behavior. Unfortunately, other exchange coupled radical-bridged lanthanide complexes have not demonstrated exceptionally high blocking temperatures.[717–722]

In Paper **VII**, a benzoquinone-bridged bimetallic Dy(III) complex [BQ{$DyCl_2(THF)_3$}$_2$] (**17**, Figure 17, BQ = 2,5-bisoxide-1,4-benzoquinone) was characterized. The original goal in the project was to reduce the BQ bridge into a radical to yield a radical-bridged complex. Cyclic voltammetry and EPR measurements support the formation of the radical complex; however, no crystals of the radical complex suitable for X-ray crystallography could be obtained, and the possible radical-bridged system could not be structurally characterized. Thus, computational studies were only carried out on the complex **17** with a diamagnetic bridge. A very similar complex with a chloroanilate bridge was recently prepared by van Slageren and co-workers;[723] they also characterized the radical-bridged complex by spectroscopic methods but were unable to obtain a crystal structure.

Ac susceptibility measurements were carried out on **17**, but no out-of-phase signal was observed, indicating that **17** is not a SMM. Properties of the eight lowest Kramers doublets corresponding to the CF-split components of the Dy(III) ground $^6H_{15/2}$ multiplet were calculated at CASSCF/SO-RASSI level. The calculations were carried out by replacing the Dy(III) ion of the other center by the diamagnetic Y(III) ion, which has a very similar ionic radius. The two centers are related by a symmetry operation and are therefore equivalent. Calculations were carried out on both centers but the results differ due to some numerical noise only; thus, only one set of values is reported in Table 9. It is immediately

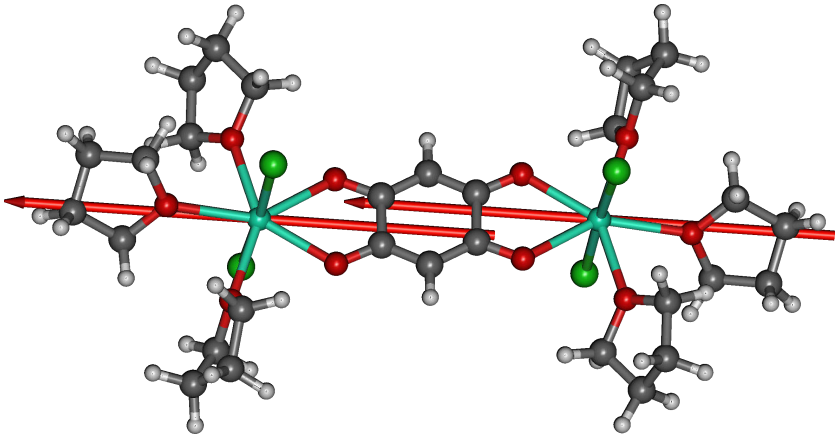

FIGURE 17 The structure of **17** and the principal magnetic axes of the ground doublets of the two Dy(III) ions.

TABLE 9 The energies, principal components of the $\tilde{\mathbf{g}}$-tensors, and directions of the principal magnetic axes of the eight lowest Kramers doublets (KDs) corresponding to the CF-split components of the Dy(III) ground $^6H_{15/2}$ multiplet in **17**

KD	E / cm^{-1}	$\tilde{g}_x$	$\tilde{g}_y$	$\tilde{g}_z$	θ^a
1	0	0.252	0.817	18.604	0.0°
2	44	0.206	0.300	19.359	91.0°
3	74	2.500	4.525	11.653	9.8°
4	132	8.008	5.110	0.185	82.2°
5	196	3.068	4.124	11.027	93.0°
6	251	0.075	1.352	14.788	75.8°
7	288	0.985	2.392	12.182	95.0°
8	306	0.842	2.359	14.483	92.6°

[a] The angle between the principal magnetic axis of the doublet and that of the ground doublet.

clear that the transversal components of the $\tilde{\mathbf{g}}$-tensor of the ground doublet are too large to effectively suppress QTM, explaining the lack of SMM behavior. It is also interesting to note that the principal magnetic axes of the ground doublets are not aligned along the pseudo-C_5 axes of the pentagonal bipyramidal coordination environments, but rather lie in the molecular plane (Figure 17). This is easy to understand by considering the formal charges on the oxygen atoms in the equatorial coordination positions; those of the BQ ligand have formal $-1/2$ charges, whereas those in the THF ligands are formally neutral. This means that the actual pseudo-symmetry of the CF is C_{2v} with the main rotational axis lying in the molecular plane. C_{2v} symmetry (exact or distorted) is not high enough to enforce axiality of the $\tilde{\mathbf{g}}$-tensor.[105]

Even though the $\tilde{\mathbf{g}}$-tensor of the ground doublet in **17** is not axial, it is still in principle possible that the QTM would be suppressed by exchange interaction between the two Dy(III) ions. This type of suppression has been observed in

bimetallic Dy(III) complexes with somewhat similar coordination environments and exchange coupling constants with magnitudes ranging from $3\,\mathrm{cm}^{-1}$ to $7\,\mathrm{cm}^{-1}$ as determined with the Lines model.[724,725] To study why this suppression is not effective in **17**, the exchange interaction was modeled by the Lines model and the exchange parameter $J_{\mathrm{Lines}} = 0.142\,\mathrm{cm}^{-1}$ was extracted by a fit of the *ab initio* calculated single-ion properties to experimental χT data. The parameter is very weak owning to the large distance between the two ions, and thus, the exchange interaction is simply too weak to effectively suppress the QTM. The exchange interaction could be considerably enhanced by introducing unpaired spin into the bridging BQ ligand, and future work will focus on this.

8 THEORETICAL DESCRIPTION OF ANISOTROPIC SPIN-DEPENDENT DELOCALIZATION

The favorable SMM properties observed in strongly exchange coupled lanthanide complexes[115,116,716] have highlighted the importance in understanding the nature of exchange interactions in the presence of strong SOC. Within the limit of applicability of the *LS* coupling scheme, the pseudospin Hamiltonian describing the direct or superexchange interaction between two trivalent lanthanide ions has been derived starting from the microscopic Hamiltonian[119,120] and the model has been applied to the description of strongly exchange coupled radical-bridged bimetallic lanthanide complexes.[121] Likewise, the conditions for Ising-type exchange interactions in lanthanide systems have been established.[235] The double exchange interaction, however, has so far not been addressed even in the limit of weak SOC. In molecular lanthanide systems, spin-dependent delocalization involving trivalent lanthanide ions has never been observed; therefore, there has not been a dire need for a pseudospin Hamiltonian model. Highly delocalized unpaired electrons have, however, been well-characterized in endohedral metallofullerenes (EMFs),[726–728] where lanthanide dimers $[Ln_2]^{5+}$ (Ln = La, Gd, Lu) are isolated in fullerene[729] or aza-fullerene[730–732] cages. The steric protection and the high electron affinity of the cages can stabilize lanthanide dimers with strong positive charge. The dimer can be thought of as consisting of two trivalent lanthanide ions with one "extra" electron resonating between the ions. DFT calculations have shown that this electron is highly delocalized over the two ions,[733,734] and interactions between lanthanide ions arising from the delocalization have been described as a one-electron covalent metal–metal bond.[735,736]

The experimental and theoretical studies on bilanthanide EMFs have so far mostly focused on the lanthanide ions, which are either diamagnetic or isotropic in their trivalent oxidation states. Very recently, Popov and co-workers experimentally characterized a bidysprosium EMF $Dy_2@C_{80}(CH_2Ph)$ (Figure 4b), which is a SMM with a blocking temperature of 18 K.[117] The paper also includes a rudimentary theoretical analysis. By the time Popov's paper was published, the research included in this dissertation was already in its final stage, and there was no time left to analyze the $Dy_2@C_{80}(CH_2Ph)$ EMF. However, Paper **VIII** included

in this thesis, analyzes the strongly anisotropic spin-dependent delocalization in the excited states of two experimentally characterized EMFs $[Gd_2@C_{78}]^-$ (**18**) and $[Gd_2@C_{80}]^-$ (**19**).[a] The focus in Paper **VIII** is on the anisotropy of the delocalized electron, whereas the anisotropy in $Dy_2@C_{80}(CH_2Ph)$ originates from the 4f electrons of the Dy ions. The consolidation of the concept of spin dependent delocalization and the 4f anisotropy into a single pseudospin Hamiltonian model is currently underway by the author of the present work but will not be discussed here. The work presented in Paper **VIII** forms an important foundation for the development of models to understand the anisotropy in more complicated systems.

Although Paper **VIII** discussed the anisotropic spin-dependent delocalization in the context of the EMFs **18** and **19**, the theory is not specific to these systems and can, if certain assumptions are valid, be applied to other systems as well. The fullerene cages in **18** and **19** can be considered as microscopic laboratories, which allow one to study the properties of the simple $[Gd_2]^{5+}$ dimers. We will first discuss the general features of the electronic structures and the ground state magnetic properties of **18** and **19** and then proceed to describe the anisotropic exchange in the excited states.

8.1 Computational details

The EMFs **18** and **19** have only been characterized in frozen solution; thus, no crystal structure geometry is available. The geometries were optimized at DFT level using the PBE0 hybrid XC functional in a non-relativistic framework. An ECP53MWB ECP[737,738] with a core-polarized valence part corresponding to a [311111/31111/21111/111/11] contraction[739,740] was used for the Gd ions. This basis includes the 4f electrons in the ECP definition; hence, the calculations can be carried out as if for a closed-shell system. Ahlrichs' older TZVP basis[621] was used for the carbon atoms in the geometry optimizations. All further DFT calculations were carried out in a scalar relativistic framework using the ZORA Hamiltonian as implemented in Orca.[392] The triple-ζ double-polarized SARC-ZORA-TZVPP basis[627] was used for the Gd ions, and the polarized double-ζ basis ZORA-def2-SVP[624] was used for the carbon atoms. Energies of higher-lying states were calculated using the DFT/ROCIS (DFT restricted open-shell CI singles) method.[617–619] The hybrid PBE0 XC functional was used along with the default set of parameters for the scaling of the CI matrix elements. The CI matrix was constructed by generating all single excitations from the SOMOs into all virtual orbitals up to 5.0 Hartree energy units considering the reference state multiplicity

[a] The experimental data has not yet been published and is based on personal correspondence with prof. T. Kato (Kyoto University). The characterization has been discussed in a conference abstract by T. Yamaguchi, N. Nakatori, T. Mitani, K. Kikuchi, T. Kodama, K. Furukawa, and T. Kato presented at *The 50th Fullerenes- Nanotubes- Graphene General Symposium* in 2016.

and the multiplicities which differ from the reference state by ± 1. The 200 lowest roots were solved. SOC was introduced by mixing the DFT/ROCIS solutions using the QDPT formalism and the SOMF operator. All DFT calculations were carried out with the ORCA code.[251,252] Version 3.0.2 was used for the geometry optimizations, version 4.0.0 for the DFT/ROCIS calculations, and version 3.0.3 for all other DFT calculations.

In order to extract effective single-ion parameters used in the construction of the model Hamiltonians, multireference *ab initio* calculations at CASSCF/XMS-CASPT2 level were carried out on a free Gd(II) ion. The calculations utilized the ANO-RCC-VQZP basis,[699] and scalar relativistic effects were introduced using the X2C approach. An (8,12) active space consisting of the seven 4f orbitals and the five 5d orbitals was used. In two SA-CASSCF calculations, one for each multiplicity, five roots with $S = 4$ and another five roots with $S = 3$ corresponding to the ^9D and ^7D terms arising from the $4f^7 5d^1$ configuration of the Gd(II) ion were solved. The XMS-CASPT2 corrections were only calculated for the CASSCF energies and no mixing of states by the electron correlation outside the active space was considered. SOC was introduced using the SO-RASSI methodology and the AMFI operator.

8.2 Electronic structures of $[Gd_2@C_{78}]^-$ and $[Gd_2@C_{80}]^-$

The optimized structures of **18** and **19** are illustrated in Figure 18a. **18** retains the D_{3h} symmetry of an elongated C_{78}-$D_{3h}(5)$ fullerene cage, whereas in **19**, the I_h symmetry of the C_{80}-I_h cage is lowered to an approximate D_{2h} symmetry. The Gd–Gd distances in **18** and **19** are 408.8 pm and 387.4 pm, respectively. Experimental EPR measurements show that both systems have a $S = {}^{15}/_2$ ground state, where all fifteen unpaired electrons are coupled to a FM configuration. The $(2S + 1)$-fold degeneracy is weakly split by SOC.

The electronic structures of **18** and **19** were studied by DFT calculations. To separate the effects of the electronic structure, which can be associated purely to the $[Gd_2]^{5+}$ dimers from those arising from the interaction with the cage, the calculations were also carried out on simple dimers **18'** and **19'**, which consist only of two Gd ions assigned with a $+5$ charge and fixed at the same distance as in the respective caged structures. The KS orbitals calculated for **18**, **19**, **18'**, and **19'** show that fourteen of the fifteen unpaired electrons in the ground $S = {}^{15}/_2$ spin state occupy combinations of the Gd 4f orbitals. The one resonating electron occupies a σ-type orbital, which is delocalized over both ions and has large amplitude in the Gd–Gd bonding region. The σ orbital consist mainly of the Gd $5d_{z^2}$, 6s, and $6p_z$ atomic orbitals. The lowest virtual 5d orbital combinations in **18** and **19** are extremely diffuse and strongly mix with the cage orbitals. In the simple dimers **18'** and **19'**, however, the virtual 5d orbital combinations can be easily identified, and they are illustrated in Figure 18b. It is easy to see that the virtual orbitals represent bonding and anti-bonding π- and δ-symmetric

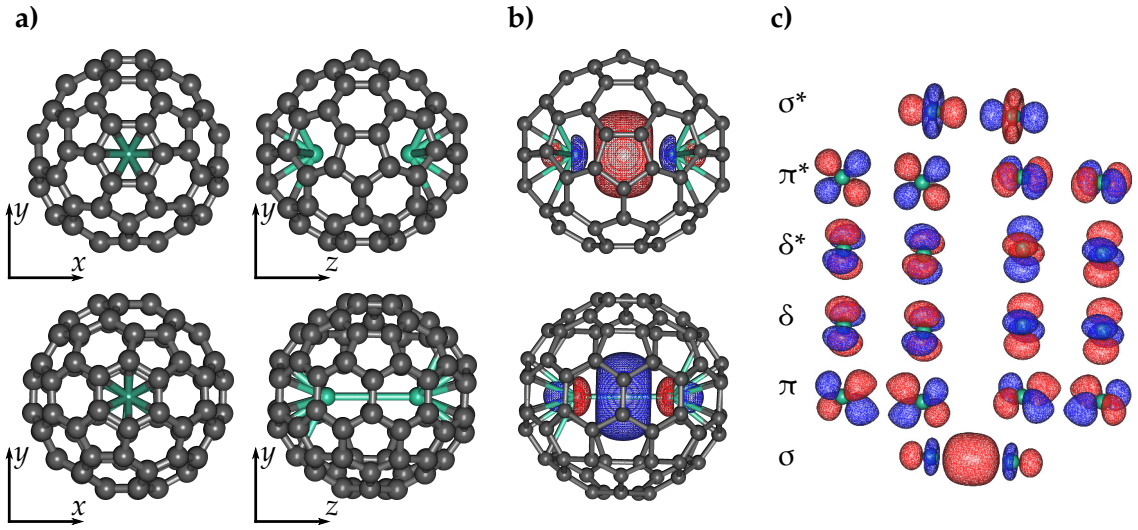

FIGURE 18 **a)** The optimized geometries of **18** and **19**, **b)** the σ-symmetric bonding orbitals in **18** and **19**, and **c)** the 5d orbital combinations in **18'**. The orbital combinations in **19'** are very similar.

combination of the 5d orbitals and the anti-bonding σ type combination. Unlike the occupied σ-type orbital, the virtual orbitals are very weakly mixed with s, p, or other orbitals and retain their 5d-like character. To keep the notation simple, we will refer to both the σ-type orbital and the actual virtual 5d orbital combinations as 5d orbital combinations.

The relative energies of configurations, where the σ electron is promoted to one of the virtual 5d combinations, was examined by DFT/ROCIS calculations, and the results are listed in Table 10. The calculations were carried out both for the full caged systems and for the dimers. The nature of the excitations was determined by visual examination of the natural transition orbitals. In the case of the caged systems **18** and **19**, only the lowest two excitations could be assigned to 5d→5d transitions. The higher energy excitations become energetically intertwined with various 5d→cage and cage→cage excitations. In case of the dimers **18'** and **19'**, all 5d→5d excitations could be identified and the lowest excitation energies match the excitation energies calculated for the caged systems reasonably well. The main difference between the caged systems and the dimers is that the π- and δ-symmetric orbitals are exactly degenerate by symmetry in the dimers. The D_{3h} symmetry of **18** should be able to enforce the degeneracy as well and the two calculated $\sigma \rightarrow \pi$ excitations of **18** have almost the same energies. The small deviation results most likely from the fact that the symmetry was not explicitly enforced on the wave function and from numerical inaccuracies. In **19**, the pseudo-D_{2h} symmetry should not retain any degeneracies and an energy difference of 1576 cm^{-1} is observed between the two $\sigma \rightarrow \pi$ excitations. The excitation energies calculated for the dimers **18'** and **19'** were used as approximations to the respective excitation energies of **18** and **19** in the subsequent analysis.

TABLE 10 5d→5d excitation energies (in cm^{-1}) calculated for **18**, **19**, **18′**, and **19′** using the DFT/ROCIS method

Excitation	**18**	**19**	**18′**	**19′**
$\sigma \rightarrow \pi$	23293.2	21334.8	19357.2	21237.8
$\sigma \rightarrow \pi$	23331.5	22910.9	19357.2	21237.8
$\sigma \rightarrow \delta$			23630.4	26894.6
$\sigma \rightarrow \delta$			23630.5	26894.7
$\sigma \rightarrow \delta^*$			24177.2	27733.9
$\sigma \rightarrow \delta^*$			24177.3	27734.0
$\sigma \rightarrow \pi^*$			24577.2	28532.7
$\sigma \rightarrow \pi^*$			24577.2	28532.7
$\sigma \rightarrow \sigma^*$			25115.8	29441.0

8.3 Spin Hamiltonian description

8.3.1 Exchange interaction in Σ states

The ground states of **18** and **19** do not have any first-order angular momentum and give rise to Σ terms. Here, we are using the same labeling of electronic states as is used in linear molecules.[741] In the case of the 5d orbitals of **18**, this does not introduce any approximations as the Σ, Π, and Δ representations of the $D_{\infty h}$ group have direct correspondence with the A, E', and E'' representations of the D_{3h} group.[245] In the case of **19**, this is an approximation as the Π and Δ representations do not directly correspond to any irreducible representation of the D_{2h} group. The ground configuration where the 5d electron occupies the bonding σ orbital gives rise to a Σ_g term, and the configuration where the electron occupies the σ^* orbital gives rise to a Σ_u term. The strong electron delocalization, referred to as transfer interaction or resonance, strongly splits these two terms, leaving the Σ_g term as an energetically well-separated ground state term. The exchange interaction between the σ electron and the 4f electrons in the two Gd ions further splits the Σ_g into a manifold of different exchange states. Due to the strong delocalization of the σ electron, the Hund's rule coupling between the σ and 4f electrons is weak compared to the effects of electron transfer. This is the opposite case to what is encountered in conventional double exchange, where the exchange splitting is stronger than the splitting of terms due to the transfer interaction. Thus, the system is better described as a three-site spin system where one of the sites is formed by the σ electron, which is resonating between the two ions, and the other two sites are formed by the Gd 4f spins. We only need to consider the case where all seven 4f electrons at each site have the same spin as any non-Hund state is much higher in energy. This model is described by the HDvV-type Hamiltonian

$$\hat{H}_{\mathrm{HDvV}} = -J_{\mathrm{4f-4f}}\hat{\mathbf{S}}_{0,a} \cdot \hat{\mathbf{S}}_{0,b} - J_{\mathrm{4f}-\sigma}\left(\hat{\mathbf{s}} \cdot \hat{\mathbf{S}}_{0,a} + \hat{\mathbf{s}} \cdot \hat{\mathbf{S}}_{0,b}\right), \tag{222}$$

where $\hat{\mathbf{S}}_{0,a}$ and $\hat{\mathbf{S}}_{0,b}$ operate on the total 4f spins $S_a = S_b = 7/2$ at Gd ions a and b, $\hat{\mathbf{s}}$ operates on the σ electron, and $J_{\mathrm{4f-4f}}$ and $J_{\mathrm{4f}-\sigma}$ are the exchange coupling

constants.

The values of the exchange coupling constants were determined from BS DFT calculations. Since the sites a and b are equivalent by symmetry, three BS DFT states with unique energies can be constructed: $|\alpha\alpha\alpha\rangle$, $|\alpha\beta\alpha\rangle$, and $|\alpha\alpha\beta\rangle$, where the first index is site a, second is the σ electron, and third is site b. Following the usual procedure of interpreting the states as Ising states, the exchange coupling constants can be extracted as

$$J_{4f-4f} = \frac{1}{49}\left(2E_{\alpha\alpha\beta} - E_{\alpha\beta\alpha} - E_{\alpha\alpha\alpha}\right) \quad \text{and} \quad J_{4f-\sigma} = \frac{1}{7}\left(E_{\alpha\beta\alpha} - E_{\alpha\alpha\alpha}\right). \tag{223}$$

The values were calculated for **18'**, **19**, and **19'**. The calculations on the $|\alpha\alpha\beta\rangle$ state of **18** faced considerable convergence difficulties. However, the exchange coupling constants calculated for **19** and **19'** are very similar especially when considering the typical errors in BS DFT calculations; therefore, the exchange coupling constants calculated for **18'** were taken as a reasonable approximation to those of **18**. The obtained values are $J_{4f-4f} = -1.3\,\mathrm{cm}^{-1}$ and $J_{4f-\sigma} = 354\,\mathrm{cm}^{-1}$ for **18** and $J_{4f-4f} = -2.9\,\mathrm{cm}^{-1}$ and $J_{4f-\sigma} = 390\,\mathrm{cm}^{-1}$ for **19**. Thus, the direct exchange between the 4f spins of the two Gd ions is very weak and AFM, and the exchange coupling between the 4f spins and the σ electron is strongly FM. This should be expected, as the latter exchange originates from the Hund's rule coupling, which is always FM. Considering usual values of Hund's rule coupling, the values obtained for $J_{4f-\sigma}$ are fairly weak. This most likely owes to the strong delocalization of the σ electron compared to the respective atomic situation.

The experimental EPR measurements showed weak ZFS of the ground $S = {}^{15}/_{2}$ multiplet with ZFS parameters $D = 0.0498\,\mathrm{cm}^{-1}$ and $E = 0.00023\,\mathrm{cm}^{-1}$ for **18** and $D = 0.0339\,\mathrm{cm}^{-1}$ and $E = 0.0102\,\mathrm{cm}^{-1}$ for **19**. The values are extremely small; thus, evaluating them quantitatively using any DFT or *ab initio* multireference method is next to impossible. Therefore, the main goal was to correctly reproduce the sign of the D parameter. All common DFT-based methods for the evaluation of ZFS parameters failed to achieve this. Physically meaningful multireference calculation of the parameters was not possible, as the ZFS originates from the mixing of high-lying multiplet states into the ground multiplet under SOC and these states cannot be reduced to the set of states generated within some reasonably sized active space. The signs were ultimately reproduced correctly when the ZFS parameters where extracted from the DFT/ROCIS results. A numerical effective Hamiltonian in a model space of $\{|\tilde{S}\tilde{M}_S\rangle\}$ states, where $\tilde{S} = S$, was constructed from the DFT/ROCIS eigenvalues and eigenvectors using equation (57). Norms of the projections of the *ab initio* states on the states in the model space are ~ 1, and the resulting Hamiltonian is practically Hermitian. The CF Hamiltonian was then constructed as in equation (62) using the substitution $\hat{\mathbf{J}} \to \tilde{\mathbf{S}}$. The CF parameters enter the matrix elements in a linear fashion, and they were solved by a least-squares fit between the analytical expressions and the numerical values. The $\mathbf{D}$ matrix was then constructed from the rank $k = 2$ CF parameters using expressions obtained from the relationship between spherical

and Cartesian spherical harmonics:[97]

$$D_{xx} = -\frac{2}{105}\sqrt{\frac{3}{2}}\mathrm{Re}(B_{22}), \qquad D_{xy} = D_{yx} = -\frac{2}{105}\sqrt{\frac{3}{2}}\mathrm{Im}(B_{22}), \tag{224}$$

$$D_{yy} = \frac{2}{105}\sqrt{\frac{3}{2}}\mathrm{Re}(B_{22}), \qquad D_{zx} = D_{xz} = \frac{2}{105}\sqrt{\frac{3}{2}}\mathrm{Re}(B_{21}), \tag{225}$$

$$D_{zz} = \frac{3}{105}B_{20}, \qquad D_{zy} = D_{yz} = \frac{2}{105}\sqrt{\frac{3}{2}}\mathrm{Im}(B_{21}). \tag{226}$$

The **D** matrix was finally diagonalized, and the D and E parameters were obtained with equation (68). The values are $D = 0.297\,\mathrm{cm}^{-1}$ and $E = 0.000\,\mathrm{cm}^{-1}$ for **18** and $D = 0.375\,\mathrm{cm}^{-1}$ and $E = 0.000\,\mathrm{cm}^{-1}$ for **19**. The digits beyond the third decimal cannot be reliably distinguished from numerical noise. The calculated parameters are still an order of magnitude off, but do correctly reproduce the sign of the D parameter; and, as noted above, when considering the extremely small energy differences involved, the results are very reasonable.

8.3.2 Exchange interaction in Π and Δ states

The general model Hamiltonian describing the most relevant physical interactions in the states arising from the Π and Δ terms of **18** and **19** in the presence of first-order angular momentum is

$$\hat{H}_{\mathrm{model}} = \hat{H}^a_{\mathrm{SOC}} + \hat{H}^a_{\mathrm{Hund}} + \hat{H}^b_{\mathrm{SOC}} + \hat{H}^b_{\mathrm{Hund}} + \hat{H}^{ab}_{\mathrm{transfer}}, \tag{227}$$

which describes the SOC, Hund's rule coupling, and transfer interaction. The superscripts indicate operators that act on sites a or b, and the last term acts on both sites. We have assumed that mixing between the Σ, Π, and Δ manifolds is negligible (see the Paper **VIII** for more detailed discussion on this assumption); therefore, the Hamiltonian (227) acts in a space of Π or Δ CF doublets, which have double degeneracy due to the spatial symmetry. Under these assumptions, (227) conserves the projections of the total angular momentum M_J, the orbital angular momentum m_l, and the total spin angular momentum M_S. The explicit forms of the SOC and Hund's rule coupling operators are

$$\hat{H}^i_{\mathrm{SOC}} = \zeta\hat{\mathbf{l}}\cdot\hat{\mathbf{s}} \tag{228}$$

$$\hat{H}^i_{\mathrm{Hund}} = -J_{\mathrm{H}}\hat{\mathbf{s}}\cdot\hat{\mathbf{S}}_{0,i}, \tag{229}$$

where $i \in a, b$, ζ is the Gd(III) 5d orbital SOC constant, $\hat{\mathbf{l}}$ is an orbital angular momentum operator acting on the 5d orbital, and J_{H} is the Hund's rule coupling constant. The transfer operator is given as

$$\hat{H}^{ab}_{\mathrm{transfer}} = \sum_{m_l,m_s} t_{m_l}\left(\hat{a}^\dagger_{m_l,m_s}\hat{b}_{m_l,m_s} + \hat{b}^\dagger_{m_l,m_s}\hat{a}_{m_l,m_s}\right), \tag{230}$$

where $\hat{a}^\dagger_{m_l,m_s}$ ($\hat{a}_{m_l,m_s}$) creates (annihilates) an electron with spin projection m_s into an orbital with angular momentum projection m_l at ion a, and $\hat{b}_{m_l,m_s}$ and $\hat{b}^\dagger_{m_l,m_s}$

act accordingly at ion b. t_{m_l} is a transfer parameter between orbitals with orbital angular momentum m_l at the two sites. Under the D_{3h} symmetry, the transfer parameters between orbitals of different symmetry are zero, whereas $t_{m_l} = t_{-m_l}$.

In the absence of the transfer interaction and assuming that the resonating electron is localized at site a, the eigenvalues of the one-site Hamiltonian $\hat{H}^a_{\mathrm{SOC}} + \hat{H}^a_{\mathrm{Hund}}$ are given as

$$\begin{aligned} &E^a_{\pm}(J_{\mathrm{H}}, \zeta; S_{0,a}, M_K, m_l) \\ &\quad = \frac{1}{2}J_{\mathrm{H}} \pm \frac{1}{2}\sqrt{J^2_{\mathrm{H}}s^2(2S_{0,a}+1)^2 - 8J_{\mathrm{H}}\zeta m_l s^2 M_K + \zeta^2 m_l^2 \frac{16s^2(S_{0,a}+s)}{(2S_{0,a}+1)^2}}, \end{aligned} \tag{231}$$

where $K = S_{0,a} \pm s$ is the total one-site spin. At the limit of $J_{\mathrm{H}} \to \infty$ equation (231) reduces to

$$E^a_{J_{\mathrm{H}}\to\infty}(\zeta; M_K, m_l) = \pm\frac{2\zeta m_l s M_K}{2S_{0,a}+1}. \tag{232}$$

The transfer interaction mixes the states where the resonating electron is located at any given site to produce fully delocalized eigenstates. Unfortunately, the resulting matrix is too large for the characteristic polynomial to have analytic solutions, and the full Hamiltonian (227) can only be diagonalized numerically. If the transfer interaction is introduced as a first order perturbation correction to (232), one obtains

$$E_{\pm}(t; K, M_K, M_0, m_l) = \begin{cases} \dfrac{2\zeta m_l s M_K \pm t\,(K+M_K)}{2S_0+1} & \text{if} \quad M_0 = M_K - s \\ \dfrac{2\zeta m_l s M_K \pm t\,(K-M_K)}{2S_0+1} & \text{if} \quad M_0 = M_K + s \\ \dfrac{2\zeta m_l s M_K}{2S_0+1} & \text{else,} \end{cases} \tag{233}$$

where we have assumed $S_{0,a} = S_{0,b} \equiv S_0$. The approximate eigenvalues (233) become the exact eigenvalues of (227) at the limit $t \ll \zeta$ and $J_{\mathrm{H}} \to \infty$. It is interesting to note that the eigenvalues depend on both the total one-site spin K and its projection M_K. This Ising-type dependence on the projection introduces an anisotropy into the energy spectrum. This is in stark contrast to the conventional double-exchange case described in equation (88), where the eigenvalues only depend on the total spin quantum numbers.[24] Furthermore, the dependence on M_K emerges from both the SOC term and the transfer term in the Hamiltonian. This then implies that the anisotropy can be chemically enhanced both by enhancing the single-ion anisotropy and also by tuning the transfer interaction.

8.4 Numerical results

In order to evaluate the energy spectrum of the states in the Π and Δ manifolds, we first need to evaluate the values of the parameters ζ, J_{H}, and $\{t_{m_l}\}$. The

TABLE 11 Energies (in cm^{-1}) of the spin-orbit coupled states arising from the $4f^7 5d^1$ configuration of a free Gd(II) ion as analytical expressions obtained by a diagonalization of a model Hamiltonian, and as numerical values obtained by fitting the exact expressions to *ab initio* values as well as the *ab initio* calculated and experimental values

State	Analytical expression	Model	*Ab initio*	Exp.[742]
$^9D_2$	$\frac{1}{8}\left(-13J_H - 2\zeta - 2\sqrt{64{J_H}^2 + 64J_H\zeta + 25\zeta^2}\right)$	0	0	0
$^9D_3$	$\frac{1}{8}\left(-13J_H - 2\zeta - 2\sqrt{64{J_H}^2 + 40J_H\zeta + 25\zeta^2}\right)$	298	317	279
$^9D_4$	$\frac{1}{8}\left(-13J_H - 2\zeta - 2\sqrt{64{J_H}^2 + 8J_H\zeta + 25\zeta^2}\right)$	758	775	694
$^9D_5$	$\frac{1}{8}\left(-13J_H - 2\zeta - 2\sqrt{64{J_H}^2 - 32J_H\zeta + 25\zeta^2}\right)$	1464	1425	1310
$^9D_6$	$\frac{1}{8}(-29J_H + 8\zeta)$	2617	2393	2283
$^7D_5$	$\frac{1}{8}\left(-13J_H - 2\zeta + 2\sqrt{64{J_H}^2 - 32J_H\zeta + 25\zeta^2}\right)$	9404	9045	9356
$^7D_4$	$\frac{1}{8}\left(-13J_H - 2\zeta + 2\sqrt{64{J_H}^2 + 8J_H\zeta + 25\zeta^2}\right)$	9869	9695	9718
$^7D_3$	$\frac{1}{8}\left(-13J_H - 2\zeta + 2\sqrt{64{J_H}^2 + 40J_H\zeta + 25\zeta^2}\right)$	10137	10153	10015
$^7D_2$	$\frac{1}{8}\left(-13J_H - 2\zeta + 2\sqrt{64{J_H}^2 + 64J_H\zeta + 25\zeta^2}\right)$	10264	10470	10234
$^7D_1$	$\frac{1}{8}(3J + 8\zeta)$	10372	10672	10387

SOC and Hund's rule coupling constants are single-ion properties and can, therefore, be evaluated from a calculation on a single Gd(II) ion. The parameters can be extracted by fitting the eigenvalue spectrum of $\hat{H}_{SOC} + \hat{H}_{Hund}$ to the eigenvalues calculated at CASSCF/XMS-CASPT2 level. This procedure yielded values $\zeta = 1038\,cm^{-1}$ and $J_H = 2070\,cm^{-1}$. The energy spectrum of the Gd(II) states arising from the $4f^7 5d^1$ configuration as obtained directly from the *ab initio* calculations and as calculated using the obtained parameters along with the experimental values[742] is listed in Table 11. The values are in good agreement with the experiment. The exact expressions given in Table 11 have been derived in the supplementary material of Paper **VIII**.

The transfer parameters where obtained from DFT calculations by utilizing the one-to-one correspondence between the matrix elements of the KS Fock operator (the operator on the left-hand side of equation (186)) and that of a tight-binding Hamiltonian

$$\hat{H}_{tb} = \sum_{p,q}\sum_{\sigma} t_{pq}\left(\hat{a}^\dagger_{p\sigma}\hat{a}_{q\sigma} + \hat{a}^\dagger_{q\sigma}\hat{a}_{p\sigma}\right) \tag{234}$$

when expressed in a basis of localized atomic-like orbitals. Thus, the KS orbitals of interest (the 4f and 5d combinations) were localized to their respective Gd ions to give Wannier-type orbitals, which still retain their polarization and hybridization due to the environment. The KS Fock matrix was then transformed into this basis. Comparison of the matrix elements of the KS Fock operator and (234) allows

one to identify the off-diagonal elements as the transfer parameters $\{t_{m_l}\}$. The extraction was done on calculations carried out on the simple dimers **18'** and **19'**. Some care must be taken because in a hybrid DFT calculation, the occupied and virtual orbitals do not experience the same potential and a localization procedure, which mixes the occupied and virtual blocks of the KS Fock operator, introduces spurious contributions to the transfer parameters. However, in the actual calculations only parameters obtained from the virtual block of the KS Fock matrix were used. The t_σ parameter was obtained from the $\sigma \rightarrow \sigma^*$ excitation energy, and the explicit value was never used in the actual calculations. The values are $t_\sigma = 12557\,\mathrm{cm}^{-1}$, $t_\pi = 2610\,\mathrm{cm}^{-1}$, and $t_\delta = 273\,\mathrm{cm}^{-1}$ for **18'** and $t_\sigma = 14721\,\mathrm{cm}^{-1}$, $t_\pi = 3648\,\mathrm{cm}^{-1}$, and $t_\delta = 420\,\mathrm{cm}^{-1}$ for **19'**.

The obtained parameters were used in construction of the matrix elements of the Hamiltonian (227). A basis consisting of the states $\{|S_{0,a}sKM_K\rangle \otimes |a, lm_l\rangle \otimes |S_{0,b}M_{0,b}\rangle, |S_{0,a}M_{0,a}\rangle \otimes |b, lm_l\rangle \otimes |S_{0,a}sKM_K\rangle\}$ was used. $|S_{0,a}sKM_K\rangle$ describes the spin state of site a when the resonating electron is localized at it, and $|S_{0,b}M_{0,b}\rangle$ describes site b in the absence of the resonating electron. $|S_{0,a}M_{0,a}\rangle$ and $|S_{0,a}sKM_K\rangle$ represent the opposite situation. $|a, lm_l\rangle$ and $|b, lm_l\rangle$ describe the orbital state of the resonating electron when it is localized at site a and b, respectively. The operators $\hat{H}^a_{\mathrm{SOC}}$, $\hat{H}^a_{\mathrm{Hund}}$, $\hat{H}^b_{\mathrm{SOC}}$, and $\hat{H}^b_{\mathrm{Hund}}$ only couple basis states where the resonating electron is localized at the same site, and $\hat{H}^{ab}_{\mathrm{transfer}}$ only has non-zero matrix elements between states where the electron is localized at different sites. The matrix elements of the operators are given as (see the supplementary material of Paper **VIII** for full derivations):

$$\begin{aligned}
&\langle S_{0,a}sKM_K| \otimes \langle a, lm_l| \otimes \langle S_{0,b}M_{0,b}|\hat{H}_{\mathrm{SOC}}|S_{0,a}sK'M'_K\rangle \otimes |a, lm'_l\rangle \otimes |S_{0,b}M'_{0,b}\rangle \\
&\qquad = \delta_{m_l m'_l}\delta_{M_{0,b}M'_{0,b}}\zeta m_l \sum_{M_{0,a}, m_s} m_s C^{KM_K}_{S_{0,a}M_{0,a}, sm_s} C^{K'M'_K}_{S_{0,a}M_{0,a}, sm_s} \qquad (235)\\
&\langle S_{0,a}M_{0,a}| \otimes \langle b, lm_l| \otimes \langle S_{0,a}sKM_K|\hat{H}_{\mathrm{SOC}}|S_{0,a}M'_{0,a}\rangle \otimes |b, lm'_l\rangle \otimes |S_{0,a}sK'M'_K\rangle \\
&\qquad = \delta_{m_l m'_l}\delta_{M_{0,a}M'_{0,a}}\zeta m_l \sum_{M_{0,b}, m_s} m_s C^{KM_K}_{sm_s, S_{0,b}M_{0,b}} C^{K'M'_K}_{sm_s, S_{0,b}M_{0,b}} \qquad (236)
\end{aligned}$$

$$\begin{aligned}
&\langle S_{0,a}sKM_K| \otimes \langle a, lm_l| \otimes \langle S_{0,b}M_{0,b}|\hat{H}_{\mathrm{Hund}}|S_{0,a}sK'M'_K\rangle \otimes |a, lm'_l\rangle \otimes |S_{0,b}M'_{0,b}\rangle \\
&\qquad = -\frac{J}{2}\left[K(K+1) - S_{0,a}(S_{0,a}+1) - s(s+1)\right]\delta_{KK'}\delta_{M_K M'_K}\delta_{m_l m'_l}\delta_{M_{0,b}M'_{0,b}} \qquad (237)\\
&\langle S_{0,a}M_{0,a}| \otimes \langle b, lm_l| \otimes \langle S_{0,a}sKM_K|\hat{H}_{\mathrm{Hund}}|S_{0,a}M'_{0,a}\rangle \otimes |b, lm'_l\rangle \otimes |S_{0,a}sK'M'_K\rangle \\
&\qquad = -\frac{J}{2}\left[K(K+1) - S_{0,b}(S_{0,b}+1) - s(s+1)\right]\delta_{KK'}\delta_{M_K M'_K}\delta_{m_l m'_l}\delta_{M_{0,a}M'_{0,a}} \qquad (238)
\end{aligned}$$

$$\begin{aligned}
&\langle S_{0,a}sKM_K| \otimes \langle a, lm_l| \otimes \langle S_{0,b}M_{0,b}|\hat{H}^{ab}_{\mathrm{transfer}}|S_{0,a}M'_{0,a}\rangle \otimes |b, lm'_l\rangle \otimes |S_{0,a}sK'M'_K\rangle \\
&\qquad = \delta_{m_l m'_l} t_{m_l} \sum_{m_s} C^{KM_K}_{S_{0,a}M'_{0,a}, sm_s} C^{K'M'_K}_{sm_s, S_{0,b}M_{0,b}}, \qquad (239)
\end{aligned}$$

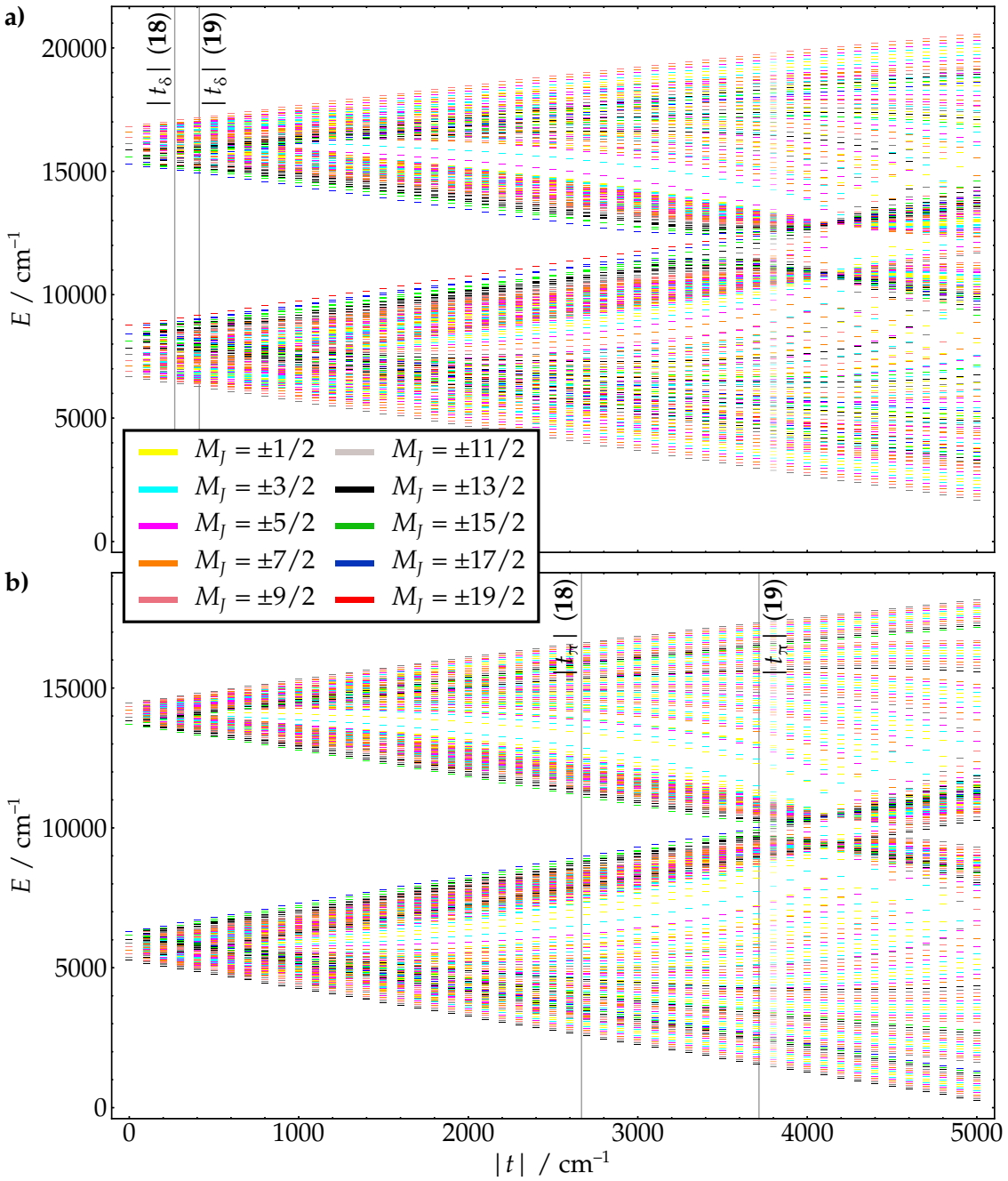

FIGURE 19 Splitting of the **a)** Δ and **b)** Π terms under the influence of SOC, Hund's rule coupling, and electron transfer. The colors of the energy levels correspond to a specific projection of the total angular momentum, and the vertical lines indicate the calculated values of the transfer parameters. The energy scale of **18** is used on the vertical axis. In **19**, all the energy levels are translated to a slightly higher energy due to the stronger CF.

where the expansion coefficients are CG coefficients. Once the matrix elements had been constructed, the Hamiltonian was numerically diagonalized. The energy spectrum originating from the Π and Δ terms of **18** as a function of the respective transfer parameter magnitude $|t|$ is given in Figure 19.

The energy spectrum shows that the states arising from the Π and Δ terms become energetically mixed even at relatively small values of $|t|$. The two manifolds at small $|t|$ arise from the states where the resonating electron is coupled into the 4f spins ferromagnetically (lower manifold) and anti-ferromagnetically (higher manifold). In the range $|t| \lesssim 2500\,\mathrm{cm}^{-1}$, these two manifolds are clearly separated from each other. The splitting within each manifold into bonding and anti-bonding states is also observable from the density of states, which is highest near the top and the bottom of the respective manifold. For larger values of $|t|$, the interaction starts to resemble that of a covalently bound system. At this limit, the states in the two manifolds with the same values of M_J become strongly mixed, and any division into some clear manifolds is lost. In the absence of SOC, the left-hand side of Figure 19 would describe the "classic" double-exchange situation (transfer interaction is much weaker than exchange interaction), whereas the right-hand side describes a one-electron covalent bond (transfer interaction dominates). Considering the transfer parameters calculated for **18** and **19** (the vertical lines in Figure 19), the states arising from the Δ terms clearly fall into the double-exchange region, whereas the states arising from the Π terms are better described as quasi-covalent states.

9 CONCLUSIONS

The overall goal of the present work has been to apply state-of-the-art computational and theoretical methods to the research conducted in the field of molecular magnetism. The discussion presented here has heavily emphasized the quantum chemical and theoretical aspects of the research. The actual work carried out in most of the papers included in this dissertation is highly multidisciplinary and in addition to the work of theoreticians, involves large, in many cases major, contributions from synthetic chemists and magnetochemists.

The work described in papers **I**, **II**, and **III** focuses on the synthesis and characterization of different exchange coupled systems. Theoretical calculations have been used to analyze the various radical–radical, metal–radical, and metal–metal exchange interactions and the weak anisotropy in the complexes characterized in Paper **I**. In all cases, it is possible to extract more parameters from the theoretical calculations than it is from fits to experimentally measured data. This allows construction of more complicated models, which better represent the macroscopic magnetic properties. In Paper **II**, the radical–radical exchange interactions between complexes **6** could only be analyzed by means of BS DFT calculations, as the strong SOC of the Dy(III) ion made such analysis based on experimental data impossible. In Paper **III**, it was shown that the simple model used to fit the experimental data is insufficient to fully describe all of the interactions taking place in the system; all necessary parameters could only be extracted from the quantum chemical calculations.

In Paper **IV** an approach to constructing organic radical systems with FM radical–radical interaction was introduced. It was shown through BS DFT calculations that by constructing radical dimers with mixed orbital symmetries, it is possible to enforce FM radical–radical interaction in these systems. It was further shown that the dimerization enthalpy of such systems can be favorable. The work presented in Paper **IV** focused on purely organic radicals, but the approach is equally applicable to organo-main-group radical systems and metal–radical complexes as long as the necessary symmetry conditions are realized.

The papers **V**, **VI**, and **VII** described the characterization and the magnetic properties mono- and bimetallic Dy(III) complexes. Theoretical calculations

offered insight into the electronic structure and the origins of the various experimentally observed phenomena or to the lack of such observations. The complexes **14** and **16** characterized in papers **V** and **VI**, respectively, represent the cutting edge of experimental research into monometallic SMMs, and **16** holds the current record for the highest magnetic blocking temperature observed in any SMM so far. The 60 K blocking temperature is over four times higher than the earlier record and approaches the temperature of liquid nitrogen.

Paper **VIII** is a purely theoretical contribution, where we discussed the interplay of spin-dependent delocalization and SOC in the ground and excited states of two experimentally characterized EMFs. The co-existence of strong electron delocalization and SOC in lanthanide systems leads to highly anisotropic energy spectrum, which is qualitatively different from what is observed in the case of the conventional double-exchange mechanism. The anisotropy depends both on the strength of the SOC and on the transfer interaction. This provides possibilities to tune the anisotropy of polymetallic lanthanide systems with strong electron delocalization and forms a solid foundation for further research.

Overall, the present work has contributed to field of molecular magnetism by providing in-depth analyses of the electronic structures and the chemical and structural factors that contribute to the magnetic properties of experimentally characterized systems. Furthermore, the present work has provided new directions to the synthesis of radical, transition metal, and lanthanide complexes, and has provided understanding of extremely complicated exchange mechanisms.

9.1 Outlook

In a closing section of this dissertation, we would like to briefly discuss the directions the computational and theoretical research in the field of molecular magnetism should be, in our opinion, taken based on the results of the present work.

i) In the case of monometallic SMMs, the chemical design criteria for obtaining high operational temperatures is generally well-understood at the molecular level. The blocking temperature ultimately depends on the interaction of the system with the low-energy phonons of the bulk material. Thus, the relaxation is a property of the material, not just the SMM. As mentioned earlier in this work, the *ab initio* study of the relaxation processes is still in its infancy, and much work is required to understand the nature of the spin–phonon interactions, the nature of the low-energy phonons in these systems, and the relationship between the chemical structure of the SMMs and the interaction with the lattice vibration.

ii) In the case of polymetallic SMMs, development is still required both in the computational methods and in the pseudospin Hamiltonian models. In case of the latter, focus should placed on generalizing the direct and

superexchange mechanism into the case when *LS* coupling is not valid and on further generalization of the double-exchange mechanism. Moreover, computational methods capable of treating two or more ions in an *ab initio* manner are required. The most promising approaches to this are DMRG in the case of multireference methods and relativistic two-component DFT in the case of BS DFT. In the absence of such methods, it would also be useful to further develop methods for the extraction of pseudospin Hamiltonian parameters from multireference *ab initio* and DFT calculations conducted on simplified or fragmented systems.

iii) Throughout the discussion in this dissertation, we have pointed out numerous shortcomings of the computational methods in the various projects. This highlights the importance of improving the computational methods that are already routinely used and, furthermore, the importance of understanding the nature and origin of these shortcomings so that the accuracy of obtained results can be assessed even when experimental reference is not available. Even if a method does not produce quantitative values, the results can still be extremely useful if the errors manifests themselves in a controlled and predictable manner. Future work should examine the nature of these errors in great detail and their relation to the more fundamental theories of wave-function-based quantum chemistry and DFT.

References

[1] W. Heitler, F. London. *Z. Phys.* **1927**, *44*, 455–472.

[2] E. Schrödinger. *Ann. Phys.* **1926**, *384*, 361–376.

[3] E. Schrödinger. *Ann. Phys.* **1926**, *384*, 489–527.

[4] E. Schrödinger. *Ann. Phys.* **1926**, *385*, 437–490.

[5] E. Schrödinger. *Ann. Phys.* **1926**, *386*, 109–139.

[6] E. Schrödinger. *Phys. Rev.* **1926**, *28*, 1049–1070.

[7] P. A. M. Dirac. *Proc. Royal Soc. A* **1926**, *112*, 661–677.

[8] P. A. M. Dirac. *Proc. Royal Soc. A* **1929**, *123*, 714–733.

[9] P. A. M. Dirac, *The Principles of Quantum Mechanics 3rd ed.*, Clarendon Press, Oxford, UK, **1948**.

[10] W. Heisenberg. *Z. Phys.* **1926**, *38*, 411–426.

[11] W. Heisenberg. *Z. Phys.* **1926**, *39*, 499–518.

[12] W. Heisenberg. *Z. Phys.* **1927**, *41*, 239–267.

[13] J. C. Slater. *Phys. Rev.* **1930**, *35*, 210–211.

[14] J. C. Slater, *Electronic Structure of Atoms and Molecules*, Tech. Rep. 3, Massachusets Institute of Technology, **1953**.

[15] W. Heisenberg. *Z. Phys.* **1928**, *49*, 619–636.

[16] J. D. Roberts, *Nuclear Magnetic Resonance. Applications Organic Chemistry*, McGraw–Hill, New York, NY, USA, **1959**.

[17] A. Abragam, *The Principles of Nuclear Magnetism*, Oxford University Press, Oxford, UK, **1961**.

[18] P. Pyykkö, *Theory of NMR parameters. From Ramsey to Relativity, 1953 to 1983* in *Calculation of NMR and EPR Parameters*, M. Kaupp, M. Bühl, V. G. Malkin (Eds.), Wiley-VHC, Weinheim, Germany, **2004**, pp. 7–19.

[19] B. Bleaney, K. W. H. Stevens. *Rep. Prog. Phys.* **1953**, *16*, 108.

[20] A. Abragam, B. Bleaney, *Electron Paramagnetic Resonance of Transition Ions*, of *International series of monographs on physics*, Clarendon Press, Oxford, UK, **1970**.

[21] F. Neese, M. L. Munzarová, *Historical Aspects of EPR Parameter Calculations* in *Calculation of NMR and EPR Parameters*, M. Kaupp, M. Bühl, V. G. Malkin (Eds.), Wiley-VHC, Weinheim, Germany, **2004**, pp. 21–32.

[22] R. L. Carlin, *Magnetochemistry*, Springer-Verlag, Berlin, Germany, **1986**.

[23] F. E. Mabbs, D. J. Machin, *Magnetism and Transition Metal Complexes*, Dover, Mineola, NY, USA, **1973**.

[24] O. Kahn, *Molecular Magnetism*, VHC, New York, NY, USA, **1993**.

[25] D. Gatteschi, R. Sessoli, J. Villain, *Molecular Nanomagnets*, Oxford University Press, Oxford, UK, **2006**.

[26] C. Benelli, D. Gatteschi, *Introduction to Molecular Magnetism. From Transition Metals to Lanthanides*, Wiley–VCH, Weinheim, Germany, **2015**.

[27] O. K. R. D. Willett, D. Gatleschi (Ed.), *Magneto-Structural Correlations in Exchange Coupled Systems*, Reidel, Dordrecht, The Neatherlands, **1985**.

[28] O. Kahn, J. Galy, Y. Journaux, J. Jaud, I. Morgenstern-Badarau. *J. Am. Chem. Soc.* **1982**, *104*, 2165–2176.

[29] A. Caneschi, D. Gatteschi, R. Sessoli, P. Rey. *Acc. Chem. Res.* **1989**, *22*, 392–398.

[30] J. S. Miller, J. C. Calabrese, H. Rommelmann, S. R. Chittipeddi, J. H. Zhang, W. M. Reiff, A. J. Epstein. *J. Am. Chem. Soc.* **1987**, *109*, 769–781.

[31] M. Tamura, Y. Nakazawa, D. Shiomi, K. Nozawa, Y. Hosokoshi, M. Ishikawa, M. Takahashi, M. Kinoshita. *Chem. Phys. Lett.* **1991**, *186*, 401–404.

[32] S. J. Blundell, F. L. Pratt. *J. Phys. Condens. Matter* **2004**, *16*, R771.

[33] C. Train, L. Norel, M. Baumgarten. *Coord. Chem. Rev.* **2009**, *253*, 2342–2351.

[34] J. S. Miller. *Chem. Soc. Rev.* **2011**, *40*, 3266–3296.

[35] I. Ratera, J. Veciana. *Chem. Soc. Rev.* **2012**, *41*, 303–349.

[36] A. J. Banister, N. Bricklebank, I. Lavender, J. M. Rawson, C. I. Gregory, B. K. Tanner, W. Clegg, M. R. J. Elsegood, F. Palacio. *Angew. Chem. Int. Ed.* **1996**, *35*, 2533–2535.

[37] S. M. Winter, R. T. Oakley, A. E. Kovalev, S. Hill. *Phys. Rev. B* **2012**, *85*, 094430.

[38] S. M. Winter, S. Hill, R. T. Oakley. *J. Am. Chem. Soc.* **2015**, *137*, 3720–3730.

[39] A. Mailman, S. M. Winter, J. W. L. Wong, C. M. Robertson, A. Assoud, P. A. Dube, R. T. Oakley. *J. Am. Chem. Soc.* **2015**, *137*, 1044–1047.

[40] R. Sessoli, H. L. Tsai, A. R. Schake, S. Wang, J. B. Vincent, K. Folting, D. Gatteschi, G. Christou, D. N. Hendrickson. *J. Am. Chem. Soc.* **1993**, *115*, 1804–1816.

[41] R. Sessoli, D. Gatteschi, A. Caneschi, M. A. Novak. *Nature* **1993**, *365*, 141–143.

[42] M. Mannini, F. Pineider, P. Sainctavit, C. Danieli, E. Otero, C. Sciancalepore, A. M. Talarico, M.-A. Arrio, A. Cornia, D. Gatteschi, R. Sessoli. *Nat. Mater.* **2009**, *8*, 194–197.

[43] K. V. Raman, A. M. Kamerbeek, A. Mukherjee, N. Atodiresei, T. K. Sen, P. Lazic, V. Caciuc, R. Michel, D. Stalke, S. K. Mandal, S. Blugel, M. Munzenberg, J. S. Moodera. *Nature* **2013**, *493*, 509–513.

[44] L. Bogani, W. Wernsdorfer. *Nat. Mater.* **2008**, *7*, 179–186.

[45] M. Urdampilleta, S. Klyatskaya, J.-P. Cleuziou, M. Ruben, W. Wernsdorfer. *Nat. Mater.* **2011**, *10*, 502–506.

[46] A. Ghirri, A. Candini, M. Affronte. *Magnetochemistry* **2017**, *3*.

[47] M. N. Leuenberger, D. Loss. *Nature* **2001**, *410*, 789–793.

[48] E. U. Condon, G. H. Shortley, *The Theory of Atomic Spectra*, Cambridge University Press, Cambridge, UK, **1935**.

[49] W. H. Moores, R. McWeeny. *Proc. Royal Soc. A* **1973**, *332*, 365–384.

[50] P. Belanzoni, E. J. Baerends, S. van Asselt, P. B. Langewen. *J. Phys. Chem.* **1995**, *99*, 13094–13102.

[51] G. Schreckenbach, T. Ziegler. *J. Phys. Chem. A* **1997**, *101*, 3388–3399.

[52] G. Schreckenbach, T. Ziegler. *Theor. Chem. Acc.* **1998**, *99*, 71–82.

[53] E. van Lenthe, P. E. S. Wormer, A. van der Avoird. *J. Chem. Phys.* **1997**, *107*, 2488–2498.

[54] E. van Lenthe, A. van der Avoird, W. R. Hagen, E. J. Reijerse. *J. Phys. Chem. A* **2000**, *104*, 2070–2077.

[55] F. Neese. *J. Chem. Phys.* **2001**, *115*, 11080–11096.

[56] J. Autschbach, T. Ziegler. *Coord. Chem. Rev.* **2003**, *238*, 83–126.

[57] J. Autschbach, B. Pritchard. *Theor. Chem. Acc.* **2011**, *129*, 453–466.

[58] M. R. Pederson, S. N. Khanna. *Phys. Rev. B* **1999**, *60*, 9566–9572.

[59] F. Neese. *J. Am. Chem. Soc.* **2006**, *128*, 10213–10222.

[60] F. Neese. *J. Chem. Phys.* **2007**, *127*, 164112.

[61] F. Neese. *Coord. Chem. Rev.* **2009**, *253*, 526–563.

[62] C. van Wüllen. *J. Chem. Phys.* **2009**, *130*, 194109.

[63] C. van Wüllen. *J. Phys. Chem. A* **2009**, *113*, 11535–11540.

[64] S. Schmitt, P. Jost, C. van Wüllen. *J. Chem. Phys.* **2011**, *134*, 194113.

[65] M. Kaupp, M. Bühl, V. G. Malkin (Eds.), *Calculation of NMR and EPR Parameters*, Wiley-VHC, Weinheim, Germany, **2004**.

[66] G. H. Lushington, F. Grein. *Theor. Chim. Acta* **1996**, *93*, 259–267.

[67] G. H. Lushington, F. Grein. *J. Chem. Phys.* **1997**, *106*, 3292–3300.

[68] G. H. Lushington. *J. Phys. Chem. A* **2000**, *104*, 2969–2974.

[69] O. Vahtras, B. Minaev, H. Ågren. *Chem. Phys. Lett.* **1997**, *281*, 186–192.

[70] L. Noodleman. *J. Chem. Phys.* **1981**, *74*, 5737–5743.

[71] L. Noodleman, E. J. Baerends. *J. Am. Chem. Soc.* **1984**, *106*, 2316–2327.

[72] L. Noodleman, J. G. Norman, Jr., J. H. Osborne, A. Aizman, D. A. Case. *J. Am. Chem. Soc.* **1985**, *107*, 3418–3426.

[73] L. Noodleman, E. R. Davidson. *Chem. Phys.* **1986**, *109*, 131–143.

[74] M. F. Charlot, M. Verdaguer, Y. Journaux, P. De Loth, J. P. Daudey. *Inorg. Chem.* **1984**, *23*, 3802–3808.

[75] P. de Loth, J.-P. Daudey, H. Astheimer, L. Walz, W. Haase. *J. Chem. Phys.* **1985**, *82*, 5048–5052.

[76] C. J. Calzado, J. Cabrero, J. P. Malrieu, R. Caballol. *J. Chem. Phys.* **2002**, *116*, 2728–2747.

[77] C. J. Calzado, J. Cabrero, J. P. Malrieu, R. Caballol. *J. Chem. Phys.* **2002**, *116*, 3985–4000.

[78] C. J. Cramer, D. G. Truhlar. *Phys. Chem. Chem. Phys.* **2009**, *11*, 10757–10816.

[79] T. Gupta, G. Rajaraman. *Chem. Commun.* **2016**, *52*, 8972–9008.

[80] R. Caballol, O. Castell, F. Illas, I. de P. R. Moreira, J. P. Malrieu. *J. Phys. Chem. A* **1997**, *101*, 7860–7866.

[81] F. Illas, I. de P. R. Moreira, C. de Graaf, V. Barone. *Theor. Chem. Acc.* **2000**, *104*, 265–272.

[82] F. Illas, I. de P. R. Moreira, J. M. Bofill, M. Filatov. *Phys. Rev. B* **2004**, *70*, 132414.

[83] F. Illas, I. de P. R. Moreira, J. Bofill, M. Filatov. *Theor. Chem. Acc.* **2006**, *116*, 587–597.

[84] E. Ruiz, S. Alvarez, J. Cano, V. Polo. *J. Chem. Phys.* **2005**, *123*, 164110.

[85] I. de P. R. Moreira, F. Illas. *Phys. Chem. Chem. Phys.* **2006**, *8*, 1645–1659.

[86] E. Ruiz, J. Cano, S. Alvarez, V. Polo. *J. Chem. Phys.* **2006**, *124*, 107102.

[87] F. Neese, E. I. Solomon. *Inorg. Chem.* **1998**, *37*, 6568–6582.

[88] F. Neese, T. Petrenko, D. Ganyushin, G. Olbrich. *Coord. Chem. Rev.* **2007**, *251*, 288–327.

[89] M. Atanasov, D. Aravena, E. Suturina, E. Bill, D. Maganas, F. Neese. *Coord. Chem. Rev.* **2015**, *289–290*, 177–214.

[90] N. Ishikawa, M. Sugita, T. Ishikawa, S.-y. Koshihara, Y. Kaizu. *J. Am. Chem. Soc.* **2003**, *125*, 8694–8695.

[91] N. Ishikawa, M. Sugita, T. Ishikawa, S.-y. Koshihara, Y. Kaizu. *J. Phys. Chem. B* **2004**, *108*, 11265–11271.

[92] D. N. Woodruff, R. E. P. Winpenny, R. A. Layfield. *Chem. Rev.* **2013**, *113*, 5110–5148.

[93] R. A. Layfield, M. Murugesu (Eds.), *Lanthanides and Actinides in Molecular Magnetism*, Wiley-VHC, Weinheim, Germany, **2015**.

[94] P. Å. Malmqvist, B. O. Roos, B. Schimmelpfennig. *Chem. Phys. Lett.* **2002**, *357*, 230–240.

[95] L. F. Chibotaru, L. Ungur. *J. Chem. Phys.* **2012**, *137*, 064112.

[96] L. Ungur, L. F. Chibotaru, *Computational Modelling of the Magnetic Properties of Lanthanide Compounds* in *Lanthanides and Actinides in Molecular Magnetism*, R. A. Layfield, M. Murugesu (Eds.), Wiley-VHC, Weinheim, Germany, **2015**, pp. 153–184.

[97] L. F. Chibotaru, Ab Initio *Methodology for Pseudospin Hamiltonians of Anisotropic Magnetic Complexes* in *Advances in Chemical Physics, Volume 153*, S. A. Rice, A. R. Dinner (Eds.), Wiley, **2013**, pp. 397–519.

[98] L. F. Chibotaru, L. Ungur, A. Soncini. *Angew. Chem.* **2008**, *120*, 4194–4197.

[99] L. Ungur, W. van den Heuvel, L. F. Chibotaru. *New J. Chem.* **2009**, *33*, 1224–1230.

[100] L. Ungur, M. Thewissen, J.-P. Costes, W. Wernsdorfer, L. F. Chibotaru. *Inorg. Chem.* **2013**, *52*, 6328–6337.

[101] L. Ungur, L. F. Chibotaru. *Chem. Eur. J.* **2017**, *23*, 3708–3718.

[102] S. K. Singh, J. Eng, M. Atanasov, F. Neese. *Coord. Chem. Rev.* **2017**, *344*, 2–25.

[103] M. Atanasov, D. Ganyushin, K. Sivalingam, F. Neese, *A Modern First-Principles View on Ligand Field Theory Through the Eyes of Correlated Multireference Wavefunctions* in *Molecular Electronic Structures of Transition Metal Complexes II*, D. M. P. Mingos, P. Day, J. P. Dahl (Eds.), Springer, Berlin, Germany, **2012**, pp. 149–220.

[104] F. Neese, D. A. Pantazis. *Faraday Discuss.* **2011**, *148*, 229–238.

[105] L. Ungur, L. F. Chibotaru. *Phys. Chem. Chem. Phys.* **2011**, *13*, 20086–20090.

[106] J. D. Rinehart, J. R. Long. *Chem. Sci.* **2011**, *2*, 2078–2085.

[107] J. Sievers. *Z. Phys. B* **1982**, *45*, 289–296.

[108] N. F. Chilton. *Inorg. Chem.* **2015**, *54*, 2097–2099.

[109] L. Ungur, L. F. Chibotaru. *Inorg. Chem.* **2016**, *55*, 10043–10056.

[110] Y.-S. Meng, Y.-Q. Zhang, Z.-M. Wang, B.-W. Wang, S. Gao. *Chem. Eur. J.* **2016**, *22*, 12724–12731.

[111] Y.-C. Chen, J.-L. Liu, L. Ungur, J. Liu, Q.-W. Li, L.-F. Wang, Z.-P. Ni, L. F. Chibotaru, X.-M. Chen, M.-L. Tong. *J. Am. Chem. Soc.* **2016**, *138*, 2829–2837.

[112] J. Liu, Y.-C. Chen, J.-L. Liu, V. Vieru, L. Ungur, J.-H. Jia, L. F. Chibotaru, Y. Lan, W. Wernsdorfer, S. Gao, X.-M. Chen, M.-L. Tong. *J. Am. Chem. Soc.* **2016**, *138*, 5441–5450.

[113] Y.-S. Ding, N. F. Chilton, R. E. P. Winpenny, Y.-Z. Zheng. *Angew. Chem. Int. Ed.* **2016**, *128*, 16305–16308.

[114] C. A. P. Goodwin, F. Ortu, D. Reta, N. F. Chilton, D. P. Mills. *Nature* **2017**, *548*, 439–442.

[115] J. D. Rinehart, M. Fang, W. J. Evans, J. R. Long. *J. Am. Chem. Soc.* **2011**, *133*, 14236–14239.

[116] J. D. Rinehart, M. Fang, W. J. Evans, J. R. Long. *Nat. Chem.* **2011**, *3*, 53–542.

[117] F. Liu, D. S. Krylov, L. Spree, S. M. Avdoshenko, N. A. Samoylova, M. Rosenkranz, A. Kostanyan, T. Greber, A. U. B. Wolter, B. Büchner, A. A. Popov. *Nat. Commun.* **2017**, *8*, 16098.

[118] M. E. Lines. *J. Chem. Phys.* **1971**, *55*, 2977–2984.

[119] N. Iwahara, L. F. Chibotaru. *Phys. Rev. B* **2015**, *91*, 174438.

[120] N. Iwahara, L. F. Chibotaru. *Sci. Rep.* **2016**, *6*, 24743.

[121] V. Vieru, N. Iwahara, L. F. Chibotaru. *Sci. Rep.* **2016**, *6*, 24046.

[122] A. Lunghi, F. Totti, R. Sessoli, S. Sanvito. *Nat. Commun.* **2017**, *8*, 14620.

[123] A. Lunghi, F. Totti, S. Sanvito, R. Sessoli. *Chem. Sci.* **2017**, *8*, 6051–6059.

[124] D. R. Hartree. *Proc. Camb. Phil. Soc.* **1928**, *24*, 89–110.

[125] H. N. Russell, A. G. Shenstone, L. A. Turner. *Phys. Rev.* **1929**, *33*, 900–906.

[126] D. R. Hartree. *Proc. Camb. Phil. Soc.* **1928**, *24*, 111–132.

[127] A. Szabo, N. S. Ostlund, *Modern Quantum Chemistry*, Macmillan Publishing Company, New York, NY, USA, **1982**.

[128] J. C. Slater. *Phys. Rev.* **1929**, *34*, 1293–1322.

[129] F. Jensen, *Introduction to Computational Chemistry 2nd ed.*, Wiley, Chichester, UK, **2007**.

[130] P. A. M. Dirac. *Proc. Royal Soc. A* **1927**, *114*, 243–265.

[131] V. Fock. *Z. Phys.* **1932**, *75*, 622–647.

[132] A. L. Fetter, J. D. Walecka, *Quantum Theory of Many-Particle Systems*, McGraw–Hill, New York, NY, USA, **1971**.

[133] T. Helgaker, P. Jørgensen, J. Olsen, *Molecular Electronic-Strucutre Theory*, Wiley, Chichester, UK, **2000**.

[134] P. Jørgensen, J. Simons, *Second Quantization-Based Methods in Quantum Chemistry*, Academic Press, New York, NY, USA, **1981**.

[135] F. Schwabl, *Advanced Quantum Mechanics 4th ed.*, Springer, Berlin, Germany, **2008**.

[136] W. Pauli. *Z. Phys.* **1925**, *31*, 765–783.

[137] W. Pauli. *Z. Phys.* **1927**, *43*, 601–623.

[138] B. R. Judd, *Second Quantization and Atomic Spectroscopy*, The Johns Hopkins Press, Baltimore, MD, USA, **1967**.

[139] P.-O. Löwdin. *Phys. Rev.* **1955**, *97*, 1474–1489.

[140] P.-O. Löwdin. *Phys. Rev.* **1955**, *97*, 1490–1508.

[141] P.-O. Löwdin. *Phys. Rev.* **1955**, *97*, 1509–1520.

[142] E. R. Davidson, *Reduced Density Matrices in Quantum Chemistry*, Academic Press, New York, NY, USA, **1976**.

[143] R. McWeeny. *Rev. Mod. Phys.* **1960**, *32*, 335–369.

[144] A. Messiah, *Quantum Mechanics*, Dover, Mineola, NY, USA, **1961–62**.

[145] R. Shankar, *Principles of Quantum Mechanics 2nd ed.*, Springer, New Delhi, India, **1994**.

[146] J. Paldus. *Phys. Rev. A* **1976**, *14*, 1620–1625.

[147] I. Shavitt. *Int. J. Quantum Chem.* **1977**, *12*, 131–148.

[148] I. Shavitt. *Int. J. Quantum Chem.* **1978**, *14*, 5–32.

[149] R. Pauncz, *Spin Eigenfunctions. Construction and use*, Plenum Press, New York, NY, USA, **1979**.

[150] B. O. Roos, R. Lindh, P. Å. Malmqvist, V. Veryazov, P.-O. Widmark, *Multiconfigurational Quantum Chemistry*, Wiley, Hoboken, NJ, USA, **2016**.

[151] R. G. Parr, W. Yang, *Density-Functional Theory of Atoms and Molecules*, of *International series of monographs on chemistry*, Clarendon Press, Oxford, UK, **1989**.

[152] J. S. Griffith, *The Theory of Transition-Metal Ions*, Cambridge University Press, Cambridge, UK, **1961**.

[153] C. Bloch. *Nucl. Phys.* **1958**, *6*, 329–347.

[154] D. E. Dugdale. *J. Phys. Condens. Matter* **1993**, *5*, 7837.

[155] M. Mostafanejad. *Int. J. Quantum Chem.* **2014**, *114*, 1495–1512.

[156] L. Sorace, D. Gatteschi, *Electronic Strucure and Magnetic Properties of Lanthanide Molecular Complexes* in *Lanthanides and Actinides in Molecular Magnetism*, R. A. Layfield, M. Murugesu (Eds.), Wiley-VHC, Weinheim, Germany, **2015**, pp. 1–25.

[157] A. R. Edmonds, *Angular Momentum in Quantum Mechanics 2nd ed.*, Princeton University Press, Princeton, NJ, USA, **1960**.

[158] E. P. Wigner, *Group Theory and its Application to the Quantum Mechanics of Atomic Spectra*, Academic Press, New York, NY, USA, **1959**.

[159] D. A. Varshalovich, A. N. Moskalev, V. K. Khersonskii, *Quantum Theory of Angular Momentum*, World Scientific Publishing, Singapore, **1988**.

[160] A. S. Davydov, *Quantum Mechanics*, Pergamon Press, Oxford, UK, **1965**.

[161] H. N. Russell, F. A. Saunders. *Astrophys. J.* **1925**, *61*, 38.

[162] G. Racah. *Phys. Rev.* **1942**, *62*, 438–462.

[163] B. R. Judd, *Operator Techniques in Atomic Spectroscopy*, McGraw–Hill, New York, NY, USA, **1963**.

[164] C. Eckart. *Rev. Mod. Phys.* **1930**, *2*, 305–380.

[165] K. W. H. Stevens. *Proc. Phys. Soc. A* **1952**, *65*, 209.

[166] H. A. Kramers. *Proc. Kon. Ned. Akad. Wetensch.* **1930**, *33*, 959–972.

[167] P. Alonso, J. Martínez. *J. Magn. Reson.* **2015**, *255*, 1–14.

[168] R. P. Feynman. *Phys. Rev.* **1939**, *56*, 340–343.

[169] P. Atkins, R. Friedman, *Molecular Quantum Mechanics 5th ed.*, Oxford University Press, Oxford, UK, **2011**.

[170] M. H. L. Pryce. *Proc. Phys. Soc. A* **1950**, *63*, 25.

[171] A. Abragam, M. H. L. Pryce. *Proc. Royal Soc. A* **1951**, *205*, 135–153.

[172] B. Bleaney. *Proc. Phys. Soc. A* **1959**, *73*, 939.

[173] G. F. Koster, H. Statz. *Phys. Rev.* **1959**, *113*, 445–454.

[174] H. Statz, G. F. Koster. *Phys. Rev.* **1959**, *115*, 1568–1577.

[175] R. Maurice, C. de Graaf, N. Guihéry. *Phys. Chem. Chem. Phys.* **2013**, *15*, 18784–18804.

[176] C. Rudowicz, M. Karbowiak. *Coord. Chem. Rev.* **2015**, *287*, 28–63.

[177] J. P. Malrieu, R. Caballol, C. J. Calzado, C. de Graaf, N. Guihéry. *Chem. Rev.* **2014**, *114*, 429–492.

[178] J. des Cloizeaux. *Nucl. Phys.* **1960**, *20*, 321–346.

[179] A. Ceulemans, L. F. Chibotaru, G. A. Heylen, K. Pierloot, L. G. Vanquickenborne. *Chem. Rev.* **2000**, *100*, 787–806.

[180] S. M. Winter, K. Riedl, R. Valentí. *Phys. Rev. B* **2017**, *95*, 060404.

[181] C. J. Ballhausen, *Introduction to Ligand Field Theory*, McGraw–Hill, New York, NY, USA, **1962**.

[182] J. H. van Vleck, A. Frank. *Phys. Rev.* **1929**, *34*, 1494–1496.

[183] J. H. van Vleck, A. Frank. *Phys. Rev.* **1929**, *34*, 1625–1625.

[184] J. H. van Vleck, *The Theory of Electric and Magnetic Susceptibilities*, Oxford University Press, Oxford, UK, **1932**.

[185] C. Rudowicz. *J. Phys. C* **1985**, *18*, 1415.

[186] C. Rudowicz. *J. Phys. C* **1985**, *18*, 3837.

[187] C. Rudowicz, C. Y. Chung. *J. Phys. Condens. Matter* **2004**, *16*, 5825.

[188] J. Becquerel. *Z. Phys.* **1929**, *58*, 205–216.

[189] H. Bethe. *Ann. Phys.* **1929**, *395*, 133–208.

[190] J. H. Van Vleck. *Phys. Rev.* **1932**, *41*, 208–215.

[191] J. H. van Vleck. *J. Chem. Phys.* **1935**, *3*, 807–813.

[192] A. Abragam, M. H. L. Pryce. *Proc. Royal Soc. A* **1951**, *206*, 173–191.

[193] K. W. H. Stevens, M. H. L. Pryce. *Proc. Royal Soc. A* **1953**, *219*, 542–555.

[194] J. Owen, J. H. M. Thornley. *Rep. Prog. Phys.* **1966**, *29*, 675.

[195] C. J. Ballhausen, *Molecular Electronic Structures of Transition Metal Complexes*, McGraw–Hill, New York, NY, USA, **1979**.

[196] J. Owen, K. W. H. Stevens. *Nature* **1953**, *171*, 836.

[197] J. M. Clemente-Juan, E. Coronado, A. Gaita-Ariño, *Mononuclear Lanthanide Complexes: Use of the Crystal Field Theory to Design Single-Ion Magnets and Spin Qubits* in *Lanthanides and Actinides in Molecular Magnetism*, R. A. Layfield, M. Murugesu (Eds.), Wiley-VHC, Weinheim, Germany, **2015**, pp. 27–59.

[198] R. McWeeny. *J. Chem. Phys.* **1965**, *42*, 1717–1725.

[199] R. McWeeney, *Spins in Chemistry*, Academic Press, New York, NY, USA, **1970**.

[200] S. Gómez-Coca, A. Urtizberea, E. Cremades, P. J. Alonso, A. Camón, E. Ruiz, F. Luis. *Nat. Commun.* **2014**, *5*, 4300.

[201] Y.-Y. Zhu, F. Liu, J.-J. Liu, Y.-S. Meng, S.-D. Jiang, A.-L. Barra, W. Wernsdorfer, S. Gao. *Inorg. Chem.* **2017**, *56*, 697–700.

[202] J. S. Griffith. *Phys. Rev.* **1963**, *132*, 316–319.

[203] C. J. Calzado, J.-P. Malrieu. *Phys. Rev. B* **2001**, *63*, 214520.

[204] C. J. Calzado, J.-P. Malrieu. *Eur. Phys. J. B* **2001**, *21*, 375–381.

[205] C. J. Calzado, C. de Graaf, E. Bordas, R. Caballol, J.-P. Malrieu. *Phys. Rev. B* **2003**, *67*, 132409.

[206] C. J. Calzado, J.-P. Malrieu. *Phys. Rev. B* **2004**, *69*, 094435.

[207] G. H. Wannier. *Phys. Rev.* **1937**, *52*, 191–197.

[208] G. H. Wannier. *Rev. Mod. Phys.* **1962**, *34*, 645–655.

[209] R. M. Martin, *Electronic Structure*, Cambridge University Press, Cambridge, UK, **2004**.

[210] J. Hubbard. *Proc. Royal Soc. A* **1963**, *276*, 238–257.

[211] P. W. Anderson. *Phys. Rev.* **1950**, *79*, 350–356.

[212] P. W. Anderson. *Phys. Rev.* **1959**, *115*, 2–13.

[213] H. A. Kramers. *Physica* **1934**, *1*, 182–192.

[214] J. B. Goodenough. *Phys. Rev.* **1955**, *100*, 564–573.

[215] J. B. Goodenough. *J. Phys. Chem. Solids* **1958**, *6*, 287–297.

[216] J. B. Goodenough, *Magnetism and the Chemical Bond*, Wiley, New York, NY, USA, **1963**.

[217] J. Kanamori. *J. Phys. Chem. Solids* **1959**, *10*, 87–98.

[218] W. Van den Heuvel, L. F. Chibotaru. *Phys. Rev. B* **2007**, *76*, 104424.

[219] C. Zener. *Phys. Rev.* **1951**, *82*, 403–405.

[220] P. W. Anderson, H. Hasegawa. *Phys. Rev.* **1955**, *100*, 675–681.

[221] P. G. de Gennes. *Phys. Rev.* **1960**, *118*, 141–154.

[222] J. H. van Vleck. *Rev. Mod. Phys.* **1945**, *17*, 27–47.

[223] J. C. Slater. *Rev. Mod. Phys.* **1953**, *25*, 199–210.

[224] G. Blondin, J. J. Girerd. *Chem. Rev.* **1990**, *90*, 1359–1376.

[225] E. Ruiz, J. Cano, S. Alvarez, P. Alemany. *J. Comp. Chem.* **1999**, *20*, 1391–1400.

[226] I. de P. R. Moreira, N. Suaud, N. Guihéry, J. P. Malrieu, R. Caballol, J. M. Bofill, F. Illas. *Phys. Rev. B* **2002**, *66*, 134430.

[227] R. Bastardis, N. Guihéry, C. de Graaf. *J. Chem. Phys.* **2008**, *129*, 104102.

[228] V. Papaefthymiou, J. J. Girerd, I. Moura, J. J. G. Moura, E. Münck. *J. Am. Chem. Soc.* **1987**, *109*, 4703–4710.

[229] T. Moriya. *Phys. Rev.* **1960**, *120*, 91–98.

[230] R. Maurice, N. Guihéry, R. Bastardis, C. d. Graaf. *J. Chem. Theory Comput.* **2010**, *6*, 55–65.

[231] I. Dzyaloshinsky. *J. Phys. Chem. Solids* **1958**, *4*, 241–255.

[232] M. L. Plumer. *Phys. Rev. B* **2007**, *76*, 144411.

[233] A. Ceulemans, G. A. Heylen, L. F. Chibotaru, T. L. Maes, K. Pierloot, C. Ribbing, L. G. Vanquickenborne. *Inorg. Chim. Acta* **1996**, *251*, 15–27.

[234] A. Palii, B. Tsukerblat, S. Klokishner, K. R. Dunbar, J. M. Clemente-Juan, E. Coronado. *Chem. Soc. Rev.* **2011**, *40*, 3130–3156.

[235] L. F. Chibotaru, N. Iwahara. *New J. Phys.* **2015**, *17*, 103028.

[236] R. Orbach. *Proc. Royal Soc. A* **1961**, *264*, 458–484.

[237] P. Debye. *Ann. Phys.* **1912**, *344*, 789–839.

[238] M. Atanasov, J. M. Zadrozny, J. R. Long, F. Neese. *Chem. Sci.* **2013**, *4*, 139–156.

[239] L. T. A. Ho, L. F. Chibotaru. *Phys. Rev. B* **2016**, *94*, 104422.

[240] L. T. A. Ho, L. F. Chibotaru. *Phys. Rev. B* **2018**, *97*, 024427.

[241] L. Escalera-Moreno, N. Suaud, A. Gaita-Ariño, E. Coronado. *J. Phys. Chem. Lett.* **2017**, *8*, 1695–1700.

[242] S. T. Liddle, J. van Slageren. *Chem. Soc. Rev.* **2015**, *44*, 6655–6669.

[243] G. R. Willey, P. R. Meehan, T. J. Woodman, M. G. Drew. *Polyhedron* **1997**, *16*, 623–627.

[244] N. Ishikawa, M. Sugita, W. Wernsdorfer. *Angew. Chem. Int. Ed.* **2005**, *44*, 2931–2935.

[245] S. L. Altmann, P. Herzig, *Point-Group Theory Tables*, Claredon Press, Oxford, UK, **1994**.

[246] J. H. van Vleck. *Phys. Rev.* **1940**, *57*, 426–447.

[247] K. S. Pedersen, J. Dreiser, H. Weihe, R. Sibille, H. V. Johannesen, M. A. Sørensen, B. E. Nielsen, M. Sigrist, H. Mutka, S. Rols, J. Bendix, S. Piligkos. *Inorg. Chem.* **2015**, *54*, 7600–7606.

[248] K. R. Meihaus, J. R. Long. *Dalton Trans.* **2015**, *44*, 2517–2528.

[249] R. J. Blagg, L. Ungur, F. Tuna, J. Speak, P. Comar, D. Collison, W. Wernsdorfer, E. J. L. McInnes, L. F. Chibotaru, R. E. P. Winpenny. *Nat. Chem.* **2013**, *5*, 673–678.

[250] K. S. Pedersen, D. N. Woodruff, J. Bendix, R. Clérac, *Experimental Aspects of Lanthanide Single-Molecule Magnet Physics* in *Lanthanides and Actinides in Molecular Magnetism*, R. A. Layfield, M. Murugesu (Eds.), Wiley-VHC, Weinheim, Germany, **2015**, pp. 125–152.

[251] F. Neese. *WIREs Comput. Mol. Sci.* **2012**, *2*, 73–78.

[252] F. Neese. *WIREs Comput. Mol. Sci.* **2017**, *8*, e1327.

[253] F. Aquilante, L. De Vico, N. Ferré, G. Ghigo, P.-å. Malmqvist, P. Neogrády, T. B. Pedersen, M. Pitoňák, M. Reiher, B. O. Roos, L. Serrano-Andrés, M. Urban, V. Veryazov, R. Lindh. *J. Comp. Chem.* **2010**, *31*, 224–247.

[254] F. Aquilante, J. Autschbach, R. K. Carlson, L. F. Chibotaru, M. G. Delcey, L. De Vico, I. Fdez. Galván, N. Ferré, L. M. Frutos, L. Gagliardi, M. Garavelli, A. Giussani, C. E. Hoyer, G. Li Manni, H. Lischka, D. Ma, P. Å. Malmqvist, T. Müller, A. Nenov, M. Olivucci, T. B. Pedersen, D. Peng, F. Plasser, B. Pritchard, M. Reiher, I. Rivalta, I. Schapiro, J. Segarra-Martí, M. Stenrup, D. G. Truhlar, L. Ungur, A. Valentini, S. Vancoillie, V. Veryazov, V. P. Vysotskiy, O. Weingart, F. Zapata, R. Lindh. *J. Comp. Chem.* **2015**, *37*, 506–541.

[255] H.-J. Werner, P. J. Knowles, G. Knizia, F. R. Manby, M. Schütz. *WIREs Comput. Mol. Sci.* **2012**, *2*, 242–253.

[256] M. Born, R. Oppenheimer. *Ann. Phys.* **1927**, *389*, 457–484.

[257] C. J. Cramer, *Essentials of Computational Chemistry*, Wiley, Chichester, UK, **2004**.

[258] C. Eckart. *Phys. Rev.* **1930**, *36*, 878–892.

[259] L. Pauling, E. B. Wilson, Jr, *Introduction to Quantum Mechanics*, Dover, NY, USA, **1935**.

[260] J. C. Slater. *Phys. Rev.* **1930**, *36*, 57–64.

[261] G. te Velde, F. M. Bickelhaupt, E. J. Baerends, C. Fonseca Guerra, S. J. A. van Gisbergen, J. G. Snijders, T. Ziegler. *J. Comp. Chem.* **2001**, *22*, 931–967.

[262] E. van Lenthe, E. J. Baerends. *J. Comp. Chem.* **2003**, *24*, 1142–1156.

[263] S. F. Boys. *Proc. Royal Soc. A* **1950**, *200*, 542–554.

[264] W. J. Hehre, R. F. Stewart, J. A. Pople. *J. Chem. Phys.* **1969**, *51*, 2657–2664.

[265] M. D. Newton, W. A. Lathan, W. J. Hehre, J. A. Pople. *J. Chem. Phys.* **1969**, *51*, 3927–3932.

[266] W. J. Hehre, R. Ditchfield, R. F. Stewart, J. A. Pople. *J. Chem. Phys.* **1970**, *52*, 2769–2773.

[267] M. D. Newton, W. A. Lathan, W. J. Hehre, J. A. Pople. *J. Chem. Phys.* **1970**, *52*, 4064–4072.

[268] R. Ditchfield, W. J. Hehre, J. A. Pople. *J. Chem. Phys.* **1970**, *52*, 5001–5007.

[269] W. J. Hehre, R. Ditchfield, J. A. Pople. *J. Chem. Phys.* **1970**, *53*, 932–935.

[270] R. Ditchfield, W. J. Hehre, J. A. Pople. *J. Chem. Phys.* **1971**, *54*, 724–728.

[271] W. J. Hehre, R. Ditchfield, J. A. Pople. *J. Chem. Phys.* **1972**, *56*, 2257–2261.

[272] W. J. Hehre, J. A. Pople. *J. Chem. Phys.* **1972**, *56*, 4233–4234.

[273] W. J. Hehre, W. A. Lathan. *J. Chem. Phys.* **1972**, *56*, 5255–5257.

[274] J. D. Dill, J. A. Pople. *J. Chem. Phys.* **1975**, *62*, 2921–2923.

[275] J. B. Collins, P. von R. Schleyer, J. S. Binkley, J. A. Pople. *J. Chem. Phys.* **1976**, *64*, 5142–5151.

[276] J. S. Binkley, J. A. Pople. *J. Chem. Phys.* **1977**, *66*, 879–880.

[277] R. Krishnan, J. S. Binkley, R. Seeger, J. A. Pople. *J. Chem. Phys.* **1980**, *72*, 650–654.

[278] M. Reiher, A. Wolf, *Relativistic Quantum Chemistry 2nd ed.*, Wiley-VHC, Weinheim, Germany, **2015**.

[279] J. C. Slater. *Phys. Rev.* **1928**, *32*, 339–348.

[280] V. Fock. *Z. Phys.* **1930**, *61*, 126–148.

[281] J. A. Pople, R. K. Nesbet. *J. Chem. Phys.* **1954**, *22*, 571–572.

[282] C. Roothaan. *Rev. Mod. Phys.* **1951**, *23*, 69–89.

[283] G. G. Hall. *Proc. Royal Soc. A* **1951**, *A205*, 541–552.

[284] J. L. Whitten. *J. Chem. Phys.* **1973**, *58*, 4496–4501.

[285] J. A. Jafri, J. L. Whitten. *J. Chem. Phys.* **1974**, *61*, 2116–2121.

[286] E. Baerends, D. Ellis, P. Ros. *Chem. Phys.* **1973**, *2*, 41–51.

[287] H. Sambe, R. H. Felton. *J. Chem. Phys.* **1975**, *62*, 1122–1126.

[288] B. I. Dunlap, J. W. D. Connolly, J. R. Sabin. *J. Chem. Phys.* **1979**, *71*, 3396–3402.

[289] B. I. Dunlap, J. W. D. Connolly, J. R. Sabin. *J. Chem. Phys.* **1979**, *71*, 4993–4999.

[290] O. Vahtras, J. Almlöf, M. Feyereisen. *Chem. Phys. Lett.* **1993**, *213*, 514–518.

[291] M. Feyereisen, G. Fitzgerald, A. Komornicki. *Chem. Phys. Lett.* **1993**, *208*, 359–363.

[292] K. Eichkorn, O. Treutler, H. Öhm, M. Häser, R. Ahlrichs. *Chem. Phys. Lett.* **1995**, *240*, 283–290.

[293] K. Eichkorn, F. Weigend, O. Treutler, R. Ahlrichs. *Theor. Chem. Acc.* **1997**, *97*, 119–124.

[294] F. Weigend, M. Häser, H. Patzelt, R. Ahlrichs. *Chem. Phys. Lett.* **1998**, *294*, 143–152.

[295] F. Neese. *J. Comp. Chem.* **2003**, *24*, 1740–1747.

[296] R. A. Kendall, H. A. Früchtl. *Theor. Chem. Acc.* **1997**, *97*, 158–163.

[297] F. Weigend. *Phys. Chem. Chem. Phys.* **2002**, *4*, 4285–4291.

[298] F. Neese, F. Wennmohs, A. Hansen, U. Becker. *Chem. Phys.* **2009**, *356*, 98–109.

[299] R. Izsák, F. Neese. *J. Chem. Phys.* **2011**, *135*, 144105.

[300] N. H. F. Beebe, J. Linderberg. *Int. J. Quantum Chem.* **1977**, *12*, 683–705.

[301] H. Koch, A. S. de Merás, T. B. Pedersen. *J. Chem. Phys.* **2003**, *118*, 9481–9484.

[302] F. Aquilante, L. Boman, J. Boström, H. Koch, R. Lindh, A. S. de Merás, T. B. Pedersen, *Cholesky Decomposition Techniques in Electronic Structure Theory* in *Linear-Scaling Techniques in Computational Chemistry and Physics: Methods and Applications*, R. Zalesny, M. G. Papadopoulos, P. G. Mezey, J. Leszczynski (Eds.), Springer, Dordrecht, Neatherlands, **2011**, pp. 301–343.

[303] W. Koch, M. C. Holthausen, *A Chemist's Guide to Density Functional Theory 2nd ed.*, Wiley–VCH, Weinheim, Germany, **2001**.

[304] M. Buijse, E. J. Baerends. *Mol. Phys.* **2002**, *100*, 401–421.

[305] J. A. Pople, R. Seeger, R. Krishnan. *Int. J. Quantum Chem.* **1977**, *12*, 149–163.

[306] R. Krishnan, H. B. Schlegel, J. A. Pople. *J. Chem. Phys.* **1980**, *72*, 4654–4655.

[307] K. Raghavachari, J. A. Pople. *Int. J. Quantum Chem.* **1981**, *20*, 1067–1071.

[308] R. J. Bartlett, M. Musiał. *Rev. Mod. Phys.* **2007**, *79*, 291–352.

[309] B. O. Roos, *The Complete Active Space Self-Consistent Field Method and its Applications in Electronic Structure Calculations* in *Advances in Chemical Physics: Ab Initio Methods in Quantum Chemistry II, Vol. 69*, K. P. Lawley (Ed.), Wiley, New York, NY, USA, **1987**, pp. 399–455.

[310] P. Siegbahn, A. Heiberg, B. Roos, B. Levy. *Phys. Scripta* **1980**, *21*, 323–327.

[311] B. O. Roos, P. R. Taylor, P. E. M. Siegbahn. *Chem. Phys.* **1980**, *48*, 157–173.

[312] P. E. M. Siegbahn, J. Almlöf, A. Heiberg, B. O. Roos. *J. Chem. Phys.* **1981**, *74*, 2384–2396.

[313] H.-J. Werner, *Matrix-Formulated Direct Multiconfiguration Self-Consistent Field and Multiconfiguration Reference Configuration-Interaction Methods* in *Advances in Chemical Physics: Ab Initio Methods in Quantum Chemistry II, Vol. 69*, K. P. Lawley (Ed.), Wiley, New York, NY, USA, **1987**, pp. 1–62.

[314] R. Shepard, *The Multiconfiguration Self-Consistent Field Method* in *Advances in Chemical Physics: Ab Initio Methods in Quantum Chemistry II, Vol. 69*, K. P. Lawley (Ed.), Wiley, New York, NY, USA, **1987**, pp. 63–200.

[315] D. R. Hartree, W. Hartree, B. Swirles. *Phil. Trans. R. Soc. A* **1939**, *238*, 229–247.

[316] A. Jucys. *Proc. Royal Soc. A* **1939**, *173*, 59–67.

[317] J. Hinze. *J. Chem. Phys.* **1973**, *59*, 6424–6432.

[318] E. Dalgaard, P. Jørgensen. *J. Chem. Phys.* **1978**, *69*, 3833–3844.

[319] B. Lévy, G. Berthier. *Int. J. Quantum Chem.* **1968**, *2*, 307–319.

[320] P. Å. Malmqvist, A. Rendell, B. O. Roos. *J. Chem. Phys.* **1990**, *94*, 5477–5482.

[321] D. Ma, G. L. Manni, L. Gagliardi. *J. Chem. Phys.* **2011**, *135*, 044128.

[322] K. D. Vogiatzis, G. Li Manni, S. J. Stoneburner, D. Ma, L. Gagliardi. *J. Chem. Theory Comput.* **2015**, *11*, 3010–3021.

[323] S. R. White. *Phys. Rev. Lett.* **1992**, *69*, 2863–2866.

[324] S. R. White. *Phys. Rev. B* **1993**, *48*, 10345–10356.

[325] K. H. Marti, M. Reiher. *Phys. Chem. Chem. Phys.* **2011**, *13*, 6750–6759.

[326] G. K.-L. Chan, S. Sharma. *Annu. Rev. Phys. Chem.* **2011**, *62*, 465–481.

[327] S. Wouters, D. van Neck. *Eur. Phys. J. D* **2014**, *68*, 272.

[328] Y. Kurashige. *Mol. Phys.* **2014**, *112*, 1485–1494.

[329] T. Yanai, Y. Kurashige, W. Mizukami, J. Chalupský, T. N. Lan, M. Saitow. *Int. J. Quantum Chem.* **2015**, *115*, 283–299.

[330] G. K.-L. Chan, A. Keselman, N. Nakatani, Z. Li, S. R. White. *J. Chem. Phys.* **2016**, *145*, 014102.

[331] As of now, there is no citations available for ICE-CI. The method is documented in the manual of Orca 4.0.0 code which is freely available at `https://orcaforum.cec.mpg.de/OrcaManual.pdf` (retrieved January 8th 2018).

[332] D. A. Mazziotti. *Acc. Chem. Res.* **2006**, *39*, 207–215.

[333] D. A. Mazziotti. *Chem. Rev.* **2012**, *112*, 244–262.

[334] Y. Kurashige, T. Yanai. *J. Chem. Phys.* **2011**, *135*, 094104.

[335] Y. Kurashige, J. ChalupskÃœ, T. N. Lan, T. Yanai. *J. Chem. Phys.* **2014**, *141*, 174111.

[336] S. Guo, M. A. Watson, W. Hu, Q. Sun, G. K.-L. Chan. *J. Chem. Theory Comput.* **2016**, *12*, 1583–1591.

[337] M. Roemelt, S. Guo, G. K.-L. Chan. *J. Chem. Phys.* **2016**, *144*, 204113.

[338] L. Freitag, S. Knecht, C. Angeli, M. Reiher. *J. Chem. Theory Comput.* **2017**, *13*, 451–459.

[339] M. Saitow, Y. Kurashige, T. Yanai. *J. Chem. Phys.* **2013**, *139*, 044118.

[340] B. O. Roos, P. Linse, P. E. Siegbahn, M. R. Blomberg. *Chem. Phys.* **1982**, *66*, 197–207.

[341] K. Andersson, P. Å. Malmqvist, B. O. Roos, A. J. Sadlej, K. Wolinski. *J. Phys. Chem.* **1990**, *94*, 5483–5488.

[342] K. Andersson, P.-Å. Malmqvist, B. O. Roos. *J. Chem. Phys.* **1992**, *96*, 1218–1226.

[343] C. Angeli, R. Cimiraglia, S. Evangelisti, T. Leininger, J.-P. Malrieu. *J. Chem. Phys.* **2001**, *114*, 10252–10264.

[344] C. Angeli, R. Cimiraglia, J.-P. Malrieu. *Chem. Phys. Lett.* **2001**, *350*, 297–305.

[345] C. Angeli, R. Cimiraglia, J.-P. Malrieu. *J. Chem. Phys.* **2002**, *117*, 9138–9153.

[346] C. Møller, M. S. Plesset. *Phys. Rev.* **1934**, *46*, 618–622.

[347] P. E. M. Siegbahn. *Int. J. Quantum Chem.* **1980**, *18*, 1229–1242.

[348] P. E. Siegbahn. *Chem. Phys.* **1977**, *25*, 197–205.

[349] W. Meyer, *Configuration Expansion by Means of Pseudonatural Orbitals* in *Methods of Electronic Structure Theory*, H. F. Schaefer (Ed.), Springer, Boston, MA, USA, **1977**, pp. 413–446.

[350] P. Celani, H.-J. Werner. *J. Chem. Phys.* **2000**, *112*, 5546–5557.

[351] B. O. Roos, K. Andersson. *Chem. Phys. Lett.* **1995**, *245*, 215–223.

[352] B. O. Roos, K. Andersson, M. P. Fülscher, L. Serrano-Andrés, K. Pierloot, M. Merchán, V. Molina. *J. Mol. Struct. THEOCHEM* **1996**, *388*, 257–276.

[353] N. Forsberg, P.-Å. Malmqvist. *Chem. Phys. Lett.* **1997**, *274*, 196–204.

[354] J. P. Zobel, J. J. Nogueira, L. González. *Chem. Sci.* **2017**, *8*, 1482–1499.

[355] J. Finley, P.-Å. Malmqvist, B. O. Roos, L. Serrano-Andrés. *Chem. Phys. Lett.* **1998**, *288*, 299–306.

[356] T. Shiozaki, W. Győrffy, P. Celani, H.-J. Werner. *J. Chem. Phys.* **2011**, *135*, 081106.

[357] A. A. Granovsky. *J. Chem. Phys.* **2011**, *134*, 214113.

[358] J. J. Baldoví, Y. Duan, R. Morales, A. Gaita-Ariño, E. Ruiz, E. Coronado. *Chem. Eur. J.* **2016**, *22*, 13532–13539.

[359] K. G. Dyall. *J. Chem. Phys.* **1995**, *102*, 4909–4918.

[360] C. Angeli, S. Borini, M. Cestari, R. Cimiraglia. *J. Chem. Phys.* **2004**, *121*, 4043–4049.

[361] I. Schapiro, K. Sivalingam, F. Neese. *J. Chem. Theory Comput.* **2013**, *9*, 3567–3580.

[362] D. Aravena, M. Atanasov, F. Neese. *Inorg. Chem.* **2016**, *55*, 4457–4469.

[363] F. Fracchia, R. Cimiraglia, C. Angeli. *J. Phys. Chem. A* **2015**, *119*, 5490–5495.

[364] K. Pierloot, Q. M. Phung, A. Domingo. *J. Chem. Theory Comput.* **2017**, *13*, 537–553.

[365] R. J. Buenker, S. D. Peyerimhoff. *Theor. Chim. Acta* **1968**, *12*, 183–199.

[366] S. D. Peyerimhoff, R. J. Buenker. *Chem. Phys. Lett.* **1972**, *16*, 235–243.

[367] R. J. Buenker, S. D. Peyerimhoff. *Theor. Chim. Acta* **1974**, *35*, 33–58.

[368] H.-J. Werner, P. J. Knowles. *J. Chem. Phys.* **1988**, *89*, 5803–5814.

[369] P. J. Knowles, H.-J. Werner. *Chem. Phys. Lett.* **1988**, *145*, 514–522.

[370] P. J. Knowles, H.-J. Werner. *Theor. Chim. Acta* **1992**, *84*, 95–103.

[371] K. R. Shamasundar, G. Knizia, H.-J. Werner. *J. Chem. Phys.* **2011**, *135*, 054101.

[372] K. Sivalingam, M. Krupicka, A. A. Auer, F. Neese. *J. Chem. Phys.* **2016**, *145*, 054104.

[373] J. Miralles, O. Castell, R. Caballol, J.-P. Malrieu. *Chem. Phys.* **1993**, *172*, 33–43.

[374] J. Miralles, J.-P. Daudey, R. Caballol. *Chem. Phys. Lett.* **1992**, *198*, 555–562.

[375] O. Castell, J. Miralles, R. Caballol. *Chem. Phys.* **1994**, *179*, 377–384.

[376] P. A. M. Dirac. *Proc. Royal Soc. A* **1928**, *117*, 610–624.

[377] P. A. M. Dirac. *Proc. Royal Soc. A* **1928**, *118*, 351–361.

[378] K. G. Dyall, K. Fægri, Jr, *Introduction to Relativistic Quantum Chemistry*, Oxford University Press, Oxford, UK, **2007**.

[379] C. Chang, M. Pelissier, P. Durand. *Physica Scripta* **1986**, *34*, 394.

[380] E. van Lenthe, E. J. Baerends, J. G. Snijders. *J. Chem. Phys.* **1993**, *99*, 4597–4610.

[381] E. van Lenthe, E. J. Baerends, J. G. Snijders. *J. Chem. Phys.* **1994**, *101*, 9783–9792.

[382] E. van Lenthe, R. van Leeuwen, E. J. Baerends, J. G. Snijders. *Int. J. Quantum Chem.* **1996**, *57*, 281–293.

[383] M. Douglas, N. M. Kroll. *Ann. Phys.* **1974**, *82*, 89–155.

[384] B. A. Hess. *Phys. Rev. A* **1986**, *33*, 3742–3748.

[385] D. Peng, M. Reiher. *Theor. Chem. Acc.* **2012**, *131*, 1081.

[386] L. Visscher, E. van Lenthe. *Chem. Phys. Lett.* **1999**, *306*, 357–365.

[387] G. Breit. *Phys. Rev.* **1929**, *34*, 553–573.

[388] G. Breit. *Phys. Rev.* **1932**, *39*, 616–624.

[389] E. van Lenthe, J. G. Snijders, E. J. Baerends. *J. Chem. Phys.* **1996**, *105*, 6505–6516.

[390] K. G. Dyall, E. van Lenthe. *J. Chem. Phys.* **1999**, *111*, 1366–1372.

[391] P. H. T. Philipsen, E. van Lenthe, J. G. Snijders, E. J. Baerends. *Phys. Rev. B* **1997**, *56*, 13556–13562.

[392] C. van Wüllen. *J. Chem. Phys.* **1998**, *109*, 392–399.

[393] M. Reiher, A. Wolf. *J. Chem. Phys.* **2004**, *121*, 10945–10956.

[394] W. Kutzelnigg, W. Liu. *J. Chem. Phys.* **2005**, *123*, 241102.

[395] W. Kutzelnigg, W. Liu. *Mol. Phys.* **2006**, *104*, 2225–2240.

[396] W. Liu, W. Kutzelnigg. *J. Chem. Phys.* **2007**, *126*, 114107.

[397] W. Liu, D. Peng. *J. Chem. Phys.* **2006**, *125*, 044102.

[398] D. Peng, W. Liu, Y. Xiao, L. Cheng. *J. Chem. Phys.* **2007**, *127*, 104106.

[399] M. Iliaš, T. Saue. *J. Chem. Phys.* **2007**, *126*, 064102.

[400] K. G. Dyall. *J. Chem. Phys.* **1994**, *100*, 2118–2127.

[401] F. Neese. *J. Chem. Phys.* **2005**, *122*, 034107.

[402] B. A. Hess, C. M. Marian, U. Wahlgren, O. Gropen. *Chem. Phys. Lett.* **1996**, *251*, 365–371.

[403] A. Berning, M. Schweizer, H.-J. Werner, P. J. Knowles, P. Palmieri. *Mol. Phys.* **2000**, *98*, 1823–1833.

[404] O. Christiansen, J. Gauss, B. Schimmelpfennig. *Phys. Chem. Chem. Phys.* **2000**, *2*, 965–971.

[405] J. Olsen, M. R. Godefroid, P. Jönsson, P. A. Malmqvist, C. F. Fischer. *Phys. Rev. E* **1995**, *52*, 4499–4508.

[406] R. Maurice, R. Bastardis, C. de Graaf, N. Suaud, T. Mallah, N. Guihéry. *J. Chem. Theory Comput.* **2009**, *5*, 2977–2984.

[407] D. Reta, I. de P. R. Moreira, F. Illas. *J. Chem. Theory Comput.* **2016**, *12*, 3228–3235.

[408] C. J. Calzado, C. Angeli, D. Taratiel, R. Caballol, J.-P. Malrieu. *J. Chem. Phys.* **2009**, *131*, 044327.

[409] C. de Graaf, C. Sousa, I. de P. R. Moreira, F. Illas. *J. Phys. Chem. A* **2001**, *105*, 11371–11378.

[410] D. Muñoz, C. de Graaf, F. Illas. *J. Comp. Chem.* **2004**, *25*, 1234–1241.

[411] C. Angeli, C. J. Calzado. *J. Chem. Phys.* **2012**, *137*, 034104.

[412] N. Queralt, D. Taratiel, C. de Graaf, R. Caballol, R. Cimiraglia, C. Angeli. *J. Comp. Chem.* **2008**, *29*, 994–1003.

[413] M. Spivak, C. Angeli, C. J. Calzado, C. de Graaf. *J. Comp. Chem.* **2014**, *35*, 1665–1671.

[414] N. Suaud, R. Ruamps, N. Guihéry, J.-P. Malrieu. *J. Chem. Theory Comput.* **2012**, *8*, 4127–4137.

[415] N. Suaud, R. Ruamps, J.-P. Malrieu, N. Guihéry. *J. Phys. Chem. A* **2014**, *118*, 5876–5884.

[416] E. Giner, C. Angeli. *J. Chem. Phys.* **2016**, *144*, 104104.

[417] R. Ruamps, R. Maurice, C. de Graaf, N. Guihéry. *Inorg. Chem.* **2014**, *53*, 4508–4516.

[418] F. Ortu, J. Liu, M. Burton, J. M. Fowler, A. Formanuik, M.-E. Boulon, N. F. Chilton, D. P. Mills. *Inorg. Chem.* **2017**, *56*, 2496–2505.

[419] A. Landé. *Z. Phys.* **1921**, *5*, 231–241.

[420] D. A. Garanin, E. M. Chudnovsky. *Phys. Rev. B* **1997**, *56*, 11102–11118.

[421] M. N. Leuenberger, D. Loss. *Phys. Rev. B* **2000**, *61*, 1286–1302.

[422] V. Dohm, P. Fulde. *Z. Phys. B* **1975**, *21*, 369–379.

[423] F. Luis, M. J. Martínez-Pérez, O. Montero, E. Coronado, S. Cardona-Serra, C. Martí-Gastaldo, J. M. Clemente-Juan, J. Sesé, D. Drung, T. Schurig. *Phys. Rev. B* **2010**, *82*, 060403.

[424] P. Hohenberg, W. Kohn. *Phys. Rev.* **1964**, *136*, B864–B871.

[425] W. Kohn, L. J. Sham. *Phys. Rev.* **1965**, *140*, A1133–A1138.

[426] H. Eschrig, *The Fundamentals of Density Functional Theory 2nd ed.*, Eagle, Leipzig, Germany, **2003**.

[427] C. Fiolhais, F. Nogueira, M. Marques, *A Primer in density functional theory*, Springer, Berlin, Germany, **2003**.

[428] K. Capelle. *Braz. J. Phys.* **2006**, *36*, 1318–1343.

[429] E. Engel, R. M. Dreizler, *Density Functional Theory. An Advanced Course*, Springer, Berlin, Germany, **2011**.

[430] E. J. Baerends. *Phys. Rev. Lett.* **2001**, *87*, 133004.

[431] A. J. Cohen, P. Mori-Sánchez, W. Yang. *J. Chem. Phys.* **2008**, *129*, 121104.

[432] A. J. Cohen, P. Mori-Sánchez, W. Yang. *Chem. Rev.* **2012**, *112*, 289–320.

[433] H. S. Yu, S. L. Li, D. G. Truhlar. *J. Chem. Phys.* **2016**, *145*, 130901.

[434] D. S. Sholl, J. A. Steckel, *Density Functional Theory. A Practical Introduction*, Wiley, Hoboken, NJ, USA, **2009**.

[435] L. H. Thomas. *Math. Proc. Cambridge Philos. Soc.* **1927**, *23*, 542–548.

[436] E. Fermi. *Rend. Accad. Naz. Lincei* **1927**, *6*, 32.

[437] F. Bloch. *Z. Phys.* **1929**, *57*, 545–555.

[438] P. A. M. Dirac. *Math. Proc. Cambridge Philos. Soc.* **1930**, *26*, 376–385.

[439] M. Levy. *Proc. Natl. Acad. Sci. USA* **1979**, *76*, 6062–6065.

[440] M. Levy. *Phys. Rev. A* **1982**, *26*, 1200–1208.

[441] E. H. Lieb. *Int. J. Quantum Chem.* **1983**, *24*, 243–277.

[442] H. Englisch, R. Englisch. *Phys. Status Solidi B* **1984**, *123*, 711–721.

[443] H. Englisch, R. Englisch. *Phys. Status Solidi B* **1984**, *124*, 373–379.

[444] T. L. Gilbert. *Phys. Rev. B* **1975**, *12*, 2111–2120.

[445] E. Runge, E. K. U. Gross. *Phys. Rev. Lett.* **1984**, *52*, 997–1000.

[446] U. von Barth, L. Hedin. *J. Phys. C* **1972**, *5*, 1629.

[447] J. P. Perdew, A. Zunger. *Phys. Rev. B* **1981**, *23*, 5048–5079.

[448] C. R. Jacob, M. Reiher. *Int. J. Quantum Chem.* **2012**, *112*, 3661–3684.

[449] A. K. Rajagopal, J. Callaway. *Phys. Rev. B* **1973**, *7*, 1912–1919.

[450] C. Fonseca Guerra, J. G. Snijders, G. te Velde, E. J. Baerends. *Theor. Chem. Acc.* **1998**, *99*, 391–403.

[451] S. H. Vosko, L. Wilk, M. Nusair. *Can. J. Phys.* **1980**, *58*, 1200–1211.

[452] J. P. Perdew, W. Yue. *Phys. Rev. B* **1986**, *33*, 8800–8802.

[453] J. P. Perdew, J. A. Chevary, S. H. Vosko, K. A. Jackson, M. R. Pederson, D. J. Singh, C. Fiolhais. *Phys. Rev. B* **1992**, *46*, 6671–6687.

[454] J. P. Perdew, J. A. Chevary, S. H. Vosko, K. A. Jackson, M. R. Pederson, D. J. Singh, C. Fiolhais. *Phys. Rev. B* **1993**, *48*, 4978–4978.

[455] A. D. Becke. *Phys. Rev. A* **1988**, *38*, 3098–3100.

[456] J. P. Perdew, K. Burke, M. Ernzerhof. *Phys. Rev. Lett.* **1996**, *77*, 3865–3868.

[457] J. P. Perdew, K. Burke, M. Ernzerhof. *Phys. Rev. Lett.* **1997**, *78*, 1396–1396.

[458] J. P. Perdew. *Phys. Rev. B* **1986**, *33*, 8822–8824.

[459] J. P. Perdew. *Phys. Rev. B* **1986**, *34*, 7406–7406.

[460] C. Lee, W. Yang, R. G. Parr. *Phys. Rev. B* **1988**, *37*, 785–789.

[461] A. D. Becke. *J. Chem. Phys.* **1997**, *107*, 8554–8560.

[462] H. L. Schmider, A. D. Becke. *J. Chem. Phys.* **1998**, *108*, 9624–9631.

[463] F. A. Hamprecht, A. J. Cohen, D. J. Tozer, N. C. Handy. *J. Chem. Phys.* **1998**, *109*, 6264–6271.

[464] P. J. Wilson, T. J. Bradley, D. J. Tozer. *J. Chem. Phys.* **2001**, *115*, 9233–9242.

[465] A. D. Boese, N. L. Doltsinis, N. C. Handy, M. Sprik. *J. Chem. Phys.* **2000**, *112*, 1670–1678.

[466] A. D. Boese, N. C. Handy. *J. Chem. Phys.* **2001**, *114*, 5497–5503.

[467] A. D. Boese, N. C. Handy. *J. Chem. Phys.* **2002**, *116*, 9559–9569.

[468] A. D. Boese, J. M. L. Martin. *J. Chem. Phys.* **2004**, *121*, 3405–3416.

[469] J. Tao, J. P. Perdew, V. N. Staroverov, G. E. Scuseria. *Phys. Rev. Lett.* **2003**, *91*, 146401.

[470] V. N. Staroverov, G. E. Scuseria, J. Tao, J. P. Perdew. *J. Chem. Phys.* **2003**, *119*, 12129–12137.

[471] Y. Zhao, D. G. Truhlar. *J. Chem. Phys.* **2006**, *125*, 194101.

[472] Y. Zhao, D. Truhlar. *Theor. Chem. Acc.* **2008**, *120*, 215–241.

[473] R. Peverati, Y. Zhao, D. G. Truhlar. *J. Phys. Chem. Lett.* **2011**, *2*, 1991–1997.

[474] A. D. Becke. *J. Chem. Phys.* **1993**, *98*, 1372–1377.

[475] A. D. Becke. *J. Chem. Phys.* **1993**, *98*, 5648–5652.

[476] O. Gunnarsson, B. I. Lundqvist. *Phys. Rev. B* **1976**, *13*, 4274–4298.

[477] D. C. Langreth, J. P. Perdew. *Phys. Rev. B* **1977**, *15*, 2884–2901.

[478] J. P. Perdew, M. Ernzerhof, K. Burke. *J. Chem. Phys.* **1996**, *105*, 9982–9985.

[479] P. J. Stephens, F. J. Devlin, C. F. Chabalowski, M. J. Frisch. *J. Phys. Chem.* **1994**, *98*, 11623–11627.

[480] M. Ernzerhof, G. E. Scuseria. *J. Chem. Phys.* **1999**, *110*, 5029–5036.

[481] C. Adamo, V. Barone. *J. Chem. Phys.* **1999**, *110*, 6158–6170.

[482] A. D. Becke. *J. Chem. Phys.* **1996**, *104*, 1040–1046.

[483] Y. Zhao, N. E. Schultz, D. G. Truhlar. *J. Chem. Phys.* **2005**, *123*, 161103.

[484] Y. Zhao, N. E. Schultz, D. G. Truhlar. *J. Chem. Theory Comput.* **2006**, *2*, 364–382.

[485] Y. Zhao, D. G. Truhlar. *J. Phys. Chem. A* **2006**, *110*, 13126–13130.

[486] Y. Zhao, D. G. Truhlar. *J. Chem. Theory Comput.* **2008**, *4*, 1849–1868.

[487] R. Peverati, D. G. Truhlar. *J. Chem. Phys.* **2011**, *135*, 191102.

[488] R. A. Donnelly, R. G. Parr. *J. Chem. Phys.* **1978**, *69*, 4431–4439.

[489] T. Tsuneda, K. Hirao. *WIREs Comput. Mol. Sci.* **2014**, *4*, 375–390.

[490] A. Savin, H.-J. Flad. *Int. J. Quantum Chem.* **1995**, *56*, 327–332.

[491] A. Savin, *On degeneracy, near-degeneracy and density functional theory* in *Recent Developments and Applications of Modern Density Functional Theory*, Vol. 4 of *Theoretical and Computational Chemistry*, J. Seminario (Ed.), Elsevier, **1996**, pp. 327–357.

[492] T. Leininger, H. Stoll, H.-J. Werner, A. Savin. *Chem. Phys. Lett.* **1997**, *275*, 151–160.

[493] H. Iikura, T. Tsuneda, T. Yanai, K. Hirao. *J. Chem. Phys.* **2001**, *115*, 3540–3544.

[494] T. Körzdörfer, J. S. Sears, C. Sutton, J.-L. Brédas. *J. Chem. Phys.* **2011**, *135*, 204107.

[495] R. Baer, E. Livshits, U. Salzner. *Annu. Rev. Phys. Chem.* **2010**, *61*, 85–109.

[496] J. Autschbach, M. Srebro. *Acc. Chem. Res.* **2014**, *47*, 2592–2602.

[497] N. Kuritz, T. Stein, R. Baer, L. Kronik. *J. Chem. Theory Comput.* **2011**, *7*, 2408–2415.

[498] L. Kronik, T. Stein, S. Refaely-Abramson, R. Baer. *J. Chem. Theory Comput.* **2012**, *8*, 1515–1531.

[499] M. E. Foster, B. M. Wong. *J. Chem. Theory Comput.* **2012**, *8*, 2682–2687.

[500] A. Karolewski, L. Kronik, S. Kümmel. *J. Chem. Phys.* **2013**, *138*, 204115.

[501] Y. Akinaga, S. Ten-no. *Chem. Phys. Lett.* **2008**, *462*, 348–351.

[502] M. Seth, T. Ziegler. *J. Chem. Theory Comput.* **2012**, *8*, 901–907.

[503] M. Seth, T. Ziegler, M. Steinmetz, S. Grimme. *J. Chem. Theory Comput.* **2013**, *9*, 2286–2299.

[504] T. Yanai, D. P. Tew, N. C. Handy. *Chem. Phys. Lett.* **2004**, *393*, 51–57.

[505] J.-D. Chai, M. Head-Gordon. *J. Chem. Phys.* **2008**, *128*, 084106.

[506] R. Peverati, D. G. Truhlar. *J. Phys. Chem. Lett.* **2012**, *3*, 117–124.

[507] R. Peverati, D. G. Truhlar. *Phys. Chem. Chem. Phys.* **2012**, *14*, 13171–13174.

[508] R. Peverati, D. G. Truhlar. *J. Chem. Theory Comput.* **2012**, *8*, 2310–2319.

[509] H. S. Yu, X. He, D. G. Truhlar. *J. Chem. Theory Comput.* **2016**, *12*, 1280–1293.

[510] R. Peverati, D. G. Truhlar. *J. Phys. Chem. Lett.* **2011**, *2*, 2810–2817.

[511] R. Peverati, D. G. Truhlar. *Phys. Chem. Chem. Phys.* **2012**, *14*, 16187–16191.

[512] H. S. Yu, X. He, S. L. Li, D. G. Truhlar. *Chem. Sci.* **2016**, *7*, 5032–5051.

[513] J. Heyd, G. E. Scuseria, M. Ernzerhof. *J. Chem. Phys.* **2003**, *118*, 8207–8215.

[514] J. Heyd, G. E. Scuseria, M. Ernzerhof. *J. Chem. Phys.* **2006**, *124*, 219906.

[515] T. M. Henderson, A. F. Izmaylov, G. Scalmani, G. E. Scuseria. *J. Chem. Phys.* **2009**, *131*, 044108.

[516] O. A. Vydrov, G. E. Scuseria. *J. Chem. Phys.* **2006**, *125*, 234109.

[517] O. A. Vydrov, J. Heyd, A. V. Krukau, G. E. Scuseria. *J. Chem. Phys.* **2006**, *125*, 074106.

[518] O. A. Vydrov, G. E. Scuseria, J. P. Perdew. *J. Chem. Phys.* **2007**, *126*, 154109.

[519] J. Heyd, G. E. Scuseria. *J. Chem. Phys.* **2004**, *120*, 7274–7280.

[520] J. Heyd, G. E. Scuseria. *J. Chem. Phys.* **2004**, *121*, 1187–1192.

[521] J. Heyd, J. E. Peralta, G. E. Scuseria, R. L. Martin. *J. Chem. Phys.* **2005**, *123*, 174101.

[522] A. F. Izmaylov, G. E. Scuseria, M. J. Frisch. *J. Chem. Phys.* **2006**, *125*, 104103.

[523] A. V. Krukau, O. A. Vydrov, A. F. Izmaylov, G. E. Scuseria. *J. Chem. Phys.* **2006**, *125*, 224106.

[524] J. Gräfenstein, D. Cremer. *Phys. Chem. Chem. Phys.* **2000**, *2*, 2091–2103.

[525] Y. He, J. Gräfenstein, E. Kraka, D. Cremer. *Mol. Phys.* **2000**, *98*, 1639–1658.

[526] D. Cremer. *Mol. Phys.* **2001**, *99*, 1899–1940.

[527] J. Gräfenstein, E. Kraka, M. Filatov, D. Cremer. *Int. J. Mol. Sci.* **2002**, *3*, 360–394.

[528] D. Cremer, M. Filatov, V. Polo, E. Kraka, S. Shaik. *Int. J. Mol. Sci.* **2002**, *3*, 604–638.

[529] V. Polo, E. Kraka, D. Cremer. *Mol. Phys.* **2002**, *100*, 1771–1790.

[530] V. Polo, J. Gräfenstein, E. Kraka, D. Cremer. *Chem. Phys. Lett.* **2002**, *352*, 469–478.

[531] V. Polo, E. Kraka, D. Cremer. *Theor. Chem. Acc.* **2002**, *107*, 291–303.

[532] V. Polo, J. Gräfenstein, E. Kraka, D. Cremer. *Theor. Chem. Acc.* **2003**, *109*, 22–35.

[533] J. Gräfenstein, D. Cremer. *Theor. Chem. Acc.* **2009**, *123*, 171–182.

[534] M. Fuchs, Y.-M. Niquet, X. Gonze, K. Burke. *J. Chem. Phys.* **2005**, *122*, 094116.

[535] T. M. Henderson, G. E. Scuseria. *Mol. Phys.* **2010**, *108*, 2511–2517.

[536] A. Hesselmann, A. Görling. *Phys. Rev. Lett.* **2011**, *106*, 093001.

[537] G. P. Chen, V. K. Voora, M. M. Agee, S. G. Balasubramani, F. Furche. *Annu. Rev. Phys. Chem.* **2017**, *68*, 421–445.

[538] M. Filatov, S. Shaik. *Chem. Phys. Lett.* **1999**, *304*, 429–437.

[539] M. Filatov, S. Shaik. *J. Phys. Chem. A* **1999**, *103*, 8885–8889.

[540] M. Filatov, S. Shaik. *J. Phys. Chem. A* **2000**, *104*, 6628–6636.

[541] M. Filatov. *WIREs Comput. Mol. Sci.* **2015**, *5*, 146–167.

[542] M. Filatov, M. Huix-Rotllant, I. Burghardt. *J. Chem. Phys.* **2015**, *142*, 184104.

[543] I. de P. R. Moreira, R. Costa, M. Filatov, F. Illas. *J. Chem. Theory Comput.* **2007**, *3*, 764–774.

[544] A. D. Becke. *J. Chem. Phys.* **2003**, *119*, 2972–2977.

[545] A. D. Becke. *J. Chem. Phys.* **2005**, *122*, 064101.

[546] A. D. Becke, E. R. Johnson. *J. Chem. Phys.* **2007**, *127*, 124108.

[547] A. D. Becke. *J. Chem. Phys.* **2013**, *138*, 074109.

[548] A. D. Becke. *Mol. Phys.* **2015**, *113*, 1884–1889.

[549] E. Proynov, Y. Shao, J. Kong. *Chem. Phys. Lett.* **2010**, *493*, 381–385.

[550] E. Proynov, F. Liu, Y. Shao, J. Kong. *J. Chem. Phys.* **2012**, *136*, 034102.

[551] E. Proynov, F. Liu, J. Kong. *Chem. Phys. Lett.* **2012**, *525–526*, 150–152.

[552] J. Kong, E. Proynov. *J. Chem. Theory Comput.* **2016**, *12*, 133–143.

[553] R. Valero, F. Illas, D. G. Truhlar. *J. Chem. Theory Comput.* **2011**, *7*, 3523–3531.

[554] H. Zhekova, M. Seth, T. Ziegler. *J. Chem. Theory Comput.* **2011**, *7*, 1858–1866.

[555] H. R. Zhekova, M. Seth, T. Ziegler. *J. Chem. Phys.* **2011**, *135*, 184105.

[556] I. Seidu, H. R. Zhekova, M. Seth, T. Ziegler. *J. Phys. Chem. A* **2012**, *116*, 2268–2277.

[557] I. Rudra, Q. Wu, T. van Voorhis. *J. Chem. Phys.* **2006**, *124*, 024103.

[558] J. J. Phillips, J. E. Peralta. *J. Chem. Phys.* **2011**, *135*, 184108.

[559] J. E. Peralta, V. Barone. *J. Chem. Phys.* **2008**, *129*, 194107.

[560] J. J. Phillips, J. E. Peralta. *J. Chem. Phys.* **2013**, *138*, 174115.

[561] J. J. Phillips, J. E. Peralta, G. Christou. *J. Chem. Theory Comput.* **2013**, *9*, 5585–5589.

[562] J. J. Phillips, J. E. Peralta. *J. Phys. Chem. A* **2014**, *118*, 5841–5847.

[563] R. P. Joshi, J. J. Phillips, J. E. Peralta. *J. Chem. Theory Comput.* **2016**.

[564] J. E. Peralta, O. Hod, G. E. Scuseria. *J. Chem. Theory Comput.* **2015**, *11*, 3661–3668.

[565] T. Steenbock, J. Tasche, A. I. Lichtenstein, C. Herrmann. *J. Chem. Theory Comput.* **2015**, *11*, 5651–5664.

[566] J. C. Slater. *Phys. Rev.* **1951**, *81*, 385–390.

[567] J. J. Girerd, Y. Journaux, O. Kahn. *Chem. Phys. Lett.* **1981**, *82*, 534–538.

[568] F. Neese. *J. Phys. Chem. Solids* **2004**, *65*, 781–785.

[569] Y. Kizashi, F. Hiroaki, F. Takayuki. *Chem. Lett.* **1986**, *15*, 625–628.

[570] K. Yamaguchi, T. Tsunekawa, Y. Toyoda, T. Fueno. *Chem. Phys. Lett.* **1988**, *143*, 371–376.

[571] K. Yamaguchi, F. Jensen, A. Dorigo, K. Houk. *Chem. Phys. Lett.* **1988**, *149*, 537–542.

[572] T. Soda, Y. Kitagawa, T. Onishi, Y. Takano, Y. Shigeta, H. Nagao, Y. Yoshioka, K. Yamaguchi. *Chem. Phys. Lett.* **2000**, *319*, 223–230.

[573] N. Ferre, N. Guihery, J.-P. Malrieu. *Phys. Chem. Chem. Phys.* **2015**, *17*, 14375–14382.

[574] E. Coulaud, N. Guihéry, J.-P. Malrieu, D. Hagebaum-Reignier, D. Siri, N. Ferré. *J. Chem. Phys.* **2012**, *137*, 114106.

[575] E. Coulaud, J.-P. Malrieu, N. Guihéry, N. Ferré. *J. Chem. Theory Comput.* **2013**, *9*, 3429–3436.

[576] C. Albonico, A. Bencini. *Inorg. Chem.* **1988**, *27*, 1934–1940.

[577] P. K. Ross, E. I. Solomon. *J. Am. Chem. Soc.* **1991**, *113*, 3246–3259.

[578] E. Ruiz, P. Alemany, S. Alvarez, J. Cano. *J. Am. Chem. Soc.* **1997**, *119*, 1297–1303.

[579] E. Ruiz, P. Alemany, S. Alvarez, J. Cano. *Inorg. Chem.* **1997**, *36*, 3683–3688.

[580] E. Ruiz, J. Cano, S. Alvarez, P. Alemany. *J. Am. Chem. Soc.* **1998**, *120*, 11122–11129.

[581] F. Fabrizi de Biani, E. Ruiz, J. Cano, J. J. Novoa, S. Alvarez. *Inorg. Chem.* **2000**, *39*, 3221–3229.

[582] M. Lundberg, P. E. M. Siegbahn. *J. Chem. Phys.* **2005**, *122*, 224103.

[583] P. Mori-Sánchez, A. J. Cohen, W. Yang. *J. Chem. Phys.* **2006**, *125*, 201102.

[584] P. Mori-Sánchez, A. J. Cohen, W. Yang. *Phys. Rev. Lett.* **2008**, *100*, 146401.

[585] E. R. Johnson, P. Mori-Sánchez, A. J. Cohen, W. Yang. *J. Chem. Phys.* **2008**, *129*, 204112.

[586] C. Adamo, V. Barone, A. Bencini, R. Broer, M. Filatov, N. M. Harrison, F. Illas, J. P. Malrieu, I. de P. R.Moreira. *J. Chem. Phys.* **2006**, *124*, 107101.

[587] J. P. Perdew, A. Savin, K. Burke. *Phys. Rev. A* **1995**, *51*, 4531–4541.

[588] F. Illas, R. L. Martin. *J. Chem. Phys.* **1998**, *108*, 2519–2527.

[589] P. Reinhardt, M. P. Habas, R. Dovesi, I. de P. R. Moreira, F. Illas. *Phys. Rev. B* **1999**, *59*, 1016–1023.

[590] D. Dai, M.-H. Whangbo. *J. Chem. Phys.* **2001**, *114*, 2887–2893.

[591] D. Dai, M.-H. Whangbo. *J. Chem. Phys.* **2003**, *118*, 29–39.

[592] R. Costa, R. Valero, D. R. Mañeru, I. de P. R. Moreira, F. Illas. *J. Chem. Theory Comput.* **2015**, *11*, 1006–1019.

[593] E. Ruiz. *Chem. Phys. Lett.* **2008**, *460*, 336–338.

[594] E. Ruiz. *J. Comp. Chem.* **2011**, *32*, 1998–2004.

[595] R. Valero, R. Costa, I. de P. R. Moreira, D. G. Truhlar, F. Illas. *J. Chem. Phys.* **2008**, *128*, 114103.

[596] P. Rivero, I. de P. R. Moreira, F. Illas, G. E. Scuseria. *J. Chem. Phys.* **2008**, *129*, 184110.

[597] N. Wannarit, C. Pakawatchai, I. Mutikainen, R. Costa, I. de P. R. Moreira, S. Youngme, F. Illas. *Phys. Chem. Chem. Phys.* **2013**, *15*, 1966–1975.

[598] D. R. Mañeru, A. K. Pal, I. de P. R. Moreira, S. N. Datta, F. Illas. *J. Chem. Theory Comput.* **2014**, *10*, 335–345.

[599] D. R. Mañeru, R. Costa, M. G. Márquez, I. de P. R. Moreira, F. Illas. *J. Chem. Theory Comput.* **2015**, *11*, 3650–3660.

[600] S. Zein, M. Poor Kalhor, L. F. Chibotaru, H. Chermette. *J. Chem. Phys.* **2009**, *131*, 224316.

[601] T. Schwabe, S. Grimme. *J. Phys. Chem. Lett.* **2010**, *1*, 1201–1204.

[602] J. E. Peralta, J. I. Melo. *J. Chem. Theory Comput.* **2010**, *6*, 1894–1899.

[603] N. A. G. Bandeira, B. L. Guennic. *J. Phys. Chem. A* **2012**, *116*, 3465–3473.

[604] T. Saito, A. Ito, T. Watanabe, T. Kawakami, M. Okumura, K. Yamaguchi. *Chem. Phys. Lett.* **2012**, *542*, 19–25.

[605] J. L. Lewin, D. E. Heppner, C. J. Cramer. *J. Biol. Inorg. Chem.* **2007**, *12*, 1221–1234.

[606] P. Comba, S. Hausberg, B. Martin. *J. Phys. Chem. A* **2009**, *113*, 6751–6755.

[607] C. Adamo, V. Barone, A. Bencini, F. Totti, I. Ciofini. *Inorg. Chem.* **1999**, *38*, 1996–2004.

[608] S. Grimme. *J. Chem. Phys.* **2006**, *124*, 034108.

[609] J. J. Phillips, J. E. Peralta. *J. Chem. Phys.* **2011**, *134*, 034108.

[610] I. de P. R. Moreira, F. Illas, R. L. Martin. *Phys. Rev. B* **2002**, *65*, 155102.

[611] X. Feng, N. M. Harrison. *Phys. Rev. B* **2004**, *70*, 092402.

[612] D. Cho, K. C. Ko, J. Y. Lee. *Int. J. Quantum Chem.* **2015**.

[613] B. Sandhoefer, F. Neese. *J. Chem. Phys.* **2012**, *137*, 094102.

[614] E. M. V. Kessler, S. Schmitt, C. van Wüllen. *J. Chem. Phys.* **2013**, *139*, 184110.

[615] A. Kubica, J. Kowalewski, D. Kruk, M. Odelius. *J. Chem. Phys.* **2013**, *138*, 064304.

[616] S. Khan, A. Kubica-Misztal, D. Kruk, J. Kowalewski, M. Odelius. *J. Chem. Phys.* **2015**, *142*, 034304.

[617] M. Roemelt, F. Neese. *J. Phys. Chem. A* **2013**, *117*, 3069–3083.

[618] M. Roemelt, D. Maganas, S. DeBeer, F. Neese. *J. Chem. Phys.* **2013**, *138*, 204101.

[619] D. Maganas, M. Roemelt, T. Weyhermuller, R. Blume, M. Havecker, A. Knop-Gericke, S. DeBeer, R. Schlogl, F. Neese. *Phys. Chem. Chem. Phys.* **2014**, *16*, 264–276.

[620] M. J. Frisch, G. W. Trucks, H. B. Schlegel, G. E. Scuseria, M. A. Robb, J. R. Cheeseman, G. Scalmani, V. Barone, B. Mennucci, G. A. Petersson, H. Nakatsuji, M. Caricato, X. Li, H. P. Hratchian, A. F. Izmaylov, J. Bloino, G. Zheng, J. L. Sonnenberg, M. Hada, M. Ehara, K. Toyota, R. Fukuda, J. Hasegawa, M. Ishida, T. Nakajima, Y. Honda, O. Kitao, H. Nakai, T. Vreven, J. A. Montgomery, Jr., J. E. Peralta, F. Ogliaro, M. Bearpark, J. J. Heyd, E. Brothers, K. N. Kudin, V. N. Staroverov, R. Kobayashi, J. Normand, K. Raghavachari, A. Rendell, J. C. Burant, S. S. Iyengar, J. Tomasi, M. Cossi, N. Rega, J. M. Millam, M. Klene, J. E. Knox, J. B. Cross, V. Bakken, C. Adamo, J. Jaramillo, R. Gomperts, R. E. Stratmann, O. Yazyev, A. J. Austin, R. Cammi, C. Pomelli, J. W. Ochterski, R. L. Martin, K. Morokuma, V. G. Zakrzewski, G. A. Voth, P. Salvador, J. J. Dannenberg, S. Dapprich, A. D. Daniels, Ã. Farkas, J. B. Foresman, J. V. Ortiz, J. Cioslowski, D. J. Fox, *Gaussian09 Revision D.01*, **2009**, Gaussian Inc., Wallingford, CT, USA.

[621] A. Schäfer, C. Huber, R. Ahlrichs. *J. Chem. Phys.* **1994**, *100*, 5829–5835.

[622] R. Seeger, J. A. Pople. *J. Chem. Phys.* **1977**, *66*, 3045–3050.

[623] R. Bauernschmitt, R. Ahlrichs. *J. Chem. Phys.* **1996**, *104*, 9047–9052.

[624] D. A. Pantazis, X.-Y. Chen, C. R. Landis, F. Neese. *J. Chem. Theory Comput.* **2008**, *4*, 908–919.

[625] D. Aravena, F. Neese, D. A. Pantazis. *J. Chem. Theory Comput.* **2016**, *12*, 1148–1156.

[626] F. Weigend, R. Ahlrichs. *Phys. Chem. Chem. Phys.* **2005**, *7*, 3297–3305.

[627] D. A. Pantazis, F. Neese. *J. Chem. Theory Comput.* **2009**, *5*, 2229–2238.

[628] J.-D. Chai, M. Head-Gordon. *Phys. Chem. Chem. Phys.* **2008**, *10*, 6615–6620.

[629] S. Grimme, J. Antony, S. Ehrlich, H. Krieg. *J. Chem. Phys.* **2010**, *132*, 154104.

[630] S. Grimme, S. Ehrlich, L. Goerigk. *J. Comp. Chem.* **2011**, *32*, 1456–1465.

[631] S. F. Boys, F. Bernardi. *Mol. Phys.* **1970**, *19*, 553–566.

[632] C. Riplinger, F. Neese. *J. Chem. Phys.* **2013**, *138*, 034106.

[633] C. Riplinger, B. Sandhoefer, A. Hansen, F. Neese. *J. Chem. Phys.* **2013**, *139*, 134101.

[634] M. Saitow, U. Becker, C. Riplinger, E. F. Valeev, F. Neese. *J. Chem. Phys.* **2017**, *146*, 164105.

[635] C. Riplinger, P. Pinski, U. Becker, E. F. Valeev, F. Neese. *J. Chem. Phys.* **2016**, *144*, 024109.

[636] Y. Guo, C. Riplinger, U. Becker, D. G. Liakos, Y. Minenkov, L. Cavallo, F. Neese. *J. Chem. Phys.* **2018**, *148*, 011101.

[637] C. Edmiston, M. Krauss. *J. Chem. Phys.* **1965**, *42*, 1119–1120.

[638] C. Edmiston, M. Krauss. *J. Chem. Phys.* **1966**, *45*, 1833–1839.

[639] P. Pulay. *Chem. Phys. Lett.* **1983**, *100*, 151–154.

[640] D. G. Liakos, F. Neese. *J. Chem. Theory Comput.* **2015**, *11*, 4054–4063.

[641] D. G. Liakos, M. Sparta, M. K. Kesharwani, J. M. L. Martin, F. Neese. *J. Chem. Theory Comput.* **2015**, *11*, 1525–1539.

[642] D. G. Liakos, F. Neese. *J. Chem. Theory Comput.* **2015**, *11*, 2137–2143.

[643] H. M. Blatter, H. Lukaszewski. *Tetrahedron Lett.* **1968**, *9*, 2701–2705.

[644] I. S. Morgan, A. Peuronen, M. M. Hänninen, R. W. Reed, R. Clérac, H. M. Tuononen. *Inorg. Chem.* **2014**, *53*, 33–35.

[645] C. Coulon, R. Clérac, W. Wernsdorfer, T. Colin, H. Miyasaka. *Phys. Rev. Lett.* **2009**, *102*, 167204.

[646] H. Miyasaka, K. Takayama, A. Saitoh, S. Furukawa, M. Yamashita, R. Clérac. *Chem. Eur. J.* **2010**, *16*, 3656–3662.

[647] I. Bhowmick, E. A. Hillard, P. Dechambenoit, C. Coulon, T. D. Harris, R. Clérac. *Chem. Commun.* **2012**, *48*, 9717–9719.

[648] J. Long, F. Habib, P.-H. Lin, I. Korobkov, G. Enright, L. Ungur, W. Wernsdorfer, L. F. Chibotaru, M. Murugesu. *J. Am. Chem. Soc.* **2011**, *133*, 5319–5328.

[649] V. Vieru, L. Ungur, L. F. Chibotaru. *J. Phys. Chem. Lett.* **2013**, *4*, 3565–3569.

[650] Y.-Q. Zhang, C.-L. Luo, B.-W. Wang, S. Gao. *J. Phys. Chem. A* **2013**, *117*, 10873–10880.

[651] H. Bürger, U. Wannagat. *Monatsh. Chem.* **1963**, *94*, 1007–1012.

[652] H. Bürger, U. Wannagat. *Monatsh. Chem.* **1964**, *95*, 1099–1102.

[653] R. A. Andersen, K. Fægri, J. C. Green, A. Haaland, M. F. Lappert, W. P. Leung, K. Rypdal. *Inorg. Chem.* **1988**, *27*, 1782–1786.

[654] A. M. Bryan, G. J. Long, F. Grandjean, P. P. Power. *Inorg. Chem.* **2013**, *52*, 12152–12160.

[655] K. Chakarawet, P. C. Bunting, J. R. Long. *J. Am. Chem. Soc.* **2018**, *in press*.

[656] D. F. Evans. *J. Chem. Soc.* **1959**, 2003–2005.

[657] S. Brehmer, H.-J. Mikeska, M. Müller, N. Nagaosa, S. Uchida. *Phys. Rev. B* **1999**, *60*, 329–334.

[658] M. Matsuda, K. Katsumata, R. S. Eccleston, S. Brehmer, H.-J. Mikeska. *Phys. Rev. B* **2000**, *62*, 8903–8908.

[659] C. Kollmar, O. Kahn. *Acc. Chem. Res.* **1993**, *26*, 259–265.

[660] K. Yoshizawa, R. Hoffmann. *J. Am. Chem. Soc.* **1995**, *117*, 6921–6926.

[661] O. Kahn, P. Tola, J. Galy, H. Coudanne. *J. Am. Chem. Soc.* **1978**, *100*, 3931–3933.

[662] V. Boekelheide, C. E. Larrabee. *J. Am. Chem. Soc.* **1950**, *72*, 1245–1249.

[663] D. H. Reid. *Chem. Ind. (London)* **1956**, 1504–1505.

[664] D. H. Reid. *Tetrahedron* **1958**, *3*, 339–352.

[665] D. H. Reid. *Q. Rev. Chem. Soc.* **1965**, *19*, 274–302.

[666] Y. Morita, S. Suzuki, K. Sato, T. Takui. *Nat. Chem.* **2011**, *3*, 197–204.

[667] Y. Morita, S. Nishida, *Phenalenyls, Cyclopentadienyls, and Other Carbon-Centered Radicals* in *Stable Radicals*, R. G. Hicks (Ed.), Wiley, Chichester, UK, **2010**, pp. 81–145.

[668] K. Goto, T. Kubo, K. Yamamoto, K. Nakasuji, K. Sato, D. Shiomi, T. Takui, M. Kubota, T. Kobayashi, K. Yakusi, J. Ouyang. *J. Am. Chem. Soc.* **1999**, *121*, 1619–1620.

[669] K. Fukui, K. Sato, D. Shiomi, T. Takui, K. Itoh, K. Gotoh, T. Kubo, K. Yamamoto, K. Nakasuji, A. Naito. *Synth. Met.* **1999**, *103*, 2257–2258.

[670] K. Fukui, K. Sato, D. Shiomi, T. Takui, K. Itoh, T. Kubo, K. Gotoh, K. Yamamoto, K. Nakasuji, A. Naito. *Mol. Cryst. Liq. Cryst.* **1999**, *334*, 49–58.

[671] Y. Morita, T. Aoki, K. Fukui, S. Nakazawa, K. Tamaki, S. Suzuki, A. Fuyuhiro, K. Yamamoto, K. Sato, D. Shiomi, A. Naito, T. Takui, K. Nakasuji. *Angew. Chem. Int. Ed.* **2002**, *41*, 1793–1796.

[672] Y. Takano, T. Taniguchi, H. Isobe, T. Kubo, Y. Morita, K. Yamamoto, K. Nakasuji, T. Takui, K. Yamaguchi. *J. Am. Chem. Soc.* **2002**, *124*, 11122–11130.

[673] Y. Takano, T. Taniguchi, H. Isobe, T. Kubo, Y. Morita, K. Yamamoto, K. Nakasuji, T. Takui, K. Yamaguchi. *Chem. Phys. Lett.* **2002**, *358*, 17–23.

[674] T. Ukai, K. Nakata, S. Yamanaka, T. Kubo, Y. Morita, T. Takada, K. Yamaguchi. *Polyhedron* **2007**, *26*, 2313–2319.

[675] D. Small, V. Zaitsev, Y. Jung, S. V. Rosokha, M. Head-Gordon, J. K. Kochi. *J. Am. Chem. Soc.* **2004**, *126*, 13850–13858.

[676] S. Suzuki, Y. Morita, K. Fukui, K. Sato, D. Shiomi, T. Takui, K. Nakasuji. *J. Am. Chem. Soc.* **2006**, *128*, 2530–2531.

[677] J. Huang, M. Kertesz. *J. Phys. Chem. A* **2007**, *111*, 6304–6315.

[678] Y.-H. Tian, M. Kertesz. *J. Am. Chem. Soc.* **2010**, *132*, 10648–10649.

[679] Y.-H. Tian, J. Huang, M. Kertesz. *Phys. Chem. Chem. Phys.* **2010**, *12*, 5084–5093.

[680] B. Kolb, M. Kertesz, T. Thonhauser. *J. Phys. Chem. A* **2013**, *117*, 3642–3649.

[681] Z.-H. Cui, H. Lischka, H. Z. Beneberu, M. Kertesz. *J. Am. Chem. Soc.* **2014**, *136*, 5539–5542.

[682] Z. Mou, K. Uchida, T. Kubo, M. Kertesz. *J. Am. Chem. Soc.* **2014**, *136*, 18009–18022.

[683] F. Mota, J. S. Miller, J. J. Novoa. *J. Am. Chem. Soc.* **2009**, *131*, 7699–7707.

[684] K. Uchida, Z. Mou, M. Kertesz, T. Kubo. *J. Am. Chem. Soc.* **2016**, *138*, 4665–4672.

[685] R.-L. Zhong, H.-L. Xu, Z.-R. Li. *J. Chem. Phys.* **2016**, *145*, 054304.

[686] Y. Morita, T. Ohba, N. Haneda, S. Maki, J. Kawai, K. Hatanaka, K. Sato, D. Shiomi, T. Takui, K. Nakasuji. *J. Am. Chem. Soc.* **2000**, *122*, 4825–4826.

[687] S. Nishida, J. Kawai, M. Moriguchi, T. Ohba, N. Haneda, K. Fukui, A. Fuyuhiro, D. Shiomi, K. Sato, T. Takui, K. Nakasuji, Y. Morita. *Chem. Eur. J.* **2013**, *19*, 11904–11915.

[688] K. Uchida, Y. Hirao, H. Kurata, T. Kubo, S. Hatano, K. Inoue. *Chem. Asian J.* **2014**, *9*, 1823–1829.

[689] Y.-C. Chen, J.-L. Liu, W. Wernsdorfer, D. Liu, L. F. Chibotaru, X.-M. Chen, M.-L. Tong. *Angew. Chem. Int. Ed.* **2017**, *56*, 4996–5000.

[690] N. F. Chilton, C. A. P. Goodwin, D. P. Mills, R. E. P. Winpenny. *Chem. Commun.* **2015**, *51*, 101–103.

[691] K. L. M. Harriman, J. L. Brosmer, L. Ungur, P. L. Diaconescu, M. Murugesu. *J. Am. Chem. Soc.* **2017**, *139*, 1420–1423.

[692] L. Norel, L. E. Darago, B. Le Guennic, K. Chakarawet, M. C. Gonzalez, J. H. Olshansky, S. Rigaut, J. R. Long. *Angew. Chem. Int. Ed.* **2018**, *in press*.

[693] P. Zhang, L. Zhang, C. Wang, S. Xue, S.-Y. Lin, J. Tang. *J. Am. Chem. Soc.* **2014**, *136*, 4484–4487.

[694] S. K. Singh, T. Gupta, G. Rajaraman. *Inorg. Chem.* **2014**, *53*, 10835–10845.

[695] S. K. Singh, B. Pandey, G. Velmurugan, G. Rajaraman. *Dalton Trans.* **2017**, *46*, 11913–11924.

[696] A. J. Brown, D. Pinkowicz, M. R. Saber, K. R. Dunbar. *Angew. Chem. Int. Ed.* **2015**, *54*, 5864–5868.

[697] P.-O. Widmark, P.-Å. Malmqvist, B. O. Roos. *Theor. Chim. Acta* **1990**, *77*, 291–306.

[698] B. O. Roos, R. Lindh, P.-Å. Malmqvist, V. Veryazov, , P.-O. Widmark. *J. Phys. Chem. A* **2004**, *108*, 2851–2858.

[699] B. O. Roos, R. Lindh, P.-Å. Malmqvist, V. Veryazov, P.-O. Widmark, A. C. Borin. *J. Phys. Chem. A* **2008**, *112*, 11431–11435.

[700] A. Schäfer, H. Horn, R. Ahlrichs. *J. Chem. Phys.* **1992**, *97*, 2571–2577.

[701] S. Stoll, A. Schweiger. *J. Magn. Reson.* **2006**, *178*, 42–55.

[702] *Matlab, R2015a*, **2015**, The MathWorks, Inc., Natick, MA, USA.

[703] R. Layfield, J. J. McDouall, S. Sulway, F. Tuna, D. Collison, R. E. Winpenny. *Chem. Eur. J.* **2010**, *16*, 4442–4446.

[704] T. Pugh, F. Tuna, L. Ungur, D. Collison, E. J. L. McInnes, L. F. Chibotaru, R. A. Layfield. *Nat. Commun.* **2015**, *6*, 7492.

[705] T. Pugh, N. F. Chilton, R. A. Layfield. *Angew. Chem. Int. Ed.* **2016**, *55*, 11082–11085.

[706] T. Pugh, V. Vieru, L. F. Chibotaru, R. A. Layfield. *Chem. Sci.* **2016**, *7*, 2128–2137.

[707] T. Pugh, N. F. Chilton, R. A. Layfield. *Chem. Sci.* **2017**, *8*, 2073–2080.

[708] S. Demir, J. M. Zadrozny, J. R. Long. *Chem. Eur. J.* **2014**, *20*, 9524–9529.

[709] S. Demir, M. D. Boshart, J. F. Corbey, D. H. Woen, M. I. Gonzalez, J. W. Ziller, K. R. Meihaus, J. R. Long, W. J. Evans. *Inorg. Chem.* **2017**, *56*, 15049–15056.

[710] C. A. P. Goodwin, D. Reta, F. Ortu, N. F. Chilton, D. P. Mills. *J. Am. Chem. Soc.* **2017**, *139*, 18714–18724.

[711] P.-H. Lin, T. Burchell, R. Clérac, M. Murugesu. *Angew. Chem. Int. Ed.* **2008**, *47*, 8848–8851.

[712] P.-H. Lin, T. Burchell, L. Ungur, L. Chibotaru, W. Wernsdorfer, M. Murugesu. *Angew. Chem. Int. Ed.* **2009**, *48*, 9489–9492.

[713] I. Hewitt, J. Tang, N. Madhu, C. Anson, Y. Lan, J. Luzon, M. Etienne, R. Sessoli, A. Powell. *Angew. Chem. Int. Ed.* **2010**, *49*, 6352–6356.

[714] R. J. Blagg, C. A. Muryn, E. J. L. McInnes, F. Tuna, R. E. P. Winpenny. *Angew. Chem. Int. Ed.* **2011**, *50*, 6530–6533.

[715] J. Tang, P. Zhang, *Polynuclear Lanthanide Single Molecule Magnets* in *Lanthanides and Actinides in Molecular Magnetism*, R. A. Layfield, M. Murugesu (Eds.), Wiley-VHC, Weinheim, Germany, **2015**, pp. 61–88.

[716] S. Demir, M. I. Gonzalez, L. E. Darago, W. J. Evans, J. R. Long. *Nat. Commun.* **2017**, *8*, 2144.

[717] S. Demir, J. M. Zadrozny, M. Nippe, J. R. Long. *J. Am. Chem. Soc.* **2012**, *134*, 18546–18549.

[718] S. Demir, M. Nippe, M. I. Gonzalez, J. R. Long. *Chem. Sci.* **2014**, *5*, 4701–4711.

[719] C. A. Gould, L. E. Darago, M. I. Gonzalez, S. Demir, J. R. Long. *Angew. Chem.* **2017**, *129*, 10237–10241.

[720] F.-S. Guo, R. A. Layfield. *Chem. Commun.* **2017**, *53*, 3130–3133.

[721] B. S. Dolinar, S. Gómez-Coca, D. I. Alexandropoulos, K. R. Dunbar. *Chem. Commun.* **2017**, *53*, 2283–2286.

[722] B. S. Dolinar, D. I. Alexandropoulos, K. R. Vignesh, T. James, K. R. Dunbar. *J. Am. Chem. Soc.* **2018**, *140*, 908–911.

[723] P. Zhang, M. Perfetti, M. Kern, P. P. Hallmen, L. Ungur, S. Lenz, M. R. Ringenberg, W. Frey, H. Stoll, G. Rauhut, J. van Slageren. *Chem. Sci.* **2018**, *9*, 1221–1230.

[724] Y.-N. Guo, G.-F. Xu, W. Wernsdorfer, L. Ungur, Y. Guo, J. Tang, H.-J. Zhang, L. F. Chibotaru, A. K. Powell. *J. Am. Chem. Soc.* **2011**, *133*, 11948–11951.

[725] Q. Chen, F. Ma, Y.-S. Meng, H.-L. Sun, Y.-Q. Zhang, S. Gao. *Inorg. Chem.* **2016**, *55*, 12904–12911.

[726] J. Zhao, X. Huang, P. Jin, Z. Chen. *Coord. Chem. Rev.* **2015**, *289–290*, 315–340.

[727] A. A. Popov, S. Yang, L. Dunsch. *Chem. Rev.* **2013**, *113*, 5989–6113.

[728] X. Lu, L. Feng, T. Akasaka, S. Nagase. *Chem. Soc. Rev.* **2012**, *41*, 7723–7760.

[729] L. Bao, M. Chen, C. Pan, T. Yamaguchi, T. Kato, M. M. Olmstead, A. L. Balch, T. Akasaka, X. Lu. *Angew. Chem. Int. Ed.* **2016**, *55*, 4242–4246.

[730] T. Zuo, L. Xu, C. M. Beavers, M. M. Olmstead, W. Fu, T. D. Crawford, A. L. Balch, H. C. Dorn. *J. Am. Chem. Soc.* **2008**, *130*, 12992–12997.

[731] W. Fu, J. Zhang, T. Fuhrer, H. Champion, K. Furukawa, T. Kato, J. E. Mahaney, B. G. Burke, K. A. Williams, K. Walker, C. Dixon, J. Ge, C. Shu, K. Harich, H. C. Dorn. *J. Am. Chem. Soc.* **2011**, *133*, 9741–9750.

[732] Z. Hu, B.-W. Dong, Z. Liu, J.-J. Liu, J. Su, C. Yu, J. Xiong, D.-E. Shi, Y. Wang, B.-W. Wang, A. Ardavan, Z. Shi, S.-D. Jiang, S. Gao. *J. Am. Chem. Soc.* **2018**, *140*, 1123–1130.

[733] M. K. Singh, N. Yadav, G. Rajaraman. *Chem. Commun.* **2015**, *51*, 17732–17735.

[734] F. Cimpoesu, B. Frecus, C. I. Oprea, H. Ramanantoanina, W. Urland, C. Daul. *Mol. Phys.* **2015**, *113*, 1712–1727.

[735] A. A. Popov, S. M. Avdoshenko, A. M. Pendás, L. Dunsch. *Chem. Commun.* **2012**, *48*, 8031–8050.

[736] N. Samoylova, S. Avdoshenko, D. Krylov, H. R. Thompson, A. Kirkhorn, M. Rosenkranz, S. Schiemenz, F. Ziegs, A. Wolter, S. Yang, S. Stevenson, A. A. Popov. *Nanoscale* **2017**, *9*, 7977–7990.

[737] M. Dolg, H. Stoll, A. Savin, H. Preuss. *Theor. Chim. Acta* **1989**, *75*, 173–194.

[738] M. Dolg, H. Stoll, H. Preuss. *Theor. Chim. Acta* **1993**, *85*, 441–450.

[739] J. Yang, M. Dolg. *Theor. Chem. Acc.* **2005**, *113*, 212–224.

[740] A. Weigand, X. Cao, J. Yang, M. Dolg. *Theor. Chem. Acc.* **2010**, *126*, 117–127.

[741] G. Herzberg, *Molecular Spectra and Molecular Structure. I. Spectra of Diatomic Molecules 2nd ed.*, D. van Nostrand Company, New York, NY, USA, **1950**.

[742] W. C. Martin, R. Zalubas, L. Hagan, *Atomic Energy Levels - The Rare-Earth Elements*, of *Nat. Stand. Ref. Data Ser., NSRDS-NBS 60*, Nat. Bur. Stand., Washington, **1978**.